Zeolitic Ice for Energy Transition

Ahmed Omran

Normandie Université

THÈSE

Pour obtenir le diplôme de doctorat

Spécialité CHIMIE

Préparée au sein de l'Université de Caen Normandie

Zeolitic Ice for Energy Transition

Présentée et soutenue par
AHMED OMRAN

Thèse soutenue le 16/12/2022 devant le jury composé de		
M. YAROSLAV FILINCHUK	Professeur, Université Catholique de Louvain (Belgique)	Rapporteur du jury
MME TZONKA MINEVA	Directeur de recherche, ENSCM Montpellier	Rapporteur du jury
M. NIKOLAY NESTERENKO	Ingénieur HDR, Sulzer	Membre du jury
MME NATHALIE TANCHOUX	Directeur de recherche au CNRS, ENSCM Montpellier	Président du jury
M. VALENTIN VALTCHEV	Directeur de recherche au CNRS, ENSICAEN	Directeur de thèse

Thèse dirigée par VALENTIN VALTCHEV (Laboratoire catalyse et spectrochimie (Caen))

UNIVERSITÉ CAEN NORMANDIE

ENSI CAEN
ÉCOLE PUBLIQUE D'INGÉNIEURS
CENTRE DE RECHERCHE

ED 591 PSIME

LCS Laboratoire Catalyse & Spectrochimie

Dedication

To my parents: Sherif and Wafaa
To my partner of Life and Success : Sahar
To my beloved Sherif and Maryam
To Egypt that keep making history
Pour La France de l'Égalité et de la Liberté

Acknowledgments

I was an ordinary person who studied hard. There are no miracle people.

-R.Feynman [Nobel Prize laureate]

The success of this work does not only come from its scientific content but also from the technical challenges associated with introducing a new research domain to LCS and the unprecedented global circumstances that surrounded us due to the pandemic and energy crisis. It would not reach that point without the help and support of many people. First and foremost, I would like to thank my supervisor ***Dr.Valentin Valtchev*** and for his guidance, trust, and kind support from both personal and technical perspectives through all this work. Thank you, Valentin! I also express my sincere gratitude to ***Dr.Nikolay Nesterenko*** for connecting me to LCS, for his advice, and for our fruitful discussions and support that helped me to overcome many challenges during this work. My sincere gratitude also extended to ***Dr.Svetlana Mintova*** for being my reference mentor and for her continuous encouragement.

All members of LCS family are also sincerely acknowledged for their help without it this work would never see the light. Marie and Benjamin for their daily support, Valarie and Hussein for their help with ICP and NMR, Jaafar for SEM and EDX, Louwanda for the valuable information and technical support even before I arrive, Sophie, Robenson and Blandine for all their kind help with the administrative staff. I am also grateful for Patrick Bousquet-Mélou et and all the team of Normandy supercomputer (CRIANN) for providing the computational resources and technical support. I would like to express my gratitude to my former supervisors *Prof.Nimir Elbashir* from Texas A&M University and *Prof.Gaber ElEnany* from Port Said University (PSU), without their kind support, I would not be here today. I also thank my friend and colleague *Dr.Ahmed Hamid* from Auburn University. Finally, I would like to thank my friends: *Hugo Cruchade, Ana Palčić, Vera Bikbaeva, Abdelhafid Bilal, Francesco Dalena, Hamza Bekkali*, and all my colleagues at LCS for making my PhD time here a lovely experience.

Contents

List of Figures

List of Tables

Chapter 1

Scope of The Thesis

Gas clathrate also called gas hydrates are crystalline nanoporous compounds with wide scale applications. Scientific research related to gas hydrates can be divided into two main categories:

1. **Their natural occurrence** which extends from earth such as natural gas hydrates reservoirs to space with many astrophysics applications related to planet and comet formations.

2. **Their technological application** which includes -but not limited to- methane storage and transportation, gas separation, desalination, flow assurance in gas processing and hydrogen storage.

With almost half of emission of coal and crude oil, natural gas -composed mainly from methane- can play an important role as a **"transition fuel"** in the current **energy transition** from fossil fuels to renewable. With the increasing energy demand, this role is translated as increasing the natural gas share in the current and near-future energy mix. However, current natural gas storage and transportation technologies are CNG (compressed natural gas), LNG (liquified natural gas), and ANG (adsorbed natural gas) are not economically feasible when it comes **long term storage** or **making use of discrete gas resources** such as shale gas and biogas. By providing safe, compact fully reversible methane storage, **synthetic gas hydrates (SGH)** can be a promising alternative or complementary technology that can be integrated with existing infrastructure to improve the current technologies. However, the industrial applicability of of SGH are hindered mainly by the slow formation kinetics and poor heat and mass transfer. Last but not least, the development of safe and practical hydrogen storage represents the major bottleneck for a sustainable hydrogen economy and enable secure energy transition. Thus, solid-state storage systems such as **hydrogen clathrates** may have a great potential to store hydrogen in a **safe, compact, and feasible** manner.

The objective of this work is to present some application of gas hydrates in the context of energy transition. In particular, fundamental understanding of processes such as **hydrate nu-**

Figure 1.1: Schematic diagram for zeolitic ice application for energy transition

cleation, gas diffusion in clathrates and selectivity and stablity for different clathrates cages has been used to overcome the problems related to **industrial applicablity and scale-up** of clathrate hydrates.

Chapter 2 will give extensive literature review with focus on the role of zeolitic ice in energy transition. The different computational methods and experimental investigations will be explained in **chapter 3**. **Chapters 4-6** are dedicated for combined experimental and first principles computational studies for methane storage in clathrate hydrates. In particular, it focuses on accelerating the methane hydrate kinetics using zeolites as green kinetic hydrate promoters and innovative reactor design. **Chapter 7** studies the hydrogen storage and diffusion into clathrate hydrates and how to increase the energy content to meet DOE (US Department of Energy) targets which are the benchmark in that field. Finally, the outcome and perspectives of this work are summarized in **Chapter 8**.

Chapter 2

Zeolitic Ice for Energy Transition: An Introduction

The beginning is the most important part of the work

-Plato

In COP 26, the international community reaffirmed its ambitious targets to reduce carbon emission to mitigate climate change according to Paris Agreement[1]. To achieve that target, a proper combination of energy efficiency and integration of renewables should be applied to ensure a smooth energy transition that balances the increasing demand and environmental commitments. Natural gas can work as a transition fuel between the polluting fossil fuels, and zero-emission renewables such as hydrogen. Carbon capture and sequestration is another important aspect that allows reducing already existing and future carbon emissions that arise from industrial processes. However, the storage and purification of natural gas, CO_2 and H_2 is still challenging and represents an overhead cost that slows down the energy transition process. This review discusses the use of "zeolitic ice" or clathrate hydrates as an environmentally benign material to help the energy transition process. Having structural topologies and properties that are identical to some zeolites and zeolitic clathrasils, those green materials showed unique properties that enable their utilization in different purposes related to the energy transition, such as gas separation, desalination, fuel cells, and others. The review especially focuses on their possible role to purify and safely store gases such as CH_4, CO_2, and H_2, which are in the heart of energy transition. Amongst the objectives of the overview is to present different possible uses of clathrates, their benchmark against existing technologies, and the possibility to integrate them into current technologies with special focus on their application for energy storage and CCS.

[1]This chapter is based on the following article: *Omran A., Nesterenko N., & Valtchev V.* Zeolitic ice: A route toward net zero emissions. Renewable and Sustainable Energy Reviews. 2022 Oct 1;168:112768.

2.1 Introduction to Clathrate Compounds

The IRENA (International Renewable Energy Agency) has defined the energy transition pathway that involves transforming the global energy mix from entirely fossil fuel-based to zero-carbon by 2050 [1]. To achieve that ambitious target, it is crucial to reduce CO_2 emissions and integrate renewable sources into the energy sector globally [2]. The polluting effects of natural gas are about half of the other fossil fuels. Therefore, natural gas is considered a transition fuel that possesses a well-established technology that can mitigate CO_2 emission while renewable energies and hydrogen economy mature both technologically and economically [3]. However, this bridging role of natural gas should be considered only as a "temporary" role because natural gas still emits CO_2 emissions [4]. In addition, the carbon emission of the natural gas processing and storage should be reduced as much as possible either through process optimization or post-processing to produce useful products [5]. Although natural gas processing and transportation are well-established, long-term storage and utilization of discrete and remote gas resources is still a challenge, an issue that is related to appropriate gas storage. Current global storage capacity is estimated to accommodate only 2% of the global annual natural gas production. This

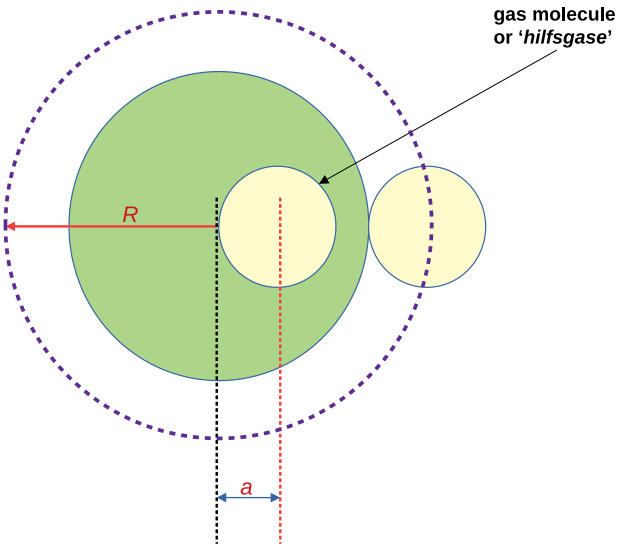

Figure 2.1: Barrer's model to calculate the intercalation heats of clathrates (adapted from [6]).

deficiency may result in an energy crisis whenever the supply chain is disturbed [7]. Moreover, the main overhead capital cost of the natural gas processing process comes from the purification process that targets the removal of acid gases and N_2 from natural gas [8]. Thus, viable and economical carbon capture and sequestration (CCS) should be coupled with the process to ensure efficiency. When it comes to hydrogen economy as a main part of the renewable energy sources, there is a significant development in the production side from both renewable and natural gas [9]. However, the bottleneck of successful hydrogen incorporation into the energy mix is connected mainly to proper and compact hydrogen storage [10].

In general, clathrates are inclusion compounds formed when guests of specific sizes (CH_4, CO_2,

H_2, Na, etc) are encaged in various host molecules (H_2O, SiO_2) or elements (Si, Ge, C, etc.) under appropriate temperature and pressure conditions [11]. According to those conditions, one or multiple guest molecules can be entrapped in the host cavity. When the host molecules are mainly silica or water, clathrates from the well-known zeolitic clathrasils or gas hydrates, respectively [12]. The two classes are structurally analogous because both materials have a framework of several cages with voids occupied by guest species **Table 2.1** [13].

Using simple models such as **Figure 2.1**, early statistical thermodynamic interpretation of van der Waals and Platteeuw could provide satisfactory information about the non-stoicheiometric nature of clathrate and the stabilizing action of guest gas as well as successfully expected the conditions under which clathrates phases are formed in most cases [6, 14, 15]. R.M. Barrer -the founding father of zeolite chemistry with a gas permeability unit named after him [16]- extended van der Waals work and dedicated a series of his early publications for those inclusion materials [6, 17–19]. Moreover, he had pointed out their structural and propertied similarities to zeolites in several others as illustrated in **Figure 2.2** [17, 20]. Based on those similarities and the success of zeolites inclusion compounds in catalysis and gas separation [21], one can anticipate that gas clathrates can have promising industrial and technological applications especially in the context of energy transition. In that particular context, gas clathrates offer the potential for environmentally benign purification and storage of natural gas, CO_2, and H_2, as shown in **Figure 2.2**.

Clathrate hydrates are non-stoichiometric nanoporous crystalline structures that are mainly composed of host water molecules [14, 15]. Connected by hydrogen bonding, those host molecules are forming three-dimensional cavities which enclose guest gas molecules. Under certain pressure and temperature conditions, they can exist in nature or be artificially synthesized. Different hydrate structures are stabilized by the encapsulation of gases such as CO_2, H_2S, CH_4, H_2, or organic solvent such as tetrahydrofuran (THF), cyclopentane, or cyclooctane (Cyclo-O). Recently, gas hydrates have been the subject of intensive research related to a wide range of energy transition applications. The existence of clathrates has been known for a long time. A description of chlorine gas crystal structure was reported by Sir Humphrey Davy back in 1810[23]. However, clathrate hydrates attracted more attention particularly with the rise of the oil and gas industry in 20^{th} [24]. In particular, the research at that period focused mainly on flow assurance and how to secure pipelines from being blocked by hydrates. Such blockage can interrupt the production from offshore reservoirs and the associated economic and safety concerns [25].

In recent decades, gas hydrates showed increasing potential for various industrial applications such as energy storage [26], gas separation [27, 28], CO_2 capture and sequestration (CCS) [29], desalination [30, 31] and fuel cells [32, 33] as shown in **Figure 2.3**. With the energy transition

Table 2.1: Clathrate types of Hydrates and Clathrasils

Clathrate Hydrate Type	I	II	H
Space group	$Pm\bar{3}n$	$Fd\bar{3}m$	$P6/mmm$
Cages	5^{12}, $5^{12}6^2$	5^{12}, $5^{12}6^4$	5^{12},$4^3 5^6 6^3$, $5^{12}6^8$
Hydrate Lattice Parameter(n.m)	a=1.2	a=1.73	a=1.22, c=1.01
Guests (Hydrates)	CH_4, CO_2	H_2,CH_4(0.25 GPa[22])	CH_4-Cyclooctane
Clathrasil IZA code	MEP	MTN	DOH
Clathrasile Lattice Parameter(n.m)	a=1.346	a=1.99	a=1.378, c=1.119
Guests (Clathrasils)	CH_4, N_2, CO_2	CH_4,N_2 Ar, $(CH_3)_3N$	N_2, $(CH_2)_5NH$

toward renewables, low-carbon and unconventional energy, electrification, and decarbonization to reduce greenhouse gases (GHGs) emissions, recent studies on gas hydrates are distributed between the following main areas: (1) the traditional field of natural gas flow assurance, (2) gas hydrate natural occurrence and the associated environmental impact and (3) possible technological applications of hydrates.

Traditionally, gas clathrate is a problem of great concern in the field of natural gas processing as it may interrupt the gas flow from offshore to onshore and affect drilling process safety [34]. Concerning clathrate's natural occurrence, the recently discovered enormous hydrates reserves, usually filled with methane, can present affordable clean energy sources and balance between the increasing energy demand and the environmental impact of using other fossil fuels such as oil and coal [35, 36]. *Clathrate gun hypothesis* refers to possible uncontrolled methane release from clathrates in oceans due to the increased temperature [37]. In such a scenario, this methane release can accelerate global warming which destabilizes more clathrate structures and invoke further warming[37, 38].
Finally, hydrates applications for green energy transition and sustainable development represent another growing area of interest. In that context, cages can be utilized for safe energy storage. With a volumetric capacity of methane that can reach about 160-180 V/V [39, 40], they can also be used to store and transport other gases of economic interest such as CO_2, N_2 and H_2 in economically feasible *P-T* conditions is one of the highly promising areas[41]. CH_4-

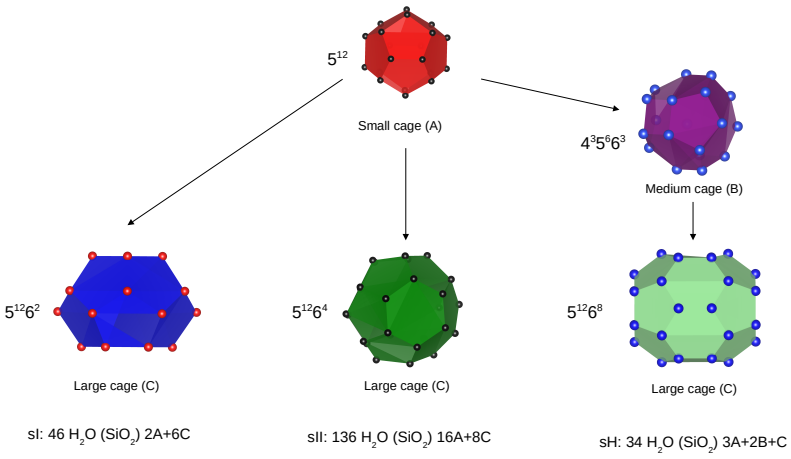

Figure 2.2: Summary of common clathrasil and gas hydrate cage structures.

CO_2 replacement in the enormous methane hydrate reservoirs is another important application that became the focus of recent research studies [42]. The interest in that technology comes from the fact that it could achieve the double benefit of simultaneous energy recovery and carbon fingerprint reduction via permanently storing CO_2 of flue gases in the deep ocean. In fact, clathrate applications can not only be regarded as "stand-alone", but also they can be integrated within exciting technologies such as LNG or biogas production.

However, despite the wide range of applications, the extensive industrial use of hydrate

Figure 2.3: Gas hydrates potential technological applications for the energy transition.

faces challenges such as slow kinetics, lack of clear understanding of phenomena such as self-preservation [43], memory effect [44] and different possibilities of cage occupancy [45]. The clathrate properties need to be further understood to resolve those problems, by combining both theoretical and experimental studies. In fact, evaluating the various interactions between the host water crystal and the enclasthrated guest molecules is an indispensable part of clathrates research. There are several detailed reviews [46–50] and early comprehensive pioneering books [23, 51] for different aspects of hydrate research. Instead of duplicating that, this paper selectively reviews the most important contributions and current state of the art of theoretical calculations, experimental studies, and industrial research, focusing on the application side. More precisely, it aims to exhibit the current problems hindering the energy transition industrial application of clathrates from scientific and engineering perspectives and propose solutions for those challenges.

2.2 Gas Clathrate Structures and Properties

The structure-property relationship within the domain of gas hydrate depends on the nature of guest molecules and various temperature and pressure conditions. This relation has a great influence on the practical application of clathrates and their impact on the environment. To illustrate, parameters such as the ability to control gas hydrate synthesis and crystallization kinetics using different methods, additives, reactor, and process design are crucial for reducing the operational cost and increasing their industrial applicability. This section will discuss different structures and properties of clathrate hydrates, which can give important insights into their applications.

2.2.1 Hydrate Structures

Although usually formed under high pressure, a combination of both experimental work and theoretical calculations in recent decades has enabled us to precisely determine the structure of those materials. Experimental techniques such as in situ NMR [52, 53], X-ray diffraction [54, 55] and Raman Spectroscopy [56, 57] provided us with important information such as the nature of host structure, cage occupancy, and guest molecules motion in the cages . For example, Okuchi *et al* used in situ NMR single-crystal XRD (SXRD) was used to get the atomic coordinates and geometries that are not provided by the conventional spectroscopic techniques [58, 59]. However, it has limited use due to the complexity of finding a suitable size clathrate single crystal. To solve that, experimental techniques can be coupled with theoretical studies to define the clathrate structure [60] or even anticipate new phases that are difficult to synthesize [61, 62]. The different nature and interactions between guest or *"helfsgase"* [63] and host molecules are crucial to understand the thermodynamic stability of different clathrates. While early theory has considered only the guest-host interactions while ignoring others [46], recent

studies showed that guest-guest and host-host interactions can also affect hydrate formation and stability[64, 65]. In general, water clathrates can be classified into two main categories: (1) clathrate hydrate and (2)ionic clathrates.

2.2.1.1 Clathrate Hydrates

Clathrate hydrates are nanoporous inclusion crystalline material with weak, non-directional van der Waal's attraction forces between the encaged hydrophobic guest molecules and the host water crystal that form a hydrogen-bonding network around them. The most common ones are sI, sII, and sH as summarized in **Figure 2.2**. They attracted more attention due to the presence of methane as a guest in all three structures depending on the formation pressure [22].

The presence of pentagonal dodecahedra (5^{12}) or small cages are common in all three structures. While sI is distinguished by the presence of large cages of tetrakaidecahedra ($5^{12}6^2$) that may host gases such as CO_2 or CH_4, sII have larger hexakaidecahedra ($5^{12}6^4$) cages that can host large solvent molecules such as THF [23, 66, 67]. Finally, sH contains medium irregular dodecahedra ($4^35^66^3$) medium cages in addition to the large icosahedra ($5^{12}6^8$) cages which can accommodate larger molecules such as cyclooctane [68]. It should be noted that smaller guest size does not always result in sI hydrate. For example, although they have relatively small kinematic diameter, hydrogen and nitrogen are naturally formed sII clathrate at elevated pressure [69]. The hydrate structure is controlled by not only by guest size but also *P*-*T* conditions. For example, increasing the pressure to 250 MPa, methane hydrate can form sII hydrate rather than structure I [22] as shown in **Figure 2.4**.

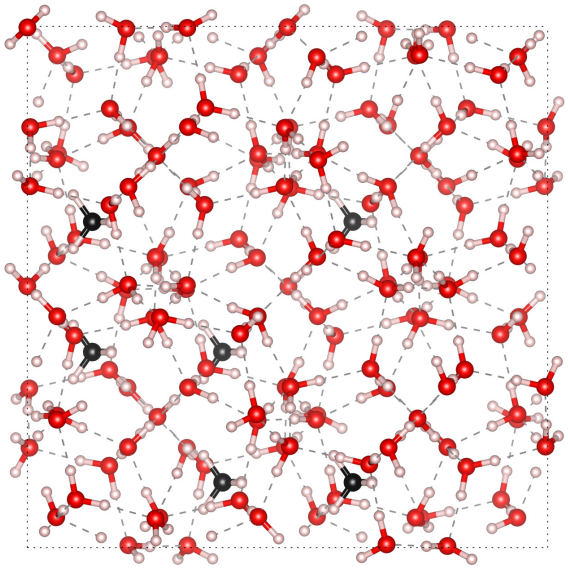

Figure 2.4: Structure II of pure methane hydrate can be formed at 0.25 GPa [22]. Hydrogen atoms are shown in pink, oxygen in red, carbon is black, and hydrogen bonds are with dashed lines.

Cage occupancy is another important factor to determine clathrate properties and storage capacity [70]. Large and small cage occupancies depend on the type of guest molecules as well as *P-T* formation conditions. While increased cage occupancies can improve clathrate stability, it is not a pre-condition to get a stable clathrate host structure [71]. For instance, pure sII hydrogen hydrate can store about 5.3 wt% at elevated pressures. In the case of binary H_2-THF sII with stoichiometric THF amount of 5.56 mol%, the large cages are completely occupied by THF and the maximum hydrogen storage capacity is about 1 wt% only but at relatively much lower pressure [72].

2.2.1.2 Semi-clathrate hydrate

Although their existence can be dated to 1893, this important class of zeolitic ice structures that has potential application in in gas separation [73], energy storage and CCS [74–76]. This kind of clathrate is usually called "ionic clathrate" due to the fact that hydrophobic cations or anions are encapsulated by host cages while a counter ion is incorporated into the host water framework. In other words, the walls of cages are partially removed or replaced by anions or guest molecules in addition to the hydrophobic inclusion that exists in clathrate hydrates [32].They can be distinguished from clathrate hydrates by exhibiting partial hydrogen bonding between the guest species and the water host cages in addition to van der Waals interactions. This latter properties result in a relatively high thermal stability in atmospheric conditions, enhanced ionic and hydrogen conductivity making them ideal candidates for applications such as solid electrolytes.

Numerous strong acids form semi-clathrates in which anion guests are encapsulated into the acidic host lattice. For example, $HAsF_6$ and HPF_6 forms sVII , which has only $4^6 6^8$ cages and is distinguished by high melting point and high ionic conductivity [77]. Acidic clathrate such as HBF_4.5.75 H_2O or $HClO_4$.5.5 H_2O can form the cubic sI clathrate. In these structure, the anions can occupy both large and small cages. HPF_6 can also form sI too, but in this case, it occupies the large cages ($5^{12}6^2$), only leaving the small cages empty. In contrast to sVI semiclathrate, sI compounds have relatively lower melting points [78]. Similarly, SF_6 neutral molecule has been shown to form sII occupying the large cages of $5^{12}6^4$ [77]. On the other hand, some ionic clathrate hydrates show strong or weak basicity by encapsulated cationic guests while the host lattice charge is balanced by anions such as OH^-, F^-, and Br^-. The base-containing semi-clathrate are more diverse than acidic ones with a general formula of $R_4N^+X^-$ where (R=CH_3, nC_3H_7, nC_4H_9, and others) while (X=OH^-, F^-, Cl^-, Br^-, and others [79].

Quaternary ammonium salts (QAS) are the most common type of these clathrates and are distinguished by a high melting point that can reach 31°C [80]. For example, tetra-*n*-butyl am-

monium bromide (TBAB) has the bromide anions constructing the cage along with host water. At the same time, the hydrophobic cation fills the cage without H-bonding to the host water molecules. In the latter case, all the dodecahedral cages are empty, providing potential storage sites for other guest molecules [81–83]. The thermal stability at ambient conditions along with the non-volatile nature of salts represent a great advantage when it comes to hydrogen storage.

2.3 Role of Zeolitic Ice for Energy Transition

In this section, we will focus on two of the main applications of gas hydrates: solid energy storage (SES) and CO_2 capture and sequestration (CCS). There is intensive research for both applications. The IPCC and Paris agreement suggested that to tackle the impacts of global warming, the carbon emissions have to be reduced systematically to zero by 2050 [84, 85]. In general, gas storage can be classified into two main categories according to the state in which the gas (for example, CH_4, CO_2 or H_2) is stored: (1) physisorption (physical storage) in which the gas is stored in molecular form, and physical adsorbed on the material surface and interact with the host material with van der Waals forces and (2) chemisorption (chemical storage) in which the gas is dissociating form ionic or covalent bond with the host.

The current CO_2 capture techniques such as adsorption, cryogenic separation, and membranes have been widely investigated. However, their economic feasibility is challenged by their high energy consumption and technical difficulties such as non-consistent performance and increased differential pressure. Thus, they are not suitable yet for industrial-scale applications, at least in the short and medium terms. When it comes to energy storage, a useful benchmark for those materials can be obtained from the United States Department of Energy (DOE), which sets some criteria for both methane and hydrogen storage for onboard applications. The purpose of this section is to focus on CCS, methane, and hydrogen storage in clathrates and compares them to other existing technologies.

2.3.1 Methane Storage

Methane clathrate formations can be from both natural and synthetic routes. Naturally occurring gas hydrates have been accumulated long geological periods in permafrost regions and mostly on the more accessible submarine continental margins representing a low carbon energy source and possible CO_2 storage sinks. Although there is considerable uncertainty about the methane hydrate reserves, the amount of methane gas is expected to be more than all other carbonaceous fuel reserves combined. One can refer the reader to some comprehensive reviews for gas hydrate reservoirs [35, 36]. We focus here on synthetic gas hydrates (SGH) as an emerging technology.

Natural gas can be stored in underground inventories such as salt caverns and depleted oil or gas reservoirs. This technique, which depends on the natural occurrence, is distinguished by the ease of gas recovery, but it may possess some environmental risks. Apart from storing natural gas in underground inventories, the main natural gas storage and transportation technologies are CNG (compressed natural gas), LNG (liquified natural gas), ANG (adsorbed natural gas), and SGH (synthetic gas hydrates). Storing and transporting methane in its native gaseous state via tanks and pipeline networks (PLG) require high volume and can be less economically feasible when it comes to discrete gas resources such as shale gas and biogas [86]. On the other hand, CNG can reduce the storage volume, but it needs expensive multistage compression, high-pressure tanks that exhibit safety concerns, and poor volumetric capacity. Thus, CNG is not applicable when it comes to large-scale natural gas storage [87]. Storage and transportation of natural gas in liquid form or LNG have been expanded rapidly to become the most convenient technology for industrial-scale and transoceanic transportation. This can be attributed to the that a single cubic meter of LNG can contain as high as 600 m^3 STP conditions. Although currently, LNG tankers are roaming around the world to transport methane, the technology possesses some drawbacks. First, it needs big reserves and long-term commitment to install expensive facilities and associated infrastructure such as cold insulation and cryogenic tanks (i.e., high CAPEX). Then, it also has a high operational cost (OPEX) coming from the energy demand for cooling methane to -161 °C, boil-off gases re-compression, and regasification at the customer end. Furthermore, the technique is not flexible to store methane for long periods such as several months or years due to the high OPEX [88, 89]. The recent pandemic and geopolitical developments disturbed gas supply and resulted in unprecedented natural gas prices increase and highlighted the need for long-term storage technologies [90]. In general, the calculation of MOFs' storage capacity calculations commonly reported in the literature were based on a single crystal assumption. Such a calculation methodology is far from practical as it ignored the packing efficiency effect. Thus, the calculations of actual or deliverable gravimetric and volumetric gas uptakes based on bulk powder are significantly lower. Furthermore, other factors like re-usability, mechanical stability, thermal conductivity, and the high cost of the material are significant challenges that impede the use of MOFs for some onboard and all industrial-scale methane storage [91, 92].

SGH can be a promising alternative or complementary technology that can be integrated with existing infrastructure to improve the current technologies. First, SGH has very competitive safety and eco-friendly advantages due to factors such as the presence of water and lower storage temperature and pressure conditions. Such factors are reflected in the non-explosive and well-controlled storage and recovery processes. Moreover, unlike chemical storage, the methane hydrate storage process depends on the physical interactions such as vdW force and thus the storage is almost fully reversible. Finally, they are economically attractive due to the simple modular synthesis arrangements and moderate storage conditions. Several studies

showed that the SGH plant can have about half the cost of LNG one of the same capacity. In addition, it is that it can reduce methane transportation costs by a quarter compared to LNG [93].However, despite the above advantages, the industrial applications of hydrate-based technologies (HBTs) are still limited. The reasons behind that can be the slow kinetics, poor heat, and mass transfer, uncertainties of scale-up storage capacities.

To solve the above problems specific additives or promoters are added during hydrate synthesis. The role of promoters can be either catalyzing the kinetics of hydrate formation (kinetic hydrate promoter or KHI) or reducing the thermodynamic requirements (thermodynamic hydrate promoter or THP). However, understanding the crystallization processes -and more specifically the nucleation process- during hydrate formation is crucial to develop a suitable kinetic model for hydrates synthesis[94]. In general, the hydrate crystallization process can be divided into three main stages: gas dissolution, nucleation, and growth. First, the gas dissolves in the aqueous medium until enough guest molecules are adsorbed in the liquid phase to start nucleation. Nucleation is usually very slow and is distinguished by its stochastic nature [95]. Two types of *microscopic nucleation* may occur (1) homogeneous nucleation or "labile cluster hypothesis" in which the crystal formation starts directly from the liquid phase and (2) heterogeneous nucleation in which the process starts on the surface of "nucleation sites" [96, 97]. On the other hand, *macroscopic nucleation* can be spotted experimentally due to the exothermic nature of the hydrate formation reaction. This temperature increase is associated with rapid pressure drop due to gas enclathration [98]. Based on that, the macroscopic induction time or "lag time" can be determined. Such a time then can be spotted by the above thermodynamic changes and the appearance of detectable hydrate crystals [23, 99]. In the last stage, catastrophic crystal growth is distinguished by a very rapid increase in the particle size as the gas becomes more concentrated in cages than in vapor[100]. At the end of that stage, the reaction is controlled by mass transfer or gas diffusion through the 'hydrate film' at the liquid-gas interface [101].

Another important phenomenon that is closely related to the understanding of the nucleation process is called the "memory effect"[51, 102, 103]. When a hydrate undergoes decomposition, the resulting solution can form hydrate more readily. In other words, it needs a relatively shorter induction time compared to a fresh solution used to make hydrate [44, 104]. The sI methane clathrate showed the highest methane uptake among all clathrate structures with volumetric storage that can reach 170 V/V relatives to STP, as shown in **Figure 2.5**. Early investigation of Vysniauskas and Bishnoi for sI methane hydrate formation kinetics showed that it depened on *P-T* conditions, gas-liquid interfacial area, and degree of supercooling [102]. After that, there were many other investigations for sI methane clathrate such as those Englezos *et al.* [105], and Kim *et al* [106]. A common observation of these studies is that at the gas-water interfaces, hydrate films grow laterally along with the interface, and it is crucial to increase the surface

area of gas-water contact to enhance both mass and heat transfer. Indirect methane hydrate formation can start from ice and could result in a high yield. However, this approach may not be economic due to the high energy spending and longer time associated with the ice formation [107].

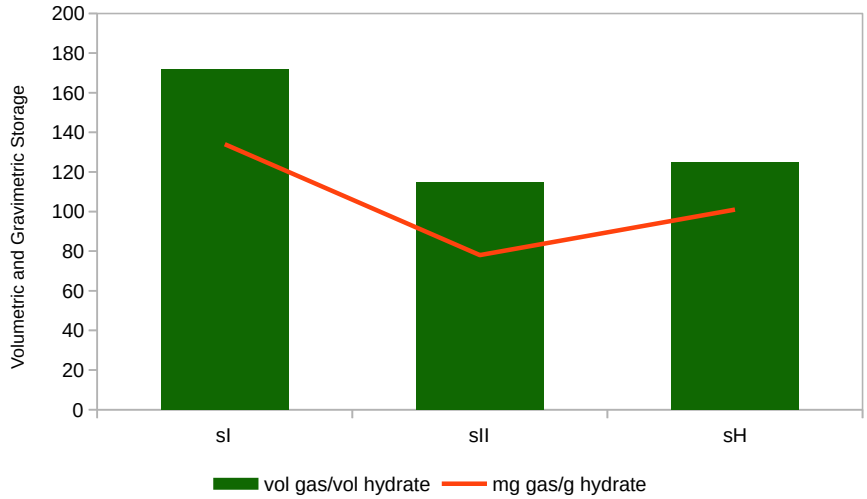

Figure 2.5: The estimated volumetric and gravimetric storage of common methane clathrate hydrate structures.

To solve the problem of slow kinetics, KHP is added to reduce the time required for hydrate synthesis without influencing thermodynamic requirements. In other words, the hydrate structure, as well as the *P-T* condition of hydrate formation, are not affected. Surfactants (anionic, cationic, and non-ionic) are commonly used for that purpose[108]. In particular, the anionic surfactant sodium dodecyl sulfate (SDS) is predominant and has extensively been studied in different concentrations [109–111]. Close to its critical micelle concentration (CMC), SDS can relatively increase the hydrate formation rate significantly [112]. Micelles formation increases methane concentration in the aqueous phase and thus enables the nucleation to start earlier [111]. Here, it's worth mentioning that selection of the suitable surfactants should take into account their Krafft temperatures. The Krafft temperature is the minimum temperature from which the micelle formation takes place. Surfactants are usually employed above their Krafft points otherwise hydrated surfactant crystals are formed [113]. To illustrate, Du *et al.* found that hydrate formation at 274 K has been little affected by dodecyltrimethylammonium chloride (DTAC) whose Krafft point below 273 K compared SDS, dodecylamine hydrochloride (DAH), and dodecyltrimethylammonium chloride (DTAC) whose Krafft points near room temperature [114]. Moreover, Zhang *et al.* explained that SDS increases the hydrate particles' surface area and the gas-liquid interfacial area while reducing surface tension [115]. Increasing the carbon chain length of sodium alkyl sulfates showed the same kinetic promotion behavior of SDS under similar conditions but required much less concentration than SDS [116, 117]. However,

the utilization of surfactants for the hydrate-based process has a serious drawback related to foaming which is a serious problem in gas processing. This has been particularly observed during hydrate dissociation and scale-up experiments [118–120]. Moreover, it has been seen the presence of surfactants at certain concentrations may have inhibiting effect probably due to the presence of sodium ions. The intrinsic water network around that hard cation collapses due to the hydrogen bond breaking and strong binding between the ion and water molecules [121, 122]. In addition to not being environmentally friendly, such drawbacks hinder the industrial applicability of this class of promoters.

In order to overcome those drawbacks, two other classes of kinetics promoters were suggested: amino acids and porous materials. It has been found that amino acids increase the rate of hydrate formation at a certain concentration [123]. Although the rate is less than SDS in some cases, the final methane uptakes are still comparable in both cases [124]. Amino acids are promising biodegradable materials that can work as hydrate promoters. Low dosage hydrophobic or aromatic amino acids such as tryptophan and methionine or have shown better performance than hydrophilic or aliphatic ones such as KHP for methane hydrate synthesis [122, 125].

Porous materials such as those from carbon origin (such as activated carbon and carbon nanotubes) or silica origin (silica gel, silica sand, hollow silica, and nano-silica), zeolites, and MOFs has been proposed as KHP [126]. In general, these materials can be utilized in two different ways: (1) in low concentrations as a nucleation site for heterogeneous nucleation to reduce the induction time [127] and (2) as host for hydrate using the confinement effect [128]. In the first approach, the porous material increases the surface area by adding another interface (or third surface) that facilitates crystallization and gas diffusion. For example, hollow silica was also examined in many studies and showed kinetic improvement. However, it needed the addition of SDS to get acceptable results when the conditions tested were near ambient conditions [129]. Xiaoya *et al.* has tested for LTA-type zeolite (3A and 5A) for methane hydrate formation and concluded that 3A has better promoting effect. However, a reasonable gas storage capacity above 120 V/V could be only achieved in presence of SDS [130, 131]. Kim *et al.* showed zeolite 13X (FAU-type) at 0.01 wt% concentration showed higher gas consumption than SDS and LTA-type zeolite, making it the most promising zeolite as KHP. The author attributed that to the small particle size and large pore diameter of 13X compared to the other zeolites studied [132]. In addition to being cheap and eco-friendly, the above zeolites are used in low concentrations and can be easily separated.

On the other hand, the porous material in the second approach can act as a medium for hydrate synthesis within the confinement approach. It has been found that high-pressure phases and reactions were found to occur in confined spaces in pressures that are magnitudes lower

than required for bulk ones [133, 134].For example, Siangsai *et al.* investigated the effect of activated carbon (AC) particle size on methane hydrate kinetics. They found that in the size range of (841–1680 μm) showed higher conversion while the highest recovery could be achieved in the range of (250–420 μm) [135]. Celzard *et al.* took advantage of activated carbon nanopore space to synthesize methane hydrate at mild conditions of (3.5 MPa and 2°C) and faster kinetics than nature [136]. It is also suggested that hydrophobic MOFs (ZIF-8) can show a high yield of methane hydrate uptake by combining methane hydrate formation and adsorption of methane in the interior pore spaces[137]. Borchardt *et al.* reviewed such an approach in detail and showed that in addition to hydrophobicity and pore size, water loading R_w (g H_2O/g soild) plays a crucial role in the uptake yield and kinetics [126]. The approach is very promising as those materials may act as both KHP and THP. However, several factors need to be examined in that approach for possible scale-up application. For example, there is packing efficiency that needs to be taken into account, additional cost to handle those materials, and the considerable loss in the gravimetric capacity.

KHP does not affect with thermodynamic conditions of hydrate formation. For that, another type of promoter is required. THP works to move the hydrate formation *P-T* conditions to a more moderate range and thus lowering the energy requirements. Depending on the nature of promoter and thermodynamic conditions, different hydrate structures can be obtained. For example, THF can direct hydrate synthesis toward sII formation. It is also reported to work in synergy with SDS to improve the kinetics [138–141]. Other sII formers such as acetone [142], cyclopentane [143], dioxlane [144], and others were reported in the literature [145]. On the other hand, sH formation needs larger molecules to stabilize the large cage of $5^{12}6^8$. Common sH formers are neohexane [54], methyl cyclohexane [146], cyclooctane [147]. Theoretically, sH can store gases such as CH_4, CO_2, or H_2 in both small and medium cages and may result in high storage capacity. A more comprehensive review of various promoters studies (KHP and THP) can be found in the literature [108]. The main drawback of using THP is the significant reduction in methane uptake compared to sI. The main reason behind that decrease is that those promoters occupy the sII or sH large cages while stabilizing the structure. However, the reduction of formation conditions closer to ambient temperatures can significantly offset that storage capacity reduction. For example, compression cost was found to be around three-quarters of the total cost of SGH formation in a pilot-scale reactor [148]. Increasing the methane formation temperature from 274.2 K to 293.2 will reduce 80% of the cooling cost as estimated by Veluswamy *et al.* [149]. The main drawback of sII and sH promoters are the potential environmental hazards and higher costs. In particular, solvent loss or volatility that requires additional solvent amount represents a big overhead on the OPEX.

2.3.2 HBCS and Simultaneous Methane Recovery

Due to various factors, such as the increasing world population, the associated global energy demand has been steadily rising, which has impacted immense pressure on dwindling fossil fuel resources. Simultaneously, environmental problems such as climate change start to affect the global economy and social stability. Consequently, the international legislation that emphasizes the importance of reducing carbon fingerprints is increasingly enforced worldwide [84, 111]. Capturable CO_2 sources can be generally divided into two main groups (1) low concentration such as air [150] and (2) high concentration such as flue gases. Although there are many advances in capturing CO_2 directly from the air [151], intensive research activities are focused on capturing it directly from the flue gas sources. The major sources of flue CO_2 gas emission are pre-combustion, post-combustion, and oxyfuel processes. The latter aims to increase the CO_2 concentration via burning the fuel in pure oxygen, which will result in easier CO_2 capture.

There are several methods to capture CO_2 from flue gases [152]. The most common ones are adsorption, absorption, cryogenic separation and membrane separation. Although each technique has some advantages, it also shows some drawbacks. For example, membrane separation is expensive with an estimated cost of 24-48$ per ton depending on working conditions [153]. Moreover, while inorganic ones do not perform well in terms of reliability and cost control, organic membranes can not simultaneously reach high selectivity and high permeability. Generally, membranes are affected by the flue gas composition and lack sustainable performance and aging resistance [154]. Adsorbent-based systems with high surface areas such as MOFs and zeolites can reduce the cost to around 14$ per ton [155, 156]. However, their sustainability can be affected by impurities, the humidity of flue gas, and complicated unit operations due to the low-temperature requirements and pressure drop. Absorption is the most common method for removing acid gases from flue gas streams, especially in gas processing plants [157]. Despite its ability to reach high CO_2 capture capacity and high separation efficiency, it has some problems such as solvent degradation, safety risk associated with high pressure in the absorber, and high energy requirement of solvent regeneration as typical regeneration is at 120°C [158]. As shown in **Figure 2.6**, the same problem of high energy consumption persists with cryogenic separation [159] of CO_2 as cooling and pressurization may consume approximately 600 kW per ton of CO_2 on average [160].

Carbon sequestration has received relatively less attention compared to carbon capture [161]. Different carbon sequestration options include but are not limited to saline aquifers, depleted and current oil and gas reservoirs, deep ocean storage, and mineral carbonation. However, many factors such as geohazard risks of the available sites and environmental, economic, social, and political factors should be considered [161]. Thus, *hydrate-based carbon capture and*

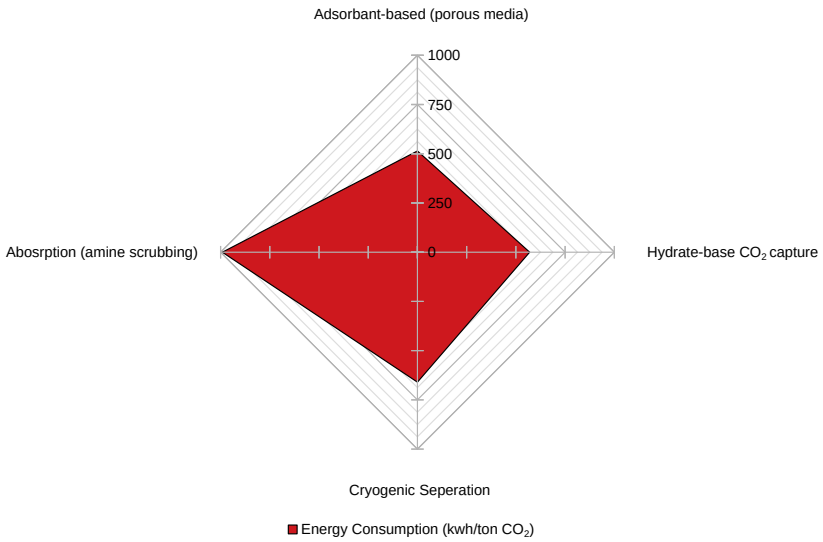

Figure 2.6: Estimated energy consumption (kw h per ton CO_2) of different carbon capture technologies. Hydrate-based technology combines both capture and sequestration methods in a single step. The figure is reproduced from Yu *et al.*[153].

sequestration **(HBCS)** has been proposed recently to overcome some of the above drawbacks of other methods while combining both capture and sequestration in a single step [162, 163]. Additionally, the recently discovered tremendous reserves of hydrates, mostly methane hydrates or natural gas hydrates (NGH), represent a huge opportunity for an affordable energy source [35, 36].The most practical NGH extraction techniques are thermal stimulation, chemical inhibitor injection, and depressurization. However, each of these methods has its advantages and deficiencies. To illustrate, CH_4 is encapsulated in a delicate crystal that can rapidly decompose in an uncontrolled or even explosive fashion under depressurization or thermal stimulation which can be a serious safety concern. In addition, methane is a high global warming potential (GWP) and can contribute to the "clathrate gun hypothesis" mentioned earlier [37].

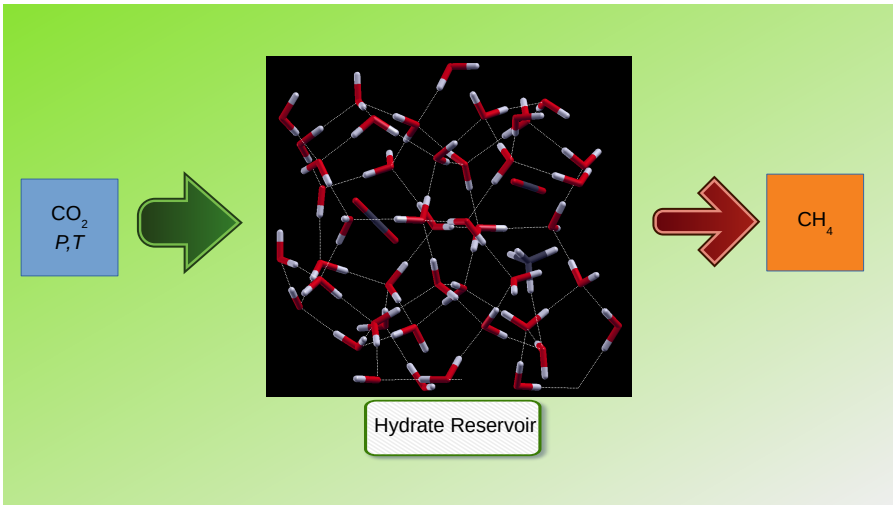

Figure 2.7: Schematic representation of methane clathrate replacement with CO_2.

Accordingly, the utilization of naturally occurring gas hydrates should be associated with a proper hazard analysis of the environmental impact. To solve the problem of uncontrolled methane release, a suitable guest molecule can be employed to replace methane in the hydrate structure. In that context, it suggested that CO_2 can replace methane in natural gas hydrate reservoirs. The formation of the more stable but geological similar CO_2 hydrates possesses a double-benefit elegant solution involving both energy recovery and combustion product sequestration as illustrated in **Figure 2.7**. Such a technique will reduce the associated greenhouse gases (GHGs) emissions [42]. In principle, the exchange possibility has already been confirmed through experimental and theoretical studies [164]. From a thermodynamics point of view, the change in Gibbs free energy (ΔG) of CH_4-CO_2 replacement in the hydrate is negative, which declares that the reaction is spontaneous without involving latent heat [165]. Thus, this exchange between injected CO_2 and methane hydrate is more economic than gas recovery via decomposition only. In addition, the thermodynamic equilibrium conditions (P, T) are more moderate in the case of CO_2 compared to CH_4 [166]. Furthermore, the process has been applied, and NGH exploitation via the CH_4-CO_2 replacement method has been used in the northern slope of Alaska since 2012 [167, 168]. The technique has many advantages and can be both economically feasible and environmentally friendly. First, it is ecofriendly as it retains the current geological structures without change. In fact, the CO_2 clathrate is more stable than the CH_4 clathrate which has been already stayed for many geological eras. Then, the exchange process is safer than mining processes from Hazard, and Operability Analysis (HAZOP) point of view. Finally, it is economically attractive as there is no need to treat the tremendous amount of water usually associated with gas hydrate dissociation. Despite the above, there is an inherited uncertainty in the economic feasibility due to the lack of enough information about the methane reserves, mechanism, and rate of the exchange reaction [169].

2.3.3 Hydrogen Storage

The hydrogen economy is a very important element in the energy transition. In this economy, hydrogen is proposed to be used extensively as the primary energy carrier. Hence, the development of hydrogen production from both natural gas (grey and blue hydrogen) and renewables (green hydrogen) is of great importance. However, safe and practical hydrogen storage represents the major bottleneck for a sustainable hydrogen economy [170]. While conventional gaseous state storage systems as pressurized hydrogen gas need very high pressure and expensive infrastructure, liquid hydrogen needs extensive refrigeration and re-compression of boil-off gas to keep the temperature near 20 K. It is very important to evaluate the specific energy consumption and CO_2 to evaluate the storage efficiency. Consequently, the above requirements pose safety and cost problems to both, onboard and large-scale applications, and do not satisfy the core objectives for a hydrogen economy [171].

Thus, solid-state storage systems have a great potential to store hydrogen in a safe, compact, and feasible manner, making it an increasingly attractive technology for hydrogen storage [172]. When they are benchmarked with chemisorption such as metal hydrides or physisorption such as metal-organic frameworks (MOFs), hydrogen hydrates possess the potential to be environmentally benign, safe, and cheap material for hydrogen storage [50]. While hydrogen storage in MOFs suffers from uptake reduction when scale-up due to packing efficiency loss as described above, zeolites and activated carbon need to work at about 77 K [173]. Chemical storage is successful in storing hydrogen at a significantly higher temperature near ambient conditions. However, it needs high energy to break the chemical bond and restore hydrogen. For example, to restore hydrogen from hydrocarbon or ammonia, it needs to undergo reforming at a high energy cost. Hydrides that seem to be the closest to attaining DOE targets need a high temperature to retrieve hydrogen as illustrared in **Figure 2.8**[174]. To illustrate, aromatic hydrogenation reactions are highly exothermic and thermodynamically favorable with the aromatic benzene ring enthalpy being ΔH_R = -68.73 kJ/mol H_2. At the same time, the dehydrogenation is endothermic with the high energy demand of 64–69 kJ/mol H_2 [175, 176]. Liquid-organic hydrogen carriers (LOHC) partially solve that problem via reducing the dehydrogenation enthalpy catalytic processes [177]. However, both hydrides and LOHC face common challenges such as safety, eco-toxicity, solid-based or liquid-based infrastructure for transportation, cost of catalyst or metal, and difficulty producing enough pure H_2 over a long life cycle. The estimated cost of different hydrate technologies are illustrated in **Figure 2.8**

In 1999, Dyadin *et al.* could utilize differential thermal analysis (DTA) to prove that pure hydrogen clathrates synthesized at $\approx$ 15 kbar are of sII clathrate (CS-II). While they anticipated H_2/H_2O ratio (R) as high as 1/3 [178], Mao *et al.* characterized sII hydrogen clathrate *in situ* by different spectroscopic methods at 145 K and 1 atm and proved that R can be $\sim$ 1/2 [179]. Unlike Villard's rule $R \sim 1/6$ in which each cage can be only occupied by a single guest[23], those higher ratios prove multiple hydrogen occupancy in both small and large cages of sII. It has been estimated that a small (5^{12}) cage can hold two hydrogen molecules while the large ($5^{12}6^4$) cages can encapsulate 4 hydrogen molecules at high pressures. With such occupancy taken into account, the pure hydrogen clathrate can exhibit a hydrogen storage capacity of 5.3 wt% or 1.8 kW.h/kg [180, 181].

H_2-THF binary clathrates have been widely investigated as THF eases the thermodynamic requirement to acceptable ranges of 7-8 MPa. However, that extra stability was at the expense of a storage capacity that significantly dropped [70, 182]. Lee *et al.* suggested tuning the THF concentration to allow hydrogen molecules to be enclathrated in the large cages of sII without compromising the moderate P-T requirements. The systematic reduction of THF concentration from 5.56 mol% to 0.2 mol% resulted in a storage capacity increase from 2.09 to 4.03

wt% at 120 bar and 270 K [183]. However, tuning phenomena is controversial in the literature. While few studies could obtain tuned H_2-THF clathrates such as Sugahara *et al.* who modified the synthesis method at $\sim$ 70 MPa and 255 K [184], many other researchers reported that such results could not be reproduced and only $\sim$ 1.0 wt% hydrogen storage could be obtained regardless of the THF concentration [185–187]. Therefore, increasing the hydrogen clathrate gravimetric and volumetric capacity in feasible *P-T* conditions remains an open area for further research. Due to their relatively higher thermal stability compared to clathrate the the the the hydrates, semi-clathrate were also studied for hydrogen storage. However, they showed lower storage capacity compared to H_2-THF binary clathrates [188].
To solve those problems, the second generation of gaseous THP promoters has been proposed to exploit the hydrate structure storage potential in small and large cages. For instance, Park *et al.* showed that N_2 can allow hydrogen multiple occupancies in sII clathrate in the presence of THF and pyrrolidine (PRD) [189]. Similarly, SF_6 and CO_2 as promoters allowed hydrogen to be stored in large cages [190]. Another ambitious direction was to use light alkane (C_1-C_3) to form hydrogen clathrate with high calorific value at affordable formation and storage conditions. According to Mao *et al.*, such a combination is expected to fulfill the US Department of Energy (DOE) energy density targets [179]. Recently, our group used *ab initio* calculations to prove that CH_4 or CO_2 can play the role of thermodynamic promoter, allowing double occupancy of methane and hydrogen in $5^{12}6^2$ large cages of sI. This double occupancy has not only enhanced the hydrogen diffusion but also pushed sI binary H_2-CH_4 volumetric and gravimetric storage capacity to meet DOE requirements [191]. Those results agreed well with previous experimental observations [192]. It has been demonstrated that different H_2-CH_4 hydrates (sI and sII) could be synthesized by varying the thermodynamic conditions [193, 194]. PXRD and Raman spectroscopy analysis of those binary clathrates showed that either sI or sII could be obtained depending on (1) *P-T* conditions, (2)initial composition, and (3) hydrate synthesis time. Interestingly, the thermodynamic requirements of such hydrates were more relaxed compared to pure H_2 or even tuned H_2-THF hydrates[195].

Similarly, ethane has been reported to form binary clathrate with hydrogen. Theoretical calculations showed that $_2$-C_2H_6 can form both cubic structures (sI and sII) at 250 K with hydrogen storage capacity of 2.5wt%, and 3.5 wt%, respectively [196]. Ghaani *et al.* reported using propane as a co-guest with hydrogen that can also reduce the thermodynamic requirements [197]. Ahn *et al.* found that for H_2-CH_4-C_2H_6 system, multiple H_2 cage occupancies in all cages of hythane hydrates of sI and sII could be achieved via guest-exchange reaction. In that approach, a double hydrogen occupancy in small cages was obtained in the formed hydrate whether it is sI or sII [41]. More recently, Moon *et al.* optimized the hydrogen concentration needed to achieve the maximum possible hydrogen storage capacity in moderate thermodynamic conditions. However, despite those promising multiple hydrogen occupancies, the GC (Gas chromatography) results indicated that most of the hydrate cages to be filled either by

methane or ethane rather than hydrogen with a composition of (51.74:17.98:30.2) mol% for (CH_4:C_2H_6:H_2) in hydrate at the best case [198].

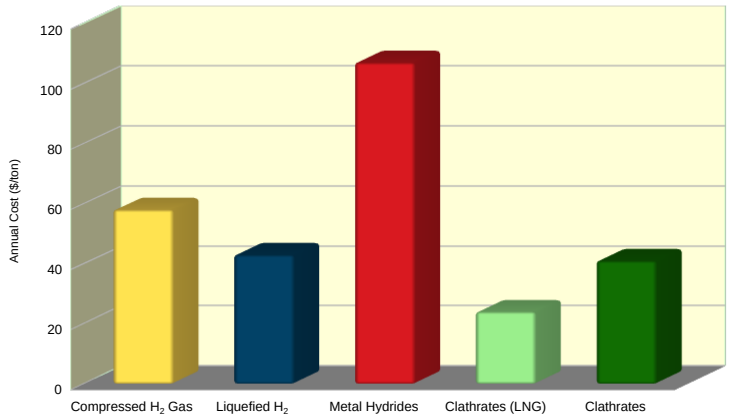

Figure 2.8: The estimated cost of different hydrogen storage technologies. Clathrate storage cost is assumed with a volumetric capacity of 3.03 wt% [199].

2.3.4 Other Hydrate-based Applications

There are many other hydrate-based applications for the energy transition as shown in **Figure 2.9**. In the *energy-water nexus*, water and energy are closely interlinked. While water can be considered as an energy source, energy is needed to transport or desalinate water. The latter is a big global challenge due to climate change and the intensive energy consumption for water desalination [200]. Thus, there is an urgent need to develop innovative technologies that can reduce such requirements and make use of waste heat from industrial sources. One clear example of that wasted energy is the cold energy of LNG re-gasification. The LNG received at the terminal at -162 °C is normally heated to 25 °C by employing seawater which is dumped back to the sea wasting the LNG cold energy. Such an amount of cold energy is huge as one tonne of LNG is estimated to require 214 kWh of cold energy removal [201]. One of the best options to utilize such wasted energy is hydrate-based desalination or (HyDesal). HyDesal work as stand-alone or in hybrid arrangement with other desalination technique to reduce the energy consumption and cost of the desalination process[30]. Such an approach can not only help to reduce the desalination energy requirements but also in GHGs capture. To illustrate, using proper hydrate former such as CH_4, CO_2, C_3H_8 at selected *P-T* range, water molecules form clathrate hydrate around gas molecules separating themselves from salty solution [23, 202]. For example, Babu *et al.* optimized the desalination conditions to reach $\sim$ 35% and salt rejection of $\sim$ 88 % for simulated seawater solution [203]. Although known from the 1940s, its commercialization faces some challenges related to reactor design to form and separate hydrate from salts and also the lack of commercial feasibility studies [202, 204].

There is increasing energy demand for space cooling along with climate change [47, 201].

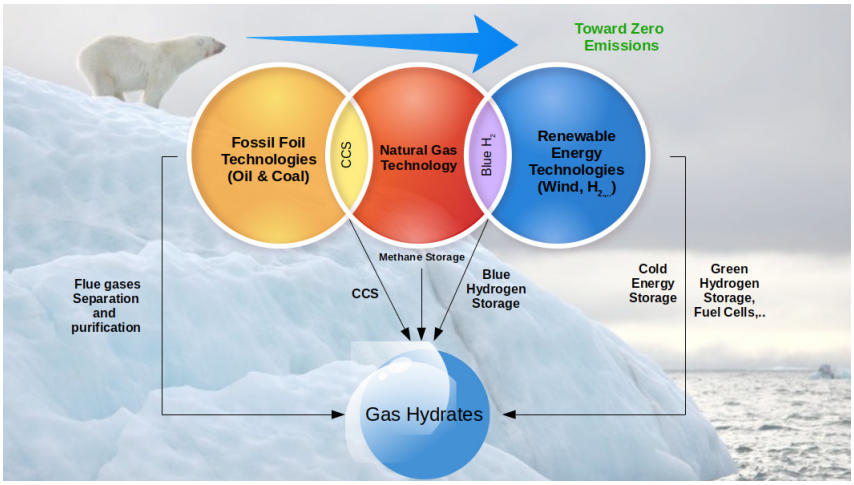

Figure 2.9: Schematic illustration of current and possible hydrate-based applications for energy transition.

Therefore, there is a growing demand to explore for the best phase change material (PCM) candidates that can efficiently take benefit of the cold energy released from the production sectors (e.g.energy from renewable sources, cheap off-peak electricity, oil and gas industry waste heat, and LNG regasification in terminals) for storage and transport applications. In that context, semi-clathrate hydrates (SCHs) are ideal candidates because of their suitable phase change temperature (5–27 °C), thermal stability (melting point can vary from -66 up to 31 °C), latent heat of fusion (190-220 kJ/kg) and relatively better heat transfer efficiency compared to clathrate hydrates [32, 205] which is suitable for various cooling requirements [206]. The process usually starts with cooling the system to form a hydrate, which is an exothermic process. The cold energy stored then could be consumed through depressurization or receiving heat from the external environment or a combination of both. CO_2 (or mixed CO_2-THF) hydrates were well-demonstrated for such an approach [207]. However, CO_2 is corrosive acid gas that will require expensive infrastructure. Although semi-clathrate hydrates can overcome those drawbacks, a more comprehensive economic assessment for the energy cycle is missing in the literature. Moreover, SCHs either in their acidic or basic ionic form showed exceptional thermal stability, ionic and proton conductivity. Such unique properties enable them to compete with solid electrolytes such as Nafion. More comprehensive research studies are highly desired to evaluate the unique physicochemical properties of such materials [32, 208, 209].

2.4 Engineering and Economic Challenges and Perspectives

Hydrate technologies for economic gas storage give promises due to the moderate production and storage condition and the ease of gas recovery compared to other means of energy storage and transportation [210]. Few studies targeted the life-cycle of NGH for transportation or mobile storage. For instance, Nogami and Oya showed that NGH is more economic in the medium

distance for 1000-6000 km distance compared to LNG, CNG, or PLG. However, for longer distances, LNG is still the optimum choice [211]. Furthermore, Nakai made a comprehensive life cycle assessment (LCA) for NGH for trucks and shipping purposes and concluded that it can reduce the cost by about 20% compared to the LNG plant of 1-1.5 MTPA (Million Tonnes per Annum)) [212]. Other cost analysis studies showed that NGH could reduce the capital cost by at least 25%-48% relative to LNG [86].

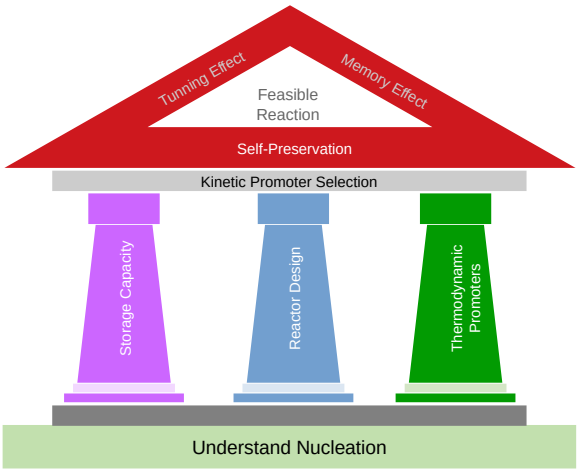

Figure 2.10: Future perspectives of hydrate research toward industrial application.

The recent sharp increases in natural gas and LNG prices due to the pandemic and recent geopolitical development revealed the need for long-term or static storage of methane especially from discrete and small gas resources (shale gas, biogas, flue gases) [90]. In that context, NGH showed a superior advantage over other technologies. In particular, it offers a high gravimetric and volumetric capacity of methane in a much controlled and safer manner compared to LNG or CNG. The safety of such a method is inherited from lower storage pressure (2-5 bar compared to 10 or MPa for CNG) and non-explosive nature due to the presence of water in excess. Economically, it can be feasible for static medium and long time storage with a relatively high storage temperature (-20°C compared to 162 °C) and less boil-off gas (BOG) re-compression requirements [88, 171]. Such unusual stability of methane clathrates even outside its zone of thermodynamic stability can be attributed to the hydrate self-preservation phenomenon [213]. For instance, an early study by Gudmundsson *et al.* showed that natural gas hydrates (92 mol% methane, 5 mol % ethane, and 3 mol% propane) can be stored in a deep freezer (-5 to -18°C) for 10 days at atmospheric pressure without significant loss of methane [214]. In a more recent study, Mimachi *et al.* showed that NGH pellets could successfully stored for 3 months at 253 K under atmospheric pressure [215]. Stability can be improved and storage can be extended for years in case of CH_4-THF sII clathrates [216] .However, this higher stability and longer storage period comes on the expense storage capacity that has been significantly reduced. To address that point, Takeya *et al.* suggested coating CH_4 hydrates with THF or cyclopentane (CP). In

case of cyclopentane-coated methane hydrate, the authors found that the hydrates remained stable for extended periods at a temperature higher than the equilibrium temperature and under atmospheric pressure[217].

Clathrate hydrates do not only reduce the cost compared to conventional storage for large-scale storage but also open the door for small and medium-size methane storage from discrete or remote resources. These resources such as shale gas, coal mine gas, offshore and onshore flue gases are not suitable for LNG which needs huge capital investment and tremendous reserves, and long-term contracts. It is important to stress here that NGH technology is complementary rather than competitive with existing technologies. In fact, NGH technology is best working in and hybrid mode due to their simple modular construction and operation which reduce the investment threshold by allowing to taking profit from the existing facilities and infrastructure [153].

In general, NGH processing technology consists of a formation step, followed by dewatering of non-converted water, cooling and depressurizing of excess gas, and finally pelletizing the hydrate for storage. While safety, storage conditions, and economics are the big advantage of NGH technology, the formation or synthesis step is the main engineering and economic obstacle that prevent the widespread of such technology [93, 211, 218]. The hydrate formation suffers from slow kinetics and severe operating condition, especially for pure methane (sI) [219]. To solve that problem, it is crucial to understand the nucleation process to shorten the induction time. The use of a carefully selected kinetic promoter (KHP) can reduce the lag time and the overall hydrate synthesis duration. In that aspect, the KHP should avoid the drawback of foaming without compromising the gas uptake. In addition to not being expensive, the selected KHP should be also eco-friendly and recyclable or degradable. The promising material in that aspect are nanoparticles [220], amino acids [221, 222], and porous materials at low concentrations [223]. The latter can be also used as the main storage medium allowing clathrates to grow inside pores at mild *P-T* conditions which is pretty similar to the THP effect [224]. Using liquid THP can reduce the hydrate formation requirements and increase the stability of formed hydrates [216]. However, the environmental impact of this promoter needs to be carefully assessed. If used in optimal concentrations, the use of those promoters can compromise between the reduced storage capacity and cooling requirement and hence minimize the overall process cost.

Recently, the use of gaseous THP such as light hydrocarbons (C_1-C_3) [225] showed promising results for both methane and blue hydrogen storage. Moreover, one the of the biggest advantages of hydrates is that they are insensitive to impurities. On the contrast, acid gases such as CO_2 and H_2S can also reduce the thermodynamic requirements of methane hydrate formation [226, 227]. For example, Gudmundsson *et al.* could store NGH of methane, ethane, and

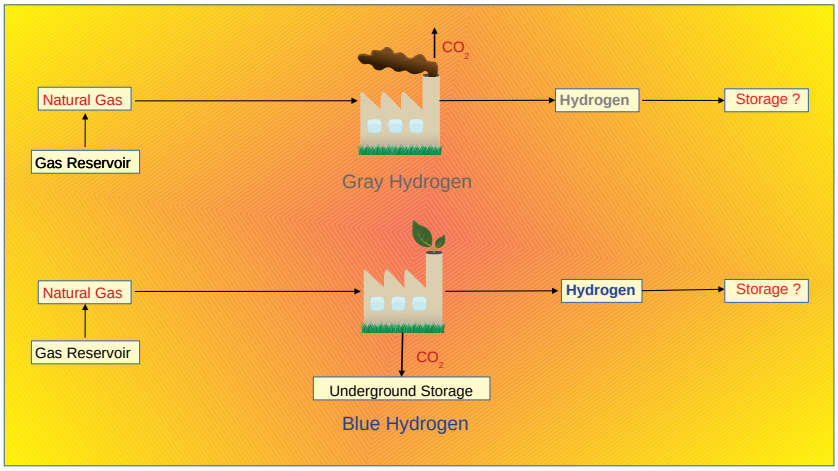

Figure 2.11: Schematic representation of gray and blue hydrogen.

propane in a normal deep freezer temprature (255.2-268.2 K) for 10 days under a pressure [214]. Overcoming the slow kinetic problem needs also innovative reactor design to enhance the gas-liquid contact, mass and heat transfer to the extent that industrial-scale application can be feasible. Current research studies in that direction, packed bed reactors [228], horizontal reactors with metallic packing [147] showed promising results. So to summarize, research perspectives for methane hydrate studies include but not limited to (1) understanding nucleation, self-preservation, structural transformation and memory phenomena, (2) proper selection of KHP, innovative (3) practical reactor design, (4) removal or optimization of THP , (5) explore the possibility of salty water and increasing pressure conditions toward the atmospheric pressure to improve the process economics and finally (6) perform detailed LCA studies.

In the case of carbon capture and sequestration (CCS), hydrate-based carbon capture and sequestration (HBCS) is a promising technique based on a simple process that is not affected by a pressure gradient, contaminants, and humidity. Moreover, the recovery or regeneration can be achieved simply by depressurization or thermal exchange at ambient conditions. This makes it energy-efficient and thus cost-effective carbon capture technology with estimated energy consumption below 0.60 kWh per ton CO_2 [153]. Although slow kinetics is still a problem, the thermodynamic requirements are much lower compared to NGH or hydrogen hydrates. Combining carbon capture and sequestration in a single process is a unique feature that favors HBCS over other carbon capture technologies. On the other hand, higher thermodynamic requirements are needed to maintain decent separation efficiency when the feed mixture has a lower CO_2 concentration. There are two possible solutions for that problem: (1) multistage HBCS and (2) hybrid hydrate CO_2 capture methods. The latter is more favored as it takes advantage of both HBCS and the conventional carbon capture method such as membrane or cryogenic separation to lower the energy requirements [229–231].

Safety and environment are priorities in the hydrogen storage process. In that aspect, hydrogen clathrate has a clear advantage over other physical and chemical storage methods. While storing hydrogen in solid clathrate is compact and needs relatively low storage pressure, storing hydrogen in reasonable amounts at its gaseous form needs a very large volume and/or high-pressure tanks which is a serious safety challenge. Moreover, it shows less CO_2 emission compared to other physical storage in both liquid and gas forms. Both economics studies show the net energy gain from hydrogen storage is competitive with chemical storage due to the less energy required to recover hydrogen [171]. On the other hand, hydrogen clathrate still faces many challenges. First and foremost, it needs very high thermodynamic requirements in terms of high pressure and low temperature. Such a challenge can be solved by blending hydrogen with natural gas to form "Hythane" in which hydrogen storage can be in a reasonable *P-T* range with multiple hydrogen cage occupancies [232]. However, further investigation is still needed to evaluate that approach especially in terms of kinetic studies and uncertainty of storage capacity.

As mentioned above for desalination, the use of wasted cold energy such as those of LNG

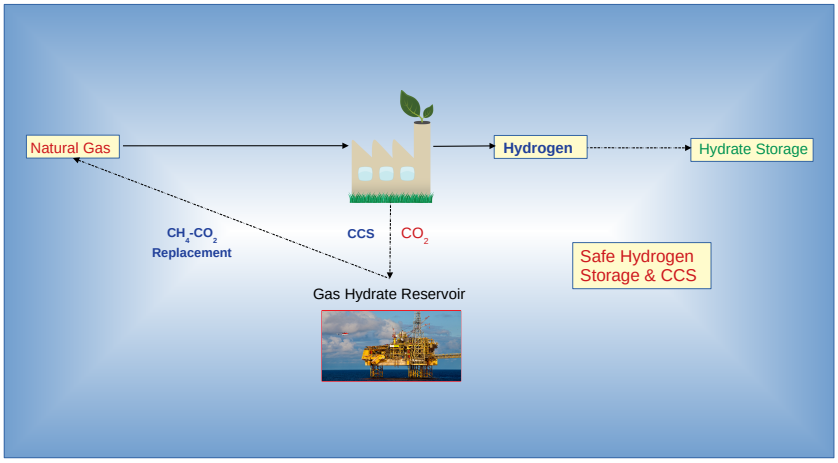

Figure 2.12: Schematic representation of possible hydrate-based blue hydrogen.

facilities can make hydrogen clathrates very competitive with the well-established hydrogen hydride or compressed hydrogen [233]. Currently, fuel cells and hydrogen hydride are the most common options for onboard hydrogen storage. While the first requires a low temperature as low as 200 K, the latter assumes a storage capacity of about 5.06 wt% hydrogen. These two conditions can be, at least theoretically, met by hydrogen clathrates [199]. However, overall cost estimates for onboard hydrogen clathrate are still needed for better evaluation. **Figure 2.10** summarizes future research areas required to enable the industrial application of gas hydrates for the energy transition.

One of the strong points of zeolitic ice technologies is their ability to be integrated with existing infrastructure and processes improving them toward greener energy transition. Having

already highlighted the role of gas hydrates for methane storage, CCS, and hydrogen storage above, one can suggest an integrated approach that can enhance the environmental feasibility of blue hydrogen production or hydrate-based blue hydrogen (HBBH). Natural gas (composed mainly of methane) is currently the primary source of hydrogen production through catalytic reactions. It is estimated that 75% of the globally produced methane is utilized for hydrogen production via processes such as steam reforming (SRM) [234] or dry reforming (DRM) [5]. Currently, the state of art hydrogen production is "gray hydrogen" which comes from steam methane reforming (SMR). Green hydrogen which refers to the hydrogen produced from clean renewable energy sources still has not had enough supply or competitive cost compared to gray hydrogen despite the rapid decrease of renewables costs[235]. To overcome the problem of GHG emissions coming from gray hydrogen, an increasing number of researchers promoted the idea of "blue hydrogen" as shown in **Figure 2.11**. The relatively new concept adds CCS to the SMR process and used to be described zero or low GHG emission technology[236]. A common gap in those 3 hydrogen production approaches (green,gray and blue), the three technologies lack a clear method for safe hydrogen storage. Such a gap is very important as it can be the bottleneck for the hydrogen economy.

To illustrate, Dawood **et al.** proposed that, in addition to production and utilization, safety and

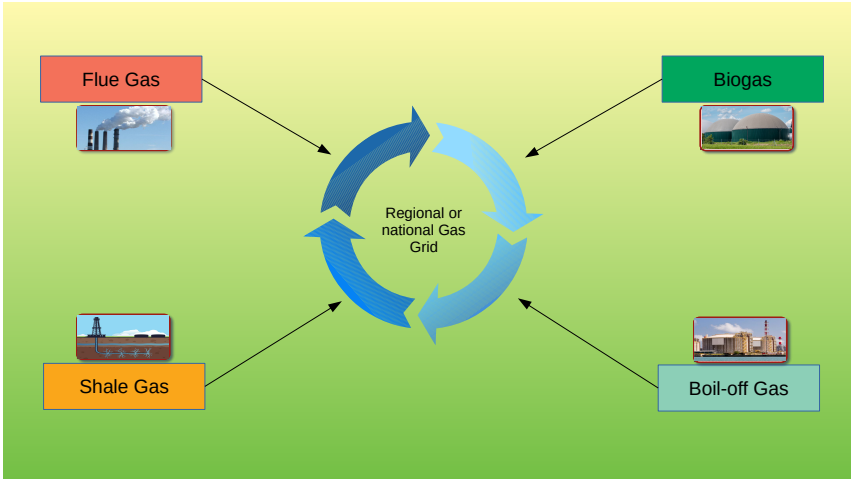

Figure 2.13: Gas Hydrate can make use of discrete gas resources by lowering the investment barrier.

storage are two important corners for hydrogen-based energy systems [237]. Although blue hydrogen technology is claimed to have a good balance between economic feasibility and GHG emissions, the steps of CO_2 capture and sequestration are two independent sub-processes. In addition, the storage is described to be in geological structures such as a saline aquifer with 800 m depth. However, a recent complete LCA by Howarth & Jacobson showed that blue hydrogen reduces carbon dioxide emission by only 9-12% less than gray hydrogen. The reason behind that is the lower amount of carbon dioxide emissions are compensated by fugitive methane emissions due to the use of natural gas to power for the carbon capture. For heating purposes, it has been found that the greenhouse gas footprint of blue hydrogen is 20% greater than natural

gas or coal [238]. A major part of those drawbacks can be avoided if hydrates are utilized for methane and CO_2 capture and sequestration in addition to hydrogen storage as shown in **Figure 2.12**. In principle, CO_2 storage can be used to recover natural gas with a double benefit of energy recovery and CCS. Resistant to contaminants, clathrate hydrates can be used to capture flue gas and fugitive methane emissions at a reasonable cost.

Finally, this review demonstrated the potential of HBT integration with existing processes for the efficient energy transition. Being flexible and implementable at a low cost, HBTs can facilitate large scale gas transportation and storage. Moreover, they can provide lower entrance barriers to utilize remote and discrete energy sources which are not feasible to transport through other gas transportation means as illustrated at **Figure 2.13**. In analogy to CCS, clathrate hydrates can be also used for methane and other GHGs capture and sequestration. Last but not least, they can be used to safely store hydrogen at a lower cost.

2.5 Conclusions

This review sheds light on increasing research interest for hydrate-based technologies (HBTs) in various fields related to energy transition and decarbonization. The main properties of hydrate (both clathrates and semi-clathrates) have been introduced to show their uniqueness and potential for industrial applications. First, we showed the advantages of NGH for methane storage and benchmarked them with existing technologies such as PLG, CNG, and LNG. NGH is suitable for medium-distance transportation, both small and large volume stationary methane storage, especially for long time storage. We concluded that NGH technology is very flexible and can be utilized in synergy with other existing methane storage technology which enables us to make use of the current infrastructure. Hydrates can also be an interesting opportunity for CCS with HBCS combining both carbon capture and sequestration in a single step. Moreover, that technique can be used for methane recovery as we showed in the CH_4-CO_2 replacement process. Then, we introduced hydrogen clathrate as a compact, safe, and environmentally benign option with a great potential for static hydrogen storage.
We have also shown the role of clathrate in the energy-water nexus with applications such as desalination. We also addressed the engineering and economic challenges that hinder the industrial application of HBTs. In our opinion, future research should focus on improving heat and mass transfer via reactor design, optimum selection and concentration of kinetic and thermodynamic hydrate promoters, and possible hybrid HBTs. Above all, detailed life-cycle economic studies will help evaluate those proposed solutions. Finally, we presented some conceptual examples of possible hydrate technology integration into the existing energy processes to enhance their performance. Presenting the current status of research, major challenges, and proposed solutions, we hope this review will attract scientists and enterprises' attention to that exciting field to reach the energy transition and low carbon economy.

References

[1] Tanay Sıdkı Uyar. *Accelerating the Transition to a 100% Renewable Energy Era*, volume 74. 2020.

[2] Xavier Garcia-Casals, Rabia Ferroukhi, and Bishal Parajuli. Measuring the socio-economic footprint of the energy transition. *Energy Transitions*, 3(1-2):105–118, 2019.

[3] C Gürsan and V. de Gooyert. The systemic impact of a transition fuel: Does natural gas help or hinder the energy transition? *Renew. Sustain. Energy Rev.*, 138(March 2020):110552, 2021.

[4] Eleanor Stephenson, Alexander Doukas, and Karena Shaw. "Greenwashing gas: Might a 'transition fuel' label legitimize carbon-intensive natural gas development?". *Energy Policy*, 46(2012):452–459, 2012.

[5] Ahmed Omran, Sun Hee Yoon, Murtaza Khan, Minhaj Ghouri, Anjaneyulu Chatla, and Nimir Elbashir. Mechanistic insights for dry reforming of methane on Cu/Ni bimetallic catalysts: DFT-assisted microkinetic analysis for coke resistance. *Catalysts*, 10(9):1–16, 2020.

[6] R. M. Barrer and W. I. Stuart. Non-stoicheiometric clathrate compounds of water. *Proc. R. Soc. London. Ser. A. Math. Phys. Sci.*, pages 172–189, 1957.

[7] Herib Blanco and André Faaij. A review at the role of storage in energy systems with a focus on Power to Gas and long-term storage. *Renew. Sustain. Energy Rev.*, 81(May 2017):1049–1086, 2018.

[8] Lars Peters, A. Hussain, M. Follmann, T. Melin, and M. B. Hägg. CO 2 removal from natural gas by employing amine absorption and membrane technology-A technical and economical analysis. *Chem. Eng. J.*, 172(2-3):952–960, 2011.

[9] Hazzim F. Abbas and W. M.A. Wan Daud. Hydrogen production by methane decomposition: A review. *Int. J. Hydrogen Energy*, 35(3):1160–1190, feb 2010.

[10] Suman Dutta. A review on production, storage of hydrogen and its utilization as an energy resource. *J. Ind. Eng. Chem.*, 20(4):1148–1156, 2014.

[11] Pramod Warrier and Carolyn A. Koh. Structure-Property-Comparisons of Clathrasils and Gas Hydrates. *Trans. Indian Inst. Met.*, 72(8):2229–2237, 2019.

[12] Koichi Momma. Clathrate compounds of silica. *J. Phys. Condens. Matter*, 26(10):103203, 2014.

[13] Juli Anna Dolyniuk, Bryan Owens-Baird, Jian Wang, Julia V. Zaikina, and Kirill Kovnir. Clathrate thermoelectrics. *Mater. Sci. Eng. R Reports*, 108:1–46, 2016.

[14] J. H. Van Der Waals. The statistical mechanics of clathrate compounds. *Trans. Faraday Soc.*, 52:184–193, 1956.

[15] J. H. van der Waals and J. C. Platteeuw. Clathrate solutions. In I. Prigogine, editor, *Adv. Chem. Phys.*, volume II, pages 1–57. John Wiley & Sons. Inc., 1958.

[16] Lovat V. C. Rees. Richard Maling Barrer. 16 June 1910–12 September 1996. *Biogr. Mem. Fellows R. Soc.*, 44:37–49, 1998.

[17] R. M. Barrer and D J Ruzicka. Non-stoichiometric clathrate compounds of water. Part 2. Formation and properties of double hydrates. *Trans. Faraday Soc.*, 58:2239–2252, 1962.

[18] R. M. Barrer and D J Ruzicka. Non-stoichiometric clathrate compounds of water. Part 3.-Inclusion Energies and Constants in the small Cavities of Structure I1 BY. *Trans. Faraday Soc.*, 58:2253–2261, 1962.

[19] R. M. Barrer and D. J. Ruzicka. Non-stoichiometric clathrate compounds of water. Part 4. - Kinetics of formation of clathrate phases. *Trans. Faraday Soc.*, 58:2262–2271, 1962.

[20] R M Barrer. Zeolite inclusion complexes. *J. Incl. Phenom.*, 1(2):105–123, 1983.

[21] Svetlana Mintova, Jean Pierre Gilson, and Valentin Valtchev. Advances in nanosized zeolites. *Nanoscale*, 5(15):6693–6703, 2013.

[22] Jinfu Shu, Xiaojia Chen, I. Ming Chou, Wenge Yang, Jingzhu Hu, Russell J. Hemley, and Ho Kwang Mao. Structural stability of methane hydrate at high pressures. *Geosci. Front.*, 2(1):93–100, 2011.

[23] E. Dendy Sloan and Carolyn Ann Koh. *Clathrate hydrates of natural gases, thrid edition*. CRC Press, third edition, 2007.

[24] Yu A. Dyadin, I. S. Terekhova, T. V. Rodionova, and D. V. Soldatov. Half-century history of clathrate chemistry. *J. Struct. Chem.*, 40(5):645–653, 1999.

[25] Xiangfang Li, Wenyuan Liu, Shujie Liu, Jinqiu Hu, Yufeng Nan, Tian Tian, and Yunjian Zhou. A prevention and control method for natural gas hydrate in pipe strings during deepwater gas well production tests. *Nat. Gas Ind. B*, 7(1):82–92, 2020.

[26] Seokyoon Moon, Sujin Hong, Yunseok Lee, Jae S. Lee, Yun Ho Ahn, and Youngjune Park. Enhancing Hydrogen Cluster Storage in Clathrate Hydrates via Defect-Mediated Lattice Engineering. *J. Phys. Chem. C*, 2021.

[27] Ali Eslamimanesh, Amir H Mohammadi, Dominique Richon, Paramespri Naidoo, and Deresh Ramjugernath. Application of gas hydrate formation in separation processes: A review of experimental studies. *J. Chem. Thermodyn.*, 46:62–71, 2012.

[28] Gyeol Ko, Joonseop Lee, and Yongwon Seo. Separation efficiency and equilibrium recovery ratio of SF6 in hydrate-based greenhouse gas separation. *Chem. Eng. J.*, 405(September 2020):126956, 2021.

[29] Wonjung Choi, Woojin Go, Yohan Lee, Junghoon Mok, and Yongwon Seo. Mechanism and kinetics of guest exchange in sII hydrate – Flue gas replacement as revealed by experimental and computational approaches for hydrocarbon recovery and CO2 sequestration. *Chem. Eng. J.*, (October):128119, 2020.

[30] Sang Hyun Lee and Kyungtae Park. Conceptual design and economic analysis of a novel cogeneration desalination process using LNG based on clathrate hydrate. *Desalination*, 498(114703):1–16, 2021.

[31] Ponnivalavan Babu, Chandradeep Bollineni, and Nagu Daraboina. Energy Analysis of Methane-Hydrate-Based Produced Water Desalination. *Energy and Fuels*, 35(3):2514–2519, 2021.

[32] Kyuchul Shin, Jong Ho Cha, Yongwon Seo, and Huen Lee. Physicochemical properties of ionic clathrate hydrates. *Chem. - An Asian J.*, 5(1):22–34, 2010.

[33] Timothy A. Strobel, Yongkwan Kim, Gary S. Andrews, Jack R. Ferrell, Carolyn A. Koh, Andrew M. Herring, and E. Dendy Sloan. Chemical-clathrate hybrid hydrogen storage: Storage in both guest and host. *J. Am. Chem. Soc.*, 130(45):14975–14977, 2008.

[34] Kyuchul Shin, Konstantin A. Udachin, Igor L. Moudrakovski, Donald M. Leek, Saman Alavi, Christopher I. Ratcliffe, and John A. Ripmeester. Methanol incorporation in clathrate hydrates and the implications for oil and gas pipeline flow assurance and icy planetary bodies. *Proc. Natl. Acad. Sci. U. S. A.*, 110(21):8437–8442, 2013.

[35] Timothy A et al Minshull. Hydrate occurrence in Europe :A review of available evidence. *Mar. Pet. Geol.*, 111:2735–2764, 2020.

[36] Roy Andrew Partain and Constantinos Yiallourides. Hydrate occurrence in Europe: Risks, rewards, and legal frameworks. *Mar. Policy*, 121(104122):1–10, 2020.

[37] Mark Maslin, Matthew Owen, Simon Day, and David Long. Linking continental-slope failures and climate change: Testing the clathrate gun hypothesis. *Geology*, 32(1):53–56, 2004.

[38] Nikolaus Froitzheim, Jaroslaw Majka, and Dmitry Zastrozhnov. Methane release from carbonate rock formations in the Siberian permafrost area during and after the 2020 heat wave. *Proc. Natl. Acad. Sci. U. S. A.*, 118(32):2020–2022, 2021.

[39] E Dendy Sloan. Gas hydrates: Review of physical/chemical properties. *Energy and Fuels*, 12(2):191–196, 1998.

[40] A Drobyshev, A Aldiyarov, V Kurnosov, K Katpaeva, E Korshikov, D Sokolov, A Shinbayeva, and A Timchenko. Physical modeling of the formation of clathrate hydrates of methane. *Low Temp. Phys.*, 41(6):429–434, 2015.

[41] Yun Ho Ahn, Seokyoon Moon, Dong Yeun Koh, Sujin Hong, Huen Lee, Jae W. Lee, and Youngjune Park. One-step formation of hydrogen clusters in clathrate hydrates stabilized via natural gas blending. *Energy Storage Mater.*, 24(March 2019):655–661, 2020.

[42] Salvatore F. Cannone, Andrea Lanzini, and Massimo Santarelli. A Review on CO2 Capture Technologies with Focus on CO2-Enhanced Methane Recovery from Hydrates. *Energies*, 14(2):387, 2021.

[43] Xuemei Lang, Caijuan Zheng, Shuanshi Fan, Yanhong Wang, Gang Li, Shenglong Wang, and Chi Yu. "Similar self-preservation" and decomposition kinetics of tetrahydrofuran-hydrogen hydrate particles. *Int. J. Hydrogen Energy*, 47(13):8457–8466, 2022.

[44] John A. Ripmeester and Saman Alavi. Some current challenges in clathrate hydrate science: Nucleation, decomposition and the memory effect. *Curr. Opin. Solid State Mater. Sci.*, 20(6):344–351, 2016.

[45] Ioannis N. Tsimpanogiannis and Ioannis G. Economou. Monte Carlo simulation studies of clathrate hydrates: A review. *J. Supercrit. Fluids*, 134(December 2017):51–60, 2018.

[46] Fernando De Azevedo Medeiros, Iuri Soter Viana Segtovich, Frederico Wanderley Tavares, and Amadeu K. Sum. Sixty Years of the van der Waals and Platteeuw Model for Clathrate Hydrates - A Critical Review from Its Statistical Thermodynamic Basis to Its Extensions and Applications. *Chem. Rev.*, 120(24):13349–13381, 2020.

[47] Zhenyuan Yin, Junjie Zheng, Hyunho Kim, Yutaek Seo, and Praveen Linga. Hydrates for cold energy storage and transport: A review. *Adv. Appl. Energy*, 2(March):100022, 2021.

[48] J. O. Abe, A. P.I. Popoola, E. Ajenifuja, and O. M. Popoola. Hydrogen energy, economy and storage: Review and recommendation. *Int. J. Hydrogen Energy*, 44(29):15072–15086, 2019.

[49] Mohammad Reza Ghaani, Judith M. Schicks, and Niall J. English. A review of reactor designs for hydrogen storage in clathrate hydrates. *Appl. Sci.*, 11(2):1–16, 2021.

[50] Aliakbar Hassanpouryouzband, Edris Joonaki, Mehrdad Vasheghani Farahani, Satoshi Takeya, Carolyn Ruppel, Jinhai Yang, Niall J. English, Judith M. Schicks, Katriona Edlmann, Hadi Mehrabian, Zachary M. Aman, and Bahman Tohidi. Gas hydrates in sustainable chemistry. *Chem. Soc. Rev.*, 49(15):5225–5309, 2020.

[51] Y.F Makogon. *Hydrates of Hydrocarbons*. Pennwell Publishing Co., 1997.

[52] Seungmin Lee, Sungwon Park, Youngjun Lee, and Yongwon Seo. Thermodynamic and 13C NMR spectroscopic verification of methane-carbon dioxide replacement in natural gas hydrates. *Chem. Eng. J.*, 225:636–640, 2013.

[53] Jong Won Lee, Jonghyub Lee, and Seong Pil Kang. 13C NMR spectroscopies and formation kinetics of gas hydrates in the presence of monoethylene glycol as an inhibitor. *Chem. Eng. Sci.*, 104:755–759, 2013.

[54] Satoshi Takeya, Konstantin A Udachin, Igor L Moudrakovski, Robin Susilo, and John A Ripmeester. Direct space methods for powder X-ray diffraction for guest-host materials: Applications to cage occupancies and guest distributions in clathrate hydrates. *J. Am. Chem. Soc.*, 132(2):524–531, 2010.

[55] Byeonggwan Lee, Kyuchul Shin, Sanehiro Muromachi, Igor L. Moudrakovski, Christopher I. Ratcliffe, and John A. Ripmeester. Enhanced methane storage in clathrate hydrates induced by antifreezes. *Chem. Eng. J.*, 418(January):129304, 2021.

[56] Amadeu K. Sum, Robert C. Burruss, and E. Dendy Sloan. Measurement of clathrate hydrates via Raman spectroscopy. *J. Phys. Chem. B*, 101(38):7371–7377, 1997.

[57] Davi Éber Sanches de Menezes, Amadeu K Sum, Arnaud Desmedt, Pedro de Alcântara Pessôa Filho, and Maria Dolores Robustillo Fuentes. Coexistence of sI and sII in methane-propane hydrate former systems at high pressures. *Chem. Eng. Sci.*, 208(115149):1–11, 2019.

[58] Michael T. Kirchner, Roland Boese, W. Edward Billups, and Lewis R. Norman. Gas hydrate single-crystal structure analyses. *J. Am. Chem. Soc.*, 126(30):9407–9412, 2004.

[59] Konstantin A. Udachin, Christopher I. Ratcliffe, and John A. Ripmeester. Single crystal diffraction studies of structure I, II and H hydrates: Structure, cage occupancy andf composition. *J. Supramol. Chem.*, 2(4-5):405–408, 2002.

[60] Yingying Huang, Keyao Li, Xue Jiang, Yan Su, Xiaoxiao Cao, and Jijun Zhao. Phase Diagram of Methane Hydrates and Discovery of MH-VI Hydrate. *J. Phys. Chem. A*, 122(28):6007–6013, 2018.

[61] Xiaoxiao Cao, Yingying Huang, Xue Jiang, Yan Su, and Jijun Zhao. Phase diagram of water-methane by first-principles thermodynamics: Discovery of MH-IV and MH-V hydrates. *Phys. Chem. Chem. Phys.*, 19(24):15996–16002, 2017.

[62] J. S. Loveday, R. J. Nelmes, M. Guthrie, D. D. Klug, and J. S. Tse. Transition from cage clathrate to filled ice: The structure of methane hydrate III. *Phys. Rev. Lett.*, 87(21):215501–1–215501–4, 2001.

[63] M von Stackelberg and W Meinhold. Feste Gashydrate III. Mischhydrate. *Zeitschrift für Elektrochemie*, 58:40–45, 1954.

[64] Ravi Radhakrishnan and Bernhardt L. Trout. A new approach for studying nucleation phenomena using molecular simulations: Application to CO2 hydrate clathrates. *J. Chem. Phys.*, 117(4):1786–1796, 2002.

[65] Qiao Shi, Pinqiang Cao, Zhengde Han, Fulong Ning, Hao Gong, Yue Xin, Zhisen Zhang, and Jianyang Wu. Role of Guest Molecules in the Mechanical Properties of Clathrate Hydrates. *Cryst. Growth Des.*, 18(11):6729–6741, 2018.

[66] M. V. Stackelberg and H. R. Müller. On the structure of gas hydrates. *J. Chem. Phys.*, 19(10):1319–1320, 1951.

[67] Thomas C. W. Mak and Richard K. McMullan. Polyhedral Clathrate Hydrates. X. Structure of the Double Hydrate of Tetrahydrofuran and Hydrogen Sulfide. *J. Chem. Phys.*, 42(8):2732–2737, 1965.

[68] John A. Ripmeester, John S. Tse, Christopher I. Ratcliffe, and Brian M. Powell. A new clathrate hydrate structure. *Nature*, 325:135–136, 1987.

[69] Claire Petuya, Françoise Damay, Bertrand Chazallon, Jean Luc Bruneel, and Arnaud Desmedt. Guest Partitioning and Metastability of the Nitrogen Gas Hydrate. *J. Phys. Chem. C*, 122(1):566–573, 2018.

[70] Ali Rasoolzadeh and Alireza Shariati. Hydrogen hydrate cage occupancy: A key parameter for hydrogen storage and transport. *Fluid Phase Equilib.*, 494:8–20, 2019.

[71] Andrzej Falenty, Thomas C. Hansen, and Werner F. Kuhs. Formation and properties of ice XVI obtained by emptying a type sII clathrate hydrate. *Nature*, 516(7530):231–233, 2014.

[72] Louw J. Florusse, Cor J. Peters, Joop Schoonman, Keith C. Hester, Carolyn A. Koh, Steven F. Dec, Kenneth N. Marsh, and E. Dendy Sloan. Stable low-pressure hydrogen clusters stored in a binary clathrate hydrate. *Science (80-.).*, 306(5695):469–471, 2004.

[73] Yasushi Kamata, Yukiyasu Yamakoshi, Takao Ebinuma, Hiroyuki Oyama, Wataru Shimada, and Hideo Narita. Hydrogen sulfide separation using tetra-n-butyl ammonium bromide semi-clathrate (TBAB) hydrate. *Energy and Fuels*, 19(4):1717–1722, 2005.

[74] Sanehiro Muromachi. CO2 capture properties of semiclathrate hydrates formed with tetra-n-butylammonium and tetra-n-butylphosphonium salts from H2 + CO2 mixed gas. *Energy*, 223:120015, 2021.

[75] Antonin Chapoy, Ross Anderson, and Bahman Tohidi. Low-pressure molecular hydrogen storage in semi-clathrate hydrates of quaternary ammonium compounds. *J. Am. Chem. Soc.*, 129(4):746–747, 2007.

[76] Ali Davoodabadi, Ashkan Mahmoudi, and Hadi Ghasemi. The potential of hydrogen hydrate as a future hydrogen storage medium. *iScience*, 24(1):101907, 2021.

[77] Dietrich Mootz, Ernst josef Oellers, and Michael Wiebcke. First Examples of Type I Clathrate Hydrates of Strong Acids: Polyhydrates of Hexafluorophosphoric, Tetrafluoroboric, and Perchloric Acid. *J. Am. Chem. Soc.*, 109(4):1200–1202, 1987.

[78] Jong Ho Cha, Kyuchul Shin, Sukjeong Choi, Sangyong Lee, and Huen Lee. Maximized proton conductivity of the HPF6 clathrate hydrate by structural transformation. *J. Phys. Chem. C*, 112(35):13332–13335, 2008.

[79] Dyadin, Yu A. and K. A. Udachin. Clathrate polyhydrates of peralkylonium salts and their analogs. *J. Struct. Chem.*, 28(44):394–432, 1987.

[80] Sungwon Park, Seungmin Lee, Youngjun Lee, and Yongwon Seo. CO2 capture from simulated fuel gas mixtures using semiclathrate hydrates formed by quaternary ammonium salts. *Environ. Sci. Technol.*, 47(13):7571–7577, 2013.

[81] Wataru Shimada, Takao Ebinuma, Hiroyuki Oyama, Yasushi Kamata, Satoshi Takeya, Tsutomu Uchida, Jiro Nagao, and Hideo Narita. Separation of gas molecule using tetra-n-butyl ammonium bromide semi-clathrate hydrate crystals. *Japanese J. Appl. Physics, Part 2 Lett.*, 42(2 A):2–5, 2003.

[82] Wataru Shimada, Motoo Shiro, Hidemasa Kondo, Satoshi Takeya, Hiroyuki Oyama, Takao Ebinuma, and Hideo Marita. Tetra-n-butylammonium bromide-water (1/38). *Acta Crystallogr. Sect. C Cryst. Struct. Commun.*, 61(2):65–66, 2005.

[83] Qiang Sun, Jinzhao Zhang, Yang Luo, Xuqiang Guo, and Aixian Liu. Separation of methane-ethylene via forming semi-clathrate hydrates with TBAB. *J. Nat. Gas Sci. Eng.*, 34:265–268, 2016.

[84] Carl-friedrich Schleussner, Joeri Rogelj, Michiel Schaeffer, Tabea Lissner, Rachel Licker, Erich M Fischer, Reto Knutti, Anders Levermann, Katja Frieler, and William Hare. Science and policy characteristics of the Paris Agreement temperature goal. *Nat. Publ. Gr.*, (July), 2016.

[85] Hideaki Kobayashi, Akihiro Hayakawa, K. D.Kunkuma A. Somarathne, and Ekenechukwu C. Okafor. Science and technology of ammonia combustion. *Proc. Combust. Inst.*, 37(1):109–133, 2019.

[86] Hari Prakash Veluswamy, Asheesh Kumar, Yutaek Seo, Ju Dong Lee, and Praveen Linga. A review of solidified natural gas (SNG) technology for gas storage via clathrate hydrates. *Appl. Energy*, 216(February):262–285, 2018.

[87] B. P. Prajwal and K. G. Ayappa. Evaluating methane storage targets: From powder samples to onboard storage systems. *Adsorption*, 20(5-6):769–776, 2014.

[88] Laura A. Pellegrini, Stefania Moioli, Fabio Brignoli, and Camilla Bellini. LNG technology: The weathering in above-ground storage tanks. *Ind. Eng. Chem. Res.*, 53(10):3931–3937, 2014.

[89] Younggy Shin and Yoon Pyo Lee. Design of a boil-off natural gas reliquefaction control system for LNG carriers. *Appl. Energy*, 86(1):37–44, 2009.

[90] Matúš Mišík. The EU needs to improve its external energy security. *Energy Policy*, 165(April), 2022.

[91] Yang Peng, Vaiva Krungleviciute, Ibrahim Eryazici, Joseph T. Hupp, Omar K. Farha, and Taner Yildirim. Methane storage in metal-organic frameworks: Current records, surprise findings, and challenges. *J. Am. Chem. Soc.*, 135(32):11887–11894, 2013.

[92] Eyas Mahmoud, Labeeb Ali, Asmaa El Sayah, Sara Awni Alkhatib, Hend Abdulsalam, Mouza Juma, and Ala'A H Al-Muhtaseb. Implementing metal-organic frameworks for natural gas storage. *Crystals*, 9(8):1–19, 2019.

[93] H. Kanda. Economic study on natural gas transportation with natural gas hydrate (NGH) pellets. *Int. Gas Union World Gas Conf. Pap.*, 4:1990–2000, 2006.

[94] Behzad Partoon and Jafar Javanmardi. Effect of Mixed Thermodynamic and Kinetic Hydrate Promoters on Methane Hydrate Phase Boundary and Formation Kinetics. *J. Chem. Eng. Data*, 58:501–509, 2013.

[95] Zhen Pan, Yi Wu, Liyan Shang, Li Zhou, and Zhien Zhang. Progress in use of surfactant in nearly static conditions in natural gas hydrate formation. *Front. Energy*, 14(3):463–481, 2020.

[96] Niall J English and J M D MacElroy. Perspectives on molecular simulation of clathrate hydrates: Progress, prospects and challenges. *Chem. Eng. Sci.*, 121:133–156, 2015.

[97] Sebastien Bergeron, Juan G. Beltrán, and Phillip Servio. Reaction rate constant of methane clathrate formation. *Fuel*, 89(2):294–301, 2010.

[98] Hari Prakash Veluswamy and Praveen Linga. Macroscopic kinetics of hydrate formation of mixed hydrates of hydrogen/tetrahydrofuran for hydrogen storage. *Int. J. Hydrogen Energy*, 38(11):4587–4596, 2013.

[99] Hari Prakash Veluswamy, Gaurav Bhattacharjee, Junxiong Liao, and Praveen Linga. Macroscopic kinetic investigations on mixed natural gas hydrate formation for gas storage application. *Energy and Fuels*, 34(12):15257–15269, 2020.

[100] Kazuya Ozawa and Ryo Ohmura. Crystal Growth of Clathrate Hydrate with Methane plus Partially Water Soluble Large-Molecule Guest Compound. *Cryst. Growth Des.*, 19(3):1689–1694, 2019.

[101] Craig J. Taylor, Kelly T. Miller, Carolyn A. Koh, and E. Dendy Sloan. Macroscopic investigation of hydrate film growth at the hydrocarbon/water interface. *Chem. Eng. Sci.*, 62(23):6524–6533, 2007.

[102] A. Vysniauskas and P. R. Bishnoi. A kinetic study of methane hydrate formation. *Chem. Eng. Sci.*, 38(7):1061–1072, 1983.

[103] Y.F. Makogon. *Hydrates of Natural Gas*. PennWell Books Tulsa, Oklahoma, 1981.

[104] John A Ripmeester and Saman Alavi. Some current challenges in clathrate hydrate science: Nucleation, decomposition and the memory effect. *Curr. Opin. Solid State Mater. Sci.*, (20):344–351, 2016.

[105] P. Englezos, N. Kalogerakis, P. D. Dholabhai, and P. R. Bishnoi. Kinetics of gas hydrate formation from mixtures of methane and ethane. *Chem. Eng. Sci.*, 42(11):2659–2666, 1987.

[106] S. S. Kim, H. C., Bishnoi, P. R., Heidemann, R. A., Rizvi. Kinetics of methane hydrate decomposition. *Chem. Eng. Sci.*, 42(7):1645–1653, 1987.

[107] M. Z. Faizullin, A. V. Vinogradov, and V. P. Koverda. Formation of clathrate hydrates under crystallization of gas-saturated amorphous ice. *Int. J. Heat Mass Transf.*, 65:649–654, 2013.

[108] Qazi Nasir, Humbul Suleman, and Yasir A. Elsheikh. A review on the role and impact of various additives as promoters/ inhibitors for gas hydrate formation. *J. Nat. Gas Sci. Eng.*, 76(December 2019):103211, 2020.

[109] Hesam Najibi, Morteza Mirzaee Shayegan, and Hassan Heidary. Experimental investigation of methane hydrate formation in the presence of copper oxide nanoparticles and SDS. *J. Nat. Gas Sci. Eng.*, 23:315–323, 2015.

[110] Zhen Pan, Zhiming Liu, Zhien Zhang, Liyan Shang, and Shihui Ma. Effect of silica sand size and saturation on methane hydrate formation in the presence of SDS. *J. Nat. Gas Sci. Eng.*, 56(February):266–280, 2018.

[111] Xiao-Yan Deng, Ying Yang, Dong-Liang Zhong, Xi-Yue Li, Bin-Bin Ge, and Jin Yan. New Insights into the Kinetics and Morphology of CO 2 Hydrate Formation in the Presence of Sodium Dodecyl Sulfate . *Energy & Fuels*, 35(17):13877–13888, 2021.

[112] Y. Zhong and R. E. Rogers. Surfactant effects on gas hydrate formation. *Chem. Eng. Sci.*, 55(19):4175–4187, 2000.

[113] Naoki Ando, Yui Kuwabara, and Yasuhiko H. Mori. Surfactant effects on hydrate formation in an unstirred gas/liquid system: An experimental study using methane and micelle-forming surfactants. *Chem. Eng. Sci.*, 73:79–85, 2012.

[114] Jianwei Du, Huijuan Li, and Liguang Wang. Effects of ionic surfactants on methane hydrate formation kinetics in a static system. *Adv. Powder Technol.*, 25(4):1227–1233, 2014.

[115] J. S. Zhang, Sangyong Lee, and Jae W. Lee. Kinetics of methane hydrate formation from SDS solution. *Ind. Eng. Chem. Res.*, 46(19):6353–6359, 2007.

[116] Young Ah Kwon, Jong Mok Park, Kwang Eun Jeong, Chul Ung Kim, Tae Wan Kim, Ho Jeong Chae, Soon Yong Jeong, Jin Heong Yim, Young Kwon Park, and Ju dong Lee. Synthesis of anionic multichain type surfactant and its effect on methane gas hydrate formation. *J. Ind. Eng. Chem.*, 17(1):120–124, 2011.

[117] Yan He, Meng-Ting Sun, Chen Chen, Guodong Zhang, Kun Chao, Yan Lin, and Fei Wang. Surfactant-based Promotion to Gas Hydrate Formation for Energy Storage. *J. Mater. Chem. A*, 2019.

[118] Gaurav Bhattacharjee, Vivek Barmecha, Omkar S. Kushwaha, and Rajnish Kumar. Kinetic promotion of methane hydrate formation by combining anionic and silicone surfactants: Scalability promise of methane storage due to prevention of foam formation. *J. Chem. Thermodyn.*, 117:248–255, 2018.

[119] Gaurav Pandey, Gaurav Bhattacharjee, Hari Prakash Veluswamy, Rajnish Kumar, Jitendra S. Sangwai, and Praveen Linga. Alleviation of Foam Formation in a Surfactant Driven Gas Hydrate System: Insights via a Detailed Morphological Study. *ACS Appl. Energy Mater.*, 1(12):6899–6911, 2018.

[120] W. X. Pang, G. J. Chen, A. Dandekar, C. Y. Sun, and C. L. Zhang. Experimental study on the scale-up effect of gas storage in the form of hydrate in a quiescent reactor. *Chem. Eng. Sci.*, 62(8):2198–2208, 2007.

[121] Ngoc N. Nguyen and Anh V. Nguyen. Hydrophobic Effect on Gas Hydrate Formation in the Presence of Additives. *Energy and Fuels*, 31(10):10311–10323, 2017.

[122] Ngoc N. Nguyen, Mirza Galib, and Anh V. Nguyen. Critical Review on Gas Hydrate Formation at Solid Surfaces and in Confined Spaces—Why and How Does Interfacial Regime Matter? *Energy & Fuels*, 34(6):6751–6760, 2020.

[123] Burla Sai Kiran, Tulluru Bhavya, and Pinnelli SR Prasad. Synergistic and antagonistic effects of amino acids in clathrate hydrates of greenhouse gases. *Chem. Eng. J. Adv.*, 7(February):100117, 2021.

[124] Jyoti Shanker Pandey, Yousef Jouljamal Daas, and Nicolas von Solms. Screening of amino acids and surfactant as hydrate promoter for CO2 capture from flue gas. *Processes*, 8(124):1–23, 2020.

[125] Ahmad A.A. Majid, Joshua Worley, and Carolyn A. Koh. Thermodynamic and Kinetic Promoters for Gas Hydrate Technological Applications. *Energy and Fuels*, 35(23):19288–19301, 2021.

[126] Lars Borchardt, Mirian Elizabeth Casco, and Joaquin Silvestre-Albero. Methane Hydrate in Confined Spaces: An Alternative Storage System. *ChemPhysChem*, 19(11):1298–1314, 2018.

[127] Maninder Khurana, Zhenyuan Yin, and Praveen Linga. A review of clathrate hydrate nucleation. *ACS Sustain. Chem. Eng.*, 5(12):11176–11203, 2017.

[128] Praveen Linga, Nagu Daraboina, John A. Ripmeester, and Peter Englezos. Enhanced rate of gas hydrate formation in a fixed bed column filled with sand compared to a stirred vessel. *Chem. Eng. Sci.*, 68(1):617–623, 2012.

[129] Katipot Inkong, Hari Prakash Veluswamy, Pramoch Rangsunvigit, Santi Kulprathipanja, and Praveen Linga. Innovative Approach to Enhance the Methane Hydrate Formation at Near-Ambient Temperature and Moderate Pressure for Gas Storage Applications. *Ind. Eng. Chem. Res.*, 58(49):22178–22192, 2019.

[130] Xiao Ya Zang, Shuan Shi Fan, De Qing Liang, Dong Liang Li, and Guang Jin Chen. Influence of 3A molecular sieve on tetrahydrofuran (THF) hydrate formation. *Sci. China, Ser. B Chem.*, 51(9):893–900, 2008.

[131] Xiao Ya Zang, De Qing Liang, Shuan Shi Fan, and Cui Ping Tang. Influence of 5A-type zeolite powder on tetrahydrofuran hydrate formation and dissociation process. *Acta Phys. - Chim. Sin.*, 25(6):1047–1052, 2009.

[132] Jun-Ho Hyun Nam-Jin Kim, Sung-Seek Park, Sang-Woong Shin and Wongee Chun. An experimental investigation into the effects of zeolites on the formation of methane hydrates. *Int. J. Energy Res.*, 39:26–32, 2015.

[133] Mirian E. Casco, Joaquín Silvestre-Albero, Anibal J. Ramírez-Cuesta, Fernando Rey, Jose L. Jordá, Atul Bansode, Atsushi Urakawa, Inma Peral, Manuel Martínez-Escandell, Katsumi Kaneko, and Francisco Rodríguez-Reinoso. Methane hydrate formation in confined nanospace can surpass nature. *Nat. Commun.*, 6, 2015.

[134] Sohaib Mohammed, Hassnain Asgar, Milind Deo, and Greeshma Gadikota. Interfacial and Confinement-Mediated Organization of Gas Hydrates, Water, Organic Fluids, and Nanoparticles for the Utilization of Subsurface Energy and Geological Resources. *Energy and Fuels*, 35(6):4687–4710, 2021.

[135] Atsadawuth Siangsai, Pramoch Rangsunvigit, Boonyarach Kitiyanan, Santi Kulprathipanja, and Praveen Linga. Investigation on the roles of activated carbon particle sizes on methane hydrate formation and dissociation. *Chem. Eng. Sci.*, 126:383–389, 2015.

[136] A. Celzard and J. F. Marêché. Optimal wetting of active carbons for methane hydrate formation. *Fuel*, 85(7-8):957–966, 2006.

[137] Mirian E Casco, Fernando Rey, José L Jordá, Svemir Rudić, François Fauth, Manuel Martínez-Escandell, Francisco Rodríguez-Reinoso, Enrique V Ramos-Fernández, and Joaquín Silvestre-Albero. Paving the way for methane hydrate formation on metal-organic frameworks (MOFs). *Chem. Sci.*, 7(6):3658–3666, 2016.

[138] Qiang Zhang, Junjie Zheng, Baoyong Zhang, and Praveen Linga. Coal mine gas separation of methane via clathrate hydrate process aided by tetrahydrofuran and amino acids. *Appl. Energy*, 287(September 2020):116576, 2021.

[139] P S R Prasad, K Shiva Prasad, and N K Thakur. Laser Raman spectroscopy of THF clathrate hydrate in the temperature range 90-300 K. *Spectrochim. Acta - Part A Mol. Biomol. Spectrosc.*, 68(4):1096–1100, 2007.

[140] Alexandr Talyzin. Feasibility of H2-THF-H2 O clathrate hydrates for hydrogen storage applications. *Int. J. Hydrogen Energy*, 33(1):111–115, 2008.

[141] Marvin Ricaurte, Christophe Dicharry, Daniel Broseta, Xavier Renaud, and Jean Philippe Torré. CO2 removal from a CO2-CH4 gas mixture by clathrate hydrate formation using THF and SDS as water-soluble hydrate promoters. *Ind. Eng. Chem. Res.*, 52(2):899–910, 2013.

[142] Behzad Partoon, Khalik M. Sabil, Hariz Roslan, Bhajan Lal, and Lau Kok Keong. Impact of acetone on phase boundary of methane and carbon dioxide mixed hydrates. *Fluid Phase Equilib.*, 412:51–56, 2016.

[143] Dong Liang Zhong, Nagu Daraboina, and Peter Englezos. Recovery of CH4 from coal mine model gas mixture (CH 4/N2) by hydrate crystallization in the presence of cyclopentane. *Fuel*, 106:425–430, 2013.

[144] Alondra Torres Trueba, Laura J. Rovetto, Louw J. Florusse, Maaike C. Kroon, and Cor J. Peters. Phase equilibrium measurements of structure II clathrate hydrates of hydrogen with various promoters. *Fluid Phase Equilib.*, 307(1):6–10, 2011.

[145] Tatsuo Maekawa. Equilibrium conditions for clathrate hydrates formed from methane and aqueous propanol solutions. *Fluid Phase Equilib.*, 267(1):1–5, 2008.

[146] Ekta Chaturvedi, Nitish Prasad, and Ajay Mandal. Enhanced formation of methane hydrate using a novel synthesized anionic surfactant for application in storage and transportation of natural gas. *J. Nat. Gas Sci. Eng.*, 56(May):246–257, 2018.

[147] Namrata Gaikwad, Gaurav Bhattacharjee, Omkar S. Kushwaha, Jitendra S. Sangwai, Praveen Linga, and Rajnish Kumar. Effect of Cyclooctane and l -Tryptophan on Hydrate Formation from an Equimolar CO2-CH4Gas Mixture Employing a Horizontal-Tray Packed Bed Reactor. *Energy and Fuels*, 34(8):9840–9851, 2020.

[148] Brinchi Lucia, Beatrice Castellani, Federico Rossi, Franco Cotana, Elena Morini, Andrea Nicolini, and Mirko Filipponi. Experimental investigations on scaled-up methane hydrate production with surfactant promotion: Energy considerations. *J. Pet. Sci. Eng.*, 120:187–193, 2014.

[149] Hari Prakash Veluswamy, Sharad Kumar, Rajnish Kumar, Pramoch Rangsunvigit, and Praveen Linga. Enhanced clathrate hydrate formation kinetics at near ambient temper-

atures and moderate pressures: Application to natural gas storage. *Fuel*, 182:907–919, 2016.

[150] Mihrimah Ozkan. Direct air capture of CO2: A response to meet the global climate targets. *MRS Energy Sustain.*, (0123456789):1–6, 2021.

[151] Eloy S. Sanz-Pérez, Christopher R. Murdock, Stephanie A. Didas, and Christopher W. Jones. Direct Capture of CO2 from Ambient Air. *Chem. Rev.*, 116(19):11840–11876, 2016.

[152] Clas Ekström, Frank Schwendig, Ole Biede, Flavio Franco, Günther Haupt, Gelein de Koeijer, Charalambos Papapavlou, and Petter E. Røkke. Techno-Economic Evaluations and Benchmarking of Pre-combustion CO2 Capture and Oxy-fuel Processes Developed in the European ENCAP Project. *Energy Procedia*, 1(1):4233–4240, 2009.

[153] Yi-Song Yu, Xianwei Zhang, Jian-Wu Liu, Yohan Lee, and Xiao-Sen Li. Natural gas hydrate resources and hydrate technologies: a review and analysis of the associated energy and global warming challenges. *Energy Environ. Sci.*, 2021.

[154] Yuan Zhang, Jaka Sunarso, Shaomin Liu, and Rong Wang. Current status and development of membranes for CO2/CH4 separation: A review. *Int. J. Greenh. Gas Control*, 12:84–107, 2013.

[155] Anshuman Sinha and Matthew J. Realff. A parametric study of the techno-economics of direct CO2 air capture systems using solid adsorbents. *AIChE J.*, 65(7):1–8, 2019.

[156] Luogang Wu, Jiaqi Liu, Hua Shang, Shishuai Li, Jiangfeng Yang, Libo Li, and Jinping Li. Capture CO2 from N2 and CH4 by zeolite L with different crystal morphology. *Microporous Mesoporous Mater.*, 316(December 2020):110956, 2021.

[157] Dennis Y.C. Leung, Giorgio Caramanna, and M. Mercedes Maroto-Valer. An overview of current status of carbon dioxide capture and storage technologies. *Renew. Sustain. Energy Rev.*, 39:426–443, 2014.

[158] Friday O. Ochedi, Jianglong Yu, Hai Yu, Yangxian Liu, and Arshad Hussain. Carbon dioxide capture using liquid absorption methods: a review. *Environ. Chem. Lett.*, 19:77–109, 2021.

[159] Dennis Y.C. Leung, Giorgio Caramanna, and M. Mercedes Maroto-Valer. An overview of current status of carbon dioxide capture and storage technologies. *Renew. Sustain. Energy Rev.*, 39:426–443, 2014.

[160] G. Göttlicher and R. Pruschek. Comparison of CO2 removal systems for fossil-fuelled power plant processes. *Energy Convers. Manag.*, 38(SUPPL. 1):173–178, 1997.

[161] Mohammed D. Aminu, Seyed Ali Nabavi, Christopher A. Rochelle, and Vasilije Manovic. A review of developments in carbon dioxide storage. *Appl. Energy*, 208(September):1389–1419, 2017.

[162] Khalik Mohamad Sabil and Behzad Partoon. Recent advances on carbon dioxide capture through a hydrate-based gas separation process. *Curr. Opin. Green Sustain. Chem.*, 11:22–26, 2018.

[163] Xiaolin Wang, Fengyuan Zhang, and Wojciech Lipiński. Research progress and challenges in hydrate-based carbon dioxide capture applications. *Appl. Energy*, 269(114928):1–26, 2020.

[164] A. Falenty, J. Qin, A. N. Salamatin, L. Yang, and W. F. Kuhs. Fluid composition and kinetics of the in situ replacement in CH4-CO2 hydrate system. *J. Phys. Chem. C*, 120(48):27159–27172, 2016.

[165] Jinxiang Liu, Yujie Yan, Jiafang Xu, Shujuan Li, Gang Chen, and Jun Zhang. Replacement micro-mechanism of CH4 hydrate by N2/CO2 mixture revealed by ab initio studies. *Comput. Mater. Sci.*, 123:106–110, 2016.

[166] Ross Anderson, Maria Llamedo, Bahman Tohidi, and Rod W. Burgass. Experimental measurement of methane and carbon dioxide clathrate hydrate equilibria in mesoporous silica. *J. Phys. Chem. B*, 107(15):3507–3514, 2003.

[167] Ray Boswell, David Schoderbek, Timothy S. Collett, Satoshi Ohtsuki, Mark White, and Brian J. Anderson. The Iġnik Sikumi field experiment, Alaska North Slope: Design, operations, and implications for CO2-CH4 exchange in gas hydrate reservoirs. *Energy and Fuels*, 31(1):140–153, 2017.

[168] T. S. Collett, R. E. Lewis, W. J. Winters, M. W. Lee, K. K. Rose, and R. M. Boswell. Downhole well log and core montages from the Mount Elbert Gas Hydrate Stratigraphic Test Well, Alaska North Slope. *Mar. Pet. Geol.*, 28(2):561–577, 2011.

[169] A. N. Salamatin, A. Falenty, and W. F. Kuhs. Diffusion Model for Gas Replacement in an Isostructural CH4-CO2 Hydrate System. *J. Phys. Chem. C*, 121(33):17603–17616, 2017.

[170] Michel Noussan, Pier Paolo Raimondi, Rossana Scita, and Manfred Hafner. The role of green and blue hydrogen in the energy transition—a technological and geopolitical perspective. *Sustain.*, 13(1):1–26, 2021.

[171] Pietro Di Profio, Simone Arca, Federico Rossi, and Mirko Filipponi. Comparison of hydrogen hydrates with existing hydrogen storage technologies: Energetic and economic evaluations. *Int. J. Hydrogen Energy*, 34(22):9173–9180, 2009.

[172] Hari Prakash Veluswamy, Rajnish Kumar, and Praveen Linga. Hydrogen storage in clathrate hydrates: Current state of the art and future directions. *Appl. Energy*, 122:112–132, 2014.

[173] Jinxiang Dong, Xiaoyan Wang, Hong Xu, Qiang Zhao, and Jinping Li. Hydrogen storage in several microporous zeolites. *Int. J. Hydrogen Energy*, 32(18):4998–5004, 2007.

[174] Huy Quoc Nguyen and Bahman Shabani. Review of metal hydride hydrogen storage thermal management for use in the fuel cell systems. *Int. J. Hydrogen Energy*, 46(62):31699–31726, 2021.

[175] Qi Long Zhu and Qiang Xu. Liquid organic and inorganic chemical hydrides for high-capacity hydrogen storage. *Energy Environ. Sci.*, 8(2):478–512, 2015.

[176] Rajesh B. Biniwale, S. Rayalu, S. Devotta, and M. Ichikawa. Chemical hydrides: A solution to high capacity hydrogen storage and supply. *Int. J. Hydrogen Energy*, 33(1):360–365, 2008.

[177] Purna Chandra Rao and Minyoung Yoon. Potential liquid-organic hydrogen carrier (Lohc) systems: A review on recent progress. *Energies*, 13(6040):1–23, 2020.

[178] Yuri A. Dyadin, Eduard G. Larionov, Andrei Yu Manakov, Fridrich V. Zhurko, Evgeny Ya Aladko, Tamara V. Mikina, and Vladislav Yu Komarov. Clathrate hydrates of hydrogen and neon. *Mendeleev Commun.*, 9(5):209–210, 1999.

[179] Wendy L Mao, Ho kwang Mao, Alexander F. Goncharov, Viktor V. Struzhkin, Quanzhong Guo, Jingzhu Hu, Jinfu Hu, Russell J. Hemley, Maddury Somayazulu, and Yusheng Zhao. Hydrogen clusters in clathrate hydrate. *Science (80-.).*, 297(5590):2247–2249, 2002.

[180] Wendy L. Mao and Ho Kwang Mao. Hydrogen storage in molecular compounds. *Proc. Natl. Acad. Sci. U. S. A.*, 101(3):708–710, 2004.

[181] Niall J. English and Christian J. Burnham. Intra-cage structure, vibrations and tetrahedral-site hopping of H2 and D2 in doubly-occupied 51264 cages in sII clathrate hydrates from path-integral and classical molecular dynamics. *Appl. Sci.*, 11(54):1–9, 2021.

[182] Keisuke Katsumasa, Kenichiro Koga, and Hideki Tanaka. On the thermodynamic stability of hydrogen clathrate hydrates. *J. Chem. Phys.*, 127(044509):1–8, 2007.

[183] Huen Lee, Jong Won Lee, Do Youn Kim, Jeasung Park, Yu Taek Seo, Huang Zeng, Igor L. Moudrakovski, Christopher I. Ratcliffe, and John A. Ripmeester. Tuning clathrate hydrates for hydrogen storage. *Mater. Sustain. Energy A Collect. Peer-Reviewed Res. Rev. Artic. from Nat. Publ. Gr.*, 434(April):285–288, 2010.

[184] Takeshi Sugahara, Joanna C. Haag, Pinnelli S.R. Prasad, Ashleigh A. Warntjes, E. Dendy Sloan, Amadeu K. Sum, and Carolyn A. Koh. Increasing hydrogen storage capacity using tetrahydrofuran. *J. Am. Chem. Soc.*, 131(41):14616–14617, 2009.

[185] Timothy A. Strobel, Craig J. Taylor, Keith C. Hester, Steven F. Dec, Carolyn A. Koh, Kelly T. Miller, and E. D. Sloan. Molecular hydrogen storage in binary THF-H2 clathrate hydrates. *J. Phys. Chem. B*, 110(34):17121–17125, 2006.

[186] Fokko M. Mulder, Marnix Wagemaker, Lambert Van Eijck, and Gordon J. Kearley. Hydrogen in porous tetrahydrofuran clathrate hydrate. *ChemPhysChem*, 9(9):1331–1337, 2008.

[187] Jr. Yorihiko Nagai, Hiroki Yoshioka, Masaki Ota, Yoshiyuki Sato, Hiroshi Inomata, Richard L. Smith. Binary Hydrogen-Tetrahydrofuran Clathrate Hydrate Formation Kinetics and Models. *AIChE J.*, 54(11):3007–3016, 2008.

[188] Hari Prakash Veluswamy, Rajnish Kumar, and Praveen Linga. Hydrogen storage in clathrate hydrates: Current state of the art and future directions. *Appl. Energy*, 122:112–132, 2014.

[189] Seongmin Park, Dong Yeun Koh, Hyery Kang, Jae W. Lee, and Huen Lee. Effect of molecular nitrogen on multiple hydrogen occupancy in clathrate hydrates. *J. Phys. Chem. C*, 118(35):20203–20208, 2014.

[190] Tomohiro Hasegawa, Paul E. Brumby, Kenji Yasuoka, and Amadeu K. Sum. Mechanism for H2 diffusion in sII hydrates by molecular dynamics simulations. *J. Chem. Phys.*, 153(5):054706–1–054706–9, 2020.

[191] Ahmed Omran, Nikolai Nesterenko, and Valentin Valtchev. Ab initio mechanistic insights into the stability, diffusion and storage capacity of sI clathrate hydrate containing hydrogen. *Int. J. Hydrogen Energy*, 47(13):8419–8433, 2022.

[192] R. Gary Grim, Prasad B. Kerkar, Michele Shebowich, Melissa Arias, E. Dendy Sloan, Carolyn A. Koh, and Amadeu K. Sum. Synthesis and characterization of sI clathrate hydrates containing hydrogen. *J. Phys. Chem. C*, 116(34):18557–18563, 2012.

[193] Sergei S. Skiba, Eduard G. Larionov, Andrey Y. Manakov, Boris A. Kolesov, and Viktor I. Kosyakov. Investigation of hydrate formation in the system H2-CH 4-H2O at a pressure up to 250 MPa. *J. Phys. Chem. B*, 111(38):11214–11220, 2007.

[194] R V Belosludov, R K Zhdanov, O S Subbotin, H Mizuseki, Yoshiyuki Kawazoe, and V R Belosludov. Theoretical study of hydrogen storage in binary hydrogen-methane clathrate hydrates. *J. Renew. Sustain. Energ*, 6:053132, 2014.

[195] Yuuki Matsumoto, R Gary Grim, Naveed M Khan, Takeshi Sugahara, Kazunari Ohgaki, E Dendy Sloan, Carolyn A Koh, and Amadeu K Sum. Investigating the thermodynamic stabilities of hydrogen and methane binary gas hydrates. *J. Phys. Chem. C*, 118(7):3581–3589, 2014.

[196] R. V. Belosludov, R. K. Zhdanov, O. S. Subbotin, H. Mizuseki, M. Souissi, Y. Kawazoe, and V. R. Belosludov. Theoretical modelling of the phase diagrams of clathrate hydrates for hydrogen storage applications. *Mol. Simul.*, 38(10):773–780, 2012.

[197] Mohammad Reza Ghaani, Satoshi Takeya, and Niall J. English. Hydrogen storage in propane-hydrate: Theoretical and experimental study. *Appl. Sci.*, 10(24):1–10, 2020.

[198] Seokyoon Moon, Yunseok Lee, Dongju Seo, Seungin Lee, Sujin Hong, Yun-Ho Ahn, and Youngjune Park. Critical hydrogen concentration of hydrogen-natural gas blends in clathrate hydrates for blue hydrogen storage. *Renew. Sustain. Energy Rev.*, 141(September 2020):110789, 2021.

[199] Anshul Gupta, Gino V. Baron, Patrice Perreault, Silvia Lenaerts, Radu George Ciocarlan, Pegie Cool, Paulo G.M. Mileo, Sven Rogge, Veronique Van Speybroeck, Geert Watson, Pascal Van Der Voort, Maarten Houlleberghs, Eric Breynaert, Johan Martens, and Joeri F.M. Denayer. Hydrogen Clathrates: Next Generation Hydrogen Storage Materials. *Energy Storage Mater.*, 41(June):69–107, 2021.

[200] R. G. Raluy, L. Serra, and J. Uche. Life cycle assessment of desalination technologies integrated with renewable energies. *Desalination*, 183(1-3):81–93, 2005.

[201] Tianbiao He, Zheng Rong Chong, Junjie Zheng, Yonglin Ju, and Praveen Linga. LNG cold energy utilization: Prospects and challenges. *Energy*, 170:557–568, 2019.

[202] Ponnivalavan Babu, Abhishek Nambiar, Tianbiao He, Iftekhar A. Karimi, Ju Dong Lee, Peter Englezos, and Praveen Linga. A Review of Clathrate Hydrate Based Desalination to Strengthen Energy-Water Nexus. *ACS Sustain. Chem. Eng.*, 6(7):8093–8107, 2018.

[203] Ponnivalavan Babu, Abhishek Nambiar, Zheng Rong Chong, Nagu Daraboina, Mohammad Albeirutty, Omar A Bamaga, and Praveen Linga. Hydrate-based desalination (HyDesal) process employing a novel prototype design. *Chem. Eng. Sci.*, 218:115563, 2020.

[204] Kyung Chan Kang, Praveen Linga, Kyeong nam Park, Sang June Choi, and Ju Dong Lee. Seawater desalination by gas hydrate process and removal characteristics of dissolved ions (Na+, K+, Mg2+, Ca2+, B3+, Cl-, SO42-). *Desalination*, 353:84–90, 2014.

[205] A. Khafaei, A., & Kamran-Pirzaman. Experimental Study of Semiclathrate Hydrates Formation TBAOH, TBAF, and TBAC in the Presence of SDS and Tween Surfactants

as a Cold Thermal Energy Storage System for Air Conditioning Applications. *J. Chem. Eng. Data*, 66(7):2901–2910, 2021.

[206] P. Zhang, Z. W. Ma, and R. Z. Wang. An overview of phase change material slurries: MPCS and CHS. *Renew. Sustain. Energy Rev.*, 14(2):598–614, 2010.

[207] Sandrine Marinhas, Anthony Delahaye, and Laurence Fournaison. Solid fraction modelling for CO2 and CO2-THF hydrate slurries used as secondary refrigerants. *Int. J. Refrig.*, 30(5):758–766, 2007.

[208] Jong Ho Cha, Kyuchul Shin, Sukjeong Choi, and Huen Lee. Ionic conductivity enhancement due to coguest inclusion in the pure ionic clathrate hydrates. *J. Phys. Chem. C*, 112(28):10573–10578, 2008.

[209] Arnaud Desmedt, Frank Stallmach, Ruep E. Lechner, Dominique Cavagnat, Jean Claude Lassègues, François Guillaume, Joseph Grondin, and Miguel A. Gonzalez. Proton dynamics in the perchloric acid clathrate hydrate HCIO 4-5.5H2O. *J. Chem. Phys.*, 121(23):11916–11926, 2004.

[210] Xiaolin Wang, Fengyuan Zhang, and Wojciech Lipiński. Carbon dioxide hydrates for cold thermal energy storage: A review. *Sol. Energy*, 211(September):11–30, 2020.

[211] T. Nogami, N. Oya, H. Ishida, and H. Matsumoto. Development of natural gas ocean transportation chain by means of natural gas hydrate (NGH). *6th Gas Hydrates Int. Conf. [ICGH] (Vancouver, Br. Columbia, 7/6-10/2008) Proc.*, (Icgh), 2008.

[212] Satoo Nakai. Development of natural gas hydrate (NGH) supply chain. *Int. Gas Union World Gas Conf. Pap.*, 4:3040–3049, 2012.

[213] Satoshi Takeya, Hiroko Mimachi, and Tetsuro Murayama. Methane storage in water frameworks: Self-preservation of methane hydrate pellets formed from NaCl solutions. *Appl. Energy*, 230(July):86–93, 2018.

[214] J. S. Gudmundsson, Mahmut Parlaktuna, and A. A. Khokhar. Storing natural gas as frozen hydrate. *SPE Prod. Facil.*, 9(1):69–73, 1994.

[215] Hiroko Mimachi, Masahiro Takahashi, Satoshi Takeya, Yoshito Gotoh, Akio Yoneyama, Kazuyuki Hyodo, Tohoru Takeda, and Tetsuro Murayama. Effect of Long-Term Storage and Thermal History on the Gas Content of Natural Gas Hydrate Pellets under Ambient Pressure. *Energy and Fuels*, 29(8):4827–4834, 2015.

[216] Gaurav Bhattacharjee and Praveen Linga. Amino Acids as Kinetic Promoters for Gas Hydrate Applications : A Mini Review. 2021.

[217] Satoshi Takeya, Sanehiro Muromachi, Akio Yoneyama, Keiichi Hirano, Kazuyuki Hyodo, and John A. Ripmeester. Superheating of Structure I Gas Hydrates within the Structure II Cyclopentane Hydrate Shell. *J. Phys. Chem. Lett.*, 13(9):2130–2136, 2022.

[218] Gregor Rehder, Robert Eckl, Markus Elfgen, Andrzej Falenty, Rainer Hamann, Nina Kähler, Werner F. Kuhs, Hans Osterkamp, and Christoph Windmeier. Methane hydrate pellet transport using the self-preservation effect: A techno-economic analysis. *Energies*, 5(7):2499–2523, 2012.

[219] Gaurav Bhattacharjee, Hari Prakash Veluswamy, Rajnish Kumar, and Praveen Linga. Rapid methane storage via sII hydrates at ambient temperature. *Appl. Energy*, 269(March):115142, 2020.

[220] Syed Y. Nahri, James L. Nielsen, and Yuanhang Chen. Effect of nanoparticles on the nucleation and agglomeration rates of hydrate growth using THF–water clathrates. *Pet. Sci.*, 17(2):467–476, 2020.

[221] Parisa Naeiji, Akram Arjomandi, and Farshad Varaminian. Journal of Natural Gas Science and Engineering Amino acids as kinetic inhibitors for tetrahydrofuran hydrate formation : Experimental study and kinetic modeling. *J. Nat. Gas Sci. Eng.*, 21:64–70, 2014.

[222] H. Fakharian, H. Ganji, A. Naderi Far, and M. Kameli. Potato starch as methane hydrate promoter. *Fuel*, 94:356–360, 2012.

[223] Avinash V. Palodkar and Amiya K. Jana. Clathrate hydrate dynamics with synthetic- and bio-surfactant in porous media: Model formulation and validation. *Chem. Eng. Sci.*, 213:115386, 2020.

[224] Mirian E. Casco, Joaquín Silvestre-Albero, Anibal J. Ramírez-Cuesta, Fernando Rey, Jose L. Jordá, Atul Bansode, Atsushi Urakawa, Inma Peral, Manuel Martínez-Escandell, Katsumi Kaneko, and Francisco Rodríguez-Reinoso. Methane hydrate formation in confined nanospace can surpass nature. *Nat. Commun.*, 6, 2015.

[225] Seokyoon Moon, Yunseok Lee, Dongju Seo, Seungin Lee, Sujin Hong, Yun-Ho Ahn, and Youngjune Park. Critical hydrogen concentration of hydrogen-natural gas blends in clathrate hydrates for blue hydrogen storage. *Renew. Sustain. Energy Rev.*, 141(September 2020):110789, 2021.

[226] Zachary T. Ward, Connor E. Deering, Robert A. Marriott, Amadeu K. Sum, E. Dendy Sloan, and Carolyn A. Koh. Phase equilibrium data and model comparisons for H2S hydrates. *J. Chem. Eng. Data*, 60(2):403–408, 2015.

[227] Ponnivalavan Babu, Ting Yang, Hari Prakash Veluswamy, Rajnish Kumar, and Praveen Linga. Hydrate phase equilibrium of ternary gas mixtures containing carbon dioxide, hydrogen and propane. *J. Chem. Thermodyn.*, 61:58–63, 2013.

[228] P. Linga and M. A. Clarke. A review of reactor designs and materials employed for increasing the rate of gas hydrate formation. *Energy and Fuels*, 31(1):1–13, 2017.

[229] Vafa Feyzi and Vahid Mohebbi. Hybrid Hydrate-Membrane Post-combustion CO2Capture: A Conceptual Process Design and Analyses. *Ind. Eng. Chem. Res.*, 59(29):13132–13142, 2020.

[230] Daria Surovtseva. *Department of Chemical Engineering Clean Gas Technologies Australia CO 2 Separation by Cryogenic and Hydrate*. PhD thesis, Curtin University of Technology, 2010.

[231] Daria Surovtseva, Robert Amin, and Ahmed Barifcani. Design and operation of pilot plant for CO2 capture from IGCC flue gases by combined cryogenic and hydrate method. *Chem. Eng. Res. Des.*, 89(9):1752–1757, 2011.

[232] Yun-Ho Ahn, Seokyoon Moon, Dong-Yeun Koh, Sujin Hong, Huen Lee, Jae W Lee, and Youngjune Park. One-step formation of hydrogen clusters in clathrate hydrates stabilized via natural gas blending. 2019.

[233] Toshio Shibata, Hiroshi Yamachi, Ryo Ohmura, and Yasuhiko H. Mori. Engineering investigation of hydrogen storage in the form of a clathrate hydrate: Conceptual designs of underground hydrate-storage silos. *Int. J. Hydrogen Energy*, 37(9):7612–7623, 2012.

[234] Luning Chen, Zhiyuan Qi, Shuchen Zhang, Ji Su, and Gabor A Somorjai. Catalytic hydrogen production from methane: A review on recent progress and prospect. *Catalysts*, 10(8), 2020.

[235] Alexandra M Oliveira, Rebecca R Beswick, and Yushan Yan. A green hydrogen economy for a renewable energy society. *Curr. Opin. Chem. Eng.*, 33:100701, 2021.

[236] Sonja van Renssen. The hydrogen solution? *Nat. Clim. Chang.*, 10(9):799–801, 2020.

[237] Furat Dawood, Martin Anda, and G M Shafiullah. Hydrogen production for energy: An overview. *Int. J. Hydrogen Energy*, 45(7):3847–3869, 2020.

[238] Robert W Howarth and Mark Z Jacobson. How green is blue hydrogen? *Energy Sci. Eng.*, 9(10):1676–1687, 2021.

Chapter 3

Experimental Techniques and Simulation Methods

Be less curious about people and more curious about ideas.

-Marie Curie

Several kinetic studies and a variety of characterization techniques were used to characterize different competent of the system including hydrates, zeolites and metallic packing. In this chapter, we start with explaining the experimental procedure and hydrate kinetic calculations. Then, we introduce the different instrument methods with focus on those we used for gas hydrate analysis, including Raman, NMR, and PXRD techniques. Additionally, we also highlight the methods used for charaterizing zeolite promoters. Finally, the *ab initio* density functional theory calculations of different systems are highlighted.

3.1 Experimental Procedure and Calculations

3.1.1 Hydrate formation experiment

First, the reactor was filled with the solution until the desired level was achieved before it was sealed, and purged with nitrogen. Further, the reactor and related connections were purged with methane to ensure the removal of any contaminants. The system then is cooled down/heated to the target temperature. The system is left to equilibrate at the desired for one hour before it is pressurized with methane up to the desired pressure. During the reaction, pressure and temperature were monitored and recorded every 10 sec via a data acquisition system (DAQ). The induction time is defined as the period between this starting point and the formation of the first hydrate crystal. Here, we monitor the end of the induction period by a simultaneous sudden pressure drop that is usually accompanied by a temperature increase due to the exother-

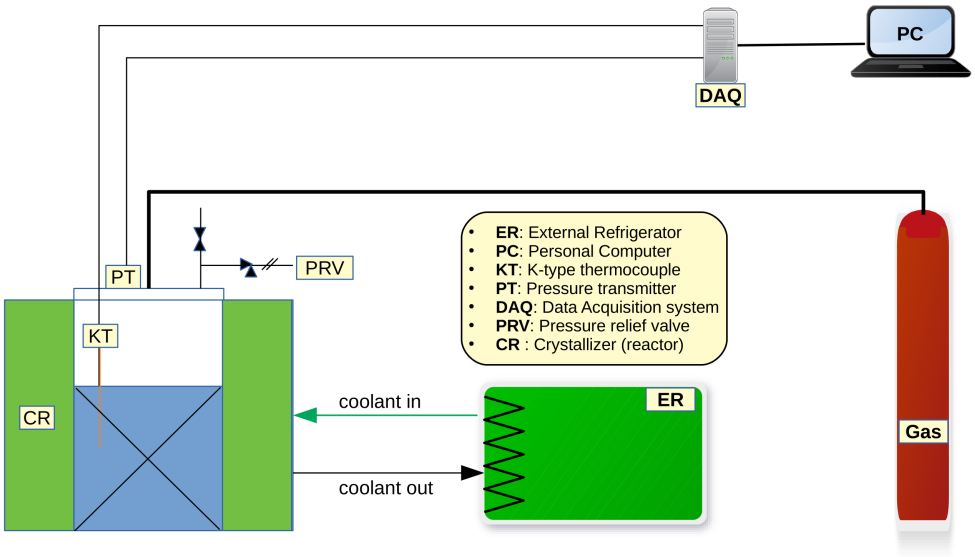

Figure 3.1: Raman shift of C-H stretching mode of several hydrocarbon hydrates

mic nature of hydrate formation. As the reaction continues, the pressure drops further, and the hydrate formation process is considered complete if there is no further significant pressure drop for 1 hour.

The number of moles of the gas consumed $(\Delta n_{H\downarrow})$ at any time t is equal to the difference between the number of moles of the gas $(n_{H,0})$ at time =0 (i.e., the start of the experiment) and the number of moles of the gas present $n_{H,t}$ at any time t in the vessel as shown by Eq.(C.1):

$$\Delta n_{H\downarrow} = n_{H_0} - n_{H_t} = \left(\frac{PV}{zRT}\right)_{G_0} - \left(\frac{PV}{zRT}\right)_{G_t} \tag{3.1}$$

Subscript G_0 and G_t represent the gas phase at the start of the experiment and time t, respectively. Here, P, T, and V are the pressure, temperature, and reactor volume, respectively. R is the universal gas constant, and z is the comprehensibility factor calculated by Pitzer's correction [1].

Normalized methane gas uptake is calculated by the following Eq.(C.2):

$$Normalized \quad uptake \quad = \frac{\Delta n_{H\downarrow}}{n_{H_2O}} \tag{3.2}$$

Finally, the volumetric capacity is calculated following Makagon method [2] where the volume

of gas stored in a unit volume of gas hydrate:

$$Q_H = \frac{V_G \delta \times 10^3}{M_h} \tag{3.3}$$

Where the density of hydrate δ is calculated as per Sloan and Koh [3] and the molecular weight of hydrate M_h is defined as:

$$M_h = M + 18.02n \tag{3.4}$$

Then, the volume of gas stored in a unit volume if hydrate at standard conditions is defined by the equation:

$$Q_{SC} = \frac{Q_H P T_0}{Z P_0 T} \tag{3.5}$$

3.1.2 Hydrate dissociation experiment

To evaluate the methane uptake, the hydrates were dissociated by increasing the temperature at the end of all experiments to 310.2 K for at least 6 hours. The selection of that temperature ensures complete hydrate dissociation as it is beyond the equilibrium phase boundary. After 6 hours, the dissociation is deemed completed when the pressure is not changing for 1 h. During dissociation, the amount of methane released from hydrate at any time t is calculated by Eq.(C.6)

$$\Delta n_{H\uparrow} = n_{H,\downarrow} - n_{H,0} = \left(\frac{PV}{zRT}\right)_{G,t} - \left(\frac{PV}{zRT}\right)_{G,0} \tag{3.6}$$

where $n_{H,\downarrow}$ is the moles of methane gas consumed for the hydrate formation at the end of the experiment. Finally, the methane recovery is calculated as in Eq.(C.7):

$$Recovery(\%) = \frac{\Delta n_{H\uparrow}}{n_{H,\downarrow}} * 100 \tag{3.7}$$

3.2 Characterization Techniques

As described in Chapter2, clathrate hydrates are non-stoichiometric crystalline compounds with different kinds of cages and different cage occupancy. In this thesis we focus our work on three commonly used instrument methods to characterize clathrate hydrates: X-ray diffraction (XRD), Nuclear mangnetic Resonance (NMR) and Raman Spectroscopy. While Raman and NMR can work better in detecting the guest molecules, XRD are performing well in characterizing the host lattice of water molecules.

3.2.1 Raman Spectroscopy

Raman spectroscopy is a category of scattering spectroscopy, which measures the changed frequency when light is scattered by molecules. Raman scattering is a series of frequencies of $\nu_0 \pm \Delta\nu_i$ that resulted from the collision of photons from incident light (i.e photons of energy $h\nu_0$) with the molecules of hydrate crystals. ($\Delta\nu_i$) is the difference between the frequencies of scattered and incident light and it defines the Raman shift. This Raman shift -regardless to the frequency or the intensity of incident light- depends on its characteristic molecular vibration or rotation energy level. Moreover, it is also affected by the applied pressure, temperature and chemical environment for specific molecule which can be used for qualitative identification [4].

Raman scattering intensity for species be expressed as:

$$A_i = I_L \sigma_i N_i \eta \tag{3.8}$$

Where $A_i, I_L, \sigma_i, N_i, \eta$ are Raman active peak integrated area, intensity of Raman laser, Raman

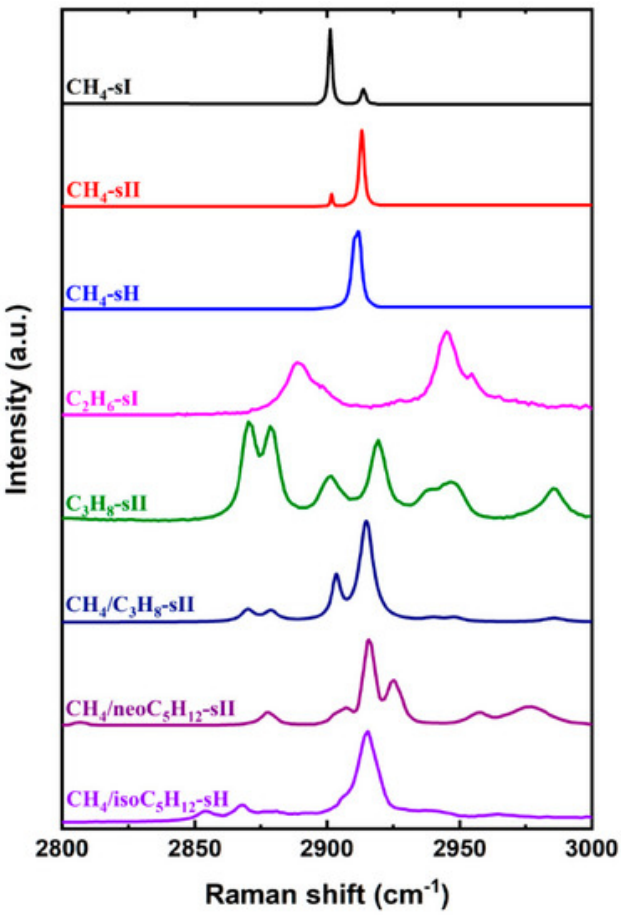

Figure 3.2: Raman shift of C-H stretching of different hydrocarbons[5].

scattering cross section, number of scattered molecules i, and Raman instrumental efficiency. When external factors (such as P-T conditions, and irradiance are constant) , then the Raman intensity is proportional to the total number of scattered molecules which can be used for quan-

titative analysis[6].

Confocal laser Raman spectroscopy is commonly used for both qualitative and quantitative characterization of gas hydrates. To illustrate, the characteristic Raman peak can provide structural information of zeolitic ice : the different gas species and their host environments (small, middle, large or other cages) which reveal the hydrate structure as shown in **A.8**. The following figure shows C-H vibration peaks of methane molecule. Quantitatively, the calculated peak areas can estimate the number of guest molecules in different cages which can be then to obtain the "cage occupancy"; a key parameter for volumetric and gravimetric storage capacity of hydrates. Raman spectroscopy is excellent tool to understand hydrate formation and dissociation, gas replacement, effect of inhibitors and promoters effects, and structure changes [7].

3.2.2 Nuclear Magnetic Resonance (NMR)

Nuclear Magnetic Resonance (NMR) is a spectroscopic technique to observe local magnetic fields around atomic nuclei. Under a uniform magnetic field (B_0), spin nuclei such as ^{1}H and ^{13}C split into separate energy levels. When irradiated with electromagnetic waves at specific frequency, the spin nuclei will absorb energy. This frequency matches the energy level difference between two state. The resonance of different nuclei occur when the imposed magnetic field is maintained constant while gradually increasing the oscillator frequency gradually. Once the resonance of the nuclei occurs, NMR signals or "chemical shifts" are observed. Normally, the chemical shift refers to relative change in resonance frequency of a sample compared to a common reference material such tetramethaylsilane (TMS). The chemical shift (δ) is calculated as:

$$\delta = \frac{\nu - \nu_{ref}}{\nu_{spec}} \times 10^6 (ppm) \tag{3.9}$$

where ν_{ref}, and ν_{spec} are the resonance frequency of standard reference compound, and instrument operating frequency, respectively. In general, the chemical shift is affected by factors such as molecular strucuture, electronegativety and chemical environment. This makes NMR ideal to be used in gas hydrates as it will give unique chemical shifts for different guest molecules [8]. More interestingly, the same guest molecules will give different chemical shifts when they are enclathrated at different cages or at gas phase. Such properties can be basis for NMR for qualitative analysis of zeoltic ice. Regarding quantitative analysis, it has been found that ^{13}C NMR signal intensity is directly proportional to the total number of corresponding guest molecules and thus can be used to determine cage occupancy. As hydrocarbons are the major components of most gas hydrates ^{13}C is most widely used for both characterization and quantitative analysis. The low resolution spectra due to chemical shift anisotropy of solid sample or inaccurate intensities due to relatively long relaxation time (compared to ^{1}H NMR) are overcome using special techniques such as magic angle rotation (MAS) or cross polarization[9, 10].

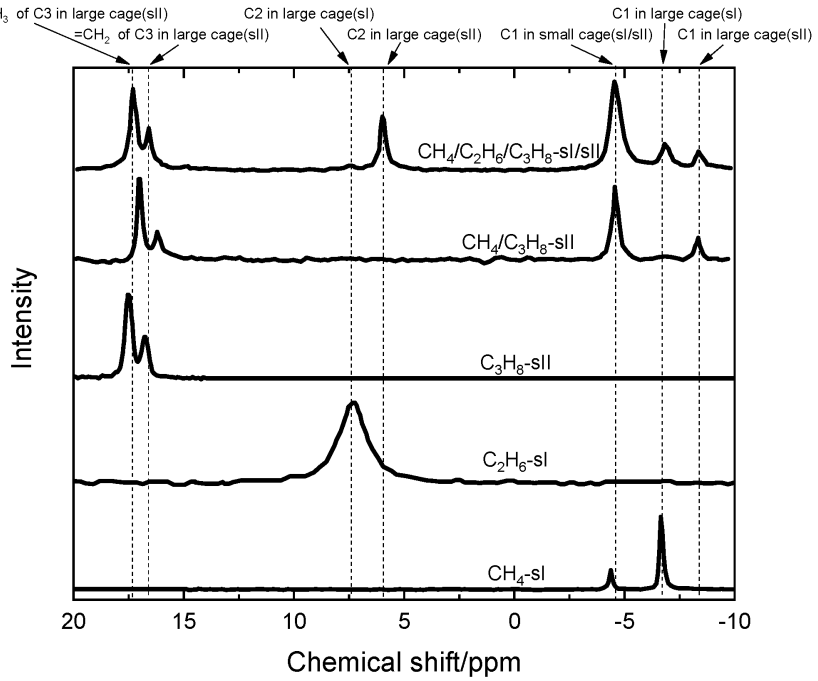

Figure 3.3: ^{13}C NMR chemical shift of different hydrocarbon clathrates

3.2.3 X-ray Diffraction

X-ray is an electromagnetic wave with a typical wave length (λ) in the range of 10^{10}m of the same order as the crystal lattice. When this electromagnetic wave enter the crystal, the outer electron of crystal atoms are excited to high energy state. As the excited electrons are returning to their ground state, photons with λ of about 100000 fm are will be emitted. As each atom is considered as a new X-ray source, there will be a spatial interference due to the periodic arrangement of atom within the crystal. The overlapping of the scattered waves can enhance the intensity in some scattering directions and neutralize each other in others, resulting in **diffraction**. The diffraction degree is a characteristic of the size of the matter and thus when this size is on the order of radiation wavelength, the degree of diffraction reaches its maximum. Diffraction patterns of specific "Laue sports" are obtained when a 3D order lattice of a single crystal is irradiated. Crystal symmetry and unit cell paramters are then determined from the relative locations of Laue spots according to Bragg's law:

$$2d \sin\theta = n\lambda \tag{3.10}$$

As zeolitic ice are crystalline solid compounds, XRD can be used to determine different hydrate structures. In particular, it can measure lattice parameters of different hydrate crystals, identify the guest species and calculate cage occupancy. The peak positions of certain hydrate XRD can identify the different crystal faces (the hlk coefficient) which shows the lattice parameter information. Thus, XRD is the most accurate technique to identify the hydrate structure type compared to other methods. For example, the position of Raman characteris-

tic peaks of different hydrate structures or same guest are too close and some time difficult to be separated. Unlike the nondestructive nature of Raman spectroscopy, NMR application for qualitative analysis is more difficult because of sample preparation and transfer. Even with *in situ* NMR, the hydrate structure identification is achieved indirectly by considering the different chemical shifts for certain molecules which may be overlapped. Both single crystal X-ray diffraction (Single-crystal XRD) and powder X-ray diffraction (PXRD) are applied for gas clathrate characterization. Single-crystal XRD has the advantage high precision to directly obtain lattice parameter, hydrate structure and cage occupancy [11]. However, high quality single crystal hydrate are difficult to synthesize. Consequently, PXRD is more commonly used for both qualitative and quantitative analysis when combined with refinement methods such as Rietveld structural refinement [12].

3.2.4 Hydrate Characterization

Structure II clathrate crystal information was obtained by powder X-ray diffraction (PXRD) [13]. The measurement was carried out at atmospheric pressure and low temperature with a PANalytical X'Pert Pro ® diffractometer system using Cu-K_α-radiation (λ = 1.5418 Å; 45 kV; 40 mA) in a continuous scan. The start position in 2θ was 10.0114°, while the end position in 2θ was 39.7500°. We used a step size in 2θ of 0.0170° and a scan step time of 50.1650 s. First, the binary CH_4-THF hydrates were synthesized in high-pressure reactor as described above using 5.56 mol% THF aqueous solution at the specified thermodynamic conditions. After the reaction is deemed complete, the unreacted gas is depressurized to the atmosphere followed by quick reactor cooling by liquid nitrogen. The hydrate sample was grounded by a mortar and pestle to prepare the uniform powder under liquid nitrogen to avoid sample dissociation. the obtained PXRD pattern is a typical sII pattern of space group $Fd\bar{3}m$ which is another indication of the presence of sII and absence of sI.

Similarly, solid-state ^{13}C MAS NMR spectra were obtained using a Bruker DRX400 spectrometer at a Larmor frequency of 100.6 MHz. Spectra were recorded at 250 K by placing the powdered hydrate samples in a 4 mm o.d. Zr-rotor that was loaded into a variable-temperature (VT) probe. All ^{13}C NMR spectra were recorded with magic angle spinning (MAS) between 2 and 4 kHz. Finally, Raman spectra of binary CH_4-THF clathrate sample are obtained using an immersion Raman probe (InPhotonics®) connected to the laser spectrometer (Horiba LabRam Evol®) via optical fibers. For excitation, a green laser at 532 nm wavelength was used with a spectral coverage of 50-3500 cm^{-1}.

3.2.5 Zeolite Promoter Characterization

PANalytical X'Pert Pro ® diffractometer was used to obtain powder X-ray diffraction (PXRD) patterns. The diffractometer system used Cu-K_α-radiation (λ = 1.5418 Å; 45 kV; 40 mA) in a

continuous scan at 25°C. The angle 2θ position was between 5.0114° and 35° while the step size in 2θ was 0.0170° in a step time of 50.1650 s. The measured specimen had a length of 10 mm. (TESCAN) MIRA-LMH scanning electron microscope (SEM) equipped with an electron emission gun and operated at 20 kV was used to obtain the electron micrographs.The same scanning electron microscope model was used for energy-dispersive X-ray spectroscopy (EDX) measurements using to confirm the elemental analysis. Prior to the measurements, the samples were sputtered with platinum to improve their electrical conductivity. In addition, chemical composition of zeolites was confirmed using inductively coupled plasma-atomic emission spectroscopy (ICP-AES) on an OPTIMA 4300 DV (Perkin-Elmer).

N_2-adsorption was employed to get the surface area and the porous volume measurements were measured via BET surface area measurement (measurement according to Brunauer, Emmet, Teller) with ASTM D3663 for the surface area and ASTM D4365 for the porous volume. The adsorption measurements were performed on Micromeritics ASAP 2020 surface area analyzer after degassing all samples under vacuum at 300°C overnight before measurement. ASAP 2020 analysis program has been used to obtain the isotherms. The *t-plot* based on the Harkins-Jura equation was used to obtain he external surface (S_{ext}), and the volume of micropores (V_{micro}). The mesoporous volume was estimated as the difference between the total and micropore volumes[14] as per Eq.(C.8)

$$V_{\text{meso}} = V_{\text{total}} - V_{\text{micro}} \tag{3.11}$$

For the data analysis, measurements were plotted with a Micromeritics Tristar 3000 analyzer. The total surface area was determined by N_2 sorption analysis according to ASTM D 4365 – 95 (reapproved 2008). Volumes of micropores and mesopores were determined according to D4641-94 (reapproved 2006).

3.2.6 Computational Methods

3.2.6.1 Overview on Density Functional Theory

Density functional theory (DFT) is a phenomenally successful approach to finding solutions to the fundamental equation that describes the quantum behavior of atoms and molecules that have been described by the Schrödinger equation. There are two important definitions related to Schrödinger equation solution and DFT: the wave function and the ground state. The definition of wave function is quantum physics state that it is a mathematical description of the quantum state of a system. The ground state of a quantum system is its lowest-energy state; the energy of the ground state is known as the zero-point energy of the system. On the other hand, an excited state is any state with energy greater than the ground state. Schrödinger equation in its famous simple form is:

$$\hat{\mathrm{H}}\,\psi = \mathrm{E}\,\psi \tag{3.12}$$

In this equation the $\hat{\mathrm{H}}$ is Hamiltonian operator and ψ is a set of solutions of the Hamiltonian. For each of these solutions ψ has an associated eigenvalue, E_n, which is a real number that satisfies the eigenvalue equation [15]. Born-Oppenheimer Approximation stated that since the electrons are small and fast compared to nuclei then the dynamics of nuclei and electron can be separated or decouple into two wave functions as follows:

$$\psi(\{r_i\},\{R_I\}) = \psi N(\{r_i\},\{R_I\}) * \psi(\{r_i\},\{R_I\}) \tag{3.13}$$

For a fixed set of atomic positions, the focus of the calculation is to solve the ground state of the electrons. Where r_i is the spatial coordinate of each i electron and R_I is the spatial coordinate of each I nucleus. Based on the above, the Schrödinger equation can be expressed as follows:

$$\hat{\mathrm{H}}\,\psi(r_1, r_2, r_3, \ldots r_N) = \mathrm{E}\,\psi(r_1, r_2, r_3, \ldots r_N) \tag{3.14}$$

Where ψ is the electronic wave function, which is a function of each of the spatial coordinate r of each of the N electrons. Solving Schrödinger equation will enable the determination of the ground state of a collection of atoms. The following equation gives a closer look at the Hamiltonian component of Schrödinger equation.

$$\left[\frac{h^2}{2m}\sum_{i=1}^{N}\nabla_i^2 + \sum_{i=1}^{N}V(\mathbf{r}_i) + \sum_{i=1}^{N}\sum_{j<i}U(\mathbf{r}_i,\mathbf{r}_j)\right]\psi = E\,\psi \tag{3.15}$$

Where the L.H.S of the above equation expresses the kinetic energy, electron nucleus interaction and the electron-electron interactions. Still, to solve Schrödinger equation for simple molecule is computational challenge as it has many-electrons problem. To illustrate this problem, consider the water molecule which possesses 10 electrons only, the Schrödinger equation will become a 30-dimensional problem as we consider 3 spatial coordinates per electron position. Similarly, we can say carbon dioxide Schrödinger equation, which will be 66-dimensional problem and so on. The strength of the Density Functional Theory (DFT) comes from its capability to utilize the electron density n(r) which is a true observable – a physical quantity that can be measured by methods such as X-ray diffraction-that contains all information in wave function. This closely related quantity is the density of electrons at a particular position in the space since it can be written in terms of the individual electron wave functions as follows:

$$n(r) = 2\sum_{i}\psi_i * (r)\,\psi_i(r) \tag{3.16}$$

The summation goes over all the individual electron wave functions that are occupied by electrons, so the term inside the summation is the probability that an electron in individual wave

function ψ_i(r) is located at position r. The factor of 2 appears due to Pauli Exclusion Principle, which states that each individual electron wave function can be occupied by two separate electrons provided they have different spins. The n(r) is function of 3 coordinates instead of 3N coordinates in case of Schrödinger equation, which converts the many-electrons problem to many-one electron problem. The density functional theory is based on two fundamental mathematical theorems proved by Kohn and Hohenberg and the derivation of a set of equations by Kohn and Sham in the mid-1960s. The first theorem, proved by Hohenberg and Kohn (HK), is: The ground-state energy from Schrödinger's equation is a unique functional of the electron density. This is very important as it support the elaborate the concept discussed above. In fact, it is possible to solve the Schrödinger equation –or in other meaning find the ground state of atoms- by finding a function of three spatial variables, the electron density, rather than a function of 3N variables, the wave function. In addition, the second Hohenberg–Kohn theorem defines another important concept of the functional: The electron density that minimizes the energy of the overall functional is the true electron density corresponding to the full solution of the Schrödinger equation [16]. The next sections will provide more specific details for the atomic models and DFT calculations used in this thesis.

3.2.6.2 Zeolite-Hydrate and Amino Acids-Hydrate Cluster Models

We performed density functional theory (DFT) calculations [16] using the projected augmented wave (PAW) method and the standard pseudopotentials supplied by Quantum Espresso (QE) software [17]. The kinetic energy cutoff for plane wave expansion of wavefunctions and charge density were 55 and 440 Ry, respectively[18]. All structures were fully optimized using a force convergence threshold of at least 10^{-4} Ry/a.u. and with a self-consistency convergence criterion of at least $1, \times 10^{-8}$. The calculations have been carried out using the Monkhorst-Pack *k*-points grid of $2 \times 2 \times 2$ in the reciprocal space. The DFT calculations for isolated cages and zeolite clusters were performed in a cubic simulation cell of volume $30 \times 30 \times 30$ Å^3. The 5^{12} small cage was modeled with a 20-molecule water cluster. In these small (5^{12}) cages, 8 oxygen atoms are located in a perfect cube (O_h). An estimated distance of 3.91 Å separates those 8 oxygen atoms from the cage center. The remaining 12 oxygen are positioned at 3.95 Å from the cage center and transform according to the (T_h) subgroup of (O_h)[19]. The results agree with the average obtained from the X-ray structure of sII as well as the optimized crystal model[20, 21]. Amino acids' interaction with the above hydrate cages was successfully monitored using DFT calculated as reported by Lee *et al.*[22]. A similar method was used to represent the zeolite promoters and their interaction with hydrate cages. In that method, we have used computationally affordable finite cluster models of zeolite crystals. Cluster models have extensively been employed to understand reactive and absorptive processes in various framework types of zeolites[23]. In particular, they have been successfully applied to understand zeolite acidity and water-zeolite interactions [24, 25].

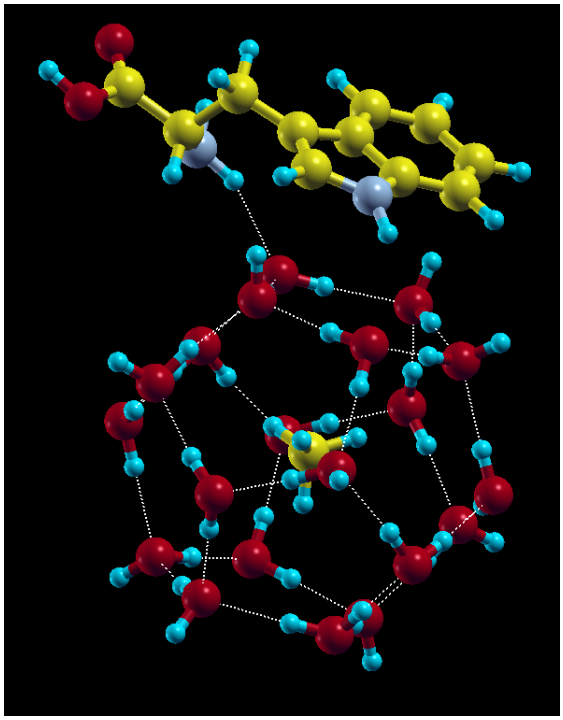

Figure 3.4: Example of Cluster Model : Optimized configuration of l-tryptophan interaction with 5^{12} methane hydrate cage

3.2.6.3 Computational Studies on Hydrate Cages and Crystal Structures

We performed here density functional theory (DFT) calculations [16] using projected augmented wave (PAW) psedopotentials with kinetic energy cutoff for wave function and charge density of 55 and 440 Ry, respectively[18]. A self consistency convergence criterion of at least 1×10^{-8} was used and all structures were fully optimized using force convergence threshold of at least 10^{-4} Ry/a.u. All calculations have been performed using $2 \times 2 \times 2$ mesh except those for sII large unit cell where we used Γ point calculation only. Gas molecules such as H_2, CH_4 and CO_2 are interacting with water frameworks by means of van der Waals forces and hydrogen bonding [3]. Moreover, it is not only the guest-host interaction but also the guest-guest and host-host interactions that affect hydrate formation and stability[26, 27]. *Ab initio* DFT calculations via Perdew-Burke-Ernzerhof generalized gradient approximation (GGA) functional[28] with revised exchange parametrization of Zhang and Yang (revPBE) has been applied self consistently[29]. The improved GGA functionals such as PBE and its revised versions revPBE and RPBE can gives more accurate chemisorption energies than the PW91 and PBE functionals [29–32], however it fails to include vdW dispersion forces or hydrogen

bonding [33, 34]. To illustrate, Pétuya *et al.* argued that the semilocal PBE functional can still reproduce experimental structural properties obtained by neutron diffraction and estimate stability of clathrates even better than non-local vdw-DF[35]. In another study, Vlasic *et al.* pointed out that revPBE works very well for gas and THF hydrates and could accurately determine their mechanical and vibrational properties. They suggested that particularly revPBE provided a unique combination of accuracy and low computational cost, when compared to other XC functionals including those that take into account long-range van der Waals interactions [36]. On the other hand, Cao *et al.* [37] suggested that the improved nonlocal van der Waals density functional (vdw-DF2) with the inclusion of a long-range term of the correlation energy is necessary to account for intermolecular dispersion interactions [38]. Accounting for the importance of these forces, we have used both revPBE and vdW-DF2 as implemented in Quantum Espresso (QE) software [17], thus addressing the discrepancies in the literature sources. The thermodynamic stability and storage capacity of mixed (CH_4 - H_2, CO_2 - H_2) sI clathrates was evaluated using the cohesive energy (E_{coh}) and binding energy (E_b).

Cohesive energy (E_{coh}) per water molecules is calculated as [39]:

$$E_{coh} = \frac{E_{hydrate} - (x.E_{H_2} + y.E_{gas} + 46E_{H_2O})}{46}$$

The binding energy (E_b) is calculated as [40, 41]:

$$E_b = E_{hydrate} - [E_{H_2} + E_{residual}]$$

where $E_{hydrate}$, E_{CO_2}, E_{gas}, E_{H_2O}, $E_{residual}$ are the energies of hydrate, hydrogen , gas (CO_2 or CH_4) , water and the hydrate with one hydrogen molecule less.The minimum energy paths (MEP) between two minima were identified using NEB and CI-NEB methods with convergence criterion (< 0.05 eV/Å). Transition state structures were confirmed by presence of only one imaginary frequency along the reaction coordinate.

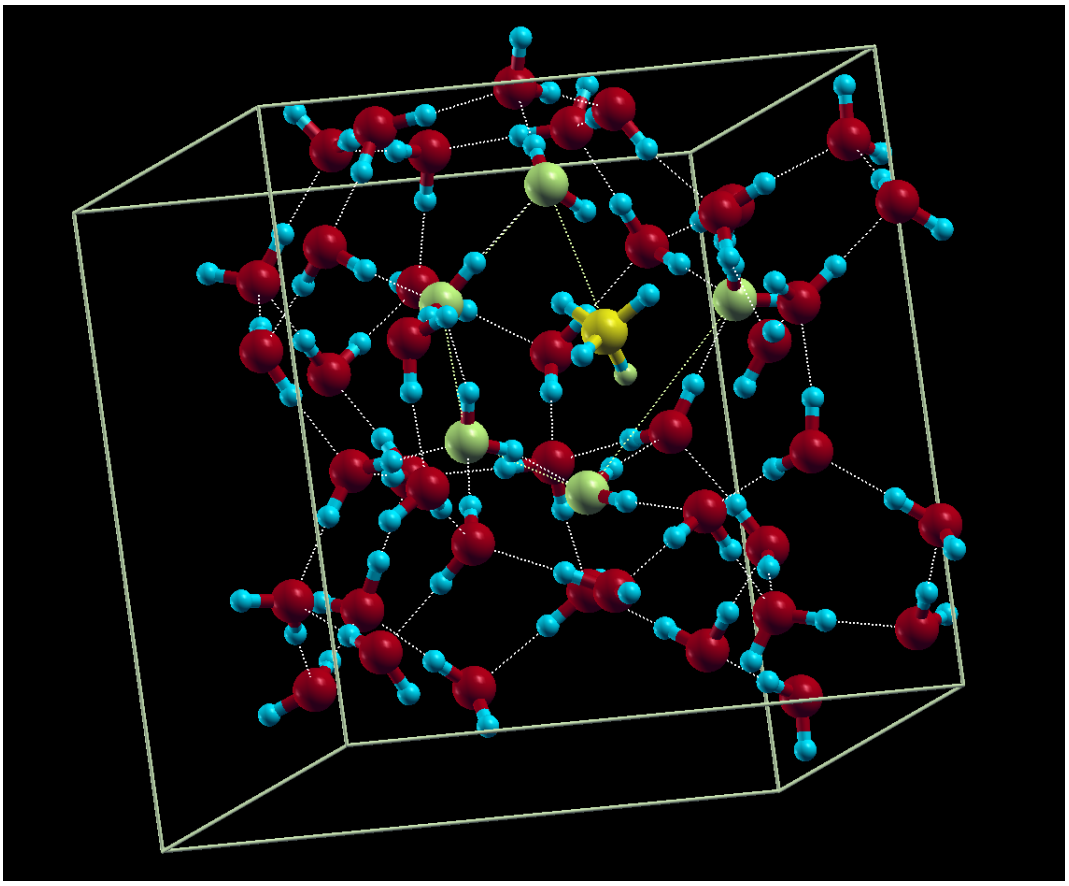

Figure 3.5: Example of Crystal Model : Diffusion of Methane in between small and large cages of sI hydrate

References

[1] Kenneth S. Pitzer, David Z. Lippmann, R. F. Curl, Charles M. Huggins, and Donald E. Petersen. The Volumetric and Thermodynamic Properties of Fluids. II. Compressibility Factor, Vapor Pressure and Entropy of Vaporization. *J. Am. Chem. Soc.*, 77(13):3433–3440, 1955.

[2] Makagon Yuri F. *Hydrates of Hydrocarbons*. Pennwell, 1997.

[3] E. Dendy Sloan and Carolyn Ann Koh. *Clathrate hydrates of natural gases, thrid edition*. CRC Press, third edition, 2007.

[4] J. W. Anthonsen, A. Kjekshus, D. G. Nicholson, J. T. Southern, J. T. Southern, Kaj Edlund, Mogens Eliasen, Carsten Herskind, Thomas Laursen, and Poul Møller Pedersen. The Raman Spectra of Some Halogen Gas Hydrates. *Acta Chem. Scand.*, 29a:175–178, 1975.

[5] Wenjiu Cai, Xin Huang, and Hailong Lu. Instrumental Methods for Cage Occupancy Estimation of Gas Hydrate. *Energies*, 15(2), 2022.

[6] Zhihua Qiao, Zhi Wang, Chenxin Zhang, Shuangjie Yuan, Yaqun Zhu, and Jixiao Wang. Quantitative Analysis of Gas Hydrates Using Raman Spectroscopy. *AIChE J.*, 59(4):215–228, 2012.

[7] Florian Rauh and Boris Mizaikoff. Spectroscopic methods in gas hydrate research. *Anal. Bioanal. Chem.*, 402(1):163–173, jan 2012.

[8] Christopher I. Ratcliffe. The Development of Clathrate Hydrate Science. *Energy and Fuels*, 2022.

[9] J. A. Ripmeester and C. I. Ratcliffe. On the contributions of NMR spectroscopy to clathrate science. *J. Struct. Chem.*, 40(5):654–662, 1999.

[10] Mingjun Yang, Zheng Rong Chong, Jianan Zheng, Yongchen Song, and Praveen Linga. Advances in nuclear magnetic resonance (NMR) techniques for the investigation of clathrate hydrates. *Renew. Sustain. Energy Rev.*, 74(December 2016):1346–1360, 2017.

[11] Konstantin A Udachin, Christopher I Ratcliffe, and John A Ripmeester. Single crystal diffraction studies of structure I, II and H hydrates: Structure, cage occupancy andf composition. *J. Supramol. Chem.*, 2(4-5):405–408, 2002.

[12] Satoshi Takeya, Konstantin A Udachin, Igor L Moudrakovski, Robin Susilo, and John A Ripmeester. Direct space methods for powder X-ray diffraction for guest-host materials: Applications to cage occupancies and guest distributions in clathrate hydrates. *J. Am. Chem. Soc.*, 132(2):524–531, 2010.

[13] Asheesh Kumar, Hari Prakash Veluswamy, Praveen Linga, and Rajnish Kumar. Molecular level investigations and stability analysis of mixed methane-tetrahydrofuran hydrates: Implications to energy storage. *Fuel*, 236(August 2018):1505–1511, 2019.

[14] Ana Palčić, Simona Moldovan, Hussein El Siblani, Aurelie Vicente, and Valentin Valtchev. Defect Sites in Zeolites: Origin and Healing. *Adv. Sci.*, 2104414:2104414, 2021.

[15] E Schrödinger. An Undulatory Theory of the Mechanics of Atoms and Molecules. *Phys. Rev.*, 28(6):1049–1070, dec 1926.

[16] W. Kohn. Nobel lecture: Electronic structure of matter - Wave functions and density functional. *Rev. Mod. Phys.*, 71(5):1253–1266, 1999.

[17] Paolo Giannozzi, Stefano Baroni, Nicola Bonini, Matteo Calandra, Roberto Car, Carlo Cavazzoni, Davide Ceresoli, Guido L. Chiarotti, Matteo Cococcioni, Ismaila Dabo, An-

drea Dal Corso, Stefano De Gironcoli, Stefano Fabris, Guido Fratesi, Ralph Gebauer, Uwe Gerstmann, Christos Gougoussis, Anton Kokalj, Michele Lazzeri, Layla Martin-Samos, Nicola Marzari, Francesco Mauri, Riccardo Mazzarello, Stefano Paolini, Alfredo Pasquarello, Lorenzo Paulatto, Carlo Sbraccia, Sandro Scandolo, Gabriele Sclauzero, Ari P. Seitsonen, Alexander Smogunov, Paolo Umari, and Renata M. Wentzcovitch. QUANTUM ESPRESSO: A modular and open-source software project for quantum simulations of materials. *J. Phys. Condens. Matter*, 21(39), 2009.

[18] P. E. Blöchl. Projector augmented-wave method. *Phys. Rev. B*, 50(24):17953–17979, 1994.

[19] Ahmed Omran, Nikolai Nesterenko, and Valentin Valtchev. Ab initio mechanistic insights into the stability, diffusion and storage capacity of sI clathrate hydrate containing hydrogen. *Int. J. Hydrogen Energy*, 47(13):8419–8433, 2022.

[20] Konstantin A. Udachin, Christopher I. Ratcliffe, and John A. Ripmeester. Single crystal diffraction studies of structure I, II and H hydrates: Structure, cage occupancy andf composition. *J. Supramol. Chem.*, 2(4-5):405–408, 2002.

[21] Michael T. Kirchner, Roland Boese, W. Edward Billups, and Lewis R. Norman. Gas hydrate single-crystal structure analyses. *J. Am. Chem. Soc.*, 126(30):9407–9412, 2004.

[22] Dongyoung Lee, Woojin Go, and Yongwon Seo. Experimental and computational investigation of methane hydrate inhibition in the presence of amino acids and ionic liquids. *Energy*, 182:632–640, 2019.

[23] Angela N. Migues, Adina Muskat, Scott M. Auerbach, Woody Sherman, and S. Vaitheeswaran. On the rational design of zeolite clusters. *ACS Catal.*, 5(5):2859–2865, 2015.

[24] Mariann Krossner and Joachim Sauer. Interaction of water with brønsted acidic sites of zeolite catalysts. ab initio study of 1:1 and 2:1 surface complexes. *J. Phys. Chem.*, 100(15):6199–6211, 1996.

[25] Frédéric Labat, Alain H. Fuchs, and Carlo Adamo. Toward an accurate modeling of the water-zeolite interaction: Calibrating the DFT approach. *J. Phys. Chem. Lett.*, 1(4):763–768, 2010.

[26] Ravi Radhakrishnan and Bernhardt L. Trout. A new approach for studying nucleation phenomena using molecular simulations: Application to CO2 hydrate clathrates. *J. Chem. Phys.*, 117(4):1786–1796, 2002.

[27] Qiao Shi, Pinqiang Cao, Zhengde Han, Fulong Ning, Hao Gong, Yue Xin, Zhisen Zhang, and Jianyang Wu. Role of Guest Molecules in the Mechanical Properties of Clathrate Hydrates. *Cryst. Growth Des.*, 18(11):6729–6741, 2018.

[28] John P. Perdew, Kieron Burke, and Matthias Ernzerhof. Generalized gradient approximation made simple. *Phys. Rev. Lett.*, 77(18):3865–3868, 1996.

[29] Yingkai Zhang and Weitao Yang. Comment on "generalized gradient approximation made simple", 1998.

[30] B Hammer, L B Hansen, and J. K. Nørskov. Improved adsorption energetics within density-functional theory using revised Perdew-Burke-Ernzerhof functionals. *Phys. Rev. B - Condens. Matter Mater. Phys.*, 59(11):7413–7421, 1999.

[31] B. Hammer and J.K. Norskov. Theoretical Surface Science and Catalysis — Calculations and Concepts. *Adv. Catal.*, 45:71–129, 2000.

[32] Ahmed Omran, Sun Hee Yoon, Murtaza Khan, Minhaj Ghouri, Anjaneyulu Chatla, and Nimir Elbashir. Mechanistic Insights for Dry Reforming of Methane on Cu/Ni Bimetallic Catalysts: DFT-Assisted Microkinetic Analysis for Coke Resistance. *Catalysts*, 10(9):1043, sep 2020.

[33] Walter Kohn, Yigal Meir, and Dmitrii E. Makarov. Van der waals energies in density functional theory. *Phys. Rev. Lett.*, 80(19):4153–4156, 1998.

[34] Tanja Van Mourik and Robert J. Gdanitz. A critical note on density functional theory studies on rare-gas dimers. *J. Chem. Phys.*, 116(22):9620–9623, 2002.

[35] Claire Pétuya, Ludovic Martin-Gondre, Philippe Aurel, Françoise Damay, and Arnaud Desmedt. Unraveling the metastability of the SI and SII carbon monoxide hydrate with a combined DFT-neutron diffraction investigation. *J. Chem. Phys.*, 150(18), 2019.

[36] Thomas M Vlasic, Phillip D Servio, and Alejandro D Rey. Infrared Spectra of Gas Hydrates from First-Principles. *J. Phys. Chem. B*, 123(4):936–947, 2019.

[37] Xiaoxiao Cao, Yingying Huang, Xue Jiang, Yan Su, and Jijun Zhao. Phase diagram of water-methane by first-principles thermodynamics: Discovery of MH-IV and MH-V hydrates. *Phys. Chem. Chem. Phys.*, 19(24):15996–16002, 2017.

[38] Kyuho Lee, Éamonn D. Murray, Lingzhu Kong, Bengt I. Lundqvist, and David C. Langreth. Higher-accuracy van der Waals density functional. *Phys. Rev. B - Condens. Matter Mater. Phys.*, 82(8):1–14, 2010.

[39] Jinxiang Liu, Jian Hou, Jiafang Xu, Haiying Liu, Gang Chen, and Jun Zhang. Ab initio study of the molecular hydrogen occupancy in pure H2 and binary H2-THF clathrate hydrates. *Int. J. Hydrogen Energy*, 42(27):17136–17143, 2017.

[40] Ping Guo, Yi Long Qiu, Long Long Li, Qiang Luo, Jian Fei Zhao, and Yi Kun Pan. Density functional theory study of structural stability for gas hydrate. *Chinese Phys. B*, 27(4), 2018.

[41] Stephen J. Cox, Michael D. Towler, Dario Alfè, and Angelos Michaelides. Benchmarking the performance of density functional theory and point charge force fields in their description of sI methane hydrate against diffusion Monte Carlo. *J. Chem. Phys.*, 140(17), 2014.

Chapter 4

Revealing Zeolites Active Sites Role as Kinetic Hydrate Promoters: Combined Computational and Experimental Study

*Curiosity – the rover and the concept – is what science is all about: the quest to **reveal** the unknown.*

-Ahmed Zewail

Clathrate hydrates are emerging as a novel storage medium for safe and compact methane storage[1]. However, their industrial-scale applicability is hindered by relatively lower gas uptake and sluggish formation kinetics. In this study, we have employed zeolites with acidic (H-Y, FAU-type) and basic (Na-X, FAU-type) surface properties as kinetic hydrate promoters (KHPs). The impact of physical parameters as pressure and the gas-to-liquid ratio has also been studied. In a combined experimental and computational study, we assessed the performance of the two types of zeolites in different concentrations and pressures for binary CH_4-THF clathrate hydrate synthesis in a non-stirred configuration. The kinetic study results showed that the acidic zeolite (H-Y) exhibited superior performance over the basic one (Na-X), reaching its optimum at 0.5 wt% zeolite, which agreed well with the DFT calculations. The methane conversion reached 94.25% at this concentration and a relatively mild pressure (6 MP). The induction time and t_{90}

(time to reach 90% of final gas uptake) were reduced by 35% and 31%, respectively. Our results open the door for a better understanding of the role of acidic zeolites as possible environmental benign KHPs that can help the utilization of water as a medium for green energy storage and transportation[1].

4.1 Introduction

The international direction toward cleaner energy resources and the increasing world population have created a strong demand for natural gas as energy source and feed for the petrochemical industry. Moreover, the natural gas is considered a "transition fuel" with cleaner-burning that represents a good compromise between conventional fossil fuels such as coal and oil. Thus there is an increasing demand for safe and long-term methane storage technology [1, 2]. There are several methods and technologies to store natural gas, and each has its advantages and disadvantages. Apart from storing natural gas in underground inventories, the main natural gas storage and transportation technologies are CNG (compressed natural gas), LNG (liquified natural gas), ANG (adsorbed natural gas), and SNG (solidified natural gas). SNG is a new technology for safe, eco-friendly, reversible, compact, and economic methane storage that can be suitable for both large reservoirs and discrete, small, inaccessible, or remote gas resources [3–7].

Despite these advantages, the applications of hydrate-based technology on an industrial scale are limited due to the slow kinetics, poor heat transfer, gas diffusion limitation, lower storage capacity in the presence of promoter, and scale-up challenges. Promoters are additives added to either catalyze the kinetics of hydrate formation (kinetic hydrate promoter or KHP) or reduce the P-T requirements (thermodynamic hydrate promoter or THP). Understanding the kinetic model of hydrate formation is essential for developing potential applications of hydrates [8]. However, it is challenging to model the kinetics as it combines a chemical reaction with phase transition. Above all, it is crucial to increase the rate of gas hydrate formation for feasible

[1]This chapter is based on the following article: *Omran A., Nesterenko N., & Valtchev V.* Revealing Zeolites Active Sites Role as Kinetic Hydrate Promoters: Combined Computational and Experimental Study. ACS Sustainable Chemistry & Engineering. 2022 Jun 9;12 (24):8002–8010.

gas storage and separation process. The crystallization process can be divided into two main steps: nucleation and growth. In the first step, a crystalline phase appears gradually directly from the liquid state (homogeneous nucleation) or occurs at nucleation sites of foreign particles or surfaces (heterogeneous nucleation) [9]. This step is usually slow, distinguished by its stochastic nature [10]. After adsorption of guest molecules in the liquid phase, it is enclathrated within the hydrate precursors, and nucleation then can be detected from the simultaneous rapid pressure decrease and temperature increase due to the exothermic reaction. The time elapsed until the appearance of a detectable volume of hydrate phase or, equivalently, until the consumption of a detectable number of gas molecules is known as induction time (or lag time) [11]. In the second step, the crystal growth is distinguished by a rapid increase in the particle size up to the full crystalline form. This step is immediate, and the gas is more concentrated in the hydrate cages than those in the vapor [12]. Well-control of growth step enhances the gas diffusion that may be hindered by'hydrate film' formation at the liquid-gas interface [5, 13].

To solve the problem of slow kinetics, KHP is added to enhance the rate of hydrate formation without influencing thermodynamics. In other words, the hydrate structure, as well as the *P-T* conditions of hydrate formation, are not affected. This kind of promoters is predominated by surfactants with all its classes (anionic, cationic and non-ionic) [14]. The most common example of those surfactants is the anionic surfactant sodium dodecyl sulfate (SDS) which has extensively been studied [15–17]. In a concentration close to or above its critical micelle concentration (CMC), it is observed that SDS increased the hydrate formation rate significantly compared to other surfactants [18]. The surfactant micelles increase methane solubility and thus initiating the nucleation [17]. Moreover, Zhang *et al.* explained that SDS increases the hydrate particles' surface area and the gas-liquid interfacial area while reducing surface tension [19]. Increasing the carbon chain length of sodium alkyl sulfates does not change the kinetics of the reaction, but requires much less surfactant concentration [20, 21]. However, the hydrate-based process suffers from foam formation, especially during gas recovery (hydrate dissociation) in pilot-scale laboratory experiments [22–24]. Adding this disadvantage to the environmental concerns of surfactant separation or degradation, makes the use them not very

attractive for a large industrial scale application. To overcome those drawbacks, other KHPs are suggested, such as porous materials.

Porous materials such as carbon forms (such as activated carbon and carbon nanotubes) and silica in different shapes (silica gel, silica sand, hollow silica, and nano-silica), zeolites, and even MOFs were used to promote hydrate formation [25, 26]. In general, these materials can be utilized in two different ways: (1) in low concentrations as nucleation sites for heterogeneous nucleation to reduce the induction time [27] and (2) as host for hydrate using the confinement effect to enable mild hydrate formation conditions [28]. Each of these two uses has its advantages and disadvantages. The use of porous materials as nucleation sites is relatively cheaper, easier to handle [29], and has higher overall gravimetric storage. However, it may suffer from slower kinetics and relatively higher thermodynamic requirements. On the other hand, the use of porous materials as a confinement medium has been proved to reduce the driving force and increase the water-to-hydrate conversion [30]. However, the high mass of porous material and complicated packing (or pelletizing) process results in a storage capacity loss[31]. Recently, pelletizing natural has been considered as a promising option for SNG transportation in many pilot plants. While they provide more flexiblibilty to transfer different quantities of solid hydrates, they add capital cost overhead due to the associated energy consumption, gas recycling and pellet dewatering processes [5].

The use of porous material as nucleation sites at low concentrations is the main focus of this article. In this approach, the porous material increases the surface area by adding another interface (or surface) that facilitates gas diffusion and crystallization [32]. Although most relevant studies showed that porous material improved the kinetic performance [33–38] , SDS is still added to get acceptable results when the conditions tested were near ambient conditions [39].

Despite their practical advantages, such as stability, large surface area, tunable acidity, and low cost, few studies investigated the use of zeolites for that purpose. For example, Xiaoya *et*

al. has tested for zeolite 3A for CH_4-THF hydrate formation and concluded that it enhanced the formation rate [40]. In 2009, the same group studied the gas storage in LTA-type zeolite (3A and 5A) in the presence and absence of SDS. They concluded that the promotion effect on hydrate formation of 3A zeolite was much more obvious than that of 5A zeolite when both zeolites are used at concentrations of 0.033 and 0.067 wt% [41]. However, the authors had to add also 0.067 wt% SDS to the initial mixture to get satisfactory kinetic performance and gas uptake. Kim *et al.* showed zeolite 13X (FAU-type) at 0.01 wt% concentration showed higher gas consumption than SDS and LTA-type zeolites, making it the most promising zeolite as KHP. The author attributed that to the small particle size and large pore diameter of 13X compared to the other zeolites studied [42]. The advantage of using the above porous materials is that they are cheap, used in low concentration, can be easily separated, and above all, they are environmentally friendly. However, a significant kinetic and gas uptake performance drop upon increasing the zeolite concentration above 0.01 wt% was observed, which remained unexplained. Other zeolites such as RHO [43], SSZ-13[26] were also studied in the confinement approach as described above, but the methane hydrate kinetic data were not reported.

In contrast with KHP, which does not intervene with thermodynamic conditions, THP shifts the hydrate formation equilibrium condition to milder *P-T*, lowering the energy requirements. Depending on the promoter, the hydrate nature may vary, but sII or sH structure types are usually obtained. The most common structure II hydrate promoter is tetrahydrofuran (THF), which is a hydrate former by itself [44]. THF is also reported to improve the kinetics either as standalone or with SDS [45–48]. Other sII formers such as cyclopentane [49], dioxlane [50], acetone [51], and others were reported in the literature [52] but showed lower performance than THF. A more comprehensive review of various promoters studies (KHP and THP) can be found in the literature [14]. The main drawback of using THP is the reduction in methane uptake compared to sI. The main reason behind that decrease is that those promoters occupy the sII or sH large cages while stabilizing the structure. However, the reduction of formation conditions closer to ambient temperatures can significantly offset that storage capacity reduction. For example, it is estimated that compression cost is approximately 70-80% of the total cost of methane hydrate

formation in a large-scale reactor of 25 L [53]. Increasing the methane formation temperature from 274.2 K to 293.2 will reduce 80% of the cooling cost as estimated by Veluswamy *et al.* [54]. Finally, we have chosen to do experiments in a non-stirring tank reactor which proved to have a higher yield while removing the additional cost of agitation. In fact, as the slurry becomes thicker, mechanical power/energy consumption will not be economical [55]. Thus, the non-stirring approach will make it easy to adopt this technology for large-scale gas storage systems[56].

The primary objective of this study was to assess the performance of environmentally benign acidic (H-Y)and basic (Na-X) zeolites, , in concentrations up to 0.5 wt%, in binary methane-THF hydrate formation. Another important objective of this study was evaluating the effects of gas-to-liquid ratio and pressure on methane hydrate at a high temperature (283.2 K). Moreover, we explored the effect of hydrophobicity, extra framework cation, and acidity of zeolites on their role as kinetic hydrate promoters. To the best of our knowledge, the latter two properties have not been explored in previous studies in that specific area. Finally, we used ab initio DFT calculation to examine the effect of the extraframework cation on hydrate formation.

4.2 Experimental Section

4.2.1 Material and apparatus

Methane (99.99% purity) was purchased from Linde Co., Tetrahyrofuran (THF, AR grade 99.99%) from Alfa Aesar, Na-X (Molecular Sieve Union Carbide Type 13X) from Fluka AG; and zeolite Y zeolite was offered by UOP. Deionized water was used in all experiments . The acidic form of zeolite Y (H-Y) was prepared by 5 consecutive exchanges of Na-Y with 10 wt% NH_4NO_3 and calcination at 450°C for 4 hours. The zeolite Na-X was used without modifications. The solution THF (5.56 mol%) solution or the mix of 5.56 mol% THF with zeolite was prepared in a volumetric flask. Full description of the apparatus used for methane hydrate formation and dissociation experiments is shown with details at supporting information.

4.2.2 Characterization Methods

The zeolite powders were characterized using powder X-ray diffraction (PXRD), scanning electron microscope (SEM), inductively coupled-atomic plasma emission spectroscopy (ICP-AES), scanning electron microscopy (SEM) equipped with energy dispersive X-ray (EDX), N_2-adsorption, and IR spectroscopy. The synthesized binary CH_4-THF hydrate was characterized with PXRD and Raman spectroscopy. Methods, procedures, calculations, and equipment are detailed in the supporting information.

4.2.3 Hydrate formation experiment

The reactor was filled with the required level of solution and sealed. Then, it was purged three times with N_2 and then with methane to ensure air removal from the system. After reaching the target 283.2 K temperature, (the target pressure was achieved; their values were recorded every 10 sec with the DAQ system. The time period between this starting point and the formation of the first hydrate crystal is referred to as induction time. The induction time was determined by a simultaneous pressure drop and temperature increase due to the exothermic nature of the hydrate formation. As the reaction continues, the pressure drops further, and the hydrate formation process is considered complete when there is no further drop for 1 h. All experiment were conducted at least 3 time and average results are reported. The number of moles of the gas consumed at any time t ($\Delta n_{H\downarrow}$) is equal to the difference between the number of moles of the gas $n_{H,0}$ at time ≒0 (i.e. the start of the experiment) and the number of moles of the gas present $n_{H,t}$ at any time t in the vessel as shown by Eq.(C.1):

$$\Delta n_{H\downarrow} = n_{H_0} - n_{H_t} = \left(\frac{PV}{zRT}\right)_{G_0} - \left(\frac{PV}{zRT}\right)_{G_t} \tag{4.1}$$

Subscript G_0 and G_t represent the gas phase at the start of the experiment and time t, respectively. Here, P, T, and V are the pressure, temperature, and reactor volume, respectively. R is the universal gas constant, and z is the comprehensibility factor calculated by Pitzer's correction [57].

Normalized methane gas uptake is calculated by the following Eq.(C.2):

$$Normalized \quad uptake \quad = \frac{\Delta n_{H\downarrow}}{n_{H_2O}} \tag{4.2}$$

Water-to-hydrate conversion, methane gas conversion as well as methane recovery percentage calculations are detailed in supporting information.

4.2.4 Computational Methods

We performed density functional theory (DFT) calculations [58] using the projected augmented wave (PAW) method and the standard pseudopotentials supplied by Quantum Espresso (QE) software [59–61]. Full description of the hydrate-zeolites systems as well as calculation details are shown in supporting information.

4.3 Results and discussion

4.3.1 Zeolite Promoters and Hydrate Characterization

N_2-adsorption measurements, PXRD, and SEM images confirmed the crystal structures of Na-X and H-Y zeolites. ICP-AES and EDX revealed that while Na-X zeolite maintained high concentration of sodium, most of the sodium extra framework cation has been exchanged, and Si/Al ratio of H-Y is 2.7 compared to 1.2 in the case of Na-X. The acidity of the H-Y zeolite and of the Na-X zeolite were determined via IR and Pyridine TPD (temperature programmed desorption). For hydrate characterization, we first confirmed sII formation using PXRD analysis. In addition, Raman spectroscopic measurements on the synthesized binary hydrate were performed. Spectroscopic data revealed methane occupancy in 5^{12} small cages of sII as a sharp peak at $\sim$ 2911.1 cm^{-1}. Detailed zeolite promoter and hydrate characterization results are provided in supporting information.

4.3.2 Effect of Reactor Level and Pressure

It is well-known that the hydrates tend to nucleate in the gas-water interface and then grow into the water bulk phase. The first set of experiments was performed with the aim to determine the effect of liquid/gas level on the gas uptake and conversion at 6 MPa and 283.22 K. During that process, the volume expansion due to hydrate growth causes the formation of a thin hydrate layer. It consumes the excess gas via diffusive transport[62]. Previous experimental observations showed that the molar liquid water-gas ratio significantly affects methane hydrates' nucleation and growth [63]. Recently, Burla and Pinnelli dedicated their study to investigate the effect liquid water–gas ratio on hydrate kinetics and storage capacity. They found that gas uptake gradually increases with the solution volume and then falls after an optimum threshold point [64]. Therefore, we systematically increased the level of THF aqueous solution without the use of any promoter to obtain the optimum uptake. As shown in **Figure 4.1**, the normalized methane gas uptake initially increased with increasing the THF solution level. After reaching an optimum level of about 53%, the amount of gas uptake decreased significantly with the increasing solution level. Similarly, the conversion followed the same trend and reached its optimum ($\approx 90\%$) at a liquid level slightly above half. Such a high conversion is important from a technical and economic point of view as it reduces the energy need to recycle that unconverted excess gas. Thus, if well-optimized, such a slight positive pressure of 2-4 bar can be used as a gas preservation blanket above the hydrate for long-term storage without further processing. The above results can be explained as follow. Initially, when there is excess gas, the rapid growth consumes the gas dissolved. Then, as the volume increases, the diffusive transport increases until a certain optimum level at which the gas uptake reaches its maximum. After that, the gas consumption decreases gradually with further solution increase. On the other hand, when there is excess THF aqueous solution, the less uptake is due to the less initial gas volume, and thus the overall gas uptake drops. Based on that, it is important to fill the reactors slightly above half of their volumetric capacity to gain the highest possible uptake, which agrees well with previous experimental observations [65, 66]. In order to increase the gas uptake and conversion, we examined two approaches: (1) introducing higher pressure (i.e., higher driving force) and (2) using a zeolite as KHP.

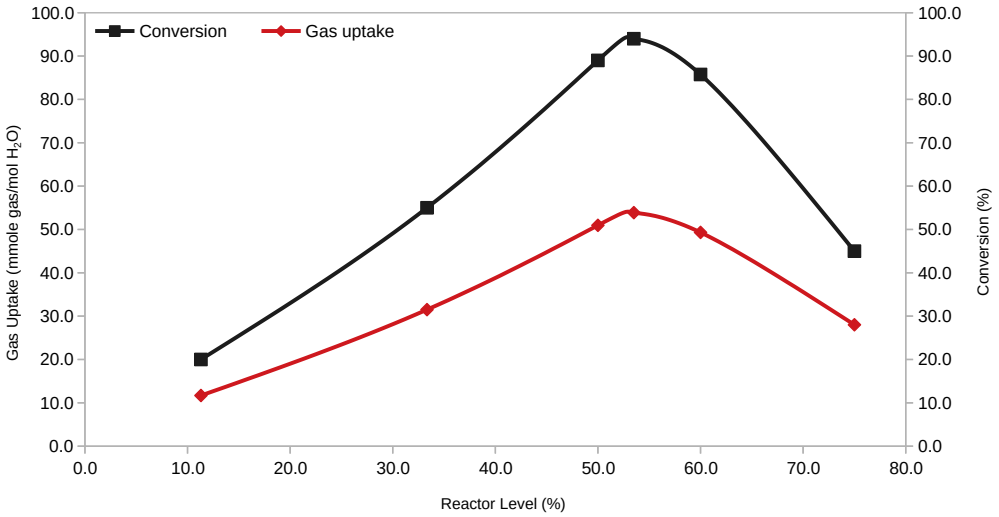

Figure 4.1: Effect of THF aqueous solution level on the gas uptake (in red) and conversion (in black) at 6 MPa.

in situ Raman showed that it had been observed that increasing the pressure would result in increasing the small cage occupancy in CH_4-THF binary hydrates [67, 68].Accordingly, we conducted experiments at pressures of 6, 7 and 8 MPa at the same temperature (283.2 K). These conditions are selected to reach the phase boundary conditions for CH_4-THF sII. As we used the same concentration of THF, we expect no change of system equilibrium due to THF composition variation and the only effect came from pressure variation as agreed in literature [39]. **Figure A.10** reports the gas uptake and conversion for blank THF aqueous solution at different pressures. One can observe that the increase in gas uptake is insignificant when the pressure increases from 6 to 7 MPa. On the contrary, increasing the pressure from 7 to 8 MPa resulted in a slight decline in gas uptake. Noteworthy, the gradual decrease of pressure from 8 to 6 MPa resulted in a significant increase in the gas conversion. The gas conversion increased from 59% to 90% when the pressure decreased from 8 MPa to 6 MPa. Thus, despite the decrease in induction time, as shown in **Table A.4 and Figure A.12** , trying to populate the small cages of (5^{12}) with methane molecules by increasing the pressure did not result in the expected increase of final gas uptake or conversion as reported **Figure 4.2**. These results indicate that increasing the pressure shorted the reaction time and did not allow methane molecules to diffuse to the majority of bulk THF solution that remained inaccessible for hydrate conversion. Hence, we employed the zeolites as KHPs at different pressures to get the appropriate trade-off between slow kinetics and gas uptake.

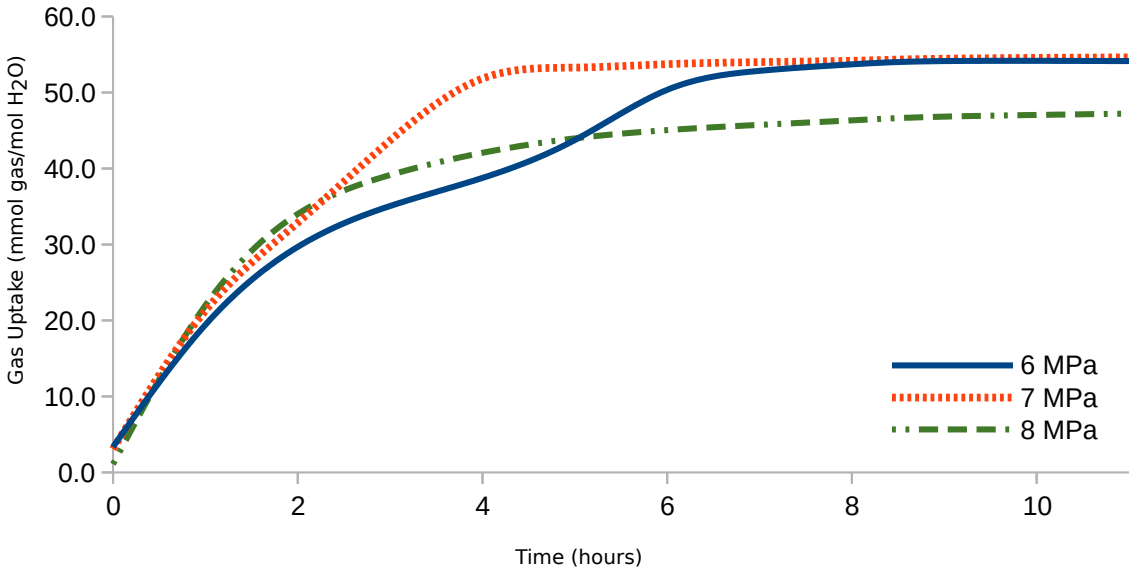

Figure 4.2: Methane uptake profiles during the hydrate formation after hydrate nucleation at 6 MPa (dark blue), 7MPa(orange), and 8 MPa(green) and 283.2 K.

4.3.3 Influence of Zeolite Kinetic Promoters

To study the kinetic performance, zeolite Na-X has been initially tested at various concentrations and pressure. Generally, the presence of Na-X zeolite increased the induction time and t_{90} compared to blank THF. For example, after adding 0.225 wt% to the THF aquous solution the induction time of hydrate formation at 8 MPa from 7.3 min to 17 min. For instance, using a concentration as low as 0.01 wt% of Na-X to test the hydrate formation at 7 MPa increased the induction time from 19.3 min to 47.3 min while the t_{90} increased by 47%. Such an increase is also associated with less conversion and gas uptake. This reduction trend in gas uptake, and conversion persists at 6 MPa despite the reduction of t_{90} as shown in **Table A.4** and **Table 4.1**.

Increasing the concentration of Na-X zeolite from 0.01 to 0.5% w/v at 7 MPa and 283.2 K, the kinetic performance and gas uptake has been significantly reduced (**Figure A.11**). Those reductions in gas uptake agree with Kim *et al.* [42] for sI methane hydrate when Na-X promoter concentration increased slightly above 0.01 wt%. A possible reason for such a behavior could be the presence of sodium as an extra framework cation. It is well-known that hard cations such as sodium strongly bind to water molecules breaking the intermolecular hydrogen bonds and thus causing the intrinsic water network to collapse [69]. This observation agrees with the experimental studies showing that Na-X act as hydrate inhibitors even at low concentrations [70]. In addition to the sodium cation, the relatively lower Si/Al ratio resulted in a more hydrophilic

Table 4.1: Average data for binary CH_4-THF Hydrate formation at different zeolite concentrations and pressures at 283.2 K.

System No.	Zeolite Conc.% w/v)	P (MPa)	Induction time(min)	Gas uptake(mmol gas/mol H_2O)[a]	Gas Conversion(%)[b]	Hydrate Yield (%)	t_{90} (min)	% Recovery[b]
X-255-80	0.255	80	17.0(±5.2)	48.68	60.70(±3.22)	41.37	257(±17)	97.40
X-001-70	0.01	70	47.3(±10.5)	49.64	72.47(±1.24)	42.19	339(±19)	96.41
X-225-70	0.255	70	110.3(±17.3)	41.20	71.88(±1.35)	23.37	387(±27)	96.10
X-500-70	0.5	70	141.2(±24.7)	8.41	12.28(±2.85)	7.15	474(±48)	96.39
X-500-60	0.5	60	53.8(±12.4)	48.95	85.38(±2.78)	41.61	295(±37)	97.70
Y-500-60	0.5	60	17.0(±3.8)	54.00	94.25(±1.47)	45.94	320(±9)	96.59
Y-255-60	0.225	60	20.0(±2.4)	51.98	90.67(±1.92)	44.19	312(±16)	97.02
Y-001-60	0.01	60	24.2(±4.7)	52.67	91.87(±0.76)	44.78	327(±31)	96.24
Y-255-70	0.225	70	11.8(±1.8)	53.54	78.18(±3.49)	45.51	218(±12)	95.83
Y-001-80	0.01	80	8.5(±2.2)	57.54	71.75(±1.33)	48.91	248(±28)	96.12
Y-255-80	0.225	80	2.5(±1.3)	57.16	71.29(±1.78)	32.41	235(±18)	95.40
Y-500-80	0.5	80	1.3(±3.5)	59.95	74.76(±1.65)	50.96	257(±25)	95.51

[a] average results of gas uptake varied within ±0.42 mmol

[b] average results of hydrate yield and %recovery varied within ± 4.17% and ±1.35 %, respectively.

nature and electrostatic structure that can reduce the water activity coefficient [11] and thus ultimately cause thermodynamic inhibition of hydrate formation. Consequently, the inhibiting effect is expected to increase with increasing the zeolite concentration.

To verify such an assumption, we have explored the acidic form of zeolite Y for hydrate formation in different concentrations and pressures, as shown in **Table 4.1**. At 8 MPa, an obvious increase in the gas uptake and water-to-hydrate conversion compared to the blank THF aqueous solution at the same pressure is observed. The raise of zeolite concentration from 0.01 wt% to 0.5 wt% results in a high gas uptake and methane conversion; despite a minor decrease in induction time. The slight increase in t_{90} is probably due to the additional time for higher gas uptake. After decreasing the pressure to 7 MPa, we observed a significant reduction in the induction time and t_{90}. However, there was no significant effect on the gas uptake or hydrate conversion relative to 8 MPa. At 6 MP, the optimum methane gas conversion of $\approx$ 94.25% along with high gas uptake could be achieved. Unlike Na-X zeolite, the increasing H-Y concentration at both 6 MPa and 8 MPa did not affect the relatively high conversion and gas uptake that was either maintained or even increased. The increase of storage capacity could be attributed to the removal of sodium cations from Y-54 zeolite and its acidity and higher hydrophobicity. It

has been shown that the presence of acidic additives, such as perchloric acid ($HClO_4$), modify the THF sII hydrates flexibility [71] by increasing gas insertion and improving the gas diffusion coefficient [72]. Thus, zeolites can be an excellent alternative to such extremely corrosive additives from environmental, safety, and economic points of view. Moreover, the adsorption involves specific interaction between the water molecule and the hydrophilic centers in zeolite, which can be either a silanol group or a cation associated with the tetrahedrally coordinated aluminum [73]. Nguyen and Nguyen demonstrated that the moderate hydrophobicity of additive results in organizing the surrounding water into a clathrate-like structure and thereby promotes hydrate formation [69]. Recently, Denning *et al.* demonstrated that the more hydrophobic SSZ-13 (Si/Al ratio = 20) promoted 2.6 more hydrate growth than the hydrophilic SAPO-34 (Si/Al ratio = 0.6) [26]. Thus, the absence of soduim cation and the higher Si/Al ratio of H-Y resulted in enhanced hydrophobicity. Along with the additional gas-to-water contact area indicated by the higher S_{ext} compared to Na-X, such hydrophobicity nature improved better orientation of water molecule for hydrate formation.

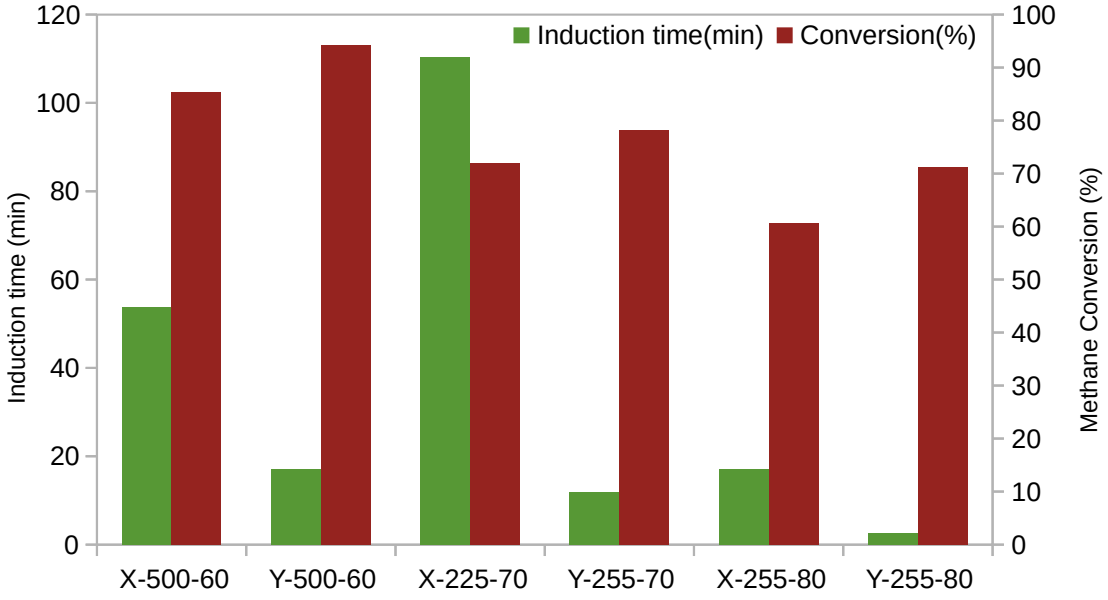

Figure 4.3: Average data of the effect equal concentrations of Na-X and H-Y zeolite promoters on the induction time (in green) and methane conversion (in dark red) of 5.56 mol% THF solution at different pressures (6-8 MPa). All experiments are conducted at 283.2 K.(For interpretation of the references to colour in this figure legend, the reader is referred to the web version of this article.)

In addition to the high gas uptake and conversion, the induction time and t_{90} have been reduced

significantly by 35% and 31% compared to blank THF aqueous solution,respectively. Similar concentrations of both zeolites were used for direct comparison at two different pressures. In all cases, H-Y outperforms Na-X kinetics at all pressures and concentrations, as shown in **Figure 5.3**. For example, at 7 MPa and a concentration of 0.255 wt%, the acidic zeolite increased gas uptake by about 30% compared to Na-X. Similarly, at 6 MPa and 0.5% w/v, the induction time is reduced 3 times in the case of H-Y compared to Na-X. In fact, Na-X showed a rather inhibiting effect at such a relatively high concentration, and the t_{90} has been reduced. The latter observation can be explained by the less gas uptake and conversion, which required less reaction time. Moreover, the positive effect of H-Y zeolite on the gas uptake could outperform SDS reported in the literature [65] at same or even lower concentrations and pressures as shown in **Figure A.13**.

To shed light on the molecular level reactions leading to these results, we have utilized DFT calculations. Recently, *ab initio* DFT calculations have been commonly used to determine the promoting or inhibiting effect of different additives on hydrate formation[74]. In this study, DFT was employed to analyze zeolite-hydrate systems in terms of 5^{12} hydrate cage energies and geometrical changes upon their interaction with finite zeolite clusters. In addition, the energetic of host-guest cage system was calculated in the presence or absence of the zeolite KHPs. The optimized geometry of $CH_4@5^{12}$ cage is shown in **Figure A.2**. The host-guest interactions are a key property that characterizes the clathrate stability [75] and can be assessed through interaction energy (ΔE^{HG}). This energy can be defined as follow:

$$\Delta E^{HG} = E(CH_4@5^{12}) - [E(CH_4) + E(5^{12})] \tag{4.3}$$

where $E(CH_4@5^{12})$, $E(CH_4)$, and $E(5^{12})$ are the energies of $CH_4@5^{12}$, methane molecule and the 5^{12} empty cage, respectively. Weak interactions such as H-bonding van der Waals forces dominate the hydrate and zeolite systems interaction.

Thus, we initially calculated the interaction energy of methane with small cage with revPBE and vdW-DF2 levels of theory. The values were +2.03 and -27.78 kJ/mol for revPBE and vdW-DF2 levels, respectively. Notably, while revPBE failed to accurately determine the host-

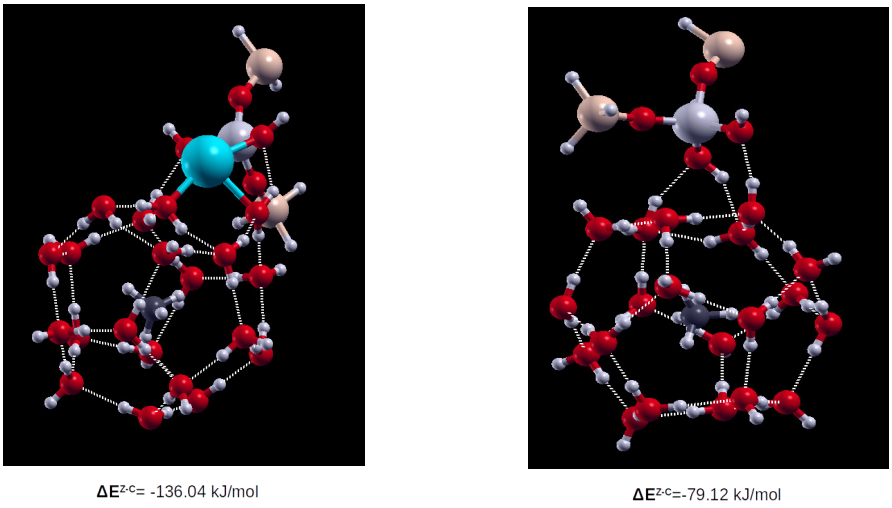

(a) Na-X **(b)** H-Y

Figure 4.4: Optimized configurations of small (5^{12}) cage with zeolite clusters of (a) Na-X and (b) H-Y . Sodium, silicon, and aluminum atoms are shown in light blue, brown, and grey colors, respectively.

guest interactions, the small difference between the value obtained from vdW-DF2 and the previously reported value of -32.55 kJ/mol at the highly accurate MP2/6-311++G(d,p) level[75] emphasized the quality of vdW-DF2 level in describing the host-guest interaction, and thus we had used it for all calculations. The optimized zeolite-cage structures are shown in **Figure 4.4**. Two types of interaction energies can be defined. The first one assesses the degree of zeolite-clathrate interactions ($\Delta E^{Z\text{-}C}$) and is defined as follow:

$$\Delta E^{Z\text{-}C} = E(Z\text{-}CH_4@5^{12}) - [E(Z) + E(CH_4@5^{12})] \tag{4.4}$$

where $\Delta E^{Z\text{-}C}$ and E(Z) are the energy of the optimized Z-$CH_4@5^{12}$ structure and isolated zeolite cluster, respectively. In this case, the more negative interaction energy between a host water molecule and the additive molecule indicates more attractive interaction or inhibitory effect [76]. The second type considers the effect of promoter host-guest interactions as calculated from (ΔE^{HG}) and eq (4.3) to get insights into the relative stability of hydrate cages in the presence and absence of zeolite promoters. This is achieved by taking into account the new arrangement of $CH_4@5^{12}$ upon interaction with zeolite. For that, single-point potential energy calculations were performed over different filled cages of $CH_4@5^{12}$ using their coordinates obtained from the optimized Z-$CH_4@5^{12}$ systems. The optimized geometries and calculated

values of $\Delta E^{Z\text{-}C}$ are illustrated in **Figure 4.4**.

While the value for Na-X zeolite is -136.04 kJ/mol, H-Y showed only -79.12 kJ/mol. The high value in the case of Na-X indicates that the zeolite binding to the clathrate cage is much stronger and thus disturbs the hydrate growth, which is attributed to the presence of sodium cation. The comparison of the optimized cage structured shown in **Figure A.14** confirms this conclusion. Clearly, the cage structure in the case of zeolite H-Y is kept intact compared to that of Na-X. This is reflected in the relative ΔE^{HG} in the presence and absence of zeolite promoter. The energy values of optimized methane cages for zeolite Na-X and H-Y are +39.56 and +15.44 kJ/mol, respectively. The higher value in the case of Na-X showed that the hydrate cage structure is destabilized. In summary, the interaction of zeolite with clathrate cage determines their function as heterogeneous nucleation sites and thus as KHPs.

The zeolite efficiency as KHP is highly affected by the (1) presence of extra framework cations, (2) zeolite hydrophobicity, and (3) acidity. The effect of H-Y zeolite particles as nucleation sites that enhance heterogeneous nucleation prevailed as the hydrophobic acidic zeolite helped the water surrounding molecules to arrange for hydrate formation and promoted further cage growth. On the other hand, the Na-X zeolite strongly binds to the clathrate cage and disturbs the hydrate growth due to sodium cation and higher hydrophilicity. Moreover, increasing the concentration Na-X zeolite makes their electrostatic interaction that restricts water molecule orientation prevails over their promoting role as a nucleation site and results in both delay in induction time and reduction of gas uptake.

4.4 Conclusions

The aim presented study is to provide a fundamental understanding of the role of zeolite as a kinetic hydrate promoter for hydrate formation at different pressures from both molecular and macroscopic levels. To achieve that, we have used combined experimental and computational techniques to compare the performance of two zeolites of FAU-type typology: Na-X and H-Y.

The effect of liquid-to-gas ratio and initial pressure on CH_4-THF hydrate formation at 283.2 K was studied. The set of results showed that the maximum conversion and gas uptake can be achieved at 53% liquid level and 6 MPa in a non-stirred tank reactor. While increasing the pressure could reduce the induction time, the gas uptake was not significantly improved, and the gas conversion was reduced. Similarly, we have found that the conversion and gas uptake is maximized at the optimum THF aqueous level at a certain pressure. Below that level, the rapid formation of thin hydrate shell hinder the excess gas diffusion and reduce the normalized gas uptake. Similarly, going above that level will also reduce the normalized gas uptake due to the excess solution and reduced initial gas volume. In the present study we have also revealed the effect of zeolite extra framework cation and surface acidity on their performance as KHPs. Our results show that increasing the Na-X concentration above 0.01 wt% has negatively affected the kinetic and reduced gas uptake and conversion. The DFT calculations showed that the sodium cation and higher hydrophilicity in Na-X zeolite destabilize the hydrate cage and thus negatively impact hydrates formation. On the other hand, the acidic and more hydrophobic H-Y showed excellent performance as KHPs. A gas uptake of 54 mmol gas/mol H_2O, methane gas conversion of 94.25%, and recovery as high as 96.59% could be achieved using 0.5 wt% H-Y at 6 MPa. Such results show the promising perspective to use zeolites as KHPs and shed light on the hydrate nucleation mechanism.

References

[1] Reza Hafezi, Amir Naser Akhavan, Saeed Pakseresht, and David A. Wood. Global natural gas demand to 2025: A learning scenario development model. *Energy*, 224:120167, 2021.

[2] Ahmed Omran, Sun Hee Yoon, Murtaza Khan, Minhaj Ghouri, Anjaneyulu Chatla, and Nimir Elbashir. Mechanistic insights for dry reforming of methane on cu/ni bimetallic catalysts: DFT-assisted microkinetic analysis for coke resistance. *Catalysts*, 10(9):1–16, 2020.

[3] J. S. Gudmundsson, Mahmut Parlaktuna, and A. A. Khokhar. Storing natural gas as frozen hydrate. *SPE Prod. Facil.*, 9(1):69–73, 1994.

[4] B. P. Prajwal and K. G. Ayappa. Evaluating methane storage targets: From powder samples to onboard storage systems. *Adsorption*, 20(5-6):769–776, 2014.

[5] Hari Prakash Veluswamy, Asheesh Kumar, Yutaek Seo, Ju Dong Lee, and Praveen Linga. A review of solidified natural gas (SNG) technology for gas storage via clathrate hydrates. *Appl. Energy*, 216(February):262–285, 2018.

[6] Laura A. Pellegrini, Stefania Moioli, Fabio Brignoli, and Camilla Bellini. LNG technology: The weathering in above-ground storage tanks. *Ind. Eng. Chem. Res.*, 53(10):3931–3937, 2014.

[7] Younggy Shin and Yoon Pyo Lee. Design of a boil-off natural gas reliquefaction control system for LNG carriers. *Appl. Energy*, 86(1):37–44, 2009.

[8] Behzad Partoon and Jafar Javanmardi. Effect of Mixed Thermodynamic and Kinetic Hydrate Promoters on Methane Hydrate Phase Boundary and Formation Kinetics. *J. Chem. Eng. Data*, 58(3):501–509, 2013.

[9] Sebastien Bergeron, Juan G. Beltrán, and Phillip Servio. Reaction rate constant of methane clathrate formation. *Fuel*, 89(2):294–301, 2010.

[10] Zhen Pan, Yi Wu, Liyan Shang, Li Zhou, and Zhien Zhang. Progress in use of surfactant in nearly static conditions in natural gas hydrate formation. *Front. Energy*, 14(3):463–481, 2020.

[11] E. Dendy Sloan and Carolyn Ann Koh. *Clathrate hydrates of natural gases, thrid edition*. CRC Press, third edition, 2007.

[12] Kazuya Ozawa and Ryo Ohmura. Crystal Growth of Clathrate Hydrate with Methane plus Partially Water Soluble Large-Molecule Guest Compound. *Cryst. Growth Des.*, 19(3):1689–1694, 2019.

[13] Craig J. Taylor, Kelly T. Miller, Carolyn A. Koh, and E. Dendy Sloan. Macroscopic investigation of hydrate film growth at the hydrocarbon/water interface. *Chem. Eng. Sci.*, 62(23):6524–6533, 2007.

[14] Qazi Nasir, Humbul Suleman, and Yasir A Elsheikh. A review on the role and impact of various additives as promoters/ inhibitors for gas hydrate formation. *J. Nat. Gas Sci. Eng.*, 76(February):103211, 2020.

[15] Hesam Najibi, Morteza Mirzaee Shayegan, and Hassan Heidary. Experimental investigation of methane hydrate formation in the presence of copper oxide nanoparticles and SDS. *J. Nat. Gas Sci. Eng.*, 23:315–323, 2015.

[16] Zhen Pan, Zhiming Liu, Zhien Zhang, Liyan Shang, and Shihui Ma. Effect of silica sand size and saturation on methane hydrate formation in the presence of SDS. *J. Nat. Gas Sci. Eng.*, 56(February):266–280, 2018.

[17] Xiao-Yan Deng, Ying Yang, Dong-Liang Zhong, Xi-Yue Li, Bin-Bin Ge, and Jin Yan. New Insights into the Kinetics and Morphology of CO 2 Hydrate Formation in the Presence of Sodium Dodecyl Sulfate . *Energy & Fuels*, 35(17):13877–13888, 2021.

[18] Y. Zhong and R. E. Rogers. Surfactant effects on gas hydrate formation. *Chem. Eng. Sci.*, 55(19):4175–4187, 2000.

[19] J. S. Zhang, Sangyong Lee, and Jae W. Lee. Kinetics of methane hydrate formation from SDS solution. *Ind. Eng. Chem. Res.*, 46(19):6353–6359, 2007.

[20] Young Ah Kwon, Jong Mok Park, Kwang Eun Jeong, Chul Ung Kim, Tae Wan Kim, Ho Jeong Chae, Soon Yong Jeong, Jin Heong Yim, Young Kwon Park, and Ju dong Lee. Synthesis of anionic multichain type surfactant and its effect on methane gas hydrate formation. *J. Ind. Eng. Chem.*, 17(1):120–124, 2011.

[21] Yan He, Meng-Ting Sun, Chen Chen, Guodong Zhang, Kun Chao, Yan Lin, and Fei Wang. Surfactant-based Promotion to Gas Hydrate Formation for Energy Storage. *J. Mater. Chem. A*, 7(38):21634–21661, 2019.

[22] Gaurav Bhattacharjee, Vivek Barmecha, Omkar S. Kushwaha, and Rajnish Kumar. Kinetic promotion of methane hydrate formation by combining anionic and silicone surfactants: Scalability promise of methane storage due to prevention of foam formation. *J. Chem. Thermodyn.*, 117:248–255, 2018.

[23] Gaurav Pandey, Gaurav Bhattacharjee, Hari Prakash Veluswamy, Rajnish Kumar, Jitendra S. Sangwai, and Praveen Linga. Alleviation of Foam Formation in a Surfactant Driven Gas Hydrate System: Insights via a Detailed Morphological Study. *ACS Appl. Energy Mater.*, 1(12):6899–6911, 2018.

[24] W. X. Pang, G. J. Chen, A. Dandekar, C. Y. Sun, and C. L. Zhang. Experimental study on the scale-up effect of gas storage in the form of hydrate in a quiescent reactor. *Chem. Eng. Sci.*, 62(8):2198–2208, 2007.

[25] Lars Borchardt, Mirian Elizabeth Casco, and Joaquin Silvestre-Albero. Methane Hydrate in Confined Spaces: An Alternative Storage System. *ChemPhysChem*, 19(11):1298–1314, 2018.

[26] Shurraya Denning, Ahmad AA Majid, James M. Crawford, Moises A. Carreon, and Carolyn A. Koh. Promoting Methane Hydrate Formation for Natural Gas Storage over Chabazite Zeolites. *ACS Appl. Energy Mater.*, 4(11):13420–13424, 2021.

[27] Maninder Khurana, Zhenyuan Yin, and Praveen Linga. A review of clathrate hydrate nucleation. *ACS Sustain. Chem. Eng.*, 5(12):11176–11203, 2017.

[28] Praveen Linga, Nagu Daraboina, John A. Ripmeester, and Peter Englezos. Enhanced rate of gas hydrate formation in a fixed bed column filled with sand compared to a stirred vessel. *Chem. Eng. Sci.*, 68(1):617–623, 2012.

[29] Hiroko Mimachi, Masahiro Takahashi, Satoshi Takeya, Yoshito Gotoh, Akio Yoneyama, Kazuyuki Hyodo, Tohoru Takeda, and Tetsuro Murayama. Effect of Long-Term Storage and Thermal History on the Gas Content of Natural Gas Hydrate Pellets under Ambient Pressure. *Energy and Fuels*, 29(8):4827–4834, 2015.

[30] Avinash Kumar Both, Yurui Gao, Xiao Cheng Zeng, and Chin Li Cheung. Gas hydrates in confined space of nanoporous materials: New frontier in gas storage technology. *Nanoscale*, 13(16):7447–7470, 2021.

[31] Yang Peng, Vaiva Krungleviciute, Ibrahim Eryazici, Joseph T. Hupp, Omar K. Farha, and Taner Yildirim. Methane storage in metal-organic frameworks: Current records, surprise findings, and challenges. *J. Am. Chem. Soc.*, 135(32):11887–11894, 2013.

[32] S. B. Cha, H. Ouar, T. R. Wildeman, and E. D. Sloan. A third-surface effect on hydrate formation. *J. Phys. Chem.*, 92(23):6492–6494, 1988.

[33] Samer Said, Varun Govindaraj, Jean Michel Herri, Yamina Ouabbas, Mohamed Khodja, Mohamed Belloum, Jitendra S. Sangwai, and Ramamurthy Nagarajan. A study on the influence of nanofluids on gas hydrate formation kinetics and their potential: Application to the CO2 capture process. *J. Nat. Gas Sci. Eng.*, 32:95–108, 2016.

[34] Jae Woo Choi, Jin Tack Chung, and Yong Tae Kang. CO2 hydrate formation at atmospheric pressure using high efficiency absorbent and surfactants. *Energy*, 78:869–876, 2014.

[35] Zhen Pan, Zhiming Liu, Zhien Zhang, Liyan Shang, and Shihui Ma. Effect of silica sand size and saturation on methane hydrate formation in the presence of SDS. *J. Nat. Gas Sci. Eng.*, 56(February):266–280, 2018.

[36] Yanhong Wang, Xuemei Lang, and Shuanshi Fan. Accelerated nucleation of tetrahydrofuran (THF) hydrate in presence of ZIF-61. *J. Nat. Gas Chem.*, 21(3):299–301, 2012.

[37] Sarocha Rungrussamee, Katipot Inkong, Santi Kulprathipanja, and Pramoch Rangsunvigit. Comparative study of methane hydrate formation and dissociation with hollow silica and activated carbon. *Chem. Eng. Trans.*, 70:1519–1524, 2018.

[38] Guodong Zhang, Bingjie Liu, Lu Xu, Runcheng Zhang, Yan He, and Fei Wang. How porous surfaces influence the nucleation and growth of methane hydrates. *Fuel*, 291:120142, 2021.

[39] Katipot Inkong, Hari Prakash Veluswamy, Pramoch Rangsunvigit, Santi Kulprathipanja, and Praveen Linga. Innovative Approach to Enhance the Methane Hydrate Formation at Near-Ambient Temperature and Moderate Pressure for Gas Storage Applications. *Ind. Eng. Chem. Res.*, 58(49):22178–22192, 2019.

[40] Xiao Ya Zang, Shuan Shi Fan, De Qing Liang, Dong Liang Li, and Guang Jin Chen. Influence of 3A molecular sieve on tetrahydrofuran (THF) hydrate formation. *Sci. China, Ser. B Chem.*, 51(9):893–900, 2008.

[41] Xiaoya ZANG, Jianwei DU, Deqing LIANG, Shuanshi FAN, and Cuiping TANG. Influence of A-type Zeolite on Methane Hydrate Formation. *Chinese J. Chem. Eng.*, 17(5):854–859, 2009.

[42] Jun-Ho Hyun Nam-Jin Kim, Sung-Seek Park, Sang-Woong Shin and Wongee Chun. An experimental investigation into the effects of zeolites on the formation of methane hydrates. *Int. J. Energy Res.*, 39:26–32, 2015.

[43] Eduardo Andres-Garcia, Alla Dikhtiarenko, Francois Fauth, Joaquin Silvestre-Albero, Enrique V. Ramos-Fernández, Jorge Gascon, Avelino Corma, and Freek Kapteijn. Methane hydrates: Nucleation in microporous materials. *Chem. Eng. J.*, 360(October 2018):569–576, 2019.

[44] Do Youn Kim, Youngjune Park, and Huen Lee. Tuning clathrate hydrates: Application to hydrogen storage. *Catal. Today*, 120(3-4 SPEC. ISS.):257–261, 2007.

[45] Qiang Zhang, Junjie Zheng, Baoyong Zhang, and Praveen Linga. Coal mine gas separation of methane via clathrate hydrate process aided by tetrahydrofuran and amino acids. *Appl. Energy*, 287(September 2020):116576, 2021.

[46] Marvin Ricaurte, Christophe Dicharry, Daniel Broseta, Xavier Renaud, and Jean Philippe Torré. CO2 removal from a CO2-CH4 gas mixture by clathrate hydrate formation using THF and SDS as water-soluble hydrate promoters. *Ind. Eng. Chem. Res.*, 52(2):899–910, 2013.

[47] P S R Prasad, K Shiva Prasad, and N K Thakur. Laser Raman spectroscopy of THF clathrate hydrate in the temperature range 90-300 K. *Spectrochim. Acta - Part A Mol. Biomol. Spectrosc.*, 68(4):1096–1100, 2007.

[48] Alexandr Talyzin. Feasibility of H2-THF-H2 O clathrate hydrates for hydrogen storage applications. *Int. J. Hydrogen Energy*, 33(1):111–115, 2008.

[49] Dong Liang Zhong, Nagu Daraboina, and Peter Englezos. Recovery of CH4 from coal mine model gas mixture (CH 4/N2) by hydrate crystallization in the presence of cyclopentane. *Fuel*, 106:425–430, 2013.

[50] Alondra Torres Trueba, Laura J. Rovetto, Louw J. Florusse, Maaike C. Kroon, and Cor J. Peters. Phase equilibrium measurements of structure II clathrate hydrates of hydrogen with various promoters. *Fluid Phase Equilib.*, 307(1):6–10, 2011.

[51] Behzad Partoon, Khalik M. Sabil, Hariz Roslan, Bhajan Lal, and Lau Kok Keong. Impact of acetone on phase boundary of methane and carbon dioxide mixed hydrates. *Fluid Phase Equilib.*, 412:51–56, 2016.

[52] Tatsuo Maekawa. Equilibrium conditions for clathrate hydrates formed from methane and aqueous propanol solutions. *Fluid Phase Equilib.*, 267(1):1–5, 2008.

[53] Brinchi Lucia, Beatrice Castellani, Federico Rossi, Franco Cotana, Elena Morini, Andrea Nicolini, and Mirko Filipponi. Experimental investigations on scaled-up methane hydrate production with surfactant promotion: Energy considerations. *J. Pet. Sci. Eng.*, 120:187–193, 2014.

[54] Hari Prakash Veluswamy, Sharad Kumar, Rajnish Kumar, Pramoch Rangsunvigit, and Praveen Linga. Enhanced clathrate hydrate formation kinetics at near ambient temperatures and moderate pressures: Application to natural gas storage. *Fuel*, 182:907–919, 2016.

[55] Yasuhiko H. Mori. On the scale-up of gas-hydrate-forming reactors: The case of gas-dispersion-type reactors. *Energies*, 8(2):1317–1335, 2015.

[56] Katipot Inkong, Pramoch Rangsunvigit, S. Kulprathipanja, and Praveen Linga. Effects of temperature and pressure on the methane hydrate formation with the presence of tetrahydrofuran (THF) as a promoter in an unstirred tank reactor. *Fuel*, 255(July):115705, 2019.

[57] Kenneth S. Pitzer, David Z. Lippmann, R. F. Curl, Charles M. Huggins, and Donald E. Petersen. The Volumetric and Thermodynamic Properties of Fluids. II. Compressibility Factor, Vapor Pressure and Entropy of Vaporization. *J. Am. Chem. Soc.*, 77(13):3433–3440, 1955.

[58] W. Kohn. Nobel lecture: Electronic structure of matter - Wave functions and density functional. *Rev. Mod. Phys.*, 71(5):1253–1266, 1999.

[59] Paolo Giannozzi, Stefano Baroni, Nicola Bonini, Matteo Calandra, Roberto Car, Carlo Cavazzoni, Davide Ceresoli, Guido L. Chiarotti, Matteo Cococcioni, Ismaila Dabo, Andrea Dal Corso, Stefano De Gironcoli, Stefano Fabris, Guido Fratesi, Ralph Gebauer, Uwe Gerstmann, Christos Gougoussis, Anton Kokalj, Michele Lazzeri, Layla Martin-Samos, Nicola Marzari, Francesco Mauri, Riccardo Mazzarello, Stefano Paolini, Alfredo Pasquarello, Lorenzo Paulatto, Carlo Sbraccia, Sandro Scandolo, Gabriele Sclauzero,

Ari P. Seitsonen, Alexander Smogunov, Paolo Umari, and Renata M. Wentzcovitch. QUANTUM ESPRESSO: A modular and open-source software project for quantum simulations of materials. *J. Phys. Condens. Matter*, 21(39):395502, 2009.

[60] Ahmed Omran, Nikolai Nesterenko, and Valentin Valtchev. Ab initio mechanistic insights into the stability, diffusion and storage capacity of sI clathrate hydrate containing hydrogen. *Int. J. Hydrogen Energy*, 47(13):8419–8433, 2022.

[61] Ahmed S. Omran. DFT Study of Copper-Nickel (111) Catalyst for Methane Dry Reforming. Master's thesis, Texas A & M University, 2019.

[62] Jong Won Jung and J. Carlos Santamarina. Hydrate formation and growth in pores. *J. Cryst. Growth*, 345(1):61–68, 2012.

[63] Wei Ke and Thor M. Svartaas. The Effect of Molar Liquid Water-Gas Ratio on Methane Hydrate Formation. *J. Mater. Sci. Eng. B*, 3(8):510–517, 2013.

[64] Sai Kiran Burla and S. R. Prasad Pinnelli. Enrichment of gas storage in clathrate hydrates by optimizing the molar liquid water–gas ratio. *RSC Adv.*, 12(4):2074–2082, 2022.

[65] Burla Sai Kiran, Kandadai Sowjanya, Pinnelli S R Prasad, and Ji Ho Yoon. Experimental investigations on tetrahydrofuran - Methane - water system: Rapid methane gas storage in hydrates. *Oil Gas Sci. Technol. – Rev. IFP Energies Nouv.*, 74:12, 2019.

[66] Hari Prakash Veluswamy, Alison Jia Hui Wong, Ponnivalavan Babu, Rajnish Kumar, Santi Kulprathipanja, Pramoch Rangsunvigit, and Praveen Linga. Rapid methane hydrate formation to develop a cost effective large scale energy storage system. *Chem. Eng. J.*, 290:161–173, 2016.

[67] Ji Ho Yoon. A theoretical prediction of cage occupancy and heat of dissociation of THF-CH4 hydrate. *Korean J. Chem. Eng.*, 29(12):1670–1673, 2012.

[68] Caroline T. Moryama, Takeshi Sugahara, Danilo Y. Yatabe Franco, and Hiroko Mimachi. In situ Raman spectroscopic studies on small-cage occupancy of methane in the simple

methane and methane + deuterated tetrahydrofuran mixed hydrates. *J. Chem. Eng. Data*, 60(12):3581–3587, 2015.

[69] Ngoc N. Nguyen and Anh V. Nguyen. Hydrophobic Effect on Gas Hydrate Formation in the Presence of Additives. *Energy and Fuels*, 31(10):10311–10323, 2017.

[70] Asheesh Kumar, Tushar Sakpal, and Rajnish Kumar. Influence of Low-Dosage Hydrate Inhibitors on Methane Clathrate Hydrate Formation and Dissociation Kinetics. *Energy Technol.*, 3(7):717–725, 2015.

[71] Arnaud Desmedt, Ludovic Martin-Gondre, The Thuong Nguyen, Claire Pétuya, Leyre Barandiaran, Odile Babot, Thierry Toupance, R Gary Grim, and Amadeu K Sum. Modifying the flexibility of water cages by co-including acidic species within clathrate hydrate. *J. Phys. Chem. C*, 119(16):8904–8911, 2015.

[72] The Thuong Nguyen, Claire Pétuya, David Talaga, and Arnaud Desmedt. Promoting the Insertion of Molecular Hydrogen in Tetrahydrofuran Hydrate With the Help of Acidic Additives. *Front. Chem.*, 8:550862, 2020.

[73] N. Y. Chen. Hydrophobic properties of zeolites. *J. Phys. Chem.*, 80(1):60–64, 1976.

[74] Dongyoung Lee, Woojin Go, and Yongwon Seo. Experimental and computational investigation of methane hydrate inhibition in the presence of amino acids and ionic liquids. *Energy*, 182:632–640, 2019.

[75] Mert Atilhan, Nezih Pala, and Santiago Aparicio. A quantum chemistry study of natural gas hydrates. *J. Mol. Model.*, 20(4):1–15, 2014.

[76] Pradeep Kumar, Brijesh Kumar Mishra, and N. Sathyamurthy. Density functional theoretic studies of host-guest interaction in gas hydrates. *Comput. Theor. Chem.*, 1029:26–32, 2014.

Chapter 5

Toward Economic Seawater-based Methane Hydrate Formation at Ambient Temperature : A Combined Experimental and Computational Study

La mer *est un espace de rigueur et de liberté.*

-Victor Hugo

Clathrate hydrates are emerging as a novel storage medium for safe and compact methane storage[1]. However, their industrial-scale applicability is hindered by sluggish formation kinetics and intense energy cooling requirements. The present study is the first report on binary methane-tetrahydrofuran (THF) formation using the combination of seawater and an unstirred reactor at ambient temperature (298.2 K) that would improve the process economics. Acidic zeolites with different Si/Al ratios (USY-40 and USY-10) as well as aliphatic (L-valine) and aromatic (L-tryptophane) amino acids are employed as environmentally benign kinetic hydrate promoters. The experimental study is combined with DFT calculations to shed light on the role of kinetic promoters in hydrate formation. The set of experimental data revealed that hydrophobic zeolites with a higher Si/Al ratio performed better than the more hydrophilic ones.

Moreover, the aliphatic amino acid L-valine showed better kinetic promotion performance for hydrate formation in natural and artificial seawater than the aromatic amino acid L-tryptophan. The optimization of the experimental condition allowed a controlled hydrate growth boosting the gas uptake to 40 mmol gas/mol water, which is the highest reported under mild conditions using seawater. In addition, the induction time is reduced to less than 10 minutes, and a methane recovery of 97% is reached without any foaming signs. Thus, this study demonstrates the possibility of controlling the stochastic nature of nucleation and hydrate growth by properly manipulating the reaction system. Our results provide a better understanding of hydrate nucleation enhancement under realistic conditions and open the door for a possible application of these environmentally benign kinetic hydrate promoters (KHPs) for synthetic natural gas (SGH) on a continuous process and industrial scale.

5.1 Introduction

Global energy demand rapid increase and movement toward less carbon emission has emphasized the role of natural gas as a transitional and clean fossil fuel toward decarbonization [1–4]. Recent disturbances in the natural supply chain due to the pandemic and geopolitical developments highlighted the need for economic long-term methane storage [5, 6]. Currently, the state-of-the-art technology of LNG (liquified natural gas) is limited by short-time storage due to the expensive cooling cost, and the need for large reserves as well as long-term contracts [7–9]. To overcome the above challenges, 'zeolitic ice' or synthetic gas hydrate (SGH) that allows methane storage in a stable, recoverable, compact, and safe solid are considered [10, 11]. Moreover, they enable the use of stranded and discrete gas resources such as flue and shale gases. However, the application of such promising material is hindered by slow kinetics and high formation condition economics [12, 13]. Desalination costs combined with the energy-intensive hydrate formation cooling requirement and agitation impose a high capital overhead on SGH technology[14, 15]. The above challenges could be faced by using accessible seawater instead of deionized water. However, the presence of salts such as sodium chloride and high

[1]This chapter is based on the following article: *Omran A., Nesterenko N., & Valtchev V.* Revealing Zeolites Active Sites Role as Kinetic Hydrate Promoters: Combined Computational and Experimental Study. ACS Sustainable Chemistry & Engineering. 2022 Jun 9;12 (24):8002–8010.

temperature can impose a double inhibitory effect on hydrate synthesis [9].

Among different reactor configurations used to study methane hydrate formation, the stirring and unstirred reactor configurations were the most common ones. Stirred reactors were used to overcome mass transfer limitations and consequently enhance methane hydrate formation by continuously disturbing the gas-liquid interface where nucleation predominantly occurs [16]. In general, this results in a relatively shorter induction time. For example, Pahlavanzadeh *et al* investigated methane hydrate formation in the stirred reactor in presence of nanofluids at 275.15 K and 5 MPa. The induction time was about 15-50 mins while gas uptake did not exceed 0.06 mol gas/mol water [17]. However, most of the research studies in stirred reactors employed a bottom-mounted stirrer (usually a magnetic stirrer). Hydrate clusters tend to float up in such an arrangement, forming a thin layer that separates the gas from bulk water. This typical mass transfer causes a quick drop in gas uptake shortly after nucleation. Thus, for example, Linga *et al.* found that fixed bed silica sand performed better than the stirred reactor [18]. Recent studies such as Gootam *et al* showed that a top-mounted stirrer can improve the rate constant due to more efficient mixing [19]. However, scale-up studies that involved both heat and mass transfer analysis showed that the stirred-reactor configuration is not favorable for any significant economic scale-up [20]. This conclusion can be explained by the lower hydrate mass in water ($\leq$ 5 wt%), agitation energy cost as the slurry thickens, and post-processing cost of filtration and packing [21]. On the other hand, unstirred and packed bed reactors showed better gas uptake and hydrate yield than the other reactor designs, including stirred reactor configuration [22, 23].

Recently, a huge experimental effort has been directed to enhance methane hydrate kinetics from natural or simulated seawater (2.7-3.5 wt% NaCl) in non-stirred reactors [24, 25]. To accelerate the hydrate formation rate in such inhibitory medium, kinetic promoters such as sodium dodecyl sulfate (SDS) and amino acids were used. For instance, Veluswamy *et al.* investigated the kinetic performance of amino acids for sII mixed methane/THF hydrate formation from saline water (3 wt% NaCl) at 283.2 K. The study showed a low concentration of

leucine (200 ppm) could improve the hydrate kinetics at 5 MPa [26]. Pandey *et al.* investigated the kinetics of binary CH_4-THF hydrate formation in the presence and absence of 3 wt% NaCl under similar thermodynamic conditions. They observed "cobweb-like" hydrate formation with no significant drop in storage capacity at 283.2 K and 5 MPa in presence of salt. However, the authors stressed the need for higher driving forces and identifying better promoters and reactors to enable the saline solutions to have reasonable gas uptakes comparable to non-saline ones [27].

Although the above efforts were useful to understand hydrates of saline solutions, they are still far from economic feasibility due to the low formation temperature. At higher temperatures, SDS (sodium dodecyl sulfate) is commonly used to improve the extremely slow kinetics. In that case, the presence of SDS may be also accompanied by higher pressure (driving force) or associated with other kinetic promoters, or both. For example, Nesterov and Reshetnikov examined pure methane hydrate formation from saline water (3 wt%) in presence of 0.1 wt% SDS at 275 K. They found that SDS micelles did not form even if the pressure increased from 8 to 16 MPa[28]. Moreover, Inkong *et al.* tested co-promoters of SDS and amino acids for binary CH_4-THF sII hydrates from a saline solution of 3.5 wt% NaCl at 8 MPa and 288 K. Despite the reduced induction time and increased hydrate formation rate in presence of SDS, it resulted in 50% reduction of methane uptake and hydrate yield compared to stand-alone amino acids [25, 29]. Thus, the effect of SDS addition to saline water is the same in both sI and sII hydrate studies. In addition to the above adverse effects of SDS as kinetic hydrate promoter (KHP), it has been found that it is not practical for any practical scale-up application due to severe foam formation even at low concentrations [30]. Thus, there is a need to explore other KHPs that can avoid those drawbacks.

Some experimental studies have also investigated hydrate formation from seawater to approach more realistic conditions. For example, Kumar *et al.* examined sII hydrate formation from both seawater and simulated seawater (3 wt% NaCl) at 7.2 MPa and 283.2 K. They highlighted that real seawater ($\sim$ 2.7 wt% salinity) showed slightly less volumetric storage of 86.3

V/V than that saline water (3 wt% NaCl) of 89.2 V/V in presence of THF. They have also highlighted that sI hydrate from saline water (without THF) could not exceed 15.5 V/V even if the condition changed to 10 MPa and 274.2 K [31]. Veluswamy *et al.* emphasized the slight lower uptake in the case of natural seawater than an artificial one [26]. In another study, the same group investigated the effect of leucine and tryptophan for sII hydrate formation from both natural and artificial seawater and found that leucine resulted in higher gas uptake than tryptophan while natural seawater (2.72 wt% salinity) outperformed artificial one (3.0 wt%) in terms of total methane uptake and reaction rate [32].

In addition to amino acids, porous material that can act as nucleation sites that accelerate the nucleation process was employed as KHPs [33–41]. Among porous materials, zeolites are green materials with low cost, large surface area, tunable acidity and hydrophobicity, and above all high stability in aqueous medium [42, 43]. The above properties of zeolites can significantly affect the kinetics of hydrate formation [44, 45]. For example, the zeolite hydrophobicity and acidity can be tuned by changing Si/Al ratio , synthesis conditions or healing the defect sites [46, 47]. Moreover, zeolites are stable in aqueous medium compared to the most common MOFs which suffer from structural deformation with their metal-coordinated linkers replaced by water molecules [48]. In spite of the advantages mentioned above, only a few studies investigated their performance as KHPs with zeolite Na-X (FAU-type) were reported as the best performing zeolite compared to different ion-exchange forms (3A and 5A) of zeolite A (LTA-type). In all above cases SDS was added to the porous material to get satisfactory condition especially when the temperature increased close to ambient [49–52]. Recently, Omran *et al.* revealed that acidic zeolite (H-Y, FAU-type) exhibited superior KHP performance over the basic one 13X (Na-X, FAU-type) for at relatively mild pressure (6 MP) without the need for SDS [45]. While there are many studies that investigated saline-based hydrate formation at elevated pressures and lower temperatures [22], it has been rarely studied at ambient temperature. Bhattacharjee *et al.* studied the formation of methane-THF hydrates at ambient temperature (298.2 K) and moderate pressure (9.5 MPa) in presence of amino acids (L-arginine and L-tryptophan). However, they had to use 0.3 mol% TBAF (tetra-n-butylammonium fluoride) as a second ther-

modynamic promoter (THP) to obtain a maximum gas uptake of 29.30 mmol methane/mol of water as the reaction could survive more than 3-4 hours in those challenging conditions. In addition to the above chemicals, below-mounted agitation with a magnetic stirrer, at least at the beginning of hydrate nucleation, was necessary [53]. This combination of multiple chemical additives and agitation increased the overall cost of the process and may cancel out the expense saved from avoiding the desalination process.

The primary objective of this study is to enhance the economic feasibility of green methane hydrate formation by maximizing the gas uptake at conditions as close as possible under realistic conditions. To achieve that objective, we investigated (1) natural seawater-based mixed methane-THF hydrate formation in (2) non-stirred reactor configuration (packed-bed) at (3) ambient temperature (298.2 K), and (4) moderate pressure (9.5 MPa). To overcome these extreme inhibitory conditions, we employed single environmentally benign KHPs of amino acids, and acidic zeolites (USY-10 and USY-40). Furthermore, the promoting mechanism of those materials was studied with both DFT (density functional theory) calculations and detailed kinetic data.

5.2 Experimental Section

5.2.1 Material and apparatus

Methane (99.99% purity) was purchased from Linde Co., Tetrahydrofuran (THF, AR grade 99.99%) from Alfa Aesar, ultra-stable acidic zeolites (H-USY40 and H-USY10) with different Si/Al ratios were obtained from Zeolyst. Amino acids L-tryptophan (reagent grade, 99 %) and L-valine (reagent grade, 99%) were purchased from Alfa Aesar. Sodium chloride (reagent grade, 99%) was purchased from Sigma-Aldrich. Fresh desalinated water were prepared in LCS (Laboratoire Catalyse et Spectrochimie), France. Natural seawater (SW) was obtained from Ouistreham coast, Caen, France. Simulated seawater (SSW) was prepared with 3 %wt NaCl. The acidic form of zeolites was calcined at 450°C for 4 hours. THF 5.56 mol% solution or its mix with zeolite or amino acid were prepared in a volumetric flask.

The instrument used for methane hydrate formation and dissociation is shown in **Figure B.1**. The set-up is composed of a 450 cm^3 high-pressure stainless-steel reactor (CR; Parr) immersed in a cooling bath. The reactor is immersed in a cooling bath whose temperature is controlled by an external refrigerator (ER; Julabo, F250) which circulates a glycol solution. The pressure and temperature measurement were monitored by a pressure transmitter (PT; UNIK 5000, GE) with a range of 0-30 MPa and 0.1 % global error and a K-type thermocouple (T) with $\pm$ 1.0 K accuracy, respectively. To monitor the data during different experiments, a data acquisition logger (DAQ; Nanodac, Eurotherm) was connected to a personal computer (PC) and collected the data every 10 seconds. To ensure reproducibility and consistency, each experiment was repeated at least three times and average data is reported. All experiments were performed an isochoric quiescent system; i.e with a fixed total volume of gas and solution or hydrate in a closed system.

5.2.2 Characterization

The zeolite powders were characterized using powder X-ray diffraction (PXRD), scanning electron microscope (SEM), inductively coupled-atomic plasma emission spectroscopy (ICP-AES), and scanning electron microscopy (SEM) equipped with energy dispersive X-ray (EDX), and N_2-adsorption. The synthesized binary CH_4-THF hydrate was characterized by PXRD and C^{13} NMR. Composition analysis of natural seawater was obtained from ICP. Methods, procedures, calculations, and equipment are detailed in the supporting information.

5.2.3 Experimental Procedure and Calculations

All experiment has been performed at ischoric and isothermal conditions. Detailed description of hydrate formation and recovery procedures and associated calculations are detailed in supporting information. Density functional theory (DFT) calculations [54] using the projected augmented wave (PAW) method and the standard pseudopotentials supplied by Quantum Espresso (QE) software [3, 55, 56]. A full description of the hydrate-zeolites systems, as well as calculation details, are shown in supporting information.

5.3 Results and discussion

5.3.1 Zeolite Promoters and Hydrate Characterization

N_2-adsorption measurements, PXRD, and SEM images confirmed the crystal structures of USY-40 and USY-10 zeolites as shown in **Table B.1**, **Figure B.2**, and **Figure B.3**, respectively. ICP-AES and EDX revealed that Si/Al ratio of USY-40 is 42 compared to 13 in the case of USY-10. For hydrate characterization, we first confirmed sII formation using PXRD analysis. In addition, C^{13} NMR measurements on the seawater-based binary hydrate were performed. Spectroscopic data revealed methane occupancy in 5^{12} small cages of sII as a sharp peak at -4.3 ppm while the other two peaks (26.2 and 69.0 ppm) indicate the large cage occupancy of THF as shown in **Figure B.4**. Details on the zeolite promoter and hydrate characterization results are provided in supporting information.

5.3.2 Effect of zeolite promoters on mixed CH_4-THF hydrate formation

The kinetic performance of different promoters employed for mixed methane-THF hydrate formation using seawater (SW) is summarized in **Table 5.1**, while similar results for freshwater (FW) and simulated seawater (SSW) are detailed in **Table B.2**. We have listed the investigated key parameters including reactor configuration, total gas uptake, induction time, t_{90} (time taken for 90% completion of methane uptake), and recovery. For each system the hydrate synthesis was investigated at a constant pressure of 9.5 MPa and ambient temperature of 298.2 K. Such a realistic condition will ensure more than 80% reduction in cooling costs as estimated by Veluswamy *et al.*[10]. The pressure of 9.5 MPa has been chosen after several trials to ensure optimum gas uptake without compromising the economic feasibility. Previous studies showed that the reaction with seawater under these conditions could not be sustained for more than 4 hours with a maximum uptake below 30 mmol gas /mol of water despite stirring and utilization of multiple thermodynamic promoters[53]. To overcome that and boost the gas uptake, a special alloy of lightweight corrosion resistance metallic packing has been utilized to enhance heat transfer. Metallic packing has been successfully employed in literature to improve the thermal conductivity during hydrate formation [57, 58].

Table 5.1: Summary of experiments carried out with THF 5.56 mol% seawater (SW) in the absence and presence of different promoters. In all listed experiments, temperature and initial pressure were 298.2 K and 9.5 MPa.

System	Experiment No.	Reactor Type	**Gas uptake(mmol gas/mol H_2O)**	Induction Time (min)	t_{90}[a]	**Revovery (%)**[b]
SW+ 5.56 mol % THF	A1	NSTR	20.93(±3.5)	13.10(±5.5)	403.70	97.30
	A2	NSTR	20.80(±1.5)	14.20(±3.8)	213.00	96.50
	A3	NSTR	20.20(±2.8)	15.70(±7.7)	375.00	96.30
SW+ 5.56 mol % THF+0.03% L-Tryptophan	B1	NSTR	29.57(±1.2)	7.70(±4.7)	271.30	98.00
	B2	NSTR	24.39(±2.6)	8.00(±1.8)	282.30	97.30
	B3	NSTR	28.70(±1.8)	7.50(±3.8)	241.50	96.70
SW+ 5.56 mol % THF+0.03% L-Valine	C1	NSTR	37.98(±1.5)	8.20(±2.7)	410.80	97.50
	C2	NSTR	35.28(±2.7)	7.20(±3.3)	409.00	97.20
	C3	NSTR	34.91(±2.9)	5.30(±2.7)	426.50	97.40
SW+ 5.56 mol % THF+0.03% US-Y-40	D1	NSTR	40.04(±1.4)	6.90(±1.8)	410.20	96.10
	D2	NSTR	38.67(±2.3)	5.20(±2.2)	410.20	97.90
	D3	NSTR	41.20(±2.7)	4.70(±3.5)	376.80	97.09
SW+ 5.56 mol % THF+0.03%US-Y-10	E1	NSTR	24.14(±1.3)	10.80(±4.2)	244.50	96.37
	E2	NSTR	20.03(±3.3)	11.20(±5.8)	267.70	96.41
	E3	NSTR	19.38(±2.1)	11.70(±4.7)	319.30	96.79

[a] average results of t_{90} varied within ±37 min

[b] average results of hydrate %recovery varied within ±1.54 %.

To study the kinetic performance of zeolite promoters, USY-40 and USY-10 have been initially tested at 300 ppm concentrations and 9.5 MPa pressure. **Figure 6.1** compares the average gas uptake due to hydrate formation from natural seawater for 5.56 % blank THF solution along with 5.56 % THF solutions with USY-40 and USY-10 zeolites. Gas uptake has been plotted for the hydrate growth phase. In other words, time zero in that figure is considered the nucleation time. As shown in the figure, pure THF solution could achieve 20 mmol of gas/mol of water, similar to those uptakes reported by Bhattacharjee *et al.* [53] without stirring or using of additional promoters such as TBAF (tetra-n-butylammonium fluoride). Then, we tested two acidic zeolites of a similar framework (FAU) type to examine the effect of different Si/Al ratios and hydrophobicity on the performance of zeolites as kinetic hydrate promoters. The selection of acidic zeolites is based on our earlier experimental studies and DFT calculations that showed that the presence of an extra framework cation such as sodium could limit zeolite's promoting effect by binding to water molecules and breaking the intermolecular hydrogen bonds preventing water arrangement for hydrate cage formation [44, 45, 59]. Such behavior resulted in disturbing the intrinsic water network of hydrate cages. As seen in **Figure 6.1**, USY-10 (Si/Al ratio $\approx$ 13) zeolite showed a slightly better promoting effect than pure THF solution.

One can observe that the induction time has been reduced by about 25% from 15 min to 11 min. However, the improvement is not high enough to be noticed especially when it comes to gas uptake which has been increased only by about 10% compared to the blank THF solution. A worth noting observation is that in both cases the uptake is relatively low and the hydrate formation was difficult to be initiated and sustained.

On the hand, USY-40 (Si/Al ratio $\approx$ 42) showed a significant increase in overall kinetic performance and enhanced the gas uptake of synthetic gas hydrates (SGH). The induction time has been reduced to less than 7 mins or more than 50% compared to the blank THF solution. When compared to USY-10, it initially showed lower uptake for the first hour. However, the hydrate formation kinetics were accelerated and the reaction could be sustained for more than 9 hours despite the presence of salt (NaCl) at high concentrations in seawater. In this particular scheme, the action of acidic zeolite as kinetic hydrate promoter comes from (1) its role as a nucleation site and (2) its ability to extract hard cations such as sodium from the aqueous solution which allows smooth hydrate growth, and (3) it does not result in foaming. The presence of these hard cations can work as hydrate inhibitors even at low concentrations [60]. Moreover, the superior performance of USY-40 over USY-10 can be attributed to its higher Si/Al ratio. The relatively lower Si/Al ratio in the case of USY-10 resulted in a more hydrophilic nature and electrostatic structure that can reduce the water activity coefficient [61] which ultimately limits the promoting effect of zeolite as KHP. To further explain, one can say that the adsorption involves specific interaction between the water molecule and the hydrophilic centers in zeolite, which can be either a silanol group or a cation associated with the tetrahedrally coordinated aluminum [62]. Nguyen and Nguyen demonstrated that the moderate hydrophobicity of additive results in organizing the surrounding water into a clathrate-like structure and thereby promotes hydrate formation [44]. Recently, Denning *et al.* demonstrated that the more hydrophobic SSZ-13 (Si/Al ratio = 20) promoted 2.6 times more water-to-hydrate conversion than the hydrophilic SAPO-34 (Si/Al ratio = 0.6) [34]. Thus, the absence of sodium cation and the higher Si/Al ratio of USY-40 resulted in enhanced hydrophobicity. Combined with the additional gas-to-water contact area indicated by the higher S_{ext} compared to USY-10, such

hydrophobicity nature improved better orientation of water molecules for hydrate formation.

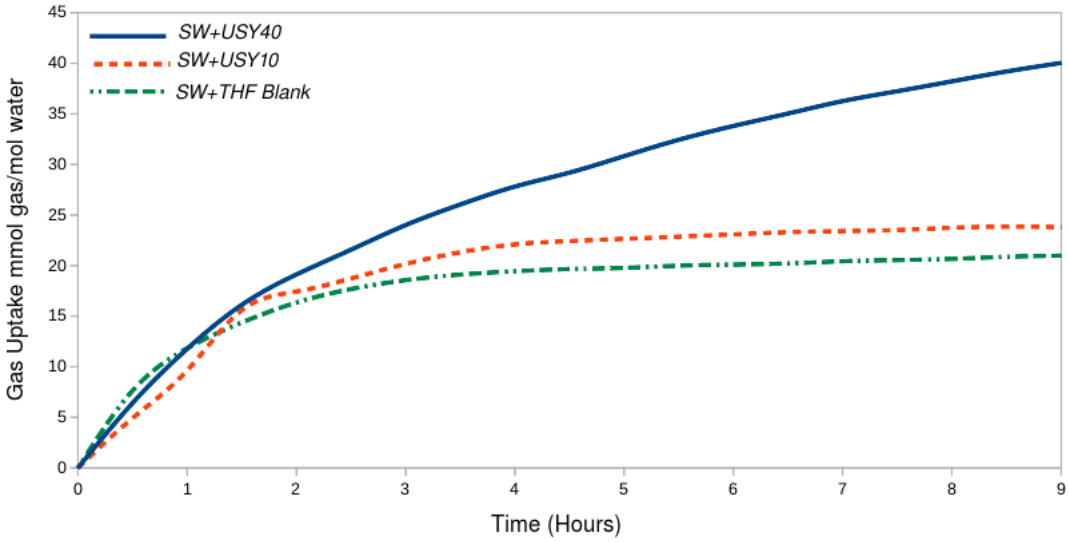

Figure 5.1: Comparison of average methane gas uptake owing to hydrate formation runs in the presence and absence of zeolite promoters: all solutions contain THF in the stoichiometric concentration of 5.56 mol% and hydrate synthesis temperature and pressure are 298.2 K and 9.5 MPa, respectively.

It is agreed that those salts such as NaCl have a thermodynamic inhibitory effect on hydrate formation in a way such as it is difficult to initiate the nucleation or maintain hydrate formation reaction [61, 63]. Thus, the presence of these salts reduces the performance of zeolite hydrate promoters as illustrated in **Figure B.6**. One can observe that zeolite kinetic promoter USY-40 performed better in natural seawater ($\approx$ 2.75 wt% salinity) compared to simulated seawater (SSW) which contains 3 wt% or 1.1 mol% NaCl. In spite of the initial higher methane uptake in the case of SSW, both natural and simulated seawater achieved the same methane uptake after about 4 hours. However, while the hydrate growth could not be sustained for more than 4 hours in the case of artificial seawater due to the high concentration of inhibitory NaCl salt, the methane uptake continued in the case of natural seawater. This can be explained by the presence of other salts in seawater that are potentially less inhibitory to hydrate growth than NaCl. Moreover, the induction time increased in the case of simulated seawater compared to the natural one. The reduced t_{90} in the case of simulated seawater can be seen as a reflection of the reduced methane uptake compared to natural seawater. On the other hand, using pure water

resulted in significantly enhanced hydrate growth kinetics and much higher methane uptake. This indicates the efficacy of USY-40 zeolite as KHP in absence of the inhibitory effect of salts.

5.3.3 Effect of Amino Acids Promoters on Mixed CH_4-THF Hydrate Formation

Amino acids are a class of eco-friendly compounds that has been recently investigated to accelerate the hydrate formation kinetics [64]. However, there is a contradiction in the literature about their role in the clathrate formation [65, 66]. For example, Sa *et al.* showed that amino acids, especially the hydrophobic ones can work as effective kinetic inhibitors for methane hydrate [67], while studies such as Veluswamy *et al.* showed they could work as promoters if used at concentrations of 300 ppm [68]. Prasad and Kiran came also to the latest conclusion but for CO_2 clathrates [69]. Thus, in this study, we have investigated two non-polar hydrophobic amino acids as kinetic promoters at concentrations as low as 300 ppm: the aliphatic amino acid (L-valine) and aromatic amino acid (L-tryptophan). The selection of hydrophobic amino acids is based on previous studies that showed that they are likely to perform better than hydrophilic ones as KHPs [44, 70, 71]. Moreover, L-valine and L-tryptophan have been previously reported to enhance hydrate kinetics in saline environments in synergism with THF [29, 32]. As shown in **Figure 6.2**, both the aliphatic (L-valine) and aromatic (L-tryptophan) showed kinetic promoting effect for mixed CH_4-THF hydrate formation at ambient temperature when compared to blank solution. The average induction time is slightly reduced in the case of L-valine compared to L-tryptophan. On the other hand, L-tryptophan showed initial higher methane uptake than L-valine. Such a high methane uptake sharply drops down after 4 hours while L-valine could sustain relatively higher methane uptake for about 9 hours. Thus, L-valine could achieve higher final methane uptake of 36 mmol gas/mol water compared to 28 mmol gas/mol water in the case of L-tryptophan.

Finally, we have explored the behavior of L-valine in artificial seawater (3 wt% or 1.1

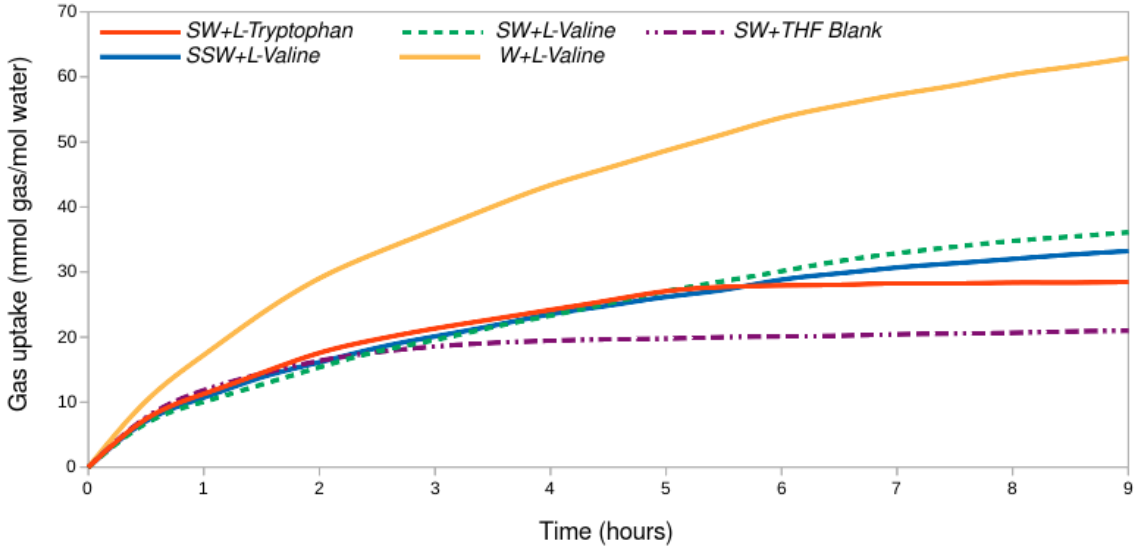

Figure 5.2: Comparison of average methane gas uptake owing to hydrate formation runs in the presence and absence of amino acid promoters: all solutions contain THF in the stoichiometric concentration of 5.56 mol% and hydrate synthesis temperature and pressure are 298.2 K and 9.5 MPa, respectively.

mol% NaCl) and freshwater. Similar to USY-40, L-valine showed slightly better performance in natural seawater than in artificial one as illustrated in **Figure 6.2**. Removing the effect of inhibitory salts, the gas uptake increased significantly by 75% to about 63 mmol gas/mol water. This reveals the real efficacy of L-valine as KHP. In addition, one can attribute the lower performance of amino acids in the seawater environment to the neutralizing effect of those salts, especially at ambient temperature. On the other hand, there was no foaming observed for both amino acids during hydrate dissociation. This crucial observation along with their kinetic performance, strengthened the possibility of their use to relieve surfactants as KHPs due to their common structural similarities. To illustrate, while surfactant such as SDS is composed of a hydrophilic head and hydrophobic tail, L-valine is composed of hydrophilic carboxylic and amine groups associated with a hydrophobic side chain. In the next section, we will employ DFT calculations to further understand the relative kinetic performance of zeolite and amino for hydrate formation on the molecular level.

5.3.4 Molecular Level Interaction of Hydrate Cages with Promoter

We have utilized DFT calculations to shed light on the molecular level interactions leading to these results. *Ab initio* DFT has been commonly used in literature to report the effect of different promoters or inhibitors on hydrate formation [72, 73]. In this study, DFT was employed to analyze zeolite-hydrate and amino acids-hydrate systems in terms of 5^{12} hydrate cage energies and geometrical changes upon their interaction either with finite zeolite clusters or with amino acid molecules. In addition, the energy of the host-guest cage system was calculated in the presence or absence of KHPs. The host-guest interactions are a key property that characterizes the clathrate stability [74] and can be assessed through interaction energy (ΔE^{HG}). This energy can be defined as follow:

$$\Delta E^{HG} = E(CH_4@5^{12}) - [E(CH_4) + E(5^{12})] \tag{5.1}$$

where $E(CH_4@5^{12})$, $E(CH_4)$, and $E(5^{12})$ are the energies of $CH_4@5^{12}$, methane molecule and the 5^{12} empty cage, respectively. The weak interactions such as H-bonding van der Waals forces dominate the hydrate, zeolite and amino acid systems interaction. Thus, the proper selection of exchange-correlation functional that capture those interactions is essential to represent those systems.

Thus, we initially calculated the interaction energy of methane with a small cage with three different levels of theory. The values were +2.03, -24.97 and -27.78 kJ/mol for revPBE, rvv-10 and vdW-DF2 levels, respectively. While rvv-10 and vdW-DF2 exchange correlation functionals could successfully capture the dispersion forces, revPBE failed to accurately determine the host-guest interactions at all. Compared to -32.55 kJ/mol obtained by the highly accurate but computationally expensive MP2/6-311++G(d,p) level of theory [74], the interaction energy value obtained from vdW-DF2 shows better accuracy in describing the host-guest interaction compared to rvv-10. Consequently, we used it for all remaining calculations.

The optimized zeolite-cage structures are shown in **Figure 5.3**. We aimed to assess the de-

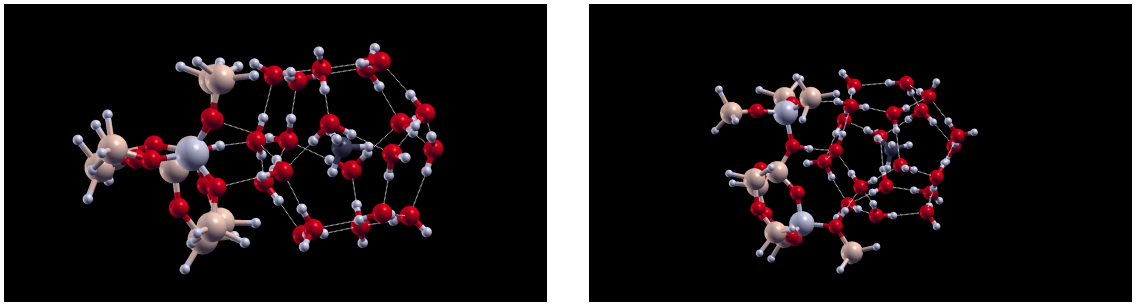

(a) USY-40 (high Si/Al cluster) **(b)** USY-10 (low Si/Al cluster)

Figure 5.3: Optimized configurations of small (5^{12}) cage with zeolite clusters of (a) USY-40 and (b) USY-10. Silicon, hydrogen, carbon, and aluminum atoms are shown in brown, white, black, and gray colors, respectively.

gree of zeolite-clathrate interactions ($\Delta E^{Z\text{-}C}$) with different Si/Al ratios. The interaction energy is defined as follows:

$$\Delta E^{Z\text{-}C} = E(Z\text{-}CH_4@5^{12}) - [E(Z) + E(CH_4@5^{12})] \tag{5.2}$$

where $\Delta E^{Z\text{-}C}$ and E(Z) are the energy of the optimized $Z\text{-}CH_4@5^{12}$ structure and isolated zeolite cluster, respectively. In this case, the lower energy values of the interaction between a host water molecule and the additive molecule indicate a more attractive interaction or inhibitory effect [75].

While the value for the low Si/Al cluster representing USY-10 zeolite is -189.957 kJ/mol, the high Si/Al cluster representing USY-40 showed only -149.69 kJ/mol. The relatively higher value in the case of a low Si/Al cluster indicates that the zeolite binding to the clathrate cage is much stronger and thus disturbs the hydrate growth. This slight stronger interaction could be explained as follows: with the presence of more Al atoms in the zeolite framework, the surface Brønsted acid sites (BAS) can form hydrogen bonds with hydrate cages as shown in **Figure 5.3**. Such an explanation is also applicable to hydrophilic surface silanol groups and agrees with the literature [76]. However, our previous studies showed that such hydrogen-bonding interactions due to BAS are much lower than that of alkali metal extra framework cations such as sodium which can cause the clathrate structure to collapse [45]. In particular, these cations possess high charge density and lower polarizability. Thus, they interact strongly with hydration shell

around them with water dipoles pointing out from it [77]. Moreover, the higher hydrophilicity which can also disturb clathrate cage formation is another consequence of the lower Si/Al ratio. Accordingly, one can say that the USY-10 zeolite strongly binds to the clathrate cage and disturbs the hydrate growth due to its high Al content and thus higher hydrophilicity which agrees with the experimental observations. On the other hand, the effect of USY-40 zeolite particles as nucleation sites that enhance heterogeneous nucleation prevailed as the more hydrophobic acidic zeolite helped the water surrounding molecules to arrange for hydrate formation and promoted further cage growth.

Similarly, as illustrated in **Figure B.7**, we have studied the interaction of both L-valine and L-tryptophane molecules with hydrate cage. The promoting effect of amphipathic amino acids depends on their chemical structure and relative hydrophobicity [44]. Our results showed that the aliphatic amino acid (L-valine) has interaction energy of -31.51 kJ/mol compared to -49.49 kJ/mol for aromatic amino acid (L-tryptophan). The more negative interaction energy in the case of L-tryptophan agrees well with our experimental observation that showed less methane uptake in the case of L-tryptophan despite the higher initial kinetic performance. The optimized structures showed that while hydrate cage disturbance L-tryptophan could be attributed to hydrogen bonding with both the amino group and secondary amine group, it comes only from the amino group in the case of L-valine. In addition, one can attribute these promoting effects of L-valine to its relatively higher hydrophobicity. According to Kyte and Doolittle, the hydrophobicity value of L-valine (+4.2) compared to (-0.9) in the case of L-tryptophan [78]. Thus, based on computational data and experimental observations, one can conclude that the hydrophobic aliphatic group in L-valine enhanced the local water structure and create an increased gas concentration around the amino acid which is finally reflected in higher gas uptake and more sustained kinetics.

5.3.5 Controlling Hydrate Growth Phase: A Step Toward Flow Chemistry of Hydrate Process

One of the main objectives of this study is to give engineering and technological perspectives on economic methane hydrate formation on an industrial scale. To achieve that goal, we have chosen realistic conditions (seawater and ambient temperature) and made technological choices (non-stirred tank reactor, selection of low cost green promoters, and pressure below 10 MPa) to boost the process economics as detailed in the introduction. However, while our approach could reduce the induction time, enabled sustained hydrate growth, and increased the gas uptake in extremely inhibitory conditions compared to literature as illustrated at **Figure 6.4** , we are aware that the reaction time is still too long for a typical economic bath process.

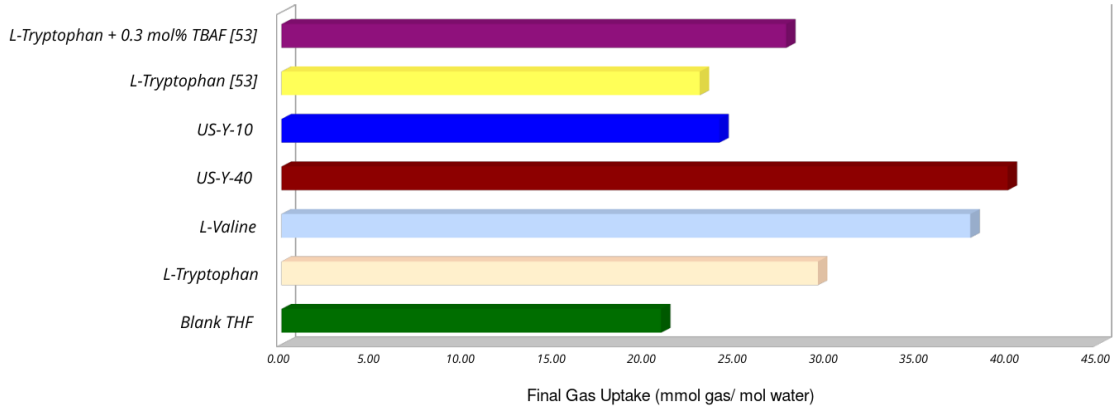

Figure 5.4: Comparison of average methane gas uptake owing to seawater-basted hydrate formation in this work compared to literature [53]: all solutions contain THF in stoichiometric concentration of 5.56 mol% and hydrate synthesis temperature and pressure are 298.2 K and 9.5 MPa, respectively.

Traditionally, the laboratory scale studies of hydrate formation are performed to increase the gas uptake in the shortest time possible. However, when it comes to pilot and industrial scales, establishing a continuous process or "flow chemistry" could save costs by eliminating multiple start-ups and shut-downs between different batches and low maintenance costs, among other reasons discussed in the literature [79]. However, continuous process requires a steady-state process with controlled reaction conditions. In this study, we could achieve a controlled hydrate growth phase during the batch reaction by carefully selecting the proper reaction systems

(reactants, reactor, and P-T condition) as shown in **Figure B.8**. This temperature control within a tight range could eliminate the usual sudden, uncontrolled and stochastic hydrate growth associated with hydrate nucleation. With such controlled behavior, it is possible to extend the process from batch to continuous hydrate production.

Finally, there is naturally inherited lower gas uptake in seawater than in freshwater due to the inhibitory effect of salts regardless of the change in the reaction system. While higher gas uptake is an advantage for stationary storage, it bears challenges in hydrate transportation either within the hydrate production facility or outside. Previous experimental and computational observations showed a greater tendency for brittleness as the hydrate saturation increased [80, 81]. Thus, increasing the gas uptake in seawater-based hydrate "slurry" while maintaining reasonable brittleness gives them an advantage during transporting hydrates without plugging the pipelines within the hydrate production plant or outside for long distances. Moreover, the above study addess the economic challenges associated with the process. At similar hydrate formation conditions (300 K and 6 MPa), Javanmardi *et al.* earlier economic simulation studies of showed that pure water SGH process can reduce the capital cost for natural gas transportation by 48% compared to LNG especially with stranded gas resource [82]. Thus, the above study is an important step toward the feasible process. Furthermore, detailed and updated economic analysis are ongoing to accurately evaluate the process using seawater.

5.4 Conclusions

The goal presented study is to provide a molecular and macroscopic understanding of the role of green promoters of acidic zeolites and amino acids as kinetic hydrate promoters. To boost the reaction economics, we investigated binary methane-THF formation using both natural and simulated seawater in the unstirred reactor at ambient temperature (298.2 K) for the first time. Two types of environmentally benign kinetic hydrate promoters, acidic zeolites with different Si/Al ratios (USY-40 and USY-10) and amino acids (L-valine and L-tryptophane), were employed. Despite the challenging, extremely inhibitory environment due to the pres-

ence of salts and high temperature, the presence of green kinetic hydrate promoter was able to enhance hydrate formation kinetics and methane uptake. Our experimental results showed that zeolite (USY-40) with high Si/Al showed superior gas uptake than the low Si/Al zeolite (USY-10). DFT calculation showed that (USY-10) disturbed the hydrate cage due to its higher hydrophilicity and hydrogen bonding with surface BAS. On the other hand, the hydrophobic zeolite (USY-40) promoted the hydrate formation as it works to arrange water surrounding molecules for hydrate formation. The aliphatic amino acid L-valine showed better kinetic promotion performance and higher gas uptake in hydrate formation than the aromatic amino acid of L-tryptophan. The computational investigation revealed that the relatively less hydrophobic and aromatic L-tryptophan slightly disturbed the hydrate growth due to hydrogen bonding between the amino and secondary amine groups and the local cage structure. On the other hand, the more hydrophobic aliphatic L-valine strengthened the local organization of the cage water structure. The use of aminoacids resulted in a substantial reduction of induction times to less than 10 minutes, and a methane recovery of 97%. The later being the highest gas uptake (40 mmol gas/mol water) reported under those challenging conditions. Finally, we have shown that the nucleation process can be controlled to a steady-state by selecting the proper reaction system, which paves the way for continuous hydrate production on an industrial scale. Our results provide a better understanding of hydrate nucleation enhancement under realistic conditions and open the door for a possible application of these green KHPs for SGH on the industrial scale.

References

[1] Reza Hafezi, Amir Naser Akhavan, Saeed Pakseresht, and David A. Wood. Global natural gas demand to 2025: A learning scenario development model. *Energy*, 224:120167, 2021.

[2] Ahmed Omran, Sun Hee Yoon, Murtaza Khan, Minhaj Ghouri, Anjaneyulu Chatla, and Nimir Elbashir. Mechanistic insights for dry reforming of methane on cu/ni bimetallic catalysts: DFT-assisted microkinetic analysis for coke resistance. *Catalysts*, 10(9):1–16, 2020.

[3] Ahmed S. Omran. *DFT Study of Copper-Nickel (111) Catalyst for Methane Dry Reforming*. PhD thesis, (Master Disseration)Texas A & M, 2019.

[4] Ahmed Omran, Minhaj Ghouri, and Nimir Elbashir. DFT study of Copper-Nickel (111) Catalyst for Methane Dry Reforming. In *Third International Computational Science and Engineering Conference*, Doha, Qatar, October 2019.

[5] Abhinandan Kumar, Pardeep Singh, Pankaj Raizada, and Chaudhery Mustansar Hussain. Impact of COVID-19 on greenhouse gases emissions: A critical review. *Sci. Total Environ.*, 806:150349, 2022.

[6] Marzia Sesini, Sara Giarola, and Adam D. Hawkes. Solidarity measures: Assessment of strategic gas storage on EU regional risk groups natural gas supply resilience. *Appl. Energy*, 308(December 2021):118356, 2022.

[7] Ahmed Omran, Nikolai Nesterenko, and Valentin Valtchev. An Eco-Friendly Approach For Improved Methane Hydrate Kinetics In Near-Ambient Temperature and Moderate

Pressure. In *ACS Research Conference : Chemistry and Chemical Engineering in MENA*, Doha, Qatar, May 2022.

[8] J. Javanmardi, Kh Nasrifar, S. H. Najibi, and Mahmood Moshfeghian. Natural gas transportation: NGH or LNG? *World Rev. Sci. Technol. Sustain. Dev.*, 4(2-3):258–267, 2007.

[9] Yuwei Yin and Jasmine Siu Lee Lam. Bottlenecks of LNG supply chain in energy transition: A case study of China using system dynamics simulation. *Energy*, 250:123803, 2022.

[10] Hari Prakash Veluswamy, Asheesh Kumar, Yutaek Seo, Ju Dong Lee, and Praveen Linga. A review of solidified natural gas (SNG) technology for gas storage via clathrate hydrates. *Appl. Energy*, 216(February):262–285, 2018.

[11] Ahmed Omran, Nikolai Nesterenko, and Valentin Valtchev. Ab initio Mechanistic Insight into the Stability, Diffusion, and Storage Capacity of H2, CH4, and CO2 in sI Clathrate Hydrate. In *European Congress and Exhibition on Advanced Materials and Processes - EUROMAT 2021*, Virtual, Austria, September 2021.

[12] Ahmed Omran, Nikolay Nesterenko, and Valentin Valtchev. Zeolitic ice : A route toward net zero emissions. *Renew. Sustain. Energy Rev.*, 168:112768, 2022.

[13] Ahmed Omran, Nikolai Nesterenko, and Valentin Valtchev. A Computational Insight of Guest Exchange Mechanism between CH4 and CO2 in SI Clathrate: CH4 Recovery and CO2 Storage Opportunities. In *TAMUQ-TotalEnergies Workshop "Successful Industry-Academia Collaboration in the Advancement of CO2 Utilization & Low Carbon Processes"*, Doha, Qatar, May 2022.

[14] Laura A. Pellegrini, Stefania Moioli, Fabio Brignoli, and Camilla Bellini. LNG technology: The weathering in above-ground storage tanks. *Ind. Eng. Chem. Res.*, 53(10):3931–3937, 2014.

[15] Younggy Shin and Yoon Pyo Lee. Design of a boil-off natural gas reliquefaction control system for LNG carriers. *Appl. Energy*, 86(1):37–44, 2009.

[16] Mohammad Reza Ghaani, Judith M. Schicks, and Niall J. English. A review of reactor designs for hydrogen storage in clathrate hydrates. *Appl. Sci.*, 11(2):1–16, 2021.

[17] Hassan Pahlavanzadeh, Sajjad Rezaei, Mehrdad Khanlarkhani, Mehrdad Manteghian, and Amir H. Mohammadi. Kinetic study of methane hydrate formation in the presence of copper nanoparticles and CTAB. *J. Nat. Gas Sci. Eng.*, 34:803–810, 2016.

[18] Praveen Linga, Nagu Daraboina, John A. Ripmeester, and Peter Englezos. Enhanced rate of gas hydrate formation in a fixed bed column filled with sand compared to a stirred vessel. *Chem. Eng. Sci.*, 68(1):617–623, 2012.

[19] Divya Gootam, Namrata Gaikwad, Rajnish Kumar, and Niket Kaisare. Modeling Growth Kinetics of Methane Hydrate in Stirred Tank Batch Reactors. *ACS Eng. Au*, 1(2):148–159, 2021.

[20] Yasuhiko H. Mori. On the scale-up of gas-hydrate-forming reactors: The case of gas-dispersion-type reactors. *Energies*, 8(2):1317–1335, 2015.

[21] Federico Rossi, Mirko Filipponi, and Beatrice Castellani. Investigation on a novel reactor for gas hydrate production. *Appl. Energy*, 99(Icgh):167–172, 2012.

[22] P. Linga and M. A. Clarke. A review of reactor designs and materials employed for increasing the rate of gas hydrate formation. *Energy and Fuels*, 31(1):1–13, 2017.

[23] Zhenyuan Yin, Maninder Khurana, Hoon Kiang Tan, and Praveen Linga. A review of gas hydrate growth kinetic models. 342:9–29, 2018.

[24] Satoshi Takeya, Hiroko Mimachi, and Tetsuro Murayama. Methane storage in water frameworks: Self-preservation of methane hydrate pellets formed from NaCl solutions. *Appl. Energy*, 230(March):86–93, 2018.

[25] Katipot Inkong, Viphada Yodpetch, Hari Prakash Veluswamy, Santi Kulprathipanja, Pramoch Rangsunvigit, and Praveen Linga. Hydrate-Based Gas Storage Application Using Simulated Seawater in the Presence of a Co-Promoter: Morphology Investigation. *Energy and Fuels*, 36(2):1100–1113, 2022.

[26] Hari Prakash Veluswamy, Asheesh Kumar, Rajnish Kumar, and Praveen Linga. Investigation of the kinetics of mixed methane hydrate formation kinetics in saline and seawater. *Appl. Energy*, 253(July):113515, 2019.

[27] Gaurav Pandey, Hari Prakash Veluswamy, Jitendra Sangwai, and Praveen Linga. Morphology study of mixed methane-tetrahydrofuran hydrates with and without the presence of salt. *Energy and Fuels*, 33(6):4865–4876, 2019.

[28] Anatoliy N. Nesterov and Aleksey M. Reshetnikov. Combined effect of NaCl and sodium dodecyl sulfate on the mechanism and kinetics of methane hydrate formation in an unstirred system. *J. Nat. Gas Sci. Eng.*, 99(October 2021):104424, 2022.

[29] Katipot Inkong, Viphada Yodpetch, Santi Kulprathipanja, Pramoch Rangsunvigit, and Praveen Linga. Influences of different co-promoters on the mixed methane hydrate formation with salt water at moderate conditions. *Fuel*, 316(August 2021):123215, 2022.

[30] W. X. Pang, G. J. Chen, A. Dandekar, C. Y. Sun, and C. L. Zhang. Experimental study on the scale-up effect of gas storage in the form of hydrate in a quiescent reactor. *Chem. Eng. Sci.*, 62(8):2198–2208, 2007.

[31] Asheesh Kumar, Hari Prakash Veluswamy, Rajnish Kumar, and Praveen Linga. Direct use of seawater for rapid methane storage via clathrate (sII) hydrates. *Appl. Energy*, 235(October 2018):21–30, 2019.

[32] Hari Prakash Veluswamy and Praveen Linga. Natural Gas Hydrate Formation Using Saline/Seawater for Gas Storage Application. *Energy and Fuels*, 35(7):5988–6002, 2021.

[33] Lars Borchardt, Mirian Elizabeth Casco, and Joaquin Silvestre-Albero. Methane Hydrate in Confined Spaces: An Alternative Storage System. *ChemPhysChem*, 19(11):1298–1314, 2018.

[34] Shurraya Denning, Ahmad AA Majid, James M. Crawford, Moises A. Carreon, and Carolyn A. Koh. Promoting Methane Hydrate Formation for Natural Gas Storage over Chabazite Zeolites. *ACS Appl. Energy Mater.*, 4(11):13420–13424, 2021.

[35] Maninder Khurana, Zhenyuan Yin, and Praveen Linga. A review of clathrate hydrate nucleation. *ACS Sustain. Chem. Eng.*, 5(12):11176–11203, 2017.

[36] Samer Said, Varun Govindaraj, Jean Michel Herri, Yamina Ouabbas, Mohamed Khodja, Mohamed Belloum, Jitendra S. Sangwai, and Ramamurthy Nagarajan. A study on the influence of nanofluids on gas hydrate formation kinetics and their potential: Application to the CO2 capture process. *J. Nat. Gas Sci. Eng.*, 32:95–108, 2016.

[37] Jae Woo Choi, Jin Tack Chung, and Yong Tae Kang. CO2 hydrate formation at atmospheric pressure using high efficiency absorbent and surfactants. *Energy*, 78:869–876, 2014.

[38] Zhen Pan, Zhiming Liu, Zhien Zhang, Liyan Shang, and Shihui Ma. Effect of silica sand size and saturation on methane hydrate formation in the presence of SDS. *J. Nat. Gas Sci. Eng.*, 56(February):266–280, 2018.

[39] Yanhong Wang, Xuemei Lang, and Shuanshi Fan. Accelerated nucleation of tetrahydrofuran (THF) hydrate in presence of ZIF-61. *J. Nat. Gas Chem.*, 21(3):299–301, 2012.

[40] Sarocha Rungrussamee, Katipot Inkong, Santi Kulprathipanja, and Pramoch Rangsunvigit. Comparative study of methane hydrate formation and dissociation with hollow silica and activated carbon. *Chem. Eng. Trans.*, 70:1519–1524, 2018.

[41] Guodong Zhang, Bingjie Liu, Lu Xu, Runcheng Zhang, Yan He, and Fei Wang. How porous surfaces influence the nucleation and growth of methane hydrates. *Fuel*, 291:120142, 2021.

[42] Yang Peng, Vaiva Krungleviciute, Ibrahim Eryazici, Joseph T. Hupp, Omar K. Farha, and Taner Yildirim. Methane storage in metal-organic frameworks: Current records, surprise findings, and challenges. *J. Am. Chem. Soc.*, 135(32):11887–11894, 2013.

[43] Eyas Mahmoud, Labeeb Ali, Asmaa El Sayah, Sara Awni Alkhatib, Hend Abdulsalam, Mouza Juma, and Ala'A H Al-Muhtaseb. Implementing metal-organic frameworks for natural gas storage. *Crystals*, 9(8):1–19, 2019.

[44] Ngoc N. Nguyen and Anh V. Nguyen. Hydrophobic Effect on Gas Hydrate Formation in the Presence of Additives. *Energy and Fuels*, 31(10):10311–10323, 2017.

[45] Ahmed Omran, Nikolay Nesterenko, and Valentin Valtchev. Revealing Zeolites Active Sites Role as Kinetic Hydrate Promoters: Combined Computational and Experimental Study. *ACS Sustain. Chem. Eng.*, 10(24):8002–8010, 2022.

[46] Ana Palčić and Valentin Valtchev. Analysis and control of acid sites in zeolites. *Appl. Catal. A Gen.*, 606(May 2020):117795, 2020.

[47] Ana Palčić, Simona Moldovan, Hussein El Siblani, Aurelie Vicente, and Valentin Valtchev. Defect Sites in Zeolites: Origin and Healing. *Adv. Sci.*, 9(4):1–11, 2022.

[48] Nicholas C. Burtch, Himanshu Jasuja, and Krista S. Walton. Water stability and adsorption in metal-organic frameworks. *Chem. Rev.*, 114(20):10575–10612, 2014.

[49] Katipot Inkong, Hari Prakash Veluswamy, Pramoch Rangsunvigit, Santi Kulprathipanja, and Praveen Linga. Innovative Approach to Enhance the Methane Hydrate Formation at Near-Ambient Temperature and Moderate Pressure for Gas Storage Applications. *Ind. Eng. Chem. Res.*, 58(49):22178–22192, 2019.

[50] Xiao Ya Zang, Shuan Shi Fan, De Qing Liang, Dong Liang Li, and Guang Jin Chen. Influence of 3A molecular sieve on tetrahydrofuran (THF) hydrate formation. *Sci. China, Ser. B Chem.*, 51(9):893–900, 2008.

[51] Xiaoya ZANG, Jianwei DU, Deqing LIANG, Shuanshi FAN, and Cuiping TANG. Influence of A-type Zeolite on Methane Hydrate Formation. *Chinese J. Chem. Eng.*, 17(5):854–859, 2009.

[52] Nam-Jin Kim, Sung-Seek Park, Sang-Woong Shin, Jun-Ho Hyun, and Wongee Chun. An experimental investigation into the effects of zeolites on the formation of methane hydrates. *International Journal of Energy Research*, 39(1):26–32, 2015.

[53] Gaurav Bhattacharjee, Hari Prakash Veluswamy, Rajnish Kumar, and Praveen Linga. Seawater based mixed methane-THF hydrate formation at ambient temperature conditions. *Appl. Energy*, 271(February):115158, 2020.

[54] W. Kohn. Nobel lecture: Electronic structure of matter - Wave functions and density functional. *Rev. Mod. Phys.*, 71(5):1253–1266, 1999.

[55] Paolo Giannozzi, Stefano Baroni, Nicola Bonini, Matteo Calandra, Roberto Car, Carlo Cavazzoni, Davide Ceresoli, Guido L. Chiarotti, Matteo Cococcioni, Ismaila Dabo, Andrea Dal Corso, Stefano De Gironcoli, Stefano Fabris, Guido Fratesi, Ralph Gebauer, Uwe Gerstmann, Christos Gougoussis, Anton Kokalj, Michele Lazzeri, Layla Martin-Samos, Nicola Marzari, Francesco Mauri, Riccardo Mazzarello, Stefano Paolini, Alfredo Pasquarello, Lorenzo Paulatto, Carlo Sbraccia, Sandro Scandolo, Gabriele Sclauzero, Ari P. Seitsonen, Alexander Smogunov, Paolo Umari, and Renata M. Wentzcovitch. QUANTUM ESPRESSO: A modular and open-source software project for quantum simulations of materials. *J. Phys. Condens. Matter*, 21(39):395502, 2009.

[56] Ahmed Omran, Nikolai Nesterenko, and Valentin Valtchev. Ab initio mechanistic insights into the stability, diffusion and storage capacity of sI clathrate hydrate containing hydrogen. *Int. J. Hydrogen Energy*, 47(13):8419–8433, 2022.

[57] Asheesh Kumar, Tushar Sakpal, Praveen Linga, and Rajnish Kumar. Enhanced carbon dioxide hydrate formation kinetics in a fixed bed reactor filled with metallic packing. *Chem. Eng. Sci.*, 122:78–85, 2015.

[58] Asheesh Kumar and Rajnish Kumar. Role of metallic packing and kinetic promoter in designing a hydrate-based gas separation process. *Energy and Fuels*, 29(7):4463–4471, 2015.

[59] Ahmed Omran, Nikolai Nesterenko, and Valentin Valtchev. Revealing Acidic Zeolites: Role as New Kinetic Hydrate Promoters: A Combined Computational and Experimental Study. In *37th meeting of French Group of Zeolite (GFZ)*, Vogüé, France, March 2022.

[60] Asheesh Kumar, Tushar Sakpal, and Rajnish Kumar. Influence of Low-Dosage Hydrate Inhibitors on Methane Clathrate Hydrate Formation and Dissociation Kinetics. *Energy Technol.*, 3(7):717–725, 2015.

[61] E. Dendy Sloan and Carolyn Ann Koh. *Clathrate hydrates of natural gases, thrid edition*. CRC Press, third edition, 2007.

[62] N. Y. Chen. Hydrophobic properties of zeolites. *J. Phys. Chem.*, 80(1):60–64, 1976.

[63] Makagon Yuri F. *Hydrates of Hydrocarbons*. Pennwell, 1997.

[64] Sai Kiran Burla, S. R. Prasad Pinnelli, and Kalachand Sain. Explicating the amino acid effects for methane storage in hydrate form. *RSC Adv.*, 12(16):10178–10185, 2022.

[65] Hadi Roosta, Ali Dashti, S Hossein Mazloumi, and Farshad Varaminian. The dual effect of amino acids on the nucleation and growth rate of gas hydrate in ethane + water, methane + propane + water and methane + THF + water systems. *Fuel*, 212:151–161, 2017.

[66] Kwangbum Kim, Sang Gyu Cho, and Jeong Hoon Sa. Natural Hydrophilic Amino Acids as Environment-Friendly Gas Hydrate Inhibitors for Carbon Capture and Sequestration. *ACS Sustain. Chem. Eng.*, 9(51):17413–17419, 2021.

[67] Jeong-hoon Sa, Gye-hoon Kwak, Bo Ram Lee, Kunwoo Han, and Kun-hong Lee. Hydrophobic amino acids as a new class of kinetic inhibitors for gas hydrate formation. *Sci. Rep.*, 3(2428):1–7, 2013.

[68] Hari Prakash Veluswamy, Asheesh Kumar, Rajnish Kumar, and Praveen Linga. Investigation of the kinetics of mixed methane hydrate formation kinetics in saline and seawater. *Appl. Energy*, 253(July):113515, 2019.

[69] Pinnelli S.R. Prasad and Burla Sai Kiran. Are the amino acids thermodynamic inhibitors or kinetic promoters for carbon dioxide hydrates? *J. Nat. Gas Sci. Eng.*, 52(January):461–466, 2018.

[70] Gaurav Bhattacharjee and Praveen Linga. Amino Acids as Kinetic Promoters for Gas Hydrate Applications: A Mini Review. *Energy & Fuels*, 35(9):7553–7571, 2021.

[71] Jianlong Wang, Jinsheng Sun, Ren Wang, Kaihe Lv, Jintang Wang, Bo Liao, Xiaomei Shi, Qibing Wang, Yuanzhi Qu, and Hongjun Huang. Mechanisms of synergistic inhibition of hydrophilic amino acids with kinetic inhibitors on hydrate formation. *Fuel*, 321(January):124012, 2022.

[72] Dongyoung Lee, Woojin Go, and Yongwon Seo. Experimental and computational investigation of methane hydrate inhibition in the presence of amino acids and ionic liquids. *Energy*, 182:632–640, 2019.

[73] Mohammad Tariq, David Rooney, Enas Othman, Santiago Aparicio, Mert Atilhan, and Majeda Khraisheh. Gas hydrate inhibition: A review of the role of ionic liquids. *Ind. Eng. Chem. Res.*, 53(46):17855–17868, 2014.

[74] Mert Atilhan, Nezih Pala, and Santiago Aparicio. A quantum chemistry study of natural gas hydrates. *J. Mol. Model.*, 20(4):1–15, 2014.

[75] Pradeep Kumar, Brijesh Kumar Mishra, and N. Sathyamurthy. Density functional theoretic studies of host-guest interaction in gas hydrates. *Comput. Theor. Chem.*, 1029:26–32, 2014.

[76] Konstantin S Smirnov. A modeling study of methane hydrate decomposition in contact with the external surface of zeolites. *Phys. Chem. Chem. Phys.*, 19(34):23095–23105, 2017.

[77] Boris Lukanov and Abbas Firoozabadi. Specific ion effects on the self-assembly of ionic surfactants: A molecular thermodynamic theory of micellization with dispersion forces. *Langmuir*, 30(22):6373–6383, 2014.

[78] Jack Kyte and Russell F. Doolittle. A simple method for displaying the hydropathic character of a protein. *J. Mol. Biol.*, 157(1):105–132, 1982.

[79] Christian Holtze and Ralf Boehling. Batch or flow chemistry? – a current industrial opinion on process selection. *Curr. Opin. Chem. Eng.*, 36:100798, 2022.

[80] Zeina M. Jendi, Phillip Servio, and Alejandro D. Rey. Ideal Strength of Methane Hydrate and Ice Ih from First-Principles. *Cryst. Growth Des.*, 15(11):5301–5309, 2015.

[81] Tae Sup Yun, Carlos J. Santamarina, and C. Ruppel. Mechanical properties of sand, silt, and clay containing tetrahydrofuran hydrate. *J. Geophys. Res. Solid Earth*, 112(B4):1–13, 2007.

[82] J. Javanmardi, Kh Nasrifar, S. H. Najibi, and M. Moshfeghian. Economic evaluation of natural gas hydrate as an alternative for natural gas transportation. *Appl. Therm. Eng.*, 25(11-12):1708–1723, 2005.

Chapter 6

Sustainable Energy Storage in Hydrates: Combining Predictive First Principle Calculations, Green Kinetic Promoters with Improved Reactor Design

***Design** is intelligence made visible.*

-Alina Wheeler

Synthetic Gas hydrates are promising materials for safe and compact energy storage but their wide-scale application is hindered by slow formation kinetics. We investigated the effect of green kinetic promoters (H-SSZ-13, l-tryptophan, l-leucine, and l-methionine) in a novel reactor design to accelerate hydrate formation at 6 MPa. In non-stirred reactor (NSR), H-SSZ-13 and l-tryptophan showed superior performance over l-leucine and l-methionine. While H-SSZ-13 showed the lowest average t_{90} (time taken for 90% completion of methane uptake) of 286 mins and the highest volumetric capacity of 115 v/v at 283 K, its kinetic performance, along with other promoters, dropped significantly at 293 K. We introduced a new fixed bed reactor (FBR) equipped with light metallic packing filaments (MPF) to increase gas diffusion and thermal conductivity. The combined effect of FBR-MFP reactor with zeolite significantly improved the kinetics overcoming NSR drawbacks. At 293.15 K, H-SSZ-13 acidic zeolite

promoter showed superior performance reducing the induction time and t_{90} to 3 and 154 mins, respectively. Furthermore, it exploited 88.6%, and 96% of the sII clathrates volumetric storage capacity at 293 K and 283 K, respectively. Finally, we showed that the synthesized hydrates can be stored at atmospheric pressure for 4 months without a significant methane loss. This multi-scale approach is paving the way for scaling up green and economical gas hydrate technology[1].

6.1 Introduction

The energy transition toward more green technologies is coupled with increasing global energy demand which poses the dilemma of balancing sustained economic growth and maintaining the environmental goals toward reducing carbon emissions [1]. In that aspect, natural gas can play an important role as a "transitional fuel" on the way from traditional fossil fuels to green energy resources [2, 3]. Although it is considered a fossil fuel, it is much cleaner than traditional oil and coal resources. It thus has been recently labeled as a green and sustainable energy source by EU taxonomy regulations [4]. Concerning the hydrogen economy, one can find that methane is currently the main feedstock for hydrogen with steam methane reforming (SMR) responsible for 48% of the global hydrogen demand compared to only 4% produced by electrolysis [5].

The natural gas supply chain has been extremely disturbed due to the recent pandemic and geopolitical developments. The current global energy crisis emphasized the need for economic methane transportation and long-term buffer storage that can absorb market shocks [6, 7]. Despite its high storage capacity, which can reach 600 v/v, the well-established gas transport technology of LNG (liquefied natural gas) is limited by very high CAPEX (capital expenditure) due to expensive infrastructure and energy-intensive cooling requirements suitable for short-term storage [8]. Moreover, LNG needs large reserves and long-term contracts to reduce operational costs, which has been proven insufficient to meet the current increasing demand or sudden market shocks [9, 10].

[1]The short version of this chapter is presented in 7th International Conference on Multifunctional, Hybrid and Nanomaterials, October 2022, Genoa, Italy.

The "zeolitic ice" or synthetic gas hydrate (SGH) is considered a promising alternative that allows physical methane storage in water through a safe, stable, compact solid form with a possibility of almost full methane recovery [11, 12]. Due to its simple and modular design, SGH technologies can allow not only purification and use of natural gas produced from conventional reservoirs but also enable the exploitation of the potential stranded and discrete gas resources such as biogas, flue, and shale gases [13–15]. Moving toward the hydrogen economy, storing hydrogen methane (25% hydrogen by weight) in the safe and compact solid form can be comparable to liquid ammonia (17.6% hydrogen by weight) especially when it is accompanied by proper carbon capture and sequestration (CCS) or pyrolysis [1, 16]. However, the industrial application of such green material is hindered by stochastic and slow kinetics and high pressures required for hydrate formation [17]. Among the most efficient solutions to overcome the above challenges are using kinetic hydrate promoters (KHPs) and innovative reactor design.

Surfactants such as sodium dodecyl sulfate (SDS) are the most common KHPs employed to accelerate methane hydrate formation [18–21]. Unfortunately, the process suffers from foam formation, which reduces methane uptake, prevents further scale-up, and creates the need for more effective promoters [22–24]. Recently, porous materials and amino acids were investigated as green KHPs to replace surfactants. Porous materials such as zeolites, MOFs, activated carbon, and others have been proven effective as KHPs [25, 26]. They provide additional gas-liquid contact surfaces and act as nucleation sites that accelerate the nucleation process and improve the hydrate kinetics [27–33]. Among porous materials, zeolites are green materials with low cost, high stability, large surface area, tunable chemical properties, and above all insensitive to aqueous medium compared to MOFs [34, 35].

Despite the advantages mentioned above, only a few studies investigated their performance as KHPs. To illustrate, zeolite Na-X (FAU-type) showed better kinetic promotion in comparison to different ion-exchange forms (3A and 5A) of zeolite A (LTA-type). However, SDS was added as a co-promoter to achieve acceptable conditions [36–39]. In a combined computational and experimental investigation, Omran *et al.* showed that acidic zeolite (H-Y, FAU-type)

exhibited better kinetic promoting performance than the basic one 13X (Na-X, FAU-type) at relatively mild pressure (6 MP) without the need for SDS. The improved performance is because the acidic form of the zeolite does not contain alkali metals that have a negative effect on hydrate nucleation [40, 41]. The acidic strength of the zeolite is also important. For instance, Denning *et al.* showed that the confinement effect and surface properties of hydrophobic SSZ-13 (CHA-type) showed a higher promoting effect than SAPO-34 of the same chabazite topology in terms of water-to-hydrate conversion when they were used at low water to zeolite mass ratios (R_w=0.3-1.2) [42]. More recently, our group compared the performance of USY zeolites in different Si/Al ratios on hydrate formation from seawater at ambient temperature. The results confirmed the superior performance of more acidic and hydrophobic zeolites compared to their hydrophilic counterparts paving the way for their use on a larger scale [43]. Amino acids are also claimed to be promising biodegradable materials that can work as hydrate promoters [44]. It has been found that the more hydrophobic amino acids such as tryptophan and methionine have shown better performance than hydrophilic ones such as glycine KHP for methane hydrate synthesis [43, 45, 46]. On the other hand, some amino acids were reported as kinetic hydrate inhibitors, perturbing the local water arrangement [47–49]. The current difficulty of correlating amino acids hydropathy scale with their promotion or inhibition effect in literature requires combining molecular simulation and experimental studies to understand their interaction mechanism with hydrate systems [50].

In addition to KHPs, different reactor designs can play an important role in enhancing the methane hydrate formation kinetics. Fixed bed reactors (FBRs) showed better gas uptake and hydrate yield than both non-stirred (NSR) and stirred reactor (SR) configurations [51–53]. The FBR design shares the same configuration as the NSR with the packing materials lying at the bottom of the reactor [54]. A common advantage of different packing media, such as porous materials, glass beads, and metallic packing, is the enhancement of gas-liquid contact surface area and the elimination of energy-intensive agitation [55]. However, the type of packing is also an important factor. For example, Babu *et al.* revealed that silica sand showed superior hydrate formation kinetics compared to silica gel, polyurethane foam packing, and stirred reac-

tor configuration [56]. Another study by Kumar and Kumar showed that FBR with structured stainless-steel (SSS) packing outperformed silica sand and the stirred reactor [57]. More recent studies with other metallic packing types and shapes such as copper foam, aluminum foam and, stainless-steel beads (SSB), confirmed the promoting role of metallic packing for hydrate growth [58–61]. This promoting effect can be attributed to the enhanced thermal conductivity and the increased surface and confinement effect in the case of dense packing. However, there are three limitations of metallic packing. First, it has a relatively high density which reduces the gravimetric capacity. To illustrate, SS-316 has a density of $\sim$ 8000 kg/m^3, which is about 5 times higher than that of sand (1520-1680 kg/m^3) [62, 63]. Thus, a proper trade-off between the kinetic advantages and maintaining the gravimetric captivity is needed.The second drawback is that they fail to improve the heat transfer at the gas phase as water and packing bed share the same height. Finally, most studies added SDS to enhance the kinetic toward an acceptable range which is not favorable as detailed above.

The primary objective of this study is to compare the formation kinetics of CH_4-tetrahydrofuran (THF) hydrates using an acidic zeolite (H-SSZ-13) and different biodegradable amino acids (l-leucine, l-methionine, and l-tryptophan) as green eco-friendly hydrate promoters. The promoting mechanism of kinetics promoters is studied by combining DFT (density functional theory) calculations and detailed experimental kinetic data. Then, we use a green approach that combines those environmentally benign promoters with innovative reactor design with metallic filament packing to maximize the hydrate growth kinetics. Finally, we explored boosting economic feasibility by increasing the temperature toward near ambient (293.15 K) and tested the long-term storage at 253.2 K for long-term storage and its implications on hydrate technology.

6.2 Experimental Section

6.2.1 Experimental Procedure

6.2.1.1 Material and apparatus

Methane (99.99% purity) was purchased from Linde Co., and Tetrahydrofuran (THF, AR grade 99.99%) from Alfa Aesar, NH_4-SSZ-13 was purchased from ACS Materials (USA). The NH_4-form of zeolite was calcined was at 450°C for 4 hours to obtain the acidic form (H-SSZ-13). Amino acids l-tryptophan (reagent grade, 99 %), l-leucine (reagent grade, 99%), l-Methionine (reagent grade, 99%), and glycine (reagent grade, 99%) were purchased from Alfa Aesar. Fresh desalinated water was prepared in LCS (Laboratoire Catalyse et Spectrochimie), France. THF 5.56 mol% solution or its mix with zeolite or amino acid was prepared in a volumetric flask and stirred for 15 mins.

The instrument used for hydrate formation and dissociation is schematically described in **Figure C.1** and details of the set-up are provided in previous studies [40, 43]. In brief, it is composed of a 450 cm^3 high-pressure stainless-steel (SS-316) reactor (CR; Parr) that is equipped with light-weight corrosion resistance metallic filament packing (MFP). The morphology and detailed elemental composition of MFP is shown in **Table C.1**, and **Figure C.2**. The temperature is controlled by immersing the reactor inside a cooling bath where an external refrigerator (ER; Julabo, F250) circulates a glycol solution. While the pressure was measured by a pressure transmitter (PT; UNIK 5000, GE) with a range of 0-30 MPa and 0.1 % global error, the temperature was monitored by a K-type thermocouple (T) with $\pm$ 1.0 K accuracy. A data acquisition logger (DAQ; Nanodac, Eurotherm) connected to a personal computer (PC) was used to monitor the data during different experiments with the data collected every 10 seconds. To ensure data consistency, each experiment was repeated at least three times, as reported in **Tables C.2-C.7**. All experiment has been performed under isochoric and isothermal conditions.

6.2.1.2 Formation, Dissociation, and Storage Procedures

A detailed description of hydrate formation and recovery experiments and calculations is reported in supporting information as described in **Sections C.2.1 and C.2.2**. For the storage procedure, the reactor content was quenched to liquid nitrogen temperature and then recovered under liquid nitrogen in an external closed stainless steel container which was preserved in a refrigerator under 253.15 K and atmospheric pressure. Periodically, the sample weight has been followed to check the methane loss.

6.2.2 Characterization of H-SSZ-13 and Binary CH_4-THF Hydrate

The calcined acidic zeolite (H-SSZ-13) was characterized using scanning electron microscope (SEM), powder X-ray diffraction (PXRD), inductively coupled-atomic plasma emission spectroscopy (ICP-AES), scanning electron microscopy (SEM) equipped with energy dispersive X-ray (EDX), and N_2 adsorption as shown in **Section C.3.1**. The synthesized binary CH_4-THF hydrate was characterized by PXRD, Raman spectra, and ^{13}C NMR. Methods, procedures, calculations, and equipment are detailed in the supporting information **Section C.3.2**.

6.2.3 Density Functional Theory Calculations

For the computational part, we used density functional theory (DFT) calculations [64] with the projected augmented wave (PAW) method and the standard pseudopotentials as implemented in Quantum Espresso (QE) software [12, 65, 66]. A full detailed description of the promoter-hydrate models and calculation parameters are shown in supporting information **Section C.4**.

6.3 Results and discussion

Zeolite promoter (H-SSZ-13) was characterized by powder X-ray diffraction (PXRD,**Figure C.3**), scanning electron microscopy (SEM, **Figure C.4**), and N_2 physisorption (**Table C.10**). All data show that the employed material is highly crystalline. ICP-AES and EDX revealed that Si/Al ratio of 9. Powder XRD analysis confirmed sII formation, which coexists with a small amount of hexagonal ice. Raman spectroscopy analysis on the synthesized binary hydrate was

also performed. The spectroscopic data revealed methane occupancy in 5^{12} small cage of sII by a sharp peak at $\sim$ 2911.1 cm^{-1}. Carbon NMR measurements confirmed the Raman result with methane occupancy in 5^{12} small cages of sII by the sharp peak at -4.3 ppm while the other two peaks (26.2 and 69.0 ppm) indicate the large cage occupancy of THF as shown in **Figure C.5**. Detailed zeolite promoter and hydrate characterization results are provided in supporting information.

6.3.1 Prediction of Amino Acids Hydrate Promoting Effect at Molecular Level

Ab initio calculation has been commonly used in literature to report the effect of different promoters or inhibitors on hydrate formation [40, 43, 67, 68]. In our previous studies, we have utilized first principle calculations to explain the promoting effect of acidic and hydrophobic zeolites, which can be applied in the case of H-SSZ-13. Here, we have studied s different amino acids to anticipate their promoting effect as KHPs. First, the molecular level investigation aimed to find the best exchange-correlation functional representing the methane hydrate 5^{12} cage and then the hydrate-amino acids system. Then, the optimized DFT calculation was employed to analyze amino acids-hydrate systems in terms of 5^{12} hydrate cage energies and geometrical changes upon their interaction with amino acid molecules. The host-guest interactions are a key property that characterizes the clathrate stability [69] and can be assessed through interaction energy (ΔE^{HG}). This energy is defined as follow:

$$\Delta E^{HG} = E(CH_4@5^{12}) - [E(CH_4) + E(5^{12})] \tag{6.1}$$

where $E(CH_4@5^{12})$, $E(CH_4)$, and $E(5^{12})$ are the energies of $CH_4@5^{12}$, methane molecule, and the 5^{12} empty cage, respectively. The weak interactions such as H-bonding van der Waals forces, dominate the hydrate-amino acid systems interaction. Thus, the proper selection of exchange-correlation functions that capture those interactions is essential to represent those systems.

Thus, we initially calculated the interaction energy of methane with a small cage with four

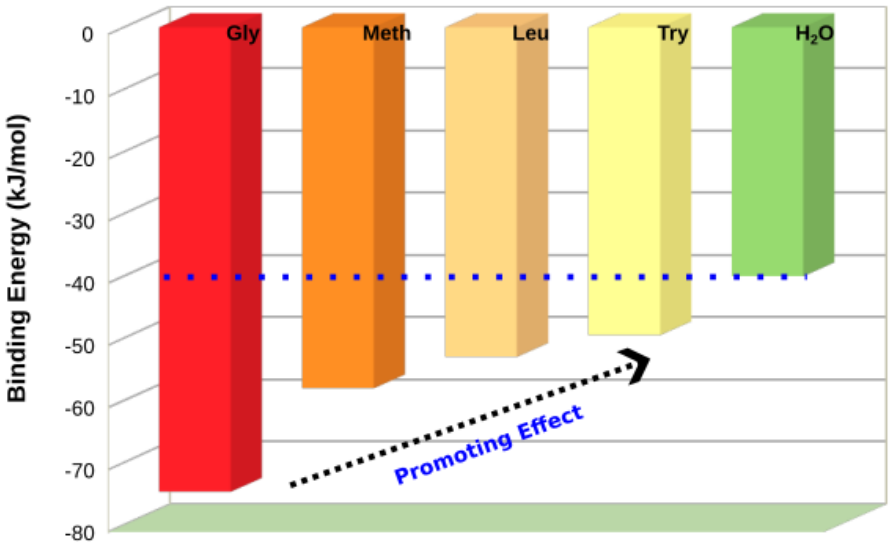

Figure 6.1: Comparison of binding energy (kJ/mol) of several amino acids to the 5^{12} methane cage compared to the interaction with H_2O. Higher binding energy shows that the amino acid disturbs the cage formation and acts as an inhibitor and *vice versa*, which agrees well with experimental observations [70–73].

different exchange-correlation functionals. Using revPBE, the calculation of binding energy resulted in +2.3 kJ/mol failing to determine the host-guest interactions accurately. Thus, we tested rVV-10, vdW-DF2, and SCAN-rvv10 exchange-correlation functionals to capture the van der Waals dispersion forces, as shown in **Figure C.8**. Compared to -32.55 kJ/mol obtained by the highly accurate but computationally expensive MP2/6-311++G(d,p) level of theory [69], the interaction energy value of -27.78 kJ/mol obtained from vdW-DF2 shows better accuracy in describing the host-guest interaction compared to rvv-10 and SCAN-rvv10 that underestimate and overestimated host-guest interactions, respectively. Consequently, we used it for all remaining calculations. After confirming the calculation accuracy on the $CH_4@5^{12}$ cage, we studied the interaction of amino acid molecules with the hydrate cage.To benchmark the promoting effect, we compare the interaction of different amino acids with $CH_4@5^{12}$ cage to that of a single water molecule with the same cage.

Based on the interaction energy of calculation, l-tryptophan showed the lowest interaction energy with -49.49 kJ/mol compared to l-methionine and l-leucine, which showed -58.03, and -52.99 kJ/mol, respectively. The more negative interaction energy indicates a more inhibitory effect for the amino acid. Accordingly, the promoting effect of amino acids is expected to be

l-tryptophan > l-leucine > l-methionine as illustrated in **Figure 6.1**. To further confirm, we did the same calculation on glycine, an amino acid known for its inhibiting effect on hydrate formation [47–49, 74], and the resulting interaction energy was -74.64 kJ/mol, which is significantly lower than all the other promoters in the study. The optimized amino-cage l-tryptophan and glycine are shown in **Figure 6.2**.

Our results show that the hydate promoting effect of amino acids does not only depend on their hydrophobicity alone but also on interactions with hydrate cage (e.g., hydrogen bonding) and thermodynamic conditions. To illustrate, while the most hydrophobic amino acids l-tryptophan showed the highest promoting effect among amino acids in all temperatures, l-leucine did not always show a more promoting effect than l-methionine despite its higher hydrophobicity according to Kyte and Doolittle scale [75, 76].

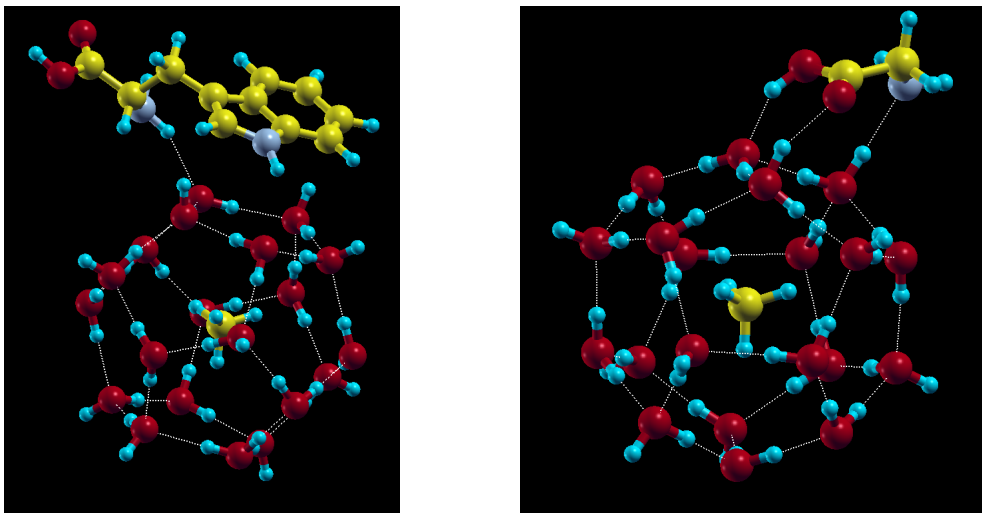

(a) **(b)**

Figure 6.2: Optimized configurations of small (5^{12}) cage with amino acids (a) l-tryptophan and (b) glycine. Nitrogen, hydrogen, carbon, and oxygen atoms are shown in violet, blue, yellow, and red colors, respectively.

6.3.2 Effect of Promoters on Binary CH_4-THF Hydrate Formation

To validate the above outcome of first principle calculations, we compared the performance of different amino acids in the non-stirring reactor (NSR) in the first set of experiments. At 283.15 K, the blank solution needed an induction time of 181.33 min. Adding 300 ppm of H-SSZ-13

has reduced the average induction time to about 11 min, while the average t_{90} (time taken for 90% completion of methane uptake) of 286.2 min outperformed other amino acids promoters, as shown in **Figure 6.3**. The presence of H-SSZ-13 has provided further liquid gas contact area and provided nucleation sites for hydrate formation. In the absence of extraframework cation as explained in the introduction, the acidity of H-SSZ-13 can increase gas insertion and improve the gas diffusion coefficient by increasing sII flexibility, similar to acidic additives such as perchloric acid ($HClO_4$) [77, 78]. This conclusion agrees well with our previous studies where the acidic forms of USY and Y zeolites were employed [79]. It is also confirmed by a recent study revealing that zeolite acidity is comparable to those of superacids [80]. Furthermore, the presence of acidic zeolite granted homogeneous nucleation through the whole aqueous bulk solution, as will be detailed in the next section.

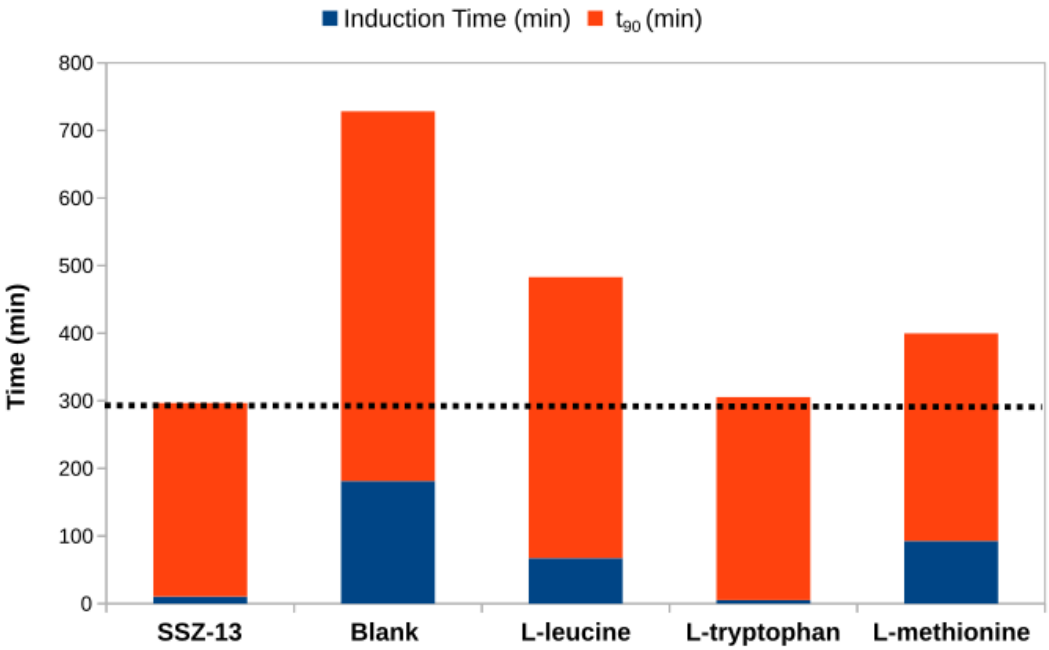

Figure 6.3: Comparison of induction time and t_{90} of H-SSZ-13 and different amino acids at 6 MPa and 283.15K

On the other hand, among the amino acids used, the hydrophobic l-tryptophan reduced the induction time significantly to 5.2 min compared to 67.3 min for l-leucine and 92.8 min for l-methionine, which agrees well with our computational expectations. When it comes to gas uptake, H-SSZ showed the highest gas uptake of 115.82 mmol gas/mol H_2O compared to

the best amino acids reported at that temperature (l-tryptophan), which showed 109.3 mmol gas/mol H_2O. This difference comes from the fact that although the amino acids increase the initial gas solubility into the THF solution, they still can slightly disturb the hydrate formation in a later stage by hydrogen bonding to the cage with both the amino group and secondary amine group. On the other hand, the H-SSZ-13 enhances the nucleation step by acting as heterogeneous nucleation sites. The enhanced kinetics uptake was also accompanied by almost full recovery (95-99 %) of the methane by slight heating up indicating a reversible process.

Increasing the temperature to 288.15 K and to near ambient (293.15K),has resulted in raised induction time and decreased gas uptake. Such behavior is a consequence of the exothermic nature of clathrate formation. **Figure 6.4** shows the gas uptake of different promoters at 293.15 K. However, one can also notice that t_{90} is at its highest at 288.15 and goes down at293.15 K as shown in **Table C.2** and **Table C.3**. While the increase of t_{90} at 288.15 K compared to 283.15 K can be justified by the slower kinetics, the lower t_{90} at 293.15 K indicates that the reaction is stopped at an earlier premature stage and accompanied by lower gas uptake. The latter can be explained by water's poor heat conductivity, which has the double role of being a reactant and a cooling medium. Another important observation is that increasing the temperature, l-tryptophan showed better kinetic performance in terms of induction time and gas uptake compared to other promoters, as shown in **Figure 6.4**. At the relative temperature and poor thermal conductivity, gas dissolution in the aqueous medium is the determining factor for kinetics. The poor performance of H-SSZ-13 at that temperature, despite the relatively short induction time, can be explained by its need for a certain critical concentration of dissolved methane to be able to trigger their role as nucleation sites. Finally, we tested the addition of 300 ppm of glycine to the THF solution. No gas uptake was observed after 24 h revealing glycine's inhibiting effect, which agrees well with previous experimental results and our DFT calculations.

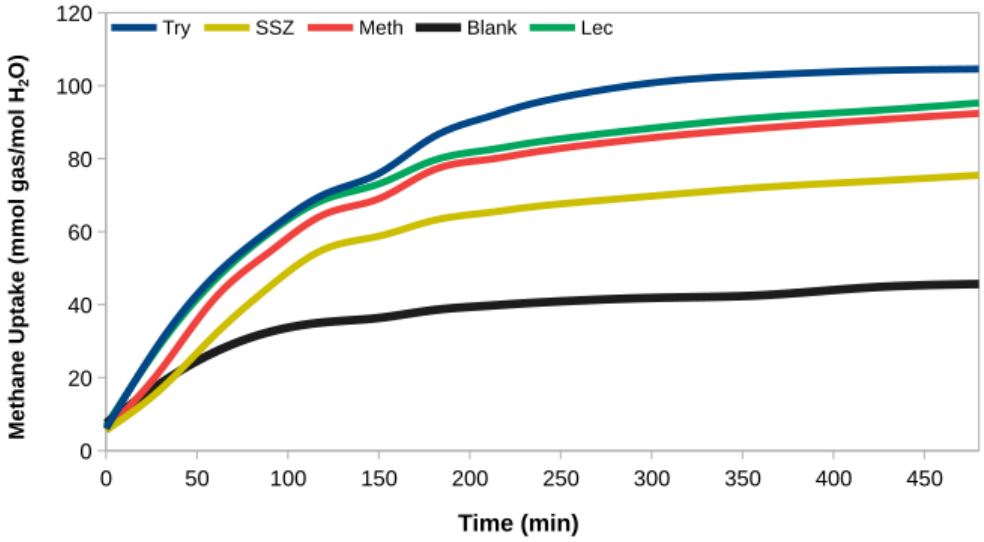

Figure 6.4: Comparison of methane uptake (mmol gas/mol H_2O)in the presence of H-SSZ-13 and different amino acids at 6 MPa and 293.15K.

6.3.3 Effect of Modified Reactor Design on Binary CH_4-THF Hydrate Formation

As has been shown above, performing the hydrate synthesis in the traditional NSR showed a high t_{90}, especially when increasing the temperature near ambient conditions to meet the economic requirements. The slow hydrate nucleation can be attributed to low gas-liquid heat transfer, and reactor design in terms of shape and cooling, i.e., the radial gradient of temperature. To illustrate, one can see that hydrate formation is more around the reactor wall due to the cooling around, which resulted in heat dissipation to the nearby aqueous solution **Figure 6.5a**.The poor heat transfer results in less hydrate formation when moving toward the center, with a clear advantage of H-SSZ-13 over amino acids (see below **Figure 6.5**).

However, even in the case of zeolites which allowed homogeneous nucleation, the formation of thin hydrate film at the surface hinders further gas-liquid mass transfer. Thus, we have utilized a light-weight metallic filaments network with a rough surface with the following objectives: (1) increase the heat conductivity, (2) break the hydrate thin film into smaller sections, (3) provide larger liquid-gas contact on the rough metal surface, and (4) extend the heat con-

(a) (b) (c)

Figure 6.5: Hydrate formation at 6 MPa and 293.15 K at (a) l-methionine at NSR (b) H-SSZ-13 at NSR and (c) H-SC.13 at FBR.

duction to the gas phase. **Figure 6.5** shows the features of hydrates formed in the NSR reactor in the presence of l-methionine (**Figure 6.5a**), H-SSZ-13 (**Figure 6.5a**), and those formed in FBR in presence of H-SSZ-13 (**Figure 6.5c**) . The zeolite improved the hydrate formation in bulk compared to l-methionine, while the presence of intervened filaments allowed exploiting the full potential of reactor volume compared to NSR. Moreover, the MFP has ruptured the hydrate thin film allowing better diffusive mass transfer and gas-liquid contact as illustrated in **Figure 6.5c** and **Figure 6.6** .

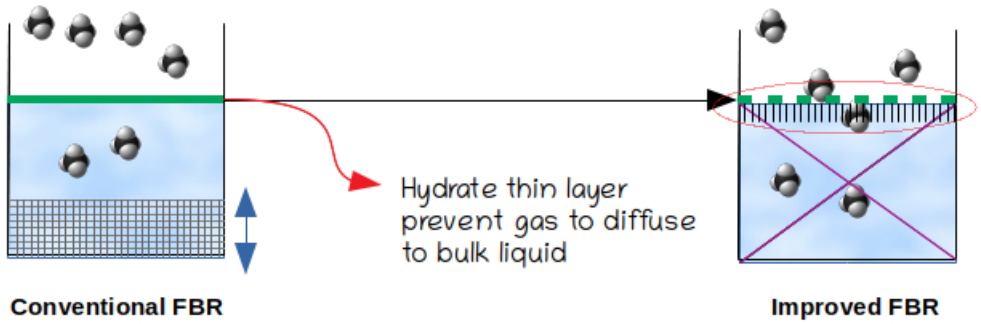

Figure 6.6: Illustration of metallic packing in hydrate FBR and the improved FBR presented in this study.

At the near-ambient temperature of 293.15 K as shown in **Table C.5**, we have found that the average induction time for a blank solution is about 81.7 min, indicating that the fixed bed reactor (FBR) is reduced by 110% compared to NSR configuration. Moreover, the utilization of promoters in the new FBR configuration has reduced the reaction time t_{90} to less than 3 hours which is feasible from both technical and economic points of view. Improving the thermal conductivity, H-SSZ-13 showed the best kinetic performance among the studied promoters with a significant simultaneous reduction in induction time to only 2.7 min (compared to 58.2

min in NSR) and the highest gas volumetric capacity of 104.5 v/v as shown in **Figure 6.7**.

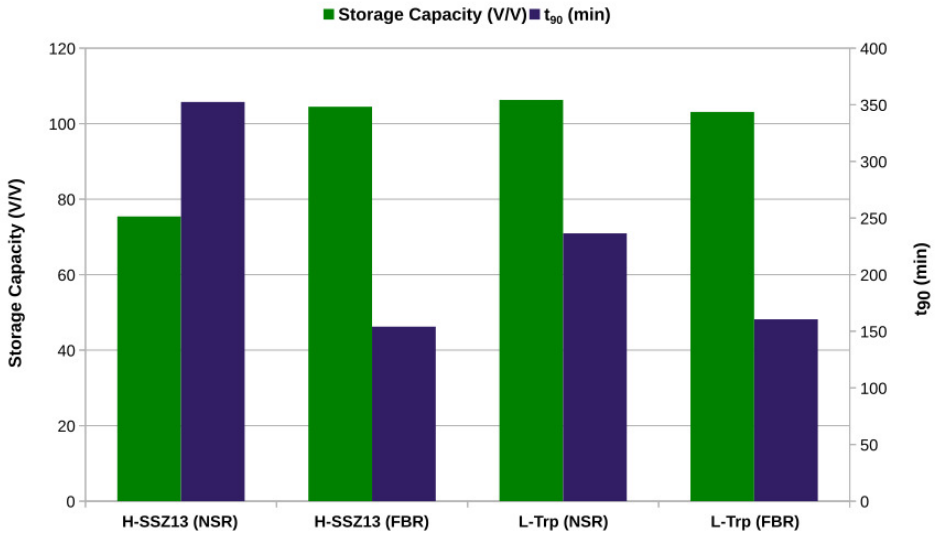

Figure 6.7: Comparison of storage capacity and t_{90} of H-SSZ-13 and l-tryptophan for hydrate synthesis in NSR and FBR at 6 MPa and 293.15K

These results point out that packing inside the reactor has successfully modified the surface properties and increased the gas mass transfer to a sufficient concentration to enhance the nucleations with acidic zeolites at the earlier stages. Moreover, it brokes the hydrate film formed early in the reaction and thus maintained suitable gas diffusion into the bulk medium. Among the amino acids, l-tryptophan slightly outperformed performed l-leucine in terms of both t_{90} and induction time but with a clear advantage of gas uptake and volumetric storage capacity of 103.73 mmol gas/mol H_2O and 103.11 v/v, respectively. Despite showing the lowest kinetic performance among the studied promoters, l-methionine in FBR still significantly reduced induction time to only 5 mins compared to 83.6 min when it was used in NSR configuration. This promoting performance of different amino acids in the case of FBR agreed well with our DFT calculation results. **Figure6.8** compares the induction time and gas uptake published in the literature at the same thermodynamic conditions. It shows that the kinetic performance and gas uptake of H-SSZ-13 and l-tryptophan outperformed hollow silica and SDS at the same temperature of 293.15 K and 6 MPa [36]. Moreover, it could get almost the same gas uptake at a higher pressure of 8 MPa with about 25 times reduction of induction time [81].

Decreasing the temperature from 288.15 to 283.15 shown in **Table C.6 and Table C.7**,

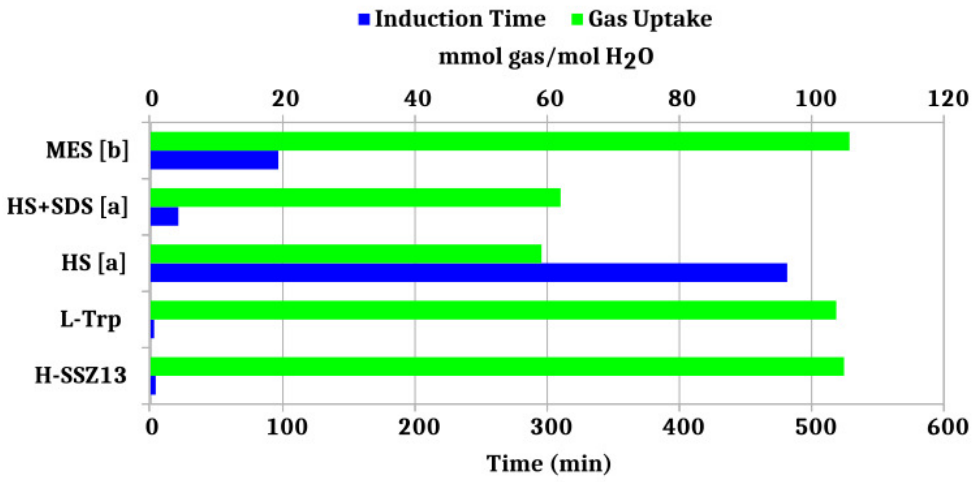

Figure 6.8: Comparison of induction time and methane uptake of this work with the literature **[a]** using hollow silica (HS) and (HS+SDS) at 6 MPa and 293.15K [36] and **[b]** using methyl ester sulfonate (MES) at 8 MPa and 293.15 K [81].

resulted in a decrease in both induction time and t_{90}. Moreover, the kinetic performance of all promoters at those temperatures outperformed those under NSR conditions. To illustrate, H-SSZ-13 resulted in a volumetric capacity of 114 v/v at 288.15 K, with an increase of 42.7% compared to NSR under the same conditions. At the same temperature, l-tryptophane resulted in a gas uptake of 115.4 mmol gas/mol H_2O, which is 22.6% higher than the same conditions at NSR. Lowering the temperature to 283.15K significantly accelerated the reaction kinetics and reduced the t_{90} to less than 80 mins. For example, there was almost instantaneous gas uptake in the case of both H-SSZ-13 and l-tryptophan. Despite the fast reaction compared to NSR and the higher temperature, H-SSZ-13 and l-tryptophan and reached an impressive volumetric capacity (110.7-117.0 mmol gas/mol H_2O). As shown in **Figure6.9**, such outstanding performance is due to the enhanced kinetic and heat transfer that resulted in a sharper temperature peak.

6.3.4 Techno-economic Aspects Implications and Long-Term Storage

One of the main goals of this study is to connect molecular-level investigation and macro-kinetic studies to the engineering and technological aspects. Establishing this connection at the early research stage will guarantee the smooth and economic scale-up process of synthetic natural gas hydrate technology (SGH). In this section, we explain the possible economic outcome of

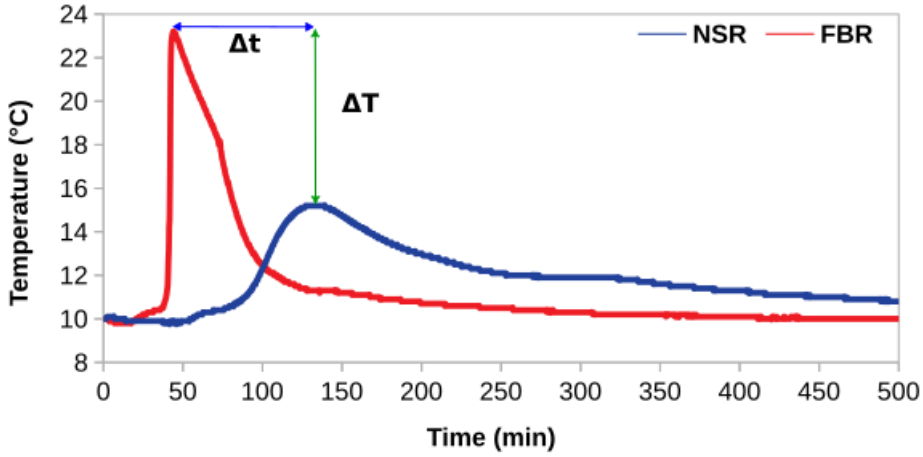

Figure 6.9: Comparison of temperature profiles of hydrate formation in NSR and FBR at 6 MPa and 283.15K.

this study's technological choices, such as realistic conditions (near-ambient temperature) and a moderate pressure of 6 MPa, the use of FBR, and the selection of low-cost green promoters to boost the hydrate formation process kinetics. Then, we show the importance and possibility of using SGH technology for long-term storage compared to other technologies such as CNG and LNG. Finally, we discuss some perspectives on the presented work.

It is important to reduce the cost of the hydrate formation process to cut the overall operating cost. According to Veluswamy *et al.*, the CAPEX (capital expenditure)/ OPEX (operating expenditure) ratio in the case of sII is 4.6 compared to 5.3 in the case of CNG with the same volumetric capacity (115 v/v) [82]. Although there is a clear advantage of SGH in terms of safety and long-term storage economics, this ratio still reflects the high cost of hydrate synthesis. Lucia *et al.* estimated that the compression cost is about 70-80 % of the total cost for methane hydrate synthesis in a large-scale 25 L reactor [83]. Thus, we have utilized THF as a thermodynamic promoter to relax the *P-T* conditions to 6 MPa and 293.15 K, significantly boosting the process economics [84].

The role of THF is not only limited to reducing the thermodynamic requirements but also extended to increase the stability of sII clathrate. The stability of binary CH_4-THF sII clathrate

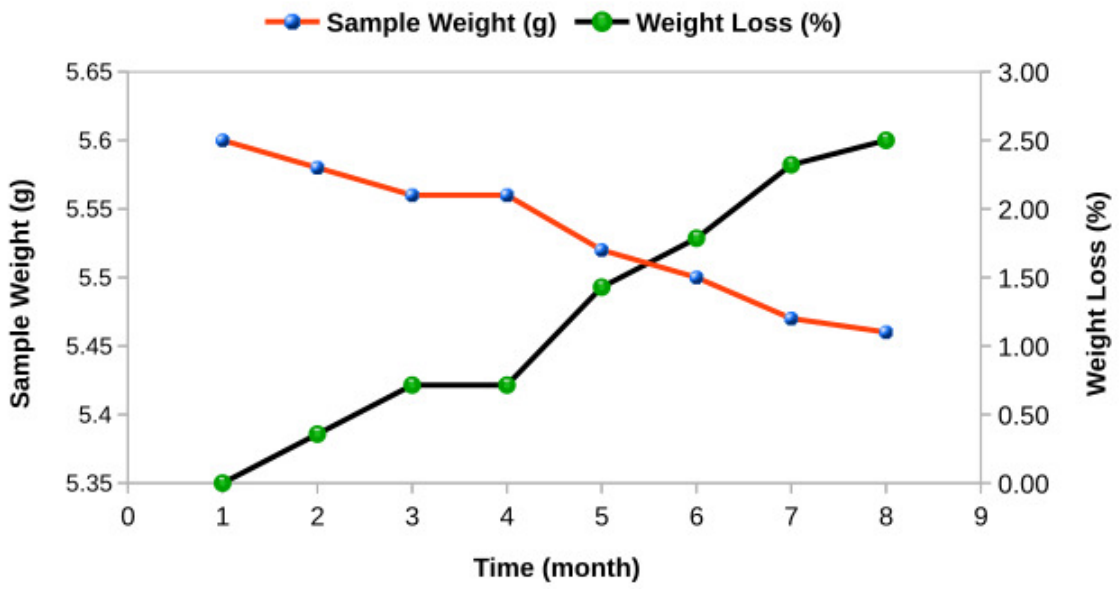

Figure 6.10: Evolution of weight loss of CH_4-THF hydrate stored in 253.15 K over 8 months.

is higher than pure THF clathrate, as revealed by high-pressure differential scanning calorimetry analysis [85]. The high stability allowed storing CH_4-THF pellets at 1.5 atm and 271.5 K for 2 months. In this study, the CH_4-THF hydrates were transferred under liquid nitrogen without further processing to a container and could be stored for 8 months at 253.15 K and atmospheric pressure. During that period, the hydrate sample weight loss did not exceed 0.6 wt% for 4 months and 2.5 wt% over 8 months from about 8.35 wt% of the stored methane as shown in **Figure 6.10**. The possibility of storing methane at atmospheric or slightly positive pressure is a clear advantage when it comes to long-term storage compared to LNG which requires extensive refrigeration to keep LNG at 113 K which is estimated to be typically **27%** of the cost or 32.4 €/GWh/d (0.5 €/t LNG/day) as per current gas prices [86]. Due to boil-off gases, LNG can suffer from 0.05 wt% loss per day in LNG or 2-6 wt% loss in cargo depending on the voyage length, typically 3 weeks [87]. Thus, the loss in long-term storage can be approximately 12 wt% over 4 months in the best cases. Based on our experimental results, methane storage at the synthesized hydrate without further processing can be more economically attractive than a typical LNG tank. As illustrated in **Figure6.11**, SGH from our experiments showed a significantly lower methane loss compared to a typical LNG tank for at least for months considering the best cases of boil-off losses [87]. After 8 months, the methane loss in the LNG is

estimated to become slightly lower compared to our SGH. Nevertheless, the storage of SNG is still much more advantageous due to the large difference between refrigeration requirements of LNG transportation and storage at 113 K (47% of LNG total cost) compared to those required for SGH at 253 K [11, 86]. Further optimization and detailed more detailed economic evaluation is required to treat other factors.

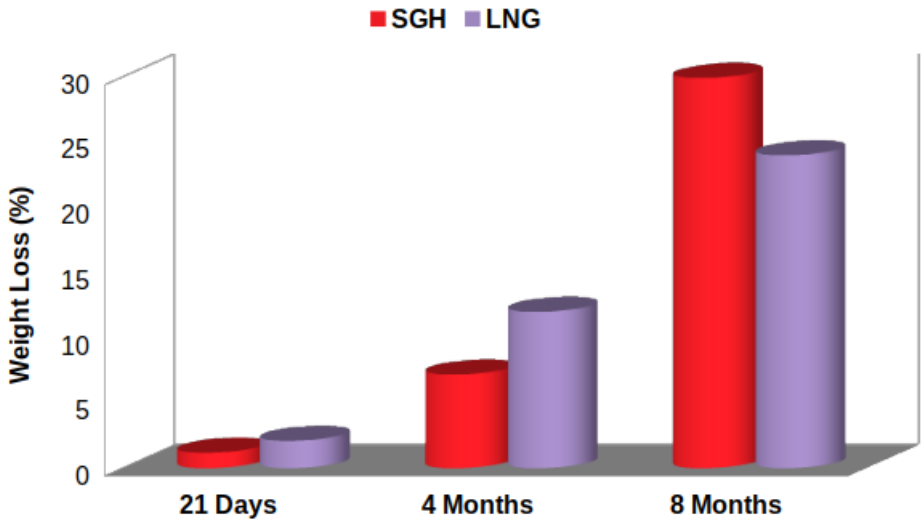

Figure 6.11: Comparison of weight loss of CH_4-THF hydrate stored in 253.15 K and LNG in 113 K over 8 months.

Finally, we have used an innovative green approach that combined green KHP and improved FBR design. Ourpacking is less than 0.08 wt/wt of the hydrate content, which is significantly lower compared to different packing reported in the literature. For example, Kumar *et al.* reported weight percentages of (0.28-1.2) for traditional stainless steel packing (SSP), 1.1 for silica gel, and even 5.0 for silica sand[88] . While this study compared FBR to NSR, here we address the economical aspects of using stirred reactors, which are the most common reactor configuration to increase the gas-liquid contact, enhance mass transfer, and shorten the induction time [89, 90]. In fact, the mass transfer in those reactors drops quickly after the nucleation as a widely used bottom-mounted laboratory magnetic stirrer does not affect the floating hydrate clusters that arrange themselves in a thin layer preventing further gas-liquid contact [91].Despite the better performance achieved by the top-mounted stirrer design [92], scale-up studies that involved both heat and mass transfer analysis showed that the stirred-reactor con-

figuration is not economically feasible [93]. Namely, the lower hydrate weight in water ($\leq$ 5 wt%) results in post-processing filtration cost and increasing agitation energy demand as the slurry thickens [94, 95]. Thus, compared to both stirred and non-stirred configurations, the improved FBR design with light-weight packing showed superior performance. Based on the above results, the perspective studies will include surveying more computationally designed green promoters, experimental studies on more acidic zeolites, and amino acids. Further improvements in the reactor design to increase the surface area of liquid-gas contact and exploring different hydrate structures is expected to enhance the storage capacity.

6.4 Conclusions

The present study provides an integrated approach for methane hydrate formation combining environmentally benign KHPs, namely acidic zeolites and amino acids, and innovative reactor design to accelerate reaction kinetics and improve the storage capacity. It also provides a first-principle methodology to evaluate the promoting efficiency of amino acid zeolite. Another important issue addressed in the study is the long-term storage in SGM compared with state-of-the-art LNG technology.

Different zeolite and amino acids KHPs at low concentrations of 300 ppm were evaluated under 6 MP and at different temperatures in a non-stirred reactor (NSR) reactor. H-SSZ-13 showed the best performance at 283 K with an average induction time of 10.5 mins, hydrate volumetric capacity of 115 v/v, and recovery of 97%. The l-tryptophane outperformed other KHPs at 283 K and 288 K in terms of induction time and gas uptake. However, the performance of all promoters dropped at 293.15 K due to low methane solubility and mass transfer limitations.

We introduced a fixed bed reactor (FBR) equipped with special metallic filament packing (MFP) to overcome the above limitations. The new MFP-FBR improved mass and heat transfer

by increasing the thermal conductivity and breaking the hydrate thin film formation without significantly affecting the gravimetric storage capacity.The experimental data showed that the presence of the green KHP H-SSZ-13 significantly reduced the reaction time and increased the volumetric storage capacity to 96% of the theoretical value. The overall performance of amino acids followed the order of l-tryptophan $>$ l-leucine $>$ l-methionine, which agreed well with our first-principle calculations. Finally, our study demonstrated the potential of SNG for long-term methane storage in economic conditions compared to LNG.

References

[1] Ahmed Omran, Nikolay Nesterenko, and Valentin Valtchev. Zeolitic ice : A route toward net zero emissions. *Renew. Sustain. Energy Rev.*, 168(112768), 2022.

[2] Reza Hafezi, Amir Naser Akhavan, Saeed Pakseresht, and David A. Wood. Global natural gas demand to 2025: A learning scenario development model. *Energy*, 224:120167, 2021.

[3] Ahmed Omran, Sun Hee Yoon, Murtaza Khan, Minhaj Ghouri, Anjaneyulu Chatla, and Nimir Elbashir. Mechanistic insights for dry reforming of methane on cu/ni bimetallic catalysts: DFT-assisted microkinetic analysis for coke resistance. *Catalysts*, 10(9):1–16, 2020.

[4] T. Klatzer, U. Bachhiesl, and S. Wogrin. State-of-the-art expansion planning of integrated power, natural gas, and hydrogen systems. *Int. J. Hydrogen Energy*, 47(47):20585–20603, jun 2022.

[5] Huchao Song, Yinhe Liu, Hao Bian, Mengfei Shen, and Xiaolong Lin. Energy, environment, and economic analyses on a novel hydrogen production method by electrified steam methane reforming with renewable energy accommodation. *Energy Convers. Manag.*, 258(January):115513, apr 2022.

[6] Abhinandan Kumar, Pardeep Singh, Pankaj Raizada, and Chaudhery Mustansar Hussain. Impact of COVID-19 on greenhouse gases emissions: A critical review. *Sci. Total Environ.*, 806:150349, 2022.

[7] Marzia Sesini, Sara Giarola, and Adam D. Hawkes. Solidarity measures: Assessment of strategic gas storage on EU regional risk groups natural gas supply resilience. *Appl. Energy*, 308(December 2021):118356, 2022.

[8] J. Javanmardi, Kh Nasrifar, S. H. Najibi, and Mahmood Moshfeghian. Natural gas transportation: NGH or LNG? *World Rev. Sci. Technol. Sustain. Dev.*, 4(2-3):258–267, 2007.

[9] Yuwei Yin and Jasmine Siu Lee Lam. Bottlenecks of LNG supply chain in energy transition: A case study of China using system dynamics simulation. *Energy*, 250:123803, 2022.

[10] Tim Tørnes Pedersen, Ebbe Kyhl Gøtske, Adam Dvorak, Gorm Bruun Andresen, and Marta Victoria. Long-term implications of reduced gas imports on the decarbonization of the European energy system. *Joule*, 6(7):1566–1580, jul 2022.

[11] Hari Prakash Veluswamy, Asheesh Kumar, Yutaek Seo, Ju Dong Lee, and Praveen Linga. A review of solidified natural gas (SNG) technology for gas storage via clathrate hydrates. *Appl. Energy*, 216(February):262–285, 2018.

[12] Ahmed Omran, Nikolai Nesterenko, and Valentin Valtchev. Ab initio mechanistic insights into the stability, diffusion and storage capacity of sI clathrate hydrate containing hydrogen. *Int. J. Hydrogen Energy*, 47(13):8419–8433, 2022.

[13] J. S. GUDMUNDSSON, V. ANDERSSON, O. I. LEVIK, and M. MORK. Hydrate Technology for Capturing Stranded Gas. *Ann. N. Y. Acad. Sci.*, 912(1):403–410, jan 2006.

[14] Zhi Ming Xia, Xiao Sen Li, Zhao Yang Chen, Gang Li, Ke Feng Yan, Chun Gang Xu, Qiu Nan Lv, and Jing Cai. Hydrate-based CO2 capture and CH4 purification from simulated biogas with synergic additives based on gas solvent. *Appl. Energy*, 162:1153–1159, 2016.

[15] Florian Filarsky, Carsten Schmuck, and Heyko Juergen Schultz. Development of a biogas production and purification process using promoted gas hydrate formation — A feasibility study. *Chem. Eng. Res. Des.*, 134:257–267, 2018.

[16] Sebastian Timmerberg, Martin Kaltschmitt, and Matthias Finkbeiner. Hydrogen and hydrogen-derived fuels through methane decomposition of natural gas – GHG emissions and costs. *Energy Convers. Manag. X*, 7(February):100043, 2020.

[17] B. P. Prajwal and K. G. Ayappa. Evaluating methane storage targets: From powder samples to onboard storage systems. *Adsorption*, 20(5-6):769–776, 2014.

[18] Hesam Najibi, Morteza Mirzaee Shayegan, and Hassan Heidary. Experimental investigation of methane hydrate formation in the presence of copper oxide nanoparticles and SDS. *J. Nat. Gas Sci. Eng.*, 23:315–323, 2015.

[19] Zhen Pan, Zhiming Liu, Zhien Zhang, Liyan Shang, and Shihui Ma. Effect of silica sand size and saturation on methane hydrate formation in the presence of SDS. *J. Nat. Gas Sci. Eng.*, 56(February):266–280, 2018.

[20] Xiao-Yan Deng, Ying Yang, Dong-Liang Zhong, Xi-Yue Li, Bin-Bin Ge, and Jin Yan. New Insights into the Kinetics and Morphology of CO 2 Hydrate Formation in the Presence of Sodium Dodecyl Sulfate . *Energy & Fuels*, 35(17):13877–13888, 2021.

[21] Abdolreza Farhadian, Andrey S Stoporev, Mikhail A Varfolomeev, Yulia F Zaripova, Vladimir V Yarkovoi, Matvei E Semenov, Airat G Kiiamov, Roman S Pavelyev, Aleksandr M Aimaletdinov, Tharaa Mohammad, and Danis K Nurgaliev. Sulfonated Castor Oil as an Efficient Biosurfactant for Improving Methane Storage in Clathrate Hydrates. *ACS Sustain. Chem. Eng.*, 10(30):9921–9932, aug 2022.

[22] Gaurav Bhattacharjee, Vivek Barmecha, Omkar S. Kushwaha, and Rajnish Kumar. Kinetic promotion of methane hydrate formation by combining anionic and silicone surfactants: Scalability promise of methane storage due to prevention of foam formation. *J. Chem. Thermodyn.*, 117:248–255, 2018.

[23] Gaurav Pandey, Gaurav Bhattacharjee, Hari Prakash Veluswamy, Rajnish Kumar, Jitendra S. Sangwai, and Praveen Linga. Alleviation of Foam Formation in a Surfactant Driven Gas Hydrate System: Insights via a Detailed Morphological Study. *ACS Appl. Energy Mater.*, 1(12):6899–6911, 2018.

[24] W. X. Pang, G. J. Chen, A. Dandekar, C. Y. Sun, and C. L. Zhang. Experimental study on the scale-up effect of gas storage in the form of hydrate in a quiescent reactor. *Chem. Eng. Sci.*, 62(8):2198–2208, 2007.

[25] Yue Qin, Zhen Pan, Zhiming Liu, Liyan Shang, and Li Zhou. Influence of the Particle Size of Porous Media on the Formation of Natural Gas Hydrate: A Review. *Energy and Fuels*, 35(15):11640–11664, 2021.

[26] Lars Borchardt, Mirian Elizabeth Casco, and Joaquin Silvestre-Albero. Methane Hydrate in Confined Spaces: An Alternative Storage System. *ChemPhysChem*, 19(11):1298–1314, 2018.

[27] Maninder Khurana, Zhenyuan Yin, and Praveen Linga. A review of clathrate hydrate nucleation. *ACS Sustain. Chem. Eng.*, 5(12):11176–11203, 2017.

[28] Samer Said, Varun Govindaraj, Jean Michel Herri, Yamina Ouabbas, Mohamed Khodja, Mohamed Belloum, Jitendra S. Sangwai, and Ramamurthy Nagarajan. A study on the influence of nanofluids on gas hydrate formation kinetics and their potential: Application to the CO2 capture process. *J. Nat. Gas Sci. Eng.*, 32:95–108, 2016.

[29] Jae Woo Choi, Jin Tack Chung, and Yong Tae Kang. CO2 hydrate formation at atmospheric pressure using high efficiency absorbent and surfactants. *Energy*, 78:869–876, 2014.

[30] Zhen Pan, Zhiming Liu, Zhien Zhang, Liyan Shang, and Shihui Ma. Effect of silica sand size and saturation on methane hydrate formation in the presence of SDS. *J. Nat. Gas Sci. Eng.*, 56(February):266–280, 2018.

[31] Yanhong Wang, Xuemei Lang, and Shuanshi Fan. Accelerated nucleation of tetrahydrofuran (THF) hydrate in presence of ZIF-61. *J. Nat. Gas Chem.*, 21(3):299–301, 2012.

[32] Sarocha Rungrussamee, Katipot Inkong, Santi Kulprathipanja, and Pramoch Rangsunvigit. Comparative study of methane hydrate formation and dissociation with hollow silica and activated carbon. *Chem. Eng. Trans.*, 70:1519–1524, 2018.

[33] Guodong Zhang, Bingjie Liu, Lu Xu, Runcheng Zhang, Yan He, and Fei Wang. How porous surfaces influence the nucleation and growth of methane hydrates. *Fuel*, 291:120142, 2021.

[34] Yang Peng, Vaiva Krungleviciute, Ibrahim Eryazici, Joseph T. Hupp, Omar K. Farha, and Taner Yildirim. Methane storage in metal-organic frameworks: Current records, surprise findings, and challenges. *J. Am. Chem. Soc.*, 135(32):11887–11894, 2013.

[35] Eyas Mahmoud, Labeeb Ali, Asmaa El Sayah, Sara Awni Alkhatib, Hend Abdulsalam, Mouza Juma, and Ala'A H Al-Muhtaseb. Implementing metal-organic frameworks for natural gas storage. *Crystals*, 9(8):1–19, 2019.

[36] Katipot Inkong, Hari Prakash Veluswamy, Pramoch Rangsunvigit, Santi Kulprathipanja, and Praveen Linga. Innovative Approach to Enhance the Methane Hydrate Formation at Near-Ambient Temperature and Moderate Pressure for Gas Storage Applications. *Ind. Eng. Chem. Res.*, 58(49):22178–22192, 2019.

[37] Xiao Ya Zang, Shuan Shi Fan, De Qing Liang, Dong Liang Li, and Guang Jin Chen. Influence of 3A molecular sieve on tetrahydrofuran (THF) hydrate formation. *Sci. China, Ser. B Chem.*, 51(9):893–900, 2008.

[38] Xiaoya ZANG, Jianwei DU, Deqing LIANG, Shuanshi FAN, and Cuiping TANG. Influence of A-type Zeolite on Methane Hydrate Formation. *Chinese J. Chem. Eng.*, 17(5):854–859, 2009.

[39] Jun-Ho Hyun Nam-Jin Kim, Sung-Seek Park, Sang-Woong Shin and Wongee Chun. An experimental investigation into the effects of zeolites on the formation of methane hydrates. *Int. J. Energy Res.*, 39:26–32, 2015.

[40] Ahmed Omran, Nikolay Nesterenko, and Valentin Valtchev. Revealing Zeolites Active Sites Role as Kinetic Hydrate Promoters: Combined Computational and Experimental Study. *ACS Sustain. Chem. Eng.*, 10(24):8002–8010, jun 2022.

[41] Ana Palčić and Valentin Valtchev. Analysis and control of acid sites in zeolites. *Appl. Catal. A Gen.*, 606(July 2020):117795, 2020.

[42] Shurraya Denning, Ahmad AA Majid, James M. Crawford, Moises A. Carreon, and Carolyn A. Koh. Promoting Methane Hydrate Formation for Natural Gas Storage over Chabazite Zeolites. *ACS Appl. Energy Mater.*, 4(11):13420–13424, 2021.

[43] Ahmed Omran, Nikolay Nesterenko, Arnold A Paecklar, Nicolas Barrier, and Valentin Valtchev. Toward Economical Seawater-Based Methane Hydrate Formation at Ambient Temperature: A Combined Experimental and Computational Study. *ACS Sustain. Chem. Eng.*, ASAP, aug 2022.

[44] Jyoti Shanker Pandey, Yousef Jouljamal Daas, and Nicolas von Solms. Screening of amino acids and surfactant as hydrate promoter for CO2 capture from flue gas. *Processes*, 8(124):1–23, 2020.

[45] Ngoc N. Nguyen, Mirza Galib, and Anh V. Nguyen. Critical Review on Gas Hydrate Formation at Solid Surfaces and in Confined Spaces—Why and How Does Interfacial Regime Matter? *Energy & Fuels*, 34(6):6751–6760, 2020.

[46] Ahmad A.A. Majid, Joshua Worley, and Carolyn A. Koh. Thermodynamic and Kinetic Promoters for Gas Hydrate Technological Applications. *Energy and Fuels*, 35(23):19288–19301, 2021.

[47] Hadi Roosta, Ali Dashti, S Hossein Mazloumi, and Farshad Varaminian. The dual effect of amino acids on the nucleation and growth rate of gas hydrate in ethane + water, methane + propane + water and methane + THF + water systems. *Fuel*, 212:151–161, 2017.

[48] Qazi Nasir, Humbul Suleman, and Yasir A Elsheikh. A review on the role and impact of various additives as promoters/ inhibitors for gas hydrate formation. *J. Nat. Gas Sci. Eng.*, 76(February):103211, 2020.

[49] Jeong Hoon Sa, Gye Hoon Kwak, Bo Ram Lee, Da Hye Park, Kunwoo Han, and Kun Hong Lee. Hydrophobic amino acids as a new class of kinetic inhibitors for gas hydrate formation. *Sci. Rep.*, 3:1–7, 2013.

[50] Cornelius B. Bavoh, Bhajan Lal, Harrison Osei, Khalik M. Sabil, and Hilmi Mukhtar. A review on the role of amino acids in gas hydrate inhibition, CO2 capture and sequestration, and natural gas storage. *J. Nat. Gas Sci. Eng.*, 64(November 2018):52–71, 2019.

[51] Praveen Linga, Nagu Daraboina, John A. Ripmeester, and Peter Englezos. Enhanced rate of gas hydrate formation in a fixed bed column filled with sand compared to a stirred vessel. *Chem. Eng. Sci.*, 68(1):617–623, 2012.

[52] P Linga and M A Clarke. A Review of Reactor Designs and Materials Employed for Increasing the Rate of Gas Hydrate Formation. *Energy Fuels*, 31:30, 2017.

[53] Zhenyuan Yin, Maninder Khurana, Hoon Kiang Tan, and Praveen Linga. A review of gas hydrate growth kinetic models, 2018.

[54] Junjie Zheng, Bao-Yong Zhang, Qiang Wu, and Praveen Linga. Kinetic Evaluation of Cyclopentane as a Promoter for CO 2 Capture via a Clathrate Process Employing Different Contact Modes. *ACS Sustain. Chem. Eng.*, 6(9):11913–11921, sep 2018.

[55] Mohammad Reza Ghaani, Judith M. Schicks, and Niall J. English. A review of reactor designs for hydrogen storage in clathrate hydrates. *Appl. Sci.*, 11(2):1–16, 2021.

[56] Ponnivalavan Babu, Praveen Linga, Rajnish Kumar, and Peter Englezos. A review of the hydrate based gas separation (HBGS) process for carbon dioxide pre-combustion capture. *Energy*, 85:261–279, jun 2015.

[57] Asheesh Kumar and Rajnish Kumar. Role of metallic packing and kinetic promoter in designing a hydrate-based gas separation process. *Energy and Fuels*, 29(7):4463–4471, 2015.

[58] Atousa Heydari and Kiana Peyvandi. Role of metallic porous media and surfactant on kinetics of methane hydrate formation and capacity of gas storage. *J. Pet. Sci. Eng.*, 181(July):106235, 2019.

[59] Namrata Gaikwad, Gaurav Bhattacharjee, Omkar S. Kushwaha, Jitendra S. Sangwai, Praveen Linga, and Rajnish Kumar. Effect of Cyclooctane and <scp>l</scp> -

Tryptophan on Hydrate Formation from an Equimolar CO2–CH4 Gas Mixture Employing a Horizontal-Tray Packed Bed Reactor. *Energy & Fuels*, 34(8):9840–9851, aug 2020.

[60] Nithin B. Kummamuru, Sammy W. Verbruggen, Silvia Lenaerts, and Patrice Perreault. Experimental investigation of methane hydrate formation in the presence of metallic packing. *Fuel*, 323(February):124269, sep 2022.

[61] Liang Yang, Chunxiao Li, Junhua Pei, Xin Wang, Ni Liu, Yingming Xie, Guomin Cui, and Daoping Liu. Enhanced clathrate hydrate phase change with open-cell copper foam for efficient methane storage. *Chem. Eng. J.*, 440(December 2021):135912, jul 2022.

[62] Michelle L. KOSMATKA, Steven H.; WILSON. *Design and Control of Concrete Mixtures The Guide to Applications, Methods and Materials.* 15 edition, 2011.

[63] Frank E Jones and Randall M Schoonover. *Handbook of mass measurement*. Chapman and Hall/CRC, mar 2002.

[64] W. Kohn. Nobel lecture: Electronic structure of matter - Wave functions and density functional. *Rev. Mod. Phys.*, 71(5):1253–1266, 1999.

[65] Paolo Giannozzi, Stefano Baroni, Nicola Bonini, Matteo Calandra, Roberto Car, Carlo Cavazzoni, Davide Ceresoli, Guido L. Chiarotti, Matteo Cococcioni, Ismaila Dabo, Andrea Dal Corso, Stefano De Gironcoli, Stefano Fabris, Guido Fratesi, Ralph Gebauer, Uwe Gerstmann, Christos Gougoussis, Anton Kokalj, Michele Lazzeri, Layla Martin-Samos, Nicola Marzari, Francesco Mauri, Riccardo Mazzarello, Stefano Paolini, Alfredo Pasquarello, Lorenzo Paulatto, Carlo Sbraccia, Sandro Scandolo, Gabriele Sclauzero, Ari P. Seitsonen, Alexander Smogunov, Paolo Umari, and Renata M. Wentzcovitch. QUANTUM ESPRESSO: A modular and open-source software project for quantum simulations of materials. *J. Phys. Condens. Matter*, 21(39):395502, 2009.

[66] Ahmed S. Omran. *DFT Study of Copper-Nickel (111) Catalyst for Methane Dry Reforming*. PhD thesis, (Master Disseration)Texas A & M, 2019.

[67] Dongyoung Lee, Woojin Go, and Yongwon Seo. Experimental and computational investigation of methane hydrate inhibition in the presence of amino acids and ionic liquids. *Energy*, 182:632–640, 2019.

[68] Mohammad Tariq, David Rooney, Enas Othman, Santiago Aparicio, Mert Atilhan, and Majeda Khraisheh. Gas hydrate inhibition: A review of the role of ionic liquids. *Ind. Eng. Chem. Res.*, 53(46):17855–17868, 2014.

[69] Mert Atilhan, Nezih Pala, and Santiago Aparicio. A quantum chemistry study of natural gas hydrates. *J. Mol. Model.*, 20(4):1–15, 2014.

[70] Dongyoung Lee, Woojin Go, Gyeol Ko, and Yongwon Seo. Inhibition synergism of glycine (an amino acid) and [BMIM][BF4] (an ionic liquid) on the growth of CH4 hydrate. *Chem. Eng. J.*, 393(February):124466, 2020.

[71] Pinnelli S.R. Prasad and Burla Sai Kiran. Are the amino acids thermodynamic inhibitors or kinetic promoters for carbon dioxide hydrates? *J. Nat. Gas Sci. Eng.*, 52(January):461–466, 2018.

[72] Yuanhao Cai, Yulong Chen, Qijie Li, Liang Li, Haoxin Huang, Suying Wang, and Weixing Wang. CO2 Hydrate Formation Promoted by a Natural Amino Acid l-Methionine for Possible Application to CO2 Capture and Storage. *Energy Technol.*, 5(8):1195–1199, 2017.

[73] Hari Prakash Veluswamy, Asheesh Kumar, Rajnish Kumar, and Praveen Linga. An innovative approach to enhance methane hydrate formation kinetics with leucine for energy storage application. *Appl. Energy*, 188:190–199, 2017.

[74] Cornelius B. Bavoh, Bhajan Lal, Harrison Osei, Khalik M. Sabil, and Hilmi Mukhtar. A review on the role of amino acids in gas hydrate inhibition, CO2 capture and sequestration, and natural gas storage. *J. Nat. Gas Sci. Eng.*, 64(November 2018):52–71, 2019.

[75] Ngoc N. Nguyen and Anh V. Nguyen. Hydrophobic Effect on Gas Hydrate Formation in the Presence of Additives. *Energy and Fuels*, 31(10):10311–10323, 2017.

[76] Jack Kyte and Russell F. Doolittle. A simple method for displaying the hydropathic character of a protein. *J. Mol. Biol.*, 157(1):105–132, 1982.

[77] Arnaud Desmedt, Ludovic Martin-Gondre, The Thuong Nguyen, Claire Pétuya, Leyre Barandiaran, Odile Babot, Thierry Toupance, R Gary Grim, and Amadeu K Sum. Modifying the flexibility of water cages by co-including acidic species within clathrate hydrate. *J. Phys. Chem. C*, 119(16):8904–8911, 2015.

[78] The Thuong Nguyen, Claire Pétuya, David Talaga, and Arnaud Desmedt. Promoting the Insertion of Molecular Hydrogen in Tetrahydrofuran Hydrate With the Help of Acidic Additives. *Front. Chem.*, 8:550862, 2020.

[79] Ahmed Omran, Nikolay Nesterenko, and Valentin Valtchev. Revealing Zeolites Active Sites Role as Kinetic Hydrate Promoters: Combined Computational and Experimental Study. *ACS Sustain. Chem. Eng.*, June 2022. Article ASAP.

[80] Georgi N Vayssilov, Hristiyan A Aleksandrov, Eddy Dib, Izabel Medeiros Costa, Nikolai Nesterenko, and Svetlana Mintova. Superacidity and spectral signatures of hydroxyl groups in zeolites. *Microporous Mesoporous Mater.*, 343(August):112144, sep 2022.

[81] Katipot Inkong, Pramoch Rangsunvigit, S. Kulprathipanja, and Praveen Linga. Effects of temperature and pressure on the methane hydrate formation with the presence of tetrahydrofuran (THF) as a promoter in an unstirred tank reactor. *Fuel*, 255(May):115705, 2019.

[82] Hari Prakash Veluswamy, Alison Jia Hui Wong, Ponnivalavan Babu, Rajnish Kumar, Santi Kulprathipanja, Pramoch Rangsunvigit, and Praveen Linga. Rapid methane hydrate formation to develop a cost effective large scale energy storage system. *Chem. Eng. J.*, 290:161–173, 2016.

[83] Brinchi Lucia, Beatrice Castellani, Federico Rossi, Franco Cotana, Elena Morini, Andrea Nicolini, and Mirko Filipponi. Experimental investigations on scaled-up methane hydrate production with surfactant promotion: Energy considerations. *J. Pet. Sci. Eng.*, 120:187–193, 2014.

[84] Ye Zhang, Gaurav Bhattacharjee, Mohana Dharshini Vijayakumar, and Praveen Linga. Rapid and energy-dense methane hydrate formation at near ambient temperature using 1,3-dioxolane as a dual-function promoter. *Appl. Energy*, 311(February):118678, apr 2022.

[85] Asheesh Kumar, Rajnish Kumar, and Praveen Linga. Sodium Dodecyl Sulfate Preferentially Promotes Enclathration of Methane in Mixed Methane-Tetrahydrofuran Hydrates. 2019.

[86] Inkyu Lee, Jinwoo Park, and Il Moon. Key Issues and Challenges on the Liquefied Natural Gas Value Chain: A Review from the Process Systems Engineering Point of View. *Ind. Eng. Chem. Res.*, 57(17):5805–5818, 2018.

[87] M. M. Faruque Hasan, Alfred Minghan Zheng, and I. A. Karimi. Minimizing Boil-Off Losses in Liquefied Natural Gas Transportation. *Ind. Eng. Chem. Res.*, 48(21):9571–9580, nov 2009.

[88] Asheesh Kumar, Tushar Sakpal, Praveen Linga, and Rajnish Kumar. Enhanced carbon dioxide hydrate formation kinetics in a fixed bed reactor filled with metallic packing. *Chem. Eng. Sci.*, 122:78–85, jan 2015.

[89] Hassan Pahlavanzadeh, Sajjad Rezaei, Mehrdad Khanlarkhani, Mehrdad Manteghian, and Amir H. Mohammadi. Kinetic study of methane hydrate formation in the presence of copper nanoparticles and CTAB. *J. Nat. Gas Sci. Eng.*, 34:803–810, 2016.

[90] P. Linga and M. A. Clarke. A Review of Reactor Designs and Materials Employed for Increasing the Rate of Gas Hydrate Formation. *Energy & Fuels*, 31(1):1–13, jan 2017.

[91] Muhammad Aifaa, Takehide Kodama, and Ryo Ohmura. Crystal growth of clathrate hydrate in a flowing liquid water system with methane gas. *Cryst. Growth Des.*, 15(2):559–563, 2015.

[92] Divya Gootam, Namrata Gaikwad, Rajnish Kumar, and Niket Kaisare. Modeling Growth Kinetics of Methane Hydrate in Stirred Tank Batch Reactors. *ACS Eng. Au*, 1(2):148–159, 2021.

[93] Yasuhiko H. Mori. On the scale-up of gas-hydrate-forming reactors: The case of gas-dispersion-type reactors. *Energies*, 8(2):1317–1335, 2015.

[94] Wenfeng Hao, Jinqu Wang, Shuanshi Fan, and Wenbin Hao. Evaluation and analysis method for natural gas hydrate storage and transportation processes. *Energy Convers. Manag.*, 49(10):2546–2553, 2008.

[95] Federico Rossi, Mirko Filipponi, and Beatrice Castellani. Investigation on a novel reactor for gas hydrate production. *Appl. Energy*, 99(Icgh):167–172, 2012.

Chapter 7

Ab *initio* Mechanistic Insights into the Stability, Diffusion and Storage Capacity of sI Clathrate Hydrate Containing Hydrogen

I think I can safely say that nobody understands quantum mechanics

-Richard Feynman

Gas hydrates are non-conventional materials offering great potential in capturing, storage, and sequestration of different gases. The weak Van der Waals interactions between a gas molecule and the pore walls stabilize these non-stoichiometric structures. The present article reports an *ab initio* improved van der Waals density functional (vdW-DF2) study devoted to the interactions associated with H_2, CH_4, and CO_2 adsorption in sI clathrate hydrate. The study provides the clathrate stability, diffusion, and energy storage of possible mixed gas occupancy in sI cages in the presence of H_2. The results also provided the hydrogen energy landscapes and the estimated diffusion activation energy barriers to the large and small cage to be 0.181 and 0.685 eV, respectively. In addition, the results showed that the presence of CH_4 or CO_2 could enhance the storage capacity, thermodynamic stability, and hydrogen diffusion in sI clathrates. The volumetric storage, gravimetric storage, and molecular hydrogen content in H_2-CH_4 binary sI clathrate are calculated to be 2.0 kW.h/kg, and 1.8 kW.h/L, and 5.0 wt%, respectively.

These results are comparable to DOE targets of hydrogen storage[1].

7.1 Introduction

Clathrate hydrates are non-stoichiometric "ice-like" structures or inclusion compounds that are formed out of water molecules connected by H-bonding to form three-dimensional cavities which are stabilized by presence of gases such as CH_4, H_2, CO_2, O_2, Ar, Kr and others. The non-stoichiometric nature of clathrates is illustrated by statistical-mechanical analysis of their stabilities which showed that the cages are not completely occupied [1, 2]. The existence of clathrates can be tracked to early 1810 when Sir Humphrey Davy described chlorine gas crystal structure [3]. According to Makagon, the discovery of gas hydrates dates back to 1778-1780. It should be related with the work of the English naturalist Joseph Priestly who described water"impregnated" SO_2 [1]. However, it was not before 1930s when hydrates attracted more attention with the discovery and improvements in the oil and gas industry [4]. At that time, the research was focused on preventing the blockage of pipelines by forming hydrates that can interrupt the production and cause safety concerns [5].

The studies on gas hydrate are related to many fields such as astrophysics[6], geosciences, chemical and petroleum engineering [7]. In addition, gas hydrates have many practical applications that includes but not limited to desalination[8], CO_2 sequesteration[9], gas separation[10] and storage[11]. The latter two applications are in the focus of the present article. With the energy transition toward renewables and decarbonization, the focus of current studies on gas hydrates is shifted equally toward to main areas: (1) their natural occurrence and environmental impact [12–14] (2) the potential technological applications in energy transition and the energy-water nexus [3]. A promising technological applications of clathrates is their usage as energy storage material to store and transport energy gases such as methane and hydrogen in moderate pressure and temperature conditions[15]. Moreover the double-benefit of replacing CH_4 in discovered hydrate reservoirs by the more stable CO_2 clathrates is the focus of

[1]This chapter is based on the following article: *Omran A., Nesterenko N., & Valtchev V. Ab initio* mechanistic insights into the stability, diffusion and storage capacity of sI clathrate hydrate containing hydrogen. International Journal of Hydrogen Energy. 2022 Feb 12;47(13):8419-33.

intense research[16]. The different interactions between host and guest molecules (host-host, host-guest, and guest-guest) are important to understand their formation, stabilization and dissociation [17].

There is a number of clathrate structures as the most common hydrates are sI, sII, and sH. Similar to other crystalline solids, the clathrate structure formation depends on factors such as pressure, temperature, and the nature of guest species [3]. For example, methane can form sI below 120 MPa. Increasing the pressure to 250 MPa, sII clathrate is obtained, and a further increase to 600 MPa will transform that structure to sH [18]. sI exhibits space group $Pm\bar{3}n$ and the unit cell consists of 46 water molecules. The water molecules are arranged in two kinds of cages - two small cages of pentagonal dodecahedra (5^{12}), and 6 large cages of tetrakaidecahedra ($5^{12}6^2$). The sII includes 136 water molecules arranged in sixteen (5^{12}) and eight hexakaidecahedra ($5^{12}6^4$) with space group of $Fd\bar{3}m$ and lattice parameter of 17.3 Å [3, 19, 20]. Reported to be isostuctural with hexagonal clathrasil dodecasil-1 H, sH showed smaller unit cell of only 34 water molecule but with 3 different sizes of the cages: 3 small (5^{12}) , 2 medium irregular dodecahedra ($4^35^66^3$) and a large icosahedra ($5^{12}6^8$) cages [21].

SI clathrate can not accommodate organic promoters and usually encapsulate single gas species such as CH_4 or CO_2 at relatively high pressures. On the other hand, the other two structures are commonly synthesized as binary clathrates such as hydrogen-tetrahydrofuran (H_2-THF) [22] and methane-cyclooctane (CH_4-Cyclo-O) [23] at more moderate conditions on the expense of storage capacity. For example, while pure methane sI clathrate can store about 172 v/v, the maximum storage capacity of binary CH_4-THF sII can reach approximately 112 v/v only [1].

Hydrogen clathrates are an attractive opportunity for green mass storage, representing a cheap alternative to the metal-organic frameworks (MOFs) or metal hydrides [24]. In 1999,

Dyadin *et al.*. found experimentally that pure hydrogen clathrate can be synthesized in the form sII clathrate but at very high pressures ($\approx$ 1.5-2 kbar)[25]. Mao *et al.* showed that the sII hydrogen clathrate is structurally stable up to 145 K at ambient pressure [26]. The estimated storage capacity of the synthesized pure sII hydrogen hydrates is approximately 5.3 wt% at those significantly elevated pressures. Such a hydrogen weight content will result in volumetric and gravimetric energy storage capacities of 1.8 kW.h/kg and 1.5 kW.h/L, respectively [27, 28]. The above estimation is based on the double occupation of small (5^{12}) and quadruple occupation of large ($5^{12}6^4$) cages of sII clathrate.

However, the above *P-T* conditions are extremely demanding and difficult to scale-up. One way to solve that is to use thermodynamic hydrate promoters (THP). In that context, H_2-THF binary clathrates have been widely studied with the goal to bring the formation conditions to reasonable ranges. However, storage capacity has been significantly reduced to about 1 wt% since H_2 enclathration is limited to 5^{12} small cages, while the $5^{12}6^4$ large cages are occupied by THF [29, 30]. Lee *et al.*suggested that the reducing of THF concentration would allow hydrogen storage in large cages in relatively moderate conditions[22]. Although supported by Sugahara *et al.* data[31],this approach was reported non-reproducible by other studies including the one by Strobel *et al.*. Thus, boosting the hydrogen capacity upon reasonable pressure-temperature conditions remains a challenge far from being met.

Another direction to solve this problem is to use gaseous thermodynamic promoter of high calorific value and hydrogen content or "blue hydrogen storage". Recently, storing hydrogen along with methane has attracted attention as they are anticipated to meet the US Department of Energy (DOE) targets of energy density while showing affordable formation and storage conditions[26]. Skiba *et al.* studied X-ray diffraction in the system H_2-CH_4-H_2O at a pressure of 20 MPa and 40 mol% of hydrogen content in the initial gas mixture. They concluded that hydrate formed is sI with cell parameter of 11.86 Å at 133 K [32] . Matsumoto *et al.* investigated H_2-CH_4 hydrates prepared at various conditions were by PXRD and Raman spectroscopy to reveal hydrate structure, cage occupancies and mole fraction of H_2 and CH_4. They noticed

that H_2-CH_4 binary hydrates can be either sI or sII depending on pressure, temperature, composition and formation time. More importantly, that they showed that in some cases sI can be formed first even before the thermodynamically stable sII and that theses hydrates can be formed at more moderate conditions than pure H_2 or tuned H_2-THF binary hydrates[33]. As hinted earlier, the presence of thermodynamic promoters in sII or sH improved the formation conditions significantly but on the expense of sharp decrease in storage capacity due to filling the large cages. So, one way to improve the clathrate storage capacity for hydrogen is to allow both small and large cage occupancies by using small gas molcules such as CH_4 and CO_2. Belosludov *et al.* theoretically investigated the hydrogen storage in binary hydrogen-methane clathrate hydrates and showed that methane concentration of 6% stabilizes the cubic sI [34, 35].

Grim *et al.*, using Raman spectroscopy and PXRD, showed that H_2 can be stored in both small and large cages of sI. They basically used pre-synthesized CH_4 and CO_2 sI clathrate as a "templates" for hydrogen clathrates. Although the storage potential was less than sII, they proved the concept that H_2 can occupy both small and large cages and multiple cage occupancy is feasible in case of sI. It should be noted that CH_4 and CO_2 sI clathrate were synthesized at 11 and 1.7 MPa, respectively. Accordingly, the CH_4 initial templates is almost fully occupied with Θ_s=0.96 and Θ_l=0.99, a value similar to CO_2 large cages Θ_l=0.98 occupancy as calculated by CSMGem [3]. Consequently, there is a big chance that cages, especially large ones, accommodate hydrogen together with CH_4 or CO_2. Such a mixed occupation would greatly impact the estimated storage capacity of those clathrates.

Generally, the cage occupancy depends mainly on two important interrelated properties: (1) the stability of those (pre-)occupied cages and (2) the ability of guest gas to diffuse into those specific cages at first place. The latter is determining factor in transport phenomena and processes such as mass transfer depend on the inter-cages transition energy barrier. Calculating those barriers will enable us to accurate estimate parameters such as diffusion constant in intact hydrate phase and therefore give better understanding of practical issue such as the slow kinetics of hydrogen storage or CO_2/CH_4 replacement[36–39]. The diffusion mechanism suggested

in the literature refers to that hydrogen diffuses most probably through hexagonal faces [40–42].

On the contrary, some other computational [43, 44] and experimental [45, 46] evidences strongly suggested that guest molecules can hop between all cages without significant overall changes to the hosting water network, despite that their nominal size exceeds the opening in the hexagonal or pentagonal face [47]. Peters *et al.* suggested that guest transport is supported by a water-hopping type mechanism to explain those contradictions. In such scenario the hydrogen bonds of a water molecule are completely dislocated and the hydrogen bond is broken while other bonds are elongated to keep the ring intact during transition [44]. Another study suggested the "help gas" mechanism in which an additional guest molecule enhance the diffusivity of the main guest by mutual interaction with the water network [48, 49]. On the other hand, a direct transition mechanism for gas diffusion in gas hydrates was proposed based on density functional theory (DFT) calculations. This approach does not involve defects or helping gases. For instance, Alvi and Ripmeester [50] considered rigid cages to calculate the diffusion of H_2 in sII hydrates using B3LYP and MP2 levels of theory. They estimated that the H_2 guest needs 5–6 kcal/mol to diffuse through a hexagonal face of the large cage. That value increases about 5 or 6 times in case of pentagonal face . Other theoretical studies suggested that the cage-to-cage hopping of gas molecules through the five- and six-membered water rings involves distortion of the local water rings and requires no other structural defects within the hydrate framework [51, 52]. However, the cage structures are partially constrained; therefore, these calculations may not be able to fully reveal the important factors related to the gas cage-to-cage hopping in gas hydrates[43].

To summarize, there are two extreme approaches try to resolve those contradiction between computational and experimental data (1) complete distortion of H-bonding network where the diffusion is facilitated by other molecule or crystal defect and (2) global structure flexibility that is enhanced by equitable sharing of the bond elongations. Thus, the proper understanding of inter-cage transport at the molecular level lies largely in the appropriate estimation of the flexible transitions.

This paper aims to study the cage occupancy and diffusion in single (H_2), mixed (CH_4 - H_2) and (CO_2 - H_2) sI clathrates. In addition, we will report the stability, binding energy, and optimum storage capacity of CH_4 and CO_2 in sI clathrate containing hydrogen. Finally, we will present all possible diffusion paths of hydrogen in sI empty and filled with frameworks. To evaluate the hydrogen bond network's ability to enhance global structure flexibility, we consider the diffusion through fully relaxed structures since the proper evaluation of diffusion is important to estimate the hydrogen storage in sI CH_4 or CO_2 clathrates.

7.2 Computational Methods

We performed here density functional theory (DFT) calculations [53] using projected augmented wave (PAW) psedopotentials with kinetic energy cutoff for wave function and charge density of 55 and 440 Ry, respectively[54]. A self consistency convergence criterion of at least 1×10^{-8} was used and all structures were fully optimized using force convergence threshold of at least 10^{-4} Ry/a.u. All calculations have been performed using $2 \times 2 \times 2$ mesh except those for sII large unit cell where we used Γ point calculation only. Gas molecules such as H_2, CH_4 and CO_2 are interacting with water frameworks by means of van der Waals forces and hydrogen bonding [3]. Moreover, it is not only the guest-host interaction but also the guest-guest and host-host interactions that affect hydrate formation and stability[55, 56]. *Ab initio* DFT calculations via Perdew-Burke-Ernzerhof generalized gradient approximation (GGA) functional[57] with revised exchange parametrization of Zhang and Yang (revPBE) has been applied self consistently[58]. The improved GGA functionals such as PBE and its revised versions revPBE and RPBE can gives more accurate chemisorption energies than the PW91 and PBE functionals [58–61], however it fails to include vdW dispersion forces or hydrogen bonding [62, 63]. To illustrate, Pétuya *et al.* argued that the semilocal PBE functional can still reproduce experimental structural properties obtained by neutron diffraction and estimate stability of clathrates even better than non-local vdw-DF[64]. In another study, Vlasic *et al.* pointed out that revPBE works very well for gas and THF hydrates and could accurately de-

termine their mechanical and vibrational properties. They suggested that particularly revPBE provided a unique combination of accuracy and low computational cost, when compared to other XC functionals including those that take into account long-range van der Waals interactions [65]. On the other hand, Cao *et al.* [66] suggested that the improved nonlocal van der Waals density functional (vdw-DF2) with the inclusion of a long-range term of the correlation energy is necessary to account for intermolecular dispersion interactions [67]. Accounting for the importance of these forces, we have used both revPBE and vdW-DF2 as implemented in Quantum Espresso (QE) software [68], thus addressing the discrepancies in the literature sources. The thermodynamic stability and storage capacity of mixed (CH_4 - H_2, CO_2 - H_2) sI clathrates was evaluated using the cohesive energy (E_{coh}) and binding energy (E_b).

Cohesive energy (E_{coh}) per water molecules is calculated as [69]:

$$E_{coh} = \frac{E_{hydrate} - (x.E_{H_2} + y.E_{gas} + 46E_{H_2O})}{46}$$

The binding energy (E_b) is calculated as [70, 71]:

$$E_b = E_{hydrate} - [E_{H_2} + E_{residual}]$$

where $E_{hydrate}$, E_{CO_2}, E_{gas}, E_{H_2O}, $E_{residual}$ are the energies of hydrate, hydrogen , gas (CO_2 or CH_4) , water and the hydrate with one hydrogen molecule less.The minimum energy paths (MEP) between two minima were identified using NEB and CI-NEB methods with convergence criterion (< 0.05 eV/Å). Transition state structures were confirmed by presence of only one imaginary frequency along the reaction coordinate. Vibrational frequency calculation for those transition states were performed via DFPT (Density-Functional Perturbation Theory) calculations as implemented in QE package. [72].

7.3 Results and discussion

7.3.1 H_2 cage occupancy

The clathrate volumetric or gravimetric storage capacity depends on hydrate's stability and cage occupancy, while the diffusion rate of a gas molecule through the cages influences the storage kinetics. A major drawback of van der Waals and Platteeuw (vdW-P) theory is that it assumes single cage occupancy and ignores guest-guest interaction [73, 90]. To overcome that, we used *ab initio* calculation of binding energy of gases in different cages to evaluate multiple cage occupancies and stability of hydrates. Calculating the binding energy in isolated cage models in order to evaluate occupancy in different cages has been proven to be a good compromise between high accuracy and computational performance [74–76]. The small cage was modelled with a 20-molecule water cluster. In this structure , 8 oxygen molecules are organized in perfect cube (O_h) at a distance of 3.91 Å from the center of the cage while the remaining 12 oxygen are positioned at 3.95 Å from cage center. For the large cage, a 24-molecule model cluster is used where oxygen atoms are positioned in between 4.04 Å and 4.64 Å from the cage center. For most of the hydrogen atoms the O-H bond length is approximately 0.96Å. Thus,the cluster models agrees will with the average x-ray structure of sI as well as the optimized crystal model [77, 78] as shown in **Figure 7.1**.

(a) **(b)**

Figure 7.1: Optimized geometries of empty (a) small (5^{12}) and (b) large ($5^{12}6^2$) cages of sI clathrate.

We calculated the binding energies as a function of the number of H_2 gas molecules bound to the sI individual cages using both vdW-DF2 and revPBE generalized gradient approximation (GGA). Here, the binding energy is defined as the energy difference between the cluster (host

cage and guest molecule(s)) and the summation of system individual components. In case of *n* multiple gas occupancies, we subtract *n* time the energies of single gas molecule. For example, in case of H_2 occupancy in 5^{12} cage, we have calculated the encapsulation energy of 1, 2 and 3 hydrogen molecules while for $5^{12}6^2$ we considered encapsulation reactions with up to 6 H_2 molecules. For either low or high occupation of *n* $H_2@5^{12}$ and $nH_2@5^{12}6^2$, it has been noticed that the calculated binding energies are not favouring the hydrogen encapsulation in both small and large sI clathrate cages even at low occupancies using revPBE as summerized in **Table 7.1**. This inconsistency with experimental evidences is not totally surprising because almost all popular PBE functionals are not able to describe vdW dispersive interactions which are dominant in the presence of non-polar gas molecules such as hydrogen[79, 80].

Table 7.1: vdW-DF2 and revPBE binding energies (eV) for H_2 in sI

Reaction	ΔE_0(revPBE)	ΔE_0(vdW-DF2)	ΔE_0 H_2-H_2 (vdW-DF2)
$1H_2+S=1H_2@S$	0.023	-0.123	-
$2H_2+S=2H_2@S$	0.258	-0.147	0.020
$3H_2+S=3H_2@S$	0.598	-0.070	0.062
$1H_2+L=1H_2@L$	0.005	-0.108	-
$2H_2+L=2H_2@L$	0.108	-0.216	-0.002
$3H_2+L=3H_2@L$	0.341	-0.210	0.013
$4H_2+L=1H_2@L$	0.546	-0.243	0.013
$5H_2+L=2H_2@L$	-	-0.225	0.037
$6H_2+L=3H_2@L$	-	-0.186	0.037

So, using vdW-DF2 we further examined the structure and stability of the H_2O/H_2 models. For $H_2@5^{12}$ model, the calculation predicted that hydrogen molecule is off-centre by only 0.2 Å. However, this distance from cage center increased to 1.27 Å in case of $5^{12}6^2$ cage. This deviation from center in large cage can be explained by the presence of different cage faces (pentagonal and hexagonal) areas that have unequal interactions with the H_2 molecule. On the other hand, the equivalent 5^{12} pentagonal faces have equal host-guest interactions areas that keep hydrogen molecule centred. For 2 $H_2@5^{12}$, the intermolecular distance in between the

centres of mass is 2.92 Å while the distances from cage center are 1.32 and 1.46 Å. Likewise for $2H_2@5^{12}6^2$, this intermolecular distance slightly increased to 3.03 Å and the two molecules stayed at remarkably equivalent distance of approximately 1.52Å from cage center.

When a third molecule is added to the small cage, the H_2 molecules are relaxed in an approximately equilateral triangle positions with intermolecular distances ranges from 2.59 to 2.64 Å and almost equal distances of average 1.51 Å from cage center. However, for 3 $H_2@5^{12}6^2$, the hydrogen molecules preferred to position at isoscele triangle fashion with H_2-H_2 distances of 2.75, 2.74, and 3.21 Å. The mass centres of those three H_2 molecules are at a distance that ranges 1.67 and 1.77 Å from the large cage center. A combination of size effect and H_2-H_2 repulsions prevents the small cage to accommodate more than 3 H_2 molecules and the binding energy become positive. On the contrary, adding a forth molecule to the large cage stabilized it at an optimum binding energy of -23.41 kJ/mol. While 2 of the 4 hydrogen molecules relaxed at cage off-center distance of 1.70 Å ,the other couple maintained approximately 1.83 Å equal distances from the cage center. In that case, the H_2-H_2 distances are between 2.74 and 3.13 Å. The geometry optimization resulted in distorted tetrahedron of H_2 molecules with center-of-mass distances between 2.72 and 4.14 Å after adding a fifth hydrogen molecule. The off-center distance range increased to 1.42-2.28 Å, with the upper limit reflecting the increasing effect of H_2-H_2 repulsion. Finally, we examined 6 hydrogen molecules cluster, and similarly H2-H2 mass center distanced between 2.74-3.98 Å.

From **Table 7.1** , we can see that an increase in the number of H_2 molecules leads to an increase in binding energy per H_2 molecule and further stabilization of the cage due to the additional interaction of H_2 molecules. This is valid until the number of hydrogen molecules reaches an optimum cluster size above which additional hydrogen molecules destabilize the cage. Accordingly, it has been found that 5^{12} cage can accommodate up to 2 H_2 molecules, while $5^{12}6^2$ had optimum cage occupancy of 4 H_2 molecules as shown in **Figure 7.2**. On the other hand, the inclusion of dispersive forces increased the stability structures in general and more specifically at higher hydrogen occupancies. For single H_2 occupancy, the differences be-

tween vdW-DF2 and revPBE is 14.12 and 10.08 kJ/mol for small and large cages, respectively. However, for the optimum occupancies, these numbers increased by 19-89% to reach 19.51 and 19.02 kJ/mol for small and large cages, respectively. In addition, our results using vdw-DF2 showed excellent agreement with those benchmark values calculated using higher level quantum chemistry methods. To illustrate, our calculated binding energies of single H_2 occupancy in small and large cages are -0.123 , -0.110 eV compared to -0.124 and -0.110 reported by Patchkovskii and Tse using second order Møller–Plesset (MP2) calculations, respectively[74].

(a) **(b)**

Figure 7.2: Optimized configurations of H_2 molecules at optimum cage occupancies inside (a) small (5^{12}) and (b) large cages ($5^{12}6^2$) of sI clathrate.

To explain this stabilization or destabilization, we should consider the relative weight of guest-guest interaction compared to host-guest interaction. To estimate the earlier we calculated the formation energies of a "bare" nH_2 cluster at the optimized geometry inside cages as shown in **Table 7.1**. Our calculations indicated that for lower cage occupancies up to the optimum, the H_2-H_2 repulsion had a minor effect at both small and large cages and did not exceed 1.91 kJ/mol. However, increasing the number of H_2 molecule by only one H_2 molecule beyond that optimum resulted in H_2-H_2 repulsion sharp increase by 3 times in case of small cage and about 2.8 time in case of large cage. In contrast, and at the same time, the attractive host-guest interactions between hydrogen and cage wall improved the cage stability to maximum at optimum occupancy. Adding further hydrogen molecules did not improve the stability as the contact area between hydrogen and cage wall has already reached the maximum at optimum occupancies. Thus, the H_2-H_2 repulsion further dominated, as shown in **Figure 7.3**.

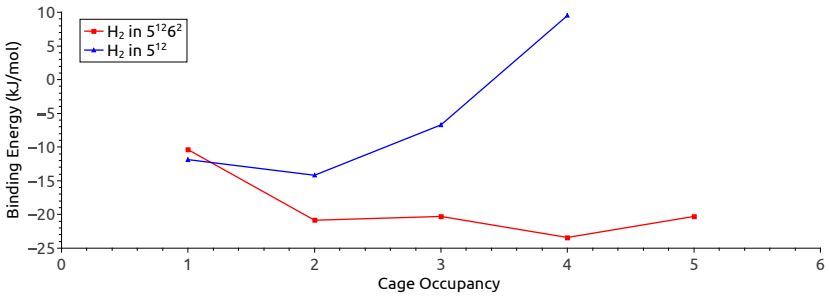

Figure 7.3: Binding energies as a function of the number of molecules for H_2 in small and large cages of sI clathrate.

7.3.2 CH_4+H_2 and CO_2+ H_2 cage occupancy

Similar to H_2, we studied the single occupancy of CO_2, CH_4, CH_4-H_2, and CO_2-H_2 in individual cages. In all cases, we have found that the adsorption energy is dominated by van der Waals interactions in line with the above results. Unlike vdW-DF2, the absence of van der Waals forces in the GGA approximation showed that the inclusion of CO_2 and CH_4 in sI cage is not energetically favorable, contradicting experimental results as shown in **Table 7.2**.

Table 7.2: Calculated interaction energy (eV) of CO_2 and CH_4.

Guest Molecule	IE (revPBE)	IE (vdW) eV	IE (MP2) eV
$1CH_4$+S=$1CH_4$@S	0.021	-0.288	-0.337[81]
$1CO_2$+S=$1CO_2$@S	0.235	-0.360	-0.390[82]
$1CH_4$+L=$1CH_4$@L	0.089	-0.283	-0.295[81]
$1CO_2$+L=$1CO_2$@L	0.063	-0.408	-0.417[81]
$2CO_2$+L=$2CO_2$@L	0.101	-0.476	-
$3CO_2$+L=$3CO_2$@L	0.310	-0.160	-

Consequently, from hereafter, vdW-DF2 results will only be considered. The geometry relaxation for CH_4 and CO_2 @ 5^{12} cage showed that the gas tends to stay at almost exactly the cage center. The single occupancy at the large cage shows some differences with the gas molecule relaxed off-centered by 0.21 and 0.52 Å for CH_4 and CO_2, respectively. Again, this small displacement is due to the unequal interactions with different faces of the large cage. One can conclude that for a single cage occupancy, the larger the molecules tend to position themselves at the cage center. More interestingly, comparing our binding energies results of single

occupancy of CO_2 and CH_4 to those calculated by Atilhan *et al.* via the highly accurate MP2 method, an excellent agreement has been obtained as shown **Table 7.2** [81]. For $CO_2@5^{12}$ cage single, cage occupancy is slightly preferred than in case of CH_4 and the results are comparable to DF-MP2/AVTZ level of theory reported by Arismendi-Arrieta *et al.* [82].

Additionally, we calculated, for the first time to the best of our knowledge, the binding energies of double occupancy of (CH_4+H_2) and (CO_2+ H_2) in both small and large cage. The binding energy values indicated that inserting hydrogen destabilizes the small cage by 18.9 kJ/mol relative to CH_4 single occupancy. At the same time, H_2 will prefer to occupy an empty cage instead as shown in **Figure 7.4**. Similarly, trying to adsorb hydrogen molecule in a small cage pre-occupied by CO_2 destabilized the cage but to lesser extent. From energetic point of view , the co-inclusion of (CO_2 + H_2) in small cage is more stable than the optimum H_2 double occupancy. On the other hand, the large cage showed flexibility to accommodate or store both molecules as detailed below. Additionally, the results showed that CO_2 occupancies in large cages is dominant over small cages. Finally, based on above results, one can conclude the separation efficiency in large cage is in the order of $CO_2 > CH_4 > H_2$ which perfectly agrees with previous experimental observations[83–85].

Except for the debatable tuning studies[86], hydrogen is generally stored in the small cages

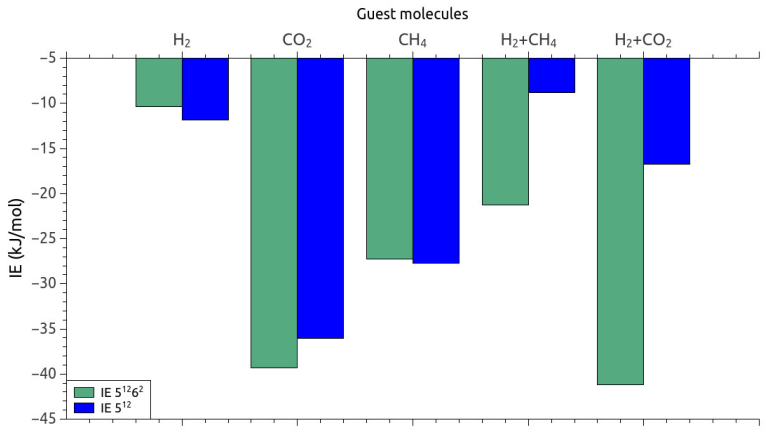

Figure 7.4: Binding energies as a function of the number of molecules for H_2 in small and large cages of sI clathrate.

of its binary clathrates such as H_2-THF or H_2-MTBE. One of the research targets of hydrogen clathrate is to store hydrogen in both small and large cages to get the full potential of clathrate

storage capacity to meet DOE targets[87, 88]. Therefore, we examined the hydrogen accommodations in $5^{12}6^2$ cage being already occupied by a small gas molecule such as CH_4 or CO_2. It was found that the H_2 inclusion in a large cage, already filled by CH_4, will stabilized the cage by 21.23 kJ/mol which is better than single, double and triplet pure H_2 occupancies. However, it is still less than the optimum quadrate occupancy as detailed in **Table 7.1**. When the large cage is filled with a single CO_2 molecules, the inclusion of H_2 molecule will stabilize the cage significantly by -41.16 kJ/mol which is more stable than all possible pure hydrogen occupancies. Because the low binding energy of only -10.4 kJ/mole in case of pure hydrogen single cage occupancy at $5^{12}6^2$ cage, such heterogeneous occupancy (H_2+CO_2 or H_2+CH_4) binding energy results can better explain H_2 single cage occupancies in sI large cages proposed by experimental studies [33, 89]. These results are in line with the concept that hydrate templates containing suitable energy gases can allow H_2 large cage occupancies, as shown in **Figure 7.4**.

7.3.3 Thermodynamic and structural properties

To further test the thermodynamic stability of the proposed mixed CH_4-H_2 occupancies in small and large cages, we evaluated the cohesive energy and binding energy when introducing H_2 to methane hydrate crystal structure. Assuming the cage is fully occupied by methane, we have found that the cohesive energy remains around -0.04 eV when filling the large cages. Similarly, the binding energy showed that introducing H_2 to the large cages increased the structure stability. However, trying to introduce a single hydrogen molecule to the small cages, the structure extremely destabilized, as indicated by both binding energy and cohesive energy values as shown in **Figure 7.5**. Similarly, the same behavior has been found when tried to introduce H_2 to CO_2 methane hydrate.

These results confirm the outcome of isolated cage calculations. Accordingly, one can draw two conclusions. First, one is methane prefers to occupy the small cage. Second, it can be further stabilized in the large cage by a single hydrogen molecule. These multiple and mixed cage occupancies have implications on the energy storage capacity of sI methane clathrate containing hydrogen, as shown in **Figure 7.6**. Based on these results, we estimate that about 5.00 wt% of molecular hydrogen can be stored in binary CH_4-H_2 sI, which meets the US DOE's

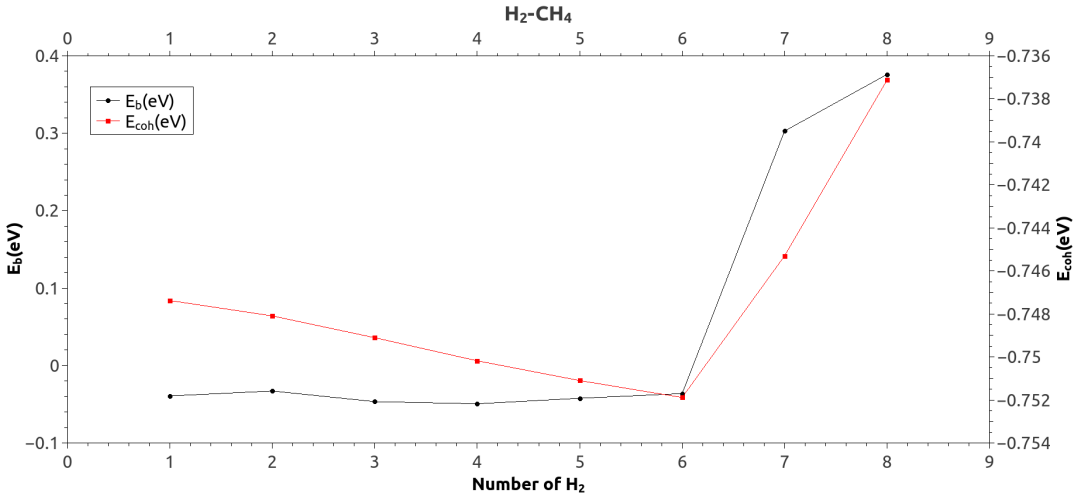

(a)

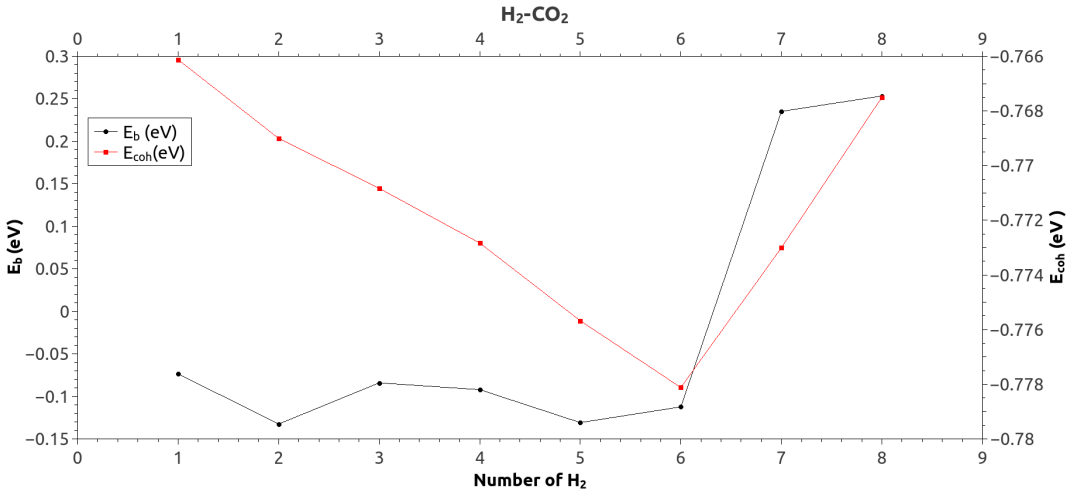

(b)

Figure 7.5: Binding and cohesive energy of (a) H_2-CH_4 and (b) H_2-CO_2 sI hydrates as function of hydrogen cage occupancy in large and small cages.

2020 4.5 wt% target. More importantly, the gravimetric and volumetric energy contents are 2.0 kW.h/kg and 1.8 kW.h/L, respectively. This higher energy density due to combining hydrogen with methane could even fulfill 2025 DOE targets of 1.7 kW.h/L .

According to vdW-P theory[73, 90], the empty hydrate is considered a metastable or hypothetical phase because the hydrate requires guest molecules to form a stable phase [91, 92]. However, Falenty *et al.* showed that those metastable structures are experimentally accessible by removing all neon guests from sII clathrate using vacuum[93]. In another study, Krishnan *et al.* evaluated the activation energy for release and uptake of neon to be 16.4 and 14.9 kJ/mol, respectivey [94]. Thus, those empty cages can be considered as a valid starting point for our

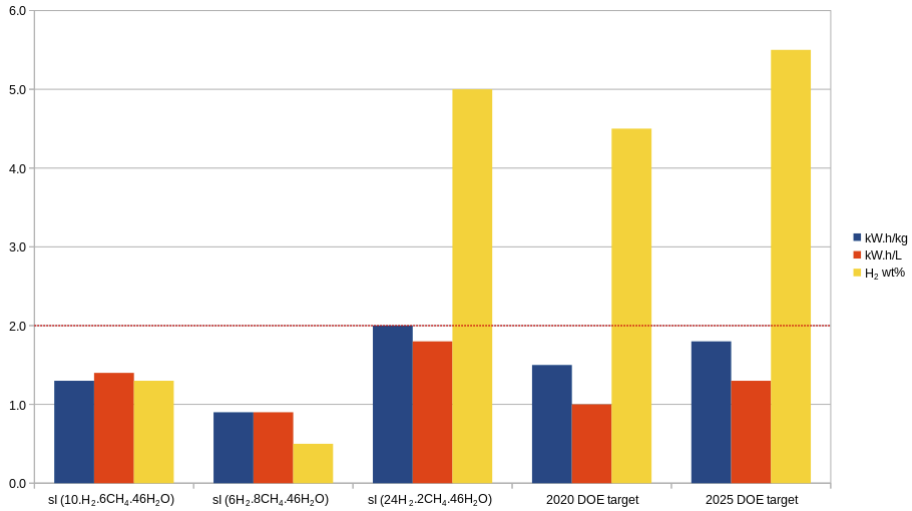

Figure 7.6: Energy density of possible binary H_2-CH_4 occupancies in sI clathrate compared to DOE targets.

hydrate crystal calculations. We have calculated the optimized lattice parameters for the three common structures sI , sII, and sH considering both empty and fully occupied cages as shown in **Table 7.3**.

Table 7.3: Calculated Lattice Parameters for sI, sII and sH of empty and filled crystal structures

Lattice Parameters		**Empty**		**Filled**			
		a [Å]	c [Å]	a [Å]	c [Å]	d_{O-H}	d_{o-o}
sI[1]	Calc.	12.03	-	11.98	-	0.99	2.79
	Exp.	12.00	-	12.00	-	0.97	2.76
sII[2]	Calc.	17.33	-	17.33	-	0.99	2.79
	Exp.	17.35	-	17.35	-	0.81	2.77
sH[3]	Calc.	12.43	10.16	12.47	10.16	0.99	2.79
	Exp.	12.33	9.92	12.33	9.92	0.78	2.78

[1] CH_4 for filled sI
[2] CH_4-THF for filled sII
[3] CH_4-Cyclooctane for filled sH

The small difference between lattice parameter of empty and filled cages for small gas guests agrees well with those reported in literature [95]. In case filled cages, we considered pure CH_4, CH_4-THF, and CH_4-Cylcooctane binary hydrates as representative examples for sI, sII and sH, respectively. In general, our results showed excellent agreement with experimental

and computational data[3, 40, 77, 96]. The small deviation from experimental distances $d_{\text{O-H}}$ in case of sII and sH can be probably due to the difficulty of accurately determining H positions in X-ray experiments [78, 95]. Accordingly, the results indicate that vdW-DF2 can not only express the system energetics, but also it can give accurate structural properties.

7.3.4 H_2 diffusion in sI clathrate

Finally, we calculated the diffusion energy barriers of the cage to cage transfer for the H_2 in both empty and filled conditions. In addition to cage occupancy, diffusion of different guest molecules through hydrate cages is important determining factor for possible gas storage, extraction and seperation [94, 97]. For example, in case of hydrogen storage, the practical application requires fast kinetics. Diffusion barriers depends on many factors but mainly on (1) gas molecules size (2) nature of gas molecule (2) cage(cavity) diameter (3) diffusion path (e.g via pentagonal or hexagonal face) and (4) cage occupancy. Through 12 images along the path from the center of one cage to another, we have calculated the diffusion barrier via nudged image elastic (NEB) folliowed climbing nudged image elastic band (cNEB) calculations . While the the first make sure that proper relaxtion are perpendicular to the path, the later fine tune the result by allowing the image of highest energy to climb along the path regardless the effect of springs. It worth saying also that the accuracy of such energy barriers are sensitive to proper relaxation of the host lattice at the first place [98, 99]. To simplify, we will use A*x*B notation to refere to diffusion path where A and B to refer to initial and final state,respectively. The number *x* then will refer to the opening type (cage face) through which the gas diffuse. A or B can be small cage (S) and large cage (L) while *x* can either represent pentagon (5) or hexagon (6). While the diffusion path between large cages can be either via the pentagon L5L or the hexagon (L6L), the diffusion path between large and small cages has only one possibility (L5S) which is not symmetric due to the different sizes of small and large cage. In addition, as we highlighted earlier in **Table 7.1** and **Table 7.2**, the different gas molecules possess different binding energies in small and large cages. Thus, there are two different activation energies for L5S and S5L depending on the direction of diffusion path. **Figure 7.7** and **Table 7.4** summarize the energy profiles of all different diffusion paths of H_2 in both empty and filled cages.

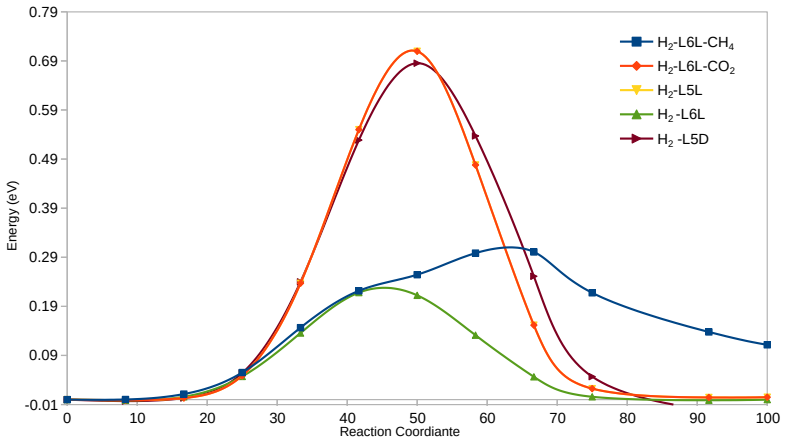

Figure 7.7: Diffusion Energy barriers of H_2 in different inter-cage transition systems (in eV) as a function of the relative progress along the reaction coordinate.

The flexibility of a cage can be estimated from the deformation of its faces upon guest hopping. Inter-cage face deformations can account for the bonds' stretching and angular changes at a time and can be directly estimated by calculating the area change of the cage face polygon defined by the oxygen atoms [54]. Those deformations and the area change values are summarized in **Figure 7.8** and **Table 7.4**.

We found the L6L hydrogen hopping is in parallel to hexagonal cage face forming intermolecular hydrogen bonding between hydrogen molecule and the oxygen atoms building the cage as shown **Fig.8 (b)**. This temporal hydrogen bonding contributes to lower the activation energy barrier that was estimated to be 0.22 eV (21.04 kJ/mol) for a hydrogen molecule hopping between empty cages. The value is significantly lower than 27.02 kJ/mol reported using vdW-DF functional for sI large cage ($5^{12}6^2$) [40] . Moreover, it perfectly agrees with the similar ($5^{12}6^4$) L6L diffusion values of 22 kJ/mole value using AIMD calculation (B3LYP) and at the lower side of 21-25 kJ/mol range reported by using MP2 methods [50, 100]. We have also investigated the hydrogen diffusion when CO_2 or CH_4 occupies the large cage. Two important observations should be underlined: first, the presence of CO_2 or CH_4 in the cage facilitated the hydrogen hopping compared to empty cages, and second, the inter-cage deformation has been minimized, as shown in **Table 7.4**. Although there is no experimental values for H_2 diffusion in sI, it should be noted that being at lower side can be considered at the right direction as experimental activation energy barrier from NMR is only 0.03 eV (3 ± 1 kJ/ mol) [101]. The large discrepancy between computational and experimental results are due to the fact that zero-point

Table 7.4: H_2 diffusion energy barriers and inter-cage deformation area of different transitions

System	Initial State	Final Sate	Ea(eV)	Ea(kJ/mol)	A(Å^2)*	ΔA%
LL	(H_2)L5L	L5L(H_2)	0.710	68.47	14.53	5.44%
	(H_2)L6L	L6L(H_2)	0.218	21.04	25.81	38.91%
	(H_2)(CH_4)L6L(CH_4)	(CH_4)L6L(CH_4)(H_2)	0.222	21.42	21.43	15.34%
	(H_2)L6L(CH_4)	L6L(CH_4)(H_2)	0.301	29.03	21.35	14.91%
	(H_2)(CH_4)L6L	(CH_4)L6L(H_2)	0.189	**18.26**	21.35	14.91%
	(H_2)(CO_2)L6L(CO_2)	(CO_2)L6L(CO_2)(H_2)	0.181	**17.46**	21.28	14.53%
	(H_2)L6L(CO_2)	L6L(CO_2)(H_2)	0.233	22.49	21.63	16.42%
	(H_2)(CO_2)L6L	(CO_2)L6L(H_2)	0.181	**17.51**	21.63	16.42%
LS	(H_2)L5S	L5S(H_2)	0.685	66.13	15.01	10.04%
	(H_2)S5L	S5L(H_2)	0.717	69.18	15.01	10.04%
	(H_2)(CH_4)L5S	(CH_4)L5S(H_2)	0.582	56.16	15.44	13.20%
	(H_2)S5L(CH_4)	S5L(CH_4)(H_2)	0.722	69.63	15.44	13.20%
	(H_2)(CO_2)L5S	(CO_2)L5S(H_2)	0.672	64.85	15.48	13.49%
	(H_2)S5L(CO_2)	S5L(CO_2)(H_2)	0.742	71.55	15.48	13.49%

*In empty cages the areas of small cage pentagonal face,large cage hexagonal and pentagonal (L5L) faces are 13.64 ,18.58 and 13.78 Å^2, respectively

energy and quantum tunnelling are not considered which decreases the effective diffusion barrier [50] and cage occupancy are not considered [100]. These factors will be considered in our future study. Nevertheless, we considered our activation energy barrier at 0 K-for the scope of this study- is enough as it has already revealed important information and proved the concept. In absence of temporary guest-cage hydrogen bonding, hydrogen molecule diffusion via pentagonal face required to overcome 0.717 and 0.685 eV for L5L and L5S transitions which are slightly lower but agrees well with Li *et al.* and Roman-Perez *et al.* calculations using vdW-DF functional [40, 95]. The higher energy barrier via pentagonal faces to/from the small cage is not sufficiently higher to underestimate its contribution to the overall diffusion. It is obvious that a lower barrier to diffuse via large cage hexagonal face channels dominates and enables faster kinetics for both adsorption and release. However, some hydrogen molecules should be retained in the small cage to get the full storage capacity of the clathrate structure. The latter can only happen through diffusion through pentagonal faces. Although those hops have relatively higher diffusion barriers, they are still affordable by the overall structure flexibility.

The other challenge for optimum hydrogen storage is the ability to retain hydrogen in large

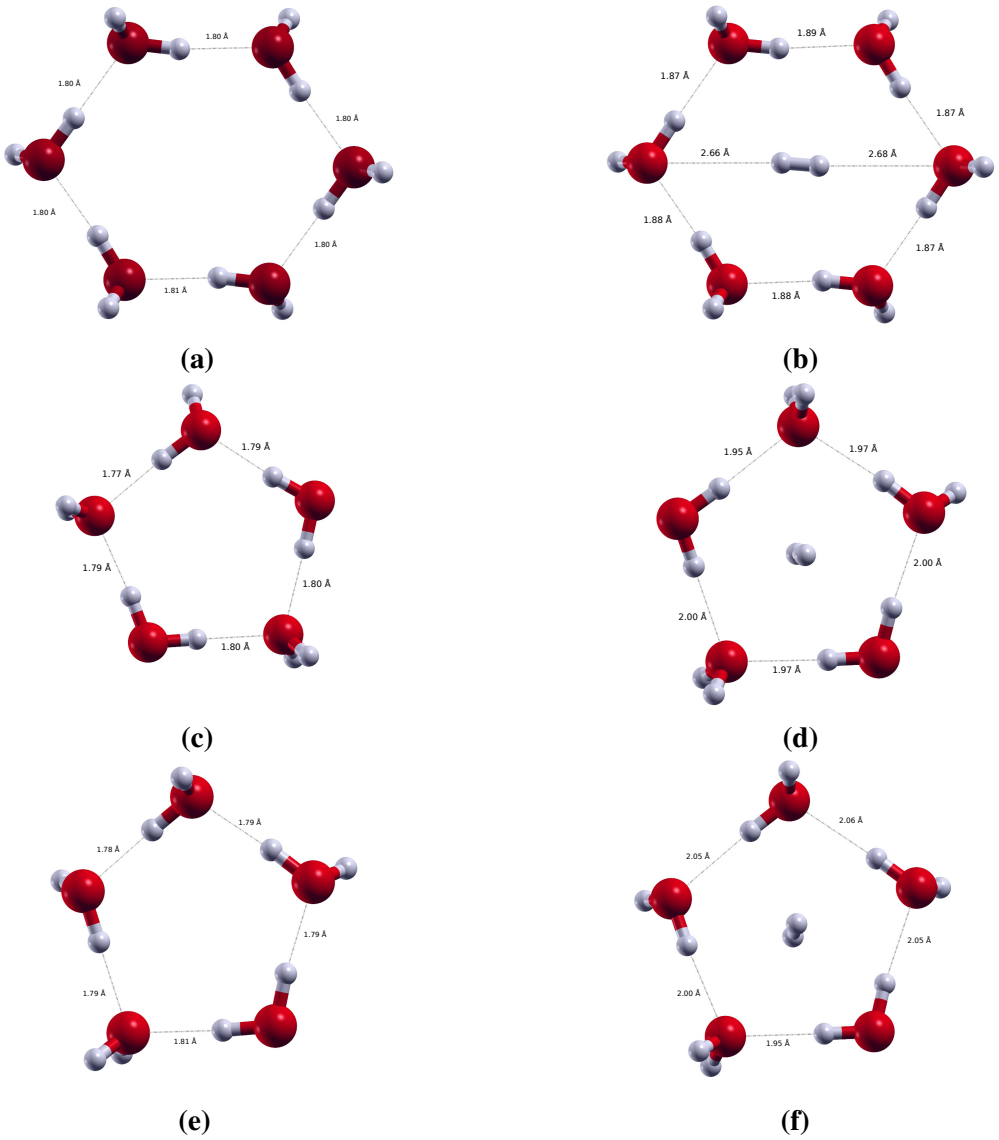

Figure 7.8: Representations of the transition state showing inter-cage face deformation during the H_2 diffusion.

cages. Based on above, the calculated 0.22 eV low barrier for hopping between large cages represent excellent opportunity for not only increasing the storage capacity but also the ease of hydrogen storage and extraction in clathrate as reported for sII[94, 97, 102]. However, our binding energy calculations showed also that even at the optimum occupancy of 4 H_2 molecules in $5^{12}6^2$ cage, the cage stability is still lower than those of CH_4 and CO_2 in large cages which supports to the 'template' concept discussed above. Several experimental pieces of evidence showed the presence of H_2 in the $5^{12}6^2$ cage of sI clathrate that have almost full large cage occupancy of CO_2 and CH_4 [33, 89]. So, these two contradicting effects leads us to think about the possibility of hydrogen diffusion to get heterogeneous H_2-CH_4 and H_2-CO_2 occupancy

with in the same large cage, which may justify the experimental results.

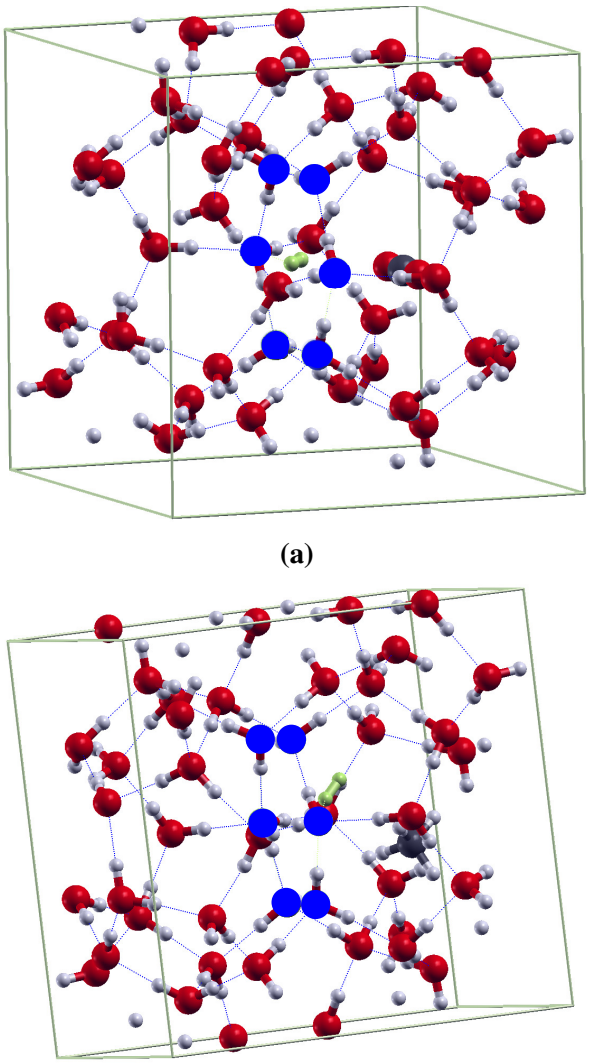

(a)

(b)

Figure 7.9: L6L system showing transition state of H_2 (green) passing through the hexagonal face (blue) from large cage filled with (a)H_2-CH_4 and (b)H_2-CO_2.

Although there are experimental and computational evidence for H_2 and H-radical diffusion to occupied large cages of pure H_2 , binary H_2-THF and H_2-C_3H_8 sII clathrates[75, 97, 103], the diatomic hydrogen diffusion between already sI occupied large cages -for the best of our knowledge- has not been reported yet. Our results showed that L6L hydrogen diffusion from the double occupied cage (DC) of (CH_4+H_2) to a large empty cage needs 18.26 kJ/mol compared 21.04 kJ/mol when hydrogen in a single occupied (SC) large cage diffuses to a neighbor empty large cage **Figure 7.9a**. However, when both large cages are occupied by CH_4, this diffusion required a slightly higher diffusion barrier of 21.42 kJ/mol. Yet, this is still feasible compared

to the higher diffusion barriers required to diffuse through the pentagonal faces for both small and large cages. Similarly, hydrogen can diffuse from DC (CO_2+H_2) to empty or (CO_2)-filled large cage with energy barrier cost of 17.51 and 17.46 kJ/mol, respectively **Figure 7.9b**. In both case, the diffusion energy barrier is reduced significantly compared to the point of hydrogen hopping to empty large cage. Double occupation, either (CH_4+H_2) or (CO_2+H_2) did not only facilitate hydrogen diffusion into neighboring large cages, but also to empty small cages. To illustrate, the diffusion energy barriers from DC large cage of (CH_4+H_2) and (CO_2+H_2) into a small empty cage are 56.16 and 64.89 kJ/mol, respectively. Both values are also less than the 66.13 kJ/mol required for hydrogen to diffuse from SC large cage to empty small cage. Based on these results, one can anticipate that heterogeneous occupancies of (CH_4+H_2) and (CO_2+H_2) are energetically feasible and can compete with pure hydrogen occupancy in large cages. More importantly, this double occupation facilitate the hydrogen diffusion to neighboring small and large cages especially the empty ones. Consequently, the H_2 storage capacity can be enhanced. This lower diffusion barrier can be attributed to the fact that small molecules such as CH_4 or CO_2 (1) stabilize the cage and (2) alter the large cage dimensions during hydrogen diffusion. This can be noticed in the smaller inter-cage expansion area (ΔA) values required for hydrogen diffusion from DC large cage (CH_4+H_2 or CO_2+H_2) into other large cages as indicated in **Table 7.4**.

7.4 Conclusion

A comprehensive stability and diffusion study was performed to evaluate the viability of sI clathrate for hydrogen storage in the presence of CO_2 and CH_4. The computational data set pointed out that energy values obtained from generalized gradient approximation (GGA) functional, such as revPBE, can not properly evaluate the stability of gas clathrate. They are not reliable to determine the cage occupancy when compared to vdW-DF2 functional, providing results that are comparable to highly accurate wave function-based methods such as MP2 and the experimental values. Consequently, we used improved van der Waals density functional (vdW-DF2) to account for dispersion forces associated with adsorption of H_2, CH_4, and CO_2

in clathrates, focusing on sI. First, we analyzed the structural properties of the common hydrate phases of sI, sII and sH, in both empty and filled conditions, and the results agreed well with previous experimental and computational studies. Our calculations showed that: (1) the order of sI gas hydrate stability is $CO_2 > CH_4 > H_2$; (2) H_2 clathrate stability can be improved in H_2-CO_2 and H_2-CH_4 mixed systems with heterogeneous occupancy of different gases in the same cage; (3) multiple cage occupancies of H_2; and (4) the volumetric storage, gravimetric storage and molecular hydrogen content in H_2-CH_4 binary sI clathrate can reach 2.0 kW.h/kg and 1.8 kW.h/L and 5.0 wt% wt, respectively. Finally, the results proved that the direct transition mechanism is theoretically feasible through a fully relaxed structure. The presence of CO_2 or CH_4 facilitates the hydrogen diffusion to large and empty small cages by reducing the cage deformation. The estimated activation energy for hydrogen diffusion from doubly occupied (H_2-CH_4) to a large and a small cage are 0.189 and 0.582 eV, respectively. This set of computational results highlights the promising properties of sI clathrate for hydrogen storage and transportation, CH_4 recovery, and CSS in sI clathrates.

References

[1] Makagon Yuri F. *Hydrates of Hydrocarbons*. Pennwell Books, 1997.

[2] Ioannis N. Tsimpanogiannis and Ioannis G. Economou. Monte Carlo simulation studies of clathrate hydrates: A review. *J. Supercrit. Fluids*, 134(December 2017):51–60, 2018.

[3] E. Dendy Sloan and Carolyn Ann Koh. *Clathrate hydrates of natural gases, thrid edition*. CRC Press, third edition, 2007.

[4] Yu A. Dyadin, I. S. Terekhova, T. V. Rodionova, and D. V. Soldatov. Half-century history of clathrate chemistry. *J. Struct. Chem.*, 40(5):645–653, 1999.

[5] Xiangfang Li, Wenyuan Liu, Shujie Liu, Jinqiu Hu, Yufeng Nan, Tian Tian, and Yunjian Zhou. A prevention and control method for natural gas hydrate in pipe strings during deepwater gas well production tests. *Nat. Gas Ind. B*, 7(1):82–92, 2020.

[6] Elodie Gloesener, Özgür Karatekin, and Véronique Dehant. Stability and composition of CH4-rich clathrate hydrates in the present martian subsurface, 2021.

[7] Bertrand Chazallon, Jennifer A. Noble, and Arnaud Desmedt. Spectroscopy of Gas Hydrates: From Fundamental Aspects to Chemical Engineering, Geophysical and Astrophysical Applications. *Gas Hydrates 1*, pages 63–112, 2017.

[8] Sang Hyun Lee and Kyungtae Park. Conceptual design and economic analysis of a novel cogeneration desalination process using LNG based on clathrate hydrate, 2021.

[9] Wonjung Choi, Woojin Go, Yohan Lee, Junghoon Mok, and Yongwon Seo. Mechanism and kinetics of guest exchange in sII hydrate – Flue gas replacement as revealed by experimental and computational approaches for hydrocarbon recovery and CO2 sequestration. *Chem. Eng. J.*, (October):128119, 2020.

[10] Gyeol Ko, Joonseop Lee, and Yongwon Seo. Separation efficiency and equilibrium recovery ratio of SF6 in hydrate-based greenhouse gas separation. *Chem. Eng. J.*, 405(September 2020):126956, 2021.

[11] Seokyoon Moon, Yunseok Lee, Dongju Seo, Seungin Lee, Sujin Hong, Yun-Ho Ahn, and Youngjune Park. Critical hydrogen concentration of hydrogen-natural gas blends in clathrate hydrates for blue hydrogen storage. *Renew. Sustain. Energy Rev.*, 141(September 2020):110789, 2021.

[12] Mark Maslin, Matthew Owen, Simon Day, and David Long. Linking continental-slope failures and climate change: Testing the clathrate gun hypothesis. *Geology*, 32(1):53–56, 2004.

[13] Timothy A. et al Minshull. Hydrate occurrence in Europe :A review of available evidence. *Mar. Pet. Geol.*, 111:2735–764, 2020.

[14] Roy Andrew Partain and Constantinos Yiallourides. Hydrate occurrence in Europe: Risks, rewards, and legal frameworks, 2020.

[15] Yun Ho Ahn, Seokyoon Moon, Dong Yeun Koh, Sujin Hong, Huen Lee, Jae W. Lee, and Youngjune Park. One-step formation of hydrogen clusters in clathrate hydrates stabilized via natural gas blending. *Energy Storage Mater.*, 24(March 2019):655–661, 2020.

[16] Salvatore F. Cannone, Andrea Lanzini, and Massimo Santarelli. A Review on CO2 Capture Technologies with Focus on CO2-Enhanced Methane Recovery from Hydrates, 2021.

[17] Seokyoon Moon, Sujin Hong, Yunseok Lee, Jae S. Lee, Yun Ho Ahn, and Youngjune Park. Enhancing Hydrogen Cluster Storage in Clathrate Hydrates via Defect-Mediated Lattice Engineering. *J. Phys. Chem. C*, 2021.

[18] Jinfu Shu, Xiaojia Chen, I Ming Chou, Wenge Yang, Jingzhu Hu, Russell J Hemley, and Ho Kwang Mao. Structural stability of methane hydrate at high pressures. *Geosci. Front.*, 2(1):93–100, 2011.

[19] M. V. Stackelberg and H. R. Müller. On the structure of gas hydrates. *J. Chem. Phys.*, 19(10):1319–1320, 1951.

[20] Thomas C. W. Mak and Richard K. McMullan. Polyhedral Clathrate Hydrates. X. Structure of the Double Hydrate of Tetrahydrofuran and Hydrogen Sulfide. *J. Chem. Phys.*, 42(8):2732–2737, 1965.

[21] Christopher I. Ratcliffe & Brian M. Powell John A. Ripmeester, John S. Tse. A new clathrate hydrate structure. *Nature*, 325:135–136, 1987.

[22] Huen Lee, Jong Won Lee, Do Youn Kim, Jeasung Park, Yu Taek Seo, Huang Zeng, Igor L. Moudrakovski, Christopher I. Ratcliffe, and John A. Ripmeester. Tuning clathrate hydrates for hydrogen storage. *Mater. Sustain. Energy A Collect. Peer-Reviewed Res. Rev. Artic. from Nat. Publ. Gr.*, 434(April):285–288, 2010.

[23] J. A. Ripmeester and C. I. Ratcliffe. 129Xe NMR studies of clathrate hydrates: New guests for structure II and structure H. *J. Phys. Chem.*, 94(25):8773–8776, 1990.

[24] Aliakbar Hassanpouryouzband, Edris Joonaki, Mehrdad Vasheghani Farahani, Satoshi Takeya, Carolyn Ruppel, Jinhai Yang, Niall J. English, Judith M. Schicks, Katriona Edlmann, Hadi Mehrabian, Zachary M. Aman, and Bahman Tohidi. Gas hydrates in sustainable chemistry. *Chem. Soc. Rev.*, 2020.

[25] Yuri A. Dyadin, Eduard G. Larionov, Andrei Yu Manakov, Fridrich V. Zhurko, Evgeny Ya Aladko, Tamara V. Mikina, and Vladislav Yu Komarov. Clathrate hydrates of hydrogen and neon. *Mendeleev Commun.*, 9(5):209–210, 1999.

[26] Wendy L Mao, Ho kwang Mao, Alexander F. Goncharov, Viktor V. Struzhkin, Quanzhong Guo, Jingzhu Hu, Jinfu Hu, Russell J. Hemley, Maddury Somayazulu, and Yusheng Zhao. Hydrogen clusters in clathrate hydrate. *Science (80-.).*, 297(5590):2247–2249, 2002.

[27] Wendy L. Mao and Ho Kwang Mao. Hydrogen storage in molecular compounds. *Proc. Natl. Acad. Sci. U. S. A.*, 101(3):708–710, 2004.

[28] Niall J. English and Christian J. Burnham. Intra-cage structure, vibrations and tetrahedral-site hopping of H2 and D2 in doubly-occupied 51264 cages in sII clathrate hydrates from path-integral and classical molecular dynamics. *Appl. Sci.*, 11(1):1–9, 2021.

[29] Ali Rasoolzadeh and Alireza Shariati. Hydrogen hydrate cage occupancy: A key parameter for hydrogen storage and transport. *Fluid Phase Equilib.*, 494:8–20, 2019.

[30] Keisuke Katsumasa, Kenichiro Koga, and Hideki Tanaka. On the thermodynamic stability of hydrogen clathrate hydrates. *J. Chem. Phys.*, 127(4), 2007.

[31] Takeshi Sugahara, Joanna C. Haag, Pinnelli S.R. Prasad, Ashleigh A. Warntjes, E. Dendy Sloan, Amadeu K. Sum, and Carolyn A. Koh. Increasing hydrogen storage capacity using tetrahydrofuran. *J. Am. Chem. Soc.*, 131(41):14616–14617, 2009.

[32] Sergei S. Skiba, Eduard G. Larionov, Andrey Y. Manakov, Boris A. Kolesov, and Viktor I. Kosyakov. Investigation of hydrate formation in the system H2-CH 4-H2O at a pressure up to 250 MPa. *J. Phys. Chem. B*, 111(38):11214–11220, 2007.

[33] Yuuki Matsumoto, R Gary Grim, Naveed M Khan, Takeshi Sugahara, Kazunari Ohgaki, E Dendy Sloan, Carolyn A Koh, and Amadeu K Sum. Investigating the thermodynamic stabilities of hydrogen and methane binary gas hydrates. *J. Phys. Chem. C*, 118(7):3581–3589, 2014.

[34] Vladimir Belosludov, Ravil K Zhdanov, Maaouia Souissi, R V Belosludov, R K Zhdanov, O S Subbotin, H Mizuseki, M Souissi, Y Kawazoe, & V R Belosludov, and V R Belosludov. Theoretical modelling of phase diagrams of clathrate hydrates for hydrogen storage applications. Molecular Simulation Theoretical modelling of the phase diagrams of clathrate hydrates for hydrogen storage applications Theoretical modelling of the phase di. 2012.

[35] R. V. Belosludov, R. K. Zhdanov, O. S. Subbotin, H. Mizuseki, Y. Kawazoe, and V. R. Belosludov. Theoretical study of hydrogen storage in binary hydrogen-methane clathrate hydrates. *J. Renew. Sustain. Energy*, 6(5), 2014.

[36] Junghoon Mok, Wonjung Choi, and Yongwon Seo. Time-dependent observation of a cage-specific guest exchange in sI hydrates for CH4 recovery and CO2 sequestration. *Chem. Eng. J.*, 389(February):124434, 2020.

[37] Geir Ersland, Jarle Husebø, Arne Graue, and Bjørn Kvamme. Transport and storage of CO2 in natural gas hydrate reservoirs. *Energy Procedia*, 1(1):3477–3484, 2009.

[38] Igor L Moudrakovski, Konstantin A Udachin, Saman Alavi, Christopher I Ratcliffe, and John A Ripmeester. Facilitating guest transport in clathrate hydrates by tuning guest-host interactions. *J. Chem. Phys.*, 142(7), 2015.

[39] Ferdi Schüth. Technology: Hydrogen and hydrates. *Nature*, 434(7034):712–713, 2005.

[40] Guillermo Román-Pérez, Mohammed Moaied, Jose M. Soler, and Felix Yndurain. Stability, adsorption, and diffusion of CH4, CO2, and H2 in clathrate hydrates. *Phys. Rev. Lett.*, 105(14):8–11, 2010.

[41] Qi Li, Brian Kolb, Guillermo Román-Pérez, José M Soler, Felix Yndurain, Lingzhu Kong, D C Langreth, and T Thonhauser. Ab initio energetics and kinetics study of H 2 and CH 4 in the SI clathrate hydrate. *Phys. Rev. B*, 84:153103, 2011.

[42] Ángel Vidal-Vidal, Martín Pérez-Rodríguez, Jean Philippe Torré, and Manuel M. Piñeiro. DFT calculation of the potential energy landscape topology and Raman spectra of type I CH4 and CO2 hydrates. *Phys. Chem. Chem. Phys.*, 17(10):6963–6975, 2015.

[43] Shuai Liang, Deqing Liang, Nengyou Wu, Lizhi Yi, and Gaowei Hu. Molecular Mechanisms of Gas Diffusion in CO2 Hydrates. *J. Phys. Chem. C*, 120(30):16298–16304, 2016.

[44] Baron Peters, Nils E.R. Zimmermann, Gregg T. Beckham, Jefferson W. Tester, and Bernhardt L. Trout. Path sampling calculation of methane diffusivity in natural gas hydrates

from a water-vacancy assisted mechanism. *J. Am. Chem. Soc.*, 130(51):17342–17350, 2008.

[45] A. N. Salamatin, A. Falenty, T. C. Hansen, and W. F. Kuhs. Guest Migration Revealed in CO2 Clathrate Hydrates. *Energy and Fuels*, 29(9):5681–5691, 2015.

[46] A. Falenty, A. N. Salamatin, and W. F. Kuhs. Kinetics of CO2-hydrate formation from ice powders: Data summary and modeling extended to low temperatures. *J. Phys. Chem. C*, 117(16):8443–8457, 2013.

[47] A. N. Salamatin, A. Falenty, and W. F. Kuhs. Diffusion Model for Gas Replacement in an Isostructural CH4-CO2 Hydrate System. *J. Phys. Chem. C*, 121(33):17603–17616, 2017.

[48] Alondra Torres Trueba, Maaike C. Kroon, Cor J. Peters, Igor L. Moudrakovski, Christopher I. Ratcliffe, Saman Alavi, and John A. Ripmeester. Inter-cage dynamics in structure I, II, and H fluoromethane hydrates as studied by NMR and molecular dynamics simulations. *J. Chem. Phys.*, 140(21), 2014.

[49] Saman Alavi and John A. Ripmeester. Effect of small cage guests on hydrogen bonding of tetrahydrofuran in binary structure II clathrate hydrates. *J. Chem. Phys.*, 137(5), 2012.

[50] Saman Alavi and John A. Ripmeester. Hydrogen-gas migration through clathrate hydrate cages. *Angew. Chemie - Int. Ed.*, 46(32):6102–6105, 2007.

[51] Ángel M. Fernández-Fernández, Manuel M. Piñeiro, and Martín Pérez-Rodríguez. Computational simulation of fluorinated methane derivatives in type I clathrate hydrate. *J. Mol. Liq.*, 314, 2020.

[52] Vidal-Vidal, M. Pérez-Rodríguez, and M. M. Piñeiro. Direct transition mechanism for molecular diffusion in gas hydrates. *RSC Adv.*, 6(3):1966–1972, 2016.

[53] W. Kohn. Nobel lecture: Electronic structure of matter - Wave functions and density functional. *Rev. Mod. Phys.*, 71(5):1253–1266, 1999.

[54] P. E. Blöchl. Projector augmented-wave method. *Phys. Rev. B*, 50(24):17953–17979, 1994.

[55] Ravi Radhakrishnan and Bernhardt L. Trout. A new approach for studying nucleation phenomena using molecular simulations: Application to CO2 hydrate clathrates. *J. Chem. Phys.*, 117(4):1786–1796, 2002.

[56] Qiao Shi, Pinqiang Cao, Zhengde Han, Fulong Ning, Hao Gong, Yue Xin, Zhisen Zhang, and Jianyang Wu. Role of Guest Molecules in the Mechanical Properties of Clathrate Hydrates. *Cryst. Growth Des.*, 18(11):6729–6741, 2018.

[57] John P. Perdew, Kieron Burke, and Matthias Ernzerhof. Generalized gradient approximation made simple. *Phys. Rev. Lett.*, 77(18):3865–3868, 1996.

[58] Yingkai Zhang and Weitao Yang. Comment on "generalized gradient approximation made simple", 1998.

[59] B Hammer, L B Hansen, and J. K. Nørskov. Improved adsorption energetics within density-functional theory using revised Perdew-Burke-Ernzerhof functionals. *Phys. Rev. B - Condens. Matter Mater. Phys.*, 59(11):7413–7421, 1999.

[60] B. Hammer and J.K. Norskov. Theoretical Surface Science and Catalysis — Calculations and Concepts. *Adv. Catal.*, 45:71–129, 2000.

[61] Ahmed Omran, Sun Hee Yoon, Murtaza Khan, Minhaj Ghouri, Anjaneyulu Chatla, and Nimir Elbashir. Mechanistic Insights for Dry Reforming of Methane on Cu/Ni Bimetallic Catalysts: DFT-Assisted Microkinetic Analysis for Coke Resistance. *Catalysts*, 10(9):1043, sep 2020.

[62] Walter Kohn, Yigal Meir, and Dmitrii E. Makarov. Van der waals energies in density functional theory. *Phys. Rev. Lett.*, 80(19):4153–4156, 1998.

[63] Tanja Van Mourik and Robert J. Gdanitz. A critical note on density functional theory studies on rare-gas dimers. *J. Chem. Phys.*, 116(22):9620–9623, 2002.

[64] Claire Pétuya, Ludovic Martin-Gondre, Philippe Aurel, Françoise Damay, and Arnaud Desmedt. Unraveling the metastability of the SI and SII carbon monoxide hydrate with a combined DFT-neutron diffraction investigation. *J. Chem. Phys.*, 150(18), 2019.

[65] Thomas M Vlasic, Phillip D Servio, and Alejandro D Rey. Infrared Spectra of Gas Hydrates from First-Principles. *J. Phys. Chem. B*, 123(4):936–947, 2019.

[66] Xiaoxiao Cao, Yingying Huang, Xue Jiang, Yan Su, and Jijun Zhao. Phase diagram of water-methane by first-principles thermodynamics: Discovery of MH-IV and MH-V hydrates. *Phys. Chem. Chem. Phys.*, 19(24):15996–16002, 2017.

[67] Kyuho Lee, Éamonn D. Murray, Lingzhu Kong, Bengt I. Lundqvist, and David C. Langreth. Higher-accuracy van der Waals density functional. *Phys. Rev. B - Condens. Matter Mater. Phys.*, 82(8):1–14, 2010.

[68] Paolo Giannozzi, Stefano Baroni, Nicola Bonini, Matteo Calandra, Roberto Car, Carlo Cavazzoni, Davide Ceresoli, Guido L. Chiarotti, Matteo Cococcioni, Ismaila Dabo, Andrea Dal Corso, Stefano De Gironcoli, Stefano Fabris, Guido Fratesi, Ralph Gebauer, Uwe Gerstmann, Christos Gougoussis, Anton Kokalj, Michele Lazzeri, Layla Martin-Samos, Nicola Marzari, Francesco Mauri, Riccardo Mazzarello, Stefano Paolini, Alfredo Pasquarello, Lorenzo Paulatto, Carlo Sbraccia, Sandro Scandolo, Gabriele Sclauzero, Ari P. Seitsonen, Alexander Smogunov, Paolo Umari, and Renata M. Wentzcovitch. QUANTUM ESPRESSO: A modular and open-source software project for quantum simulations of materials. *J. Phys. Condens. Matter*, 21(39), 2009.

[69] Jinxiang Liu, Jian Hou, Jiafang Xu, Haiying Liu, Gang Chen, and Jun Zhang. Ab initio study of the molecular hydrogen occupancy in pure H2 and binary H2-THF clathrate hydrates. *Int. J. Hydrogen Energy*, 42(27):17136–17143, 2017.

[70] Ping Guo, Yi Long Qiu, Long Long Li, Qiang Luo, Jian Fei Zhao, and Yi Kun Pan. Density functional theory study of structural stability for gas hydrate. *Chinese Phys. B*, 27(4), 2018.

[71] Stephen J. Cox, Michael D. Towler, Dario Alfè, and Angelos Michaelides. Benchmarking the performance of density functional theory and point charge force fields in their description of sI methane hydrate against diffusion Monte Carlo. *J. Chem. Phys.*, 140(17), 2014.

[72] Stefano Baroni, Stefano de Gironcoli and Andrea Dal Corso. Phonons and related crystal properties from density-functional perturbation theory. *Rev. Mod. Phys.*, 73:515–561, 2001.

[73] J H van der Waals and J C Platteeuw. Clathrate Solutions. *Adv. Chem. Phys.*, II:1–57, 1958.

[74] Serguei Patchkovskii and John S. Tse. Thermodynamic stability of hydrogen clathrates. *Proc. Natl. Acad. Sci. U. S. A.*, 100(25):14645–14650, 2003.

[75] Saman Alavi and John A. Ripmeester. Migration of hydrogen radicals through clathrate hydrate cages. *Chem. Phys. Lett.*, 479(4-6):234–237, 2009.

[76] Niraj Thakre and Amiya K. Jana. Physical and molecular insights to Clathrate hydrate thermodynamics. *Renew. Sustain. Energy Rev.*, 135(September 2019):110150, 2021.

[77] Konstantin A. Udachin, Christopher I. Ratcliffe, and John A. Ripmeester. Single crystal diffraction studies of structure I, II and H hydrates: Structure, cage occupancy andf composition. *J. Supramol. Chem.*, 2(4-5):405–408, 2002.

[78] Michael T. Kirchner, Roland Boese, W. Edward Billups, and Lewis R. Norman. Gas hydrate single-crystal structure analyses. *J. Am. Chem. Soc.*, 126(30):9407–9412, 2004.

[79] Pattanasak Teeratchanan. First-principles studies of gas hydrates and clathrates under pressure. Technical report, 2017.

[80] Xiaoxiao Cao, Yan Su, and Jijun Zhao. Stability and Vibrations of Guest Molecules in the Type II Clathrate Hydrate: A First-Principles Study of Solid Phase. *J. Phys. Chem. A*, 119(27):7063–7069, 2015.

[81] Mert Atilhan, Nezih Pala, and Santiago Aparicio. A quantum chemistry study of natural gas hydrates. *J. Mol. Model.*, 20(4), 2014.

[82] Daniel J. Arismendi-Arrieta, Álvaro Valdés, and Rita Prosmiti. A Systematic Protocol for Benchmarking Guest–Host Interactions by First-Principles Computations: Capturing CO2 in Clathrate Hydrates. *Chem. - A Eur. J.*, 24(37):9353–9363, 2018.

[83] Pinnelli S.R. Prasad and Burla Sai Kiran. Clathrate Hydrates of Greenhouse Gases in the Presence of Natural Amino Acids: Storage, Transportation and Separation Applications. *Sci. Rep.*, 8(1):1–10, 2018.

[84] Junjie Zheng, Yean Kuan Lee, Ponnivalavan Babu, Peng Zhang, and Praveen Linga. Impact of fixed bed reactor orientation, liquid saturation, bed volume and temperature on the clathrate hydrate process for pre-combustion carbon capture. *J. Nat. Gas Sci. Eng.*, 35:1499–1510, 2016.

[85] Zhiming Xia, Xiaosen Li, Zhaoyang Chen, Kefeng Yan, Chungang Xu, and Jing Cai. Hydrate-based hydrogen purification from simulated syngas with synergic additives. *Int. J. Hydrogen Energy*, 41(4):2649–2659, 2016.

[86] Timothy A. Strobel, Craig J. Taylor, Keith C. Hester, Steven F. Dec, Carolyn A. Koh, Kelly T. Miller, and E. D. Sloan. Molecular hydrogen storage in binary THF-H2 clathrate hydrates. *J. Phys. Chem. B*, 110(34):17121–17125, 2006.

[87] Niall J. English and Christian J. Burnham. Intra-cage structure, vibrations and tetrahedral-site hopping of H2 and D2 in doubly-occupied 51264 cages in sII clathrate hydrates from path-integral and classical molecular dynamics, 2021.

[88] Timothy A. Strobel, Keith C. Hester, Carolyn A. Koh, Amadeu K. Sum, and E. Dendy Sloan. Properties of the clathrates of hydrogen and developments in their applicability for hydrogen storage. *Chem. Phys. Lett.*, 478(4-6):97–109, 2009.

[89] R. Gary Grim, Prasad B. Kerkar, Michele Shebowich, Melissa Arias, E. Dendy Sloan, Carolyn A. Koh, and Amadeu K. Sum. Synthesis and characterization of sI clathrate hydrates containing hydrogen. *J. Phys. Chem. C*, 116(34):18557–18563, 2012.

[90] J. C. Platteeuw and J. H. van der Waals. Thermodynamic properties of gas hydrates. *Mol. Phys.*, 1(1):91–96, 1958.

[91] Fernando J.A.L. Cruz, Saman Alavi, and José P.B. Mota. Low-Temperature Thermodynamic Study of the Metastable Empty Clathrate Hydrates Using Molecular Simulations. *ACS Earth Sp. Chem.*, 3(5):789–799, 2019.

[92] Fernando De Azevedo Medeiros, Iuri Soter Viana Segtovich, Frederico Wanderley Tavares, and Amadeu K. Sum. Sixty Years of the van der Waals and Platteeuw Model for Clathrate Hydrates - A Critical Review from Its Statistical Thermodynamic Basis to Its Extensions and Applications. *Chem. Rev.*, 120(24):13349–13381, 2020.

[93] Andrzej Falenty, Thomas C. Hansen, and Werner F. Kuhs. Formation and properties of ice XVI obtained by emptying a type sII clathrate hydrate. *Nature*, 516(7530):231–233, 2014.

[94] Yogeshwaran Krishnan, Mohammad Reza Ghaani, and Niall J. English. Electric-Field Control of Neon Uptake and Release to and from Clathrate Hydrates. *J. Phys. Chem. C*, 2019.

[95] Qi Li, Brian Kolb, Guillermo Román-Pérez, José M. Soler, Felix Yndurain, Lingzhu Kong, D. C. Langreth, and T. Thonhauser. Ab initio energetics and kinetics study of H2 and CH4 in the SI clathrate hydrate. *Phys. Rev. B - Condens. Matter Mater. Phys.*, 84(15):2–5, 2011.

[96] Konstantin A. Udachin, Christopher I. Ratcliffe, and John A. Ripmeester. Structure, composition, and thermal expansion of CO2 hydrate from single crystal x-ray diffraction measurements. *J. Phys. Chem. B*, 105(19):4200–4204, 2001.

[97] Niall English and Christian BURNHAM. Method and apparatus for controllable storage of hydrogen, 2020.

[98] Graeme Henkelman and Hannes Jónsson. Improved tangent estimate in the nudged elastic band method for finding minimum energy paths and saddle points. *J. Chem. Phys.*, 113(22):9978–9985, 2000.

[99] Graeme Henkelman, Blas P. Uberuaga, and Hannes Jónsson. Climbing image nudged elastic band method for finding saddle points and minimum energy paths. *J. Chem. Phys.*, 113(22):9901–9904, 2000.

[100] Thuat T. Trinh, Magnus H. Waage, Titus S. Van Erp, and Signe Kjelstrup. Low barriers for hydrogen diffusion in sII clathrate. *Phys. Chem. Chem. Phys.*, 17(21):13808–13812, 2015.

[101] Takuo Okuchi, Igor L. Moudrakovski, and John A. Ripmeester. Efficient storage of hydrogen fuel into leaky cages of clathrate hydrate. *Appl. Phys. Lett.*, 91(17):2005–2008, 2007.

[102] Yanhong Wang, Kaidong Yin, Shuanshi Fan, Xuemei Lang, Chi Yu, Shenglong Wang, and Song Li. The molecular insight into the "Zeolite-ice" as hydrogen storage material. *Energy*, 217:119406, 2021.

[103] Sun Hwa Yeon, Jiwoong Seol, Youngjune Park, Dong Yeun Koh, Soo Kang Young, and Huen Lee. Spectroscopic observation of atomic hydrogen radicals entrapped in Icy hydrogen hydrate. *J. Am. Chem. Soc.*, 130(29):9208–9209, 2008.

Chapter 8

Conclusion and Perspectives

All's Well That Ends Well

-William Shakespeare

8.1 Conclusion

Gas clathrate also called gas hydrates are crystalline nanoporous compounds with wide scale applications. These zeolitic-like ices are green **nanoporous** materials with unique properties that can play an important role in the energy transition process. Composed mainly from water, these crystalline structure can have several industrial applications related to water-energy nexus and CCS. This thesis reports the work on fundamental understanding the promotion mechanism of methane hydrate nucleation using computational studies. It also included extensive kinetics studies of methane hydrate formation using zeolites as green promoters. In particular, it addressed the main problems of slow formation kinetics, and poor heat & mass transfer which prevent the wide scale of zeolitic ice technology. Moreover, it explored the future of **safe** and **economic** hydrogen storage in those environmentally benign material with the target of zero carbon emissions.

This Ph.D. thesis is composed of 8 chapters: it starts with as short introduction to the subject highlighting the importance of gas hydrates for energy transition in **Chapter 1**. Then, **Chapter 2** shows experimental and computational methods that have been used in different studies. **Chapter 3** includs detailed literature showing the structure similarities between clathrate hydrates and clathrasils and highlight how these material can improve different processes related to energy transition such as methane storage, CCS and hydrogen storage. The most important findings were as follows:

- Zeolitic ice are eco-friendly materials that can play an important in energy transition.

- Gas hydrates possess unique physicochemical properties such as selective adsorption, thermal stability, and ionic conductivity.
- Natural gas hydrates offer a unique opportunity for long-term methane storage and utilization of discrete gas resources.
- Zeolitic ice can combine carbon capture and sequestration in a single process which can be standalone or combined with exiting technologies.
- Clathrate hydrates have a promising potential for safe and cost-effective hydrogen storage.

The data in **Chapter 4** reveal for the first time the promoting effect of acidic zeolite for hydrate kinetics. The effect of ressure and the gas-to-liquid ratio has also been studied. DFT calculations and experimental results assessed the performance of the two types of zeolites in different concentrations and pressures for binary CH_4-THF clathrate hydrate synthesis in a non-stirred configuration. The results indicated that the acidic zeolite (H-Y) exhibited superior performance over the basic one (Na-X), reaching its optimum at **0.5 wt% zeolite**. A methane **conversion of 94.25%** could be obtained at this concentration in a relatively **mild formation pressure of 6 MP**.

To boost the process economics under realistic conditions, **Chapter 5** reports for the first time binary methane-tetrahydrofuran (THF) formation using the combination of *seawater* and an *unstirred reactor* at *ambient temperature (298.2 K)*.The results revealed that hydrophobic zeolites with a higher Si/Al ratio performed better than the more hydrophilic zeolites. Moreover, the aliphatic amino acid l-valine showed slightly better kinetic promotion performance for hydrate formation in natural and artificial seawater than the aromatic amino acid l-tryptophan. The optimization of the experimental conditions allowed a controlled hydrate growth, boosting the gas uptake to **40 mmol of gas/mol of water**, which is the **highest** reported under mild conditions using seawater.

In **Chapter 6** we investigate the effect of green kinetic promoters (H-SSZ-13, l-tryptophan, l-leucine, and l-methionine) in a novel fixed bed reactor design to accelerate hydrate formation at 6 MPa. The following points summarized the results obtained from that study:

- Binary CH_4 -THF hydrate is formed at **near ambient temperature (293.15 K)**.
- Green promoters H-SSZ-13 and l-tryptophan dramatically improve the crystalliza- tion kinetics of **binary CH_4-THF hydrate at 283.15 K**.
- A **new design non-stirred fixed-bed reactor** boosts the formation kinetics and storage capacity of CH4-THF hydrate.

- Experimental and **techno-economic analysis** prove that zeolitic ice is an ideal medium for safe and long-term energy storage.

Last but not least, **Chapter 7** reports DFT calculations to show the possibility of using green house gases as a thermodynamic for hydrogen storage in clathrate hydrate. After choosing the a relaible exchange-correlation functional to accurately account for van der Waals interactions, the study provided the clathrate stability, diffusion, and energy storage of possible mixed gas occupancy in sI cages in the presence of H_2. The volumetric storage, gravimetric storage, and molecular hydrogen content in H_2-CH_4 binary sI clathrate are calculated to be **2.0 kW.h/kg, and 1.8 kW.h/L, and 5.0 wt%, respectively**. These results are open the door **to achieve DOE targets** of hydrogen storage.

8.2 Perspectives

Based on the results presented in the above studies, the following points can be recommended for future studies:

- Zeolitic ice are **promising** green material for different energy transition applications such as methane storage, CCS and hydrogen storage.
- Porous material such as green and low cost **acidic zeolites** with moderate hydrophobicity showed **enhanced hydrate kinetics**. More extensive studies on different zeolite framework could provide more understanding for the **complex interactions in zeolite-hydrate** system.
- Carefully selected biodegradable **amino acids could improve gas dissolution and storage capacity**. Surveying more amino acids using computational tools can help to elect the best KHPs candidates.
- The storage capacity could be further increased by the help of **advanced reactor design** that enhance heat and mass transfer.
- Computational studies evidence showed the possibility of **safe hydrogen storage** can be achieved in presence of methane. More experimental studies on binary **CH_4-H_2 system** is needed either as standalone mixture or with addition of other thermodynamic promoters.

Appendices

Appendix A

Supporting Information for Chapter 4

A.1 Apparatus

The used methane hydrate formation and dissociation instrument is shown in **Figure C.1**. It consisted of a 450 cm^3 high-pressure stainless-steel reactor (CR; Parr) immersed in a cooling bath. An external refrigerator (ER; Julabo, F250) circulated a glycol solution to control the temperature of the cooling bath. A pressure transmitter (PT; UNIK 5000, GE) with a range of 0-30 MPa and 0.1 % global error was used to measure the system pressure, while a K-type thermocouple (T) with $\pm$ 1.0 K accuracy was used to monitor the temperature. A data acquisition logger (DAQ; Nanodac, Eurotherm) was connected to a computer to record the data during the experiment. All experiments were repeated three times to ensure consistency and carried out with a fixed amount of gas and solution in a closed system (isochoric quiescent system), and the average value was reported.

A.2 Hydrate Yield, Methane Conversion and Recovery Calculations

In Eq.(C.8), water-to-hydrate conversion is calculated based on pressure and temperature data as follows:

$$Hydrate\ yield\ (\%) = \frac{\Delta n_{H\downarrow} \times Hydrate\ Number}{n_{H_2O}} \tag{A.1}$$

Hydrate number is the number of water molecules required per methane molecule for the complete conversion. In our calculations, we used the hydrate number of 8.5 because we applied the stoichiometric mole% of THF (5.56 mole%), which resulted in the complete occupation of THF in all large cages of mixed sII hydrates [6].

Then, Eq.(A.2) describes the methane gas conversion is calculated as follow:

$$Methane \quad conversion(\%) = \frac{n_{H_f}}{n_{H_0}} * 100 \tag{A.2}$$

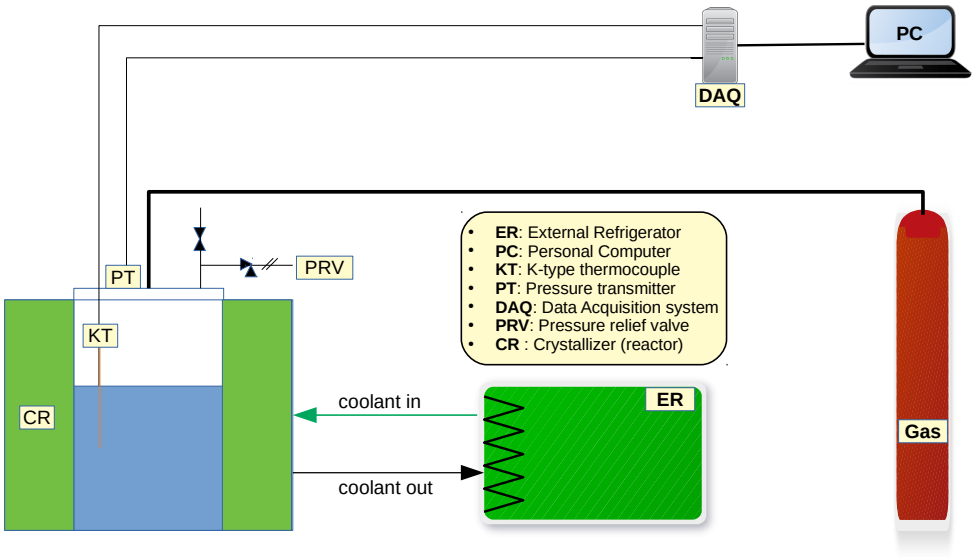

Figure A.1: Schematic diagram of hydrate formation and dissociation setup

where n_{H_0} and n_{H_f} are the initial numbers of moles of methane at the beginning of the experiment and those consumed at the end, respectively.

To evaluate the methane uptake, the hydrates were dissociated by increasing the temperature at the end of all experiments to 310.2 K for at least 6 hours. The selection of that temperature ensures complete hydrate dissociation as it is beyond the equilibrium phase boundary. After 6 hours, the dissociation is deemed completed when the pressure is not changing for 1 h. During dissociation, the amount of methane released from hydrate at any time t is calculated by Eq.(A.3)

$$\Delta n_{H\uparrow} = n_{H,\downarrow} - n_{H,0} = \left(\frac{PV}{zRT}\right)_{G,t} - \left(\frac{PV}{zRT}\right)_{G,0} \tag{A.3}$$

where $n_{H,\downarrow}$ is the moles of methane gas consumed for the hydrate formation at the end of experiment. Finally the methane recovery is calculated as in Eq.(A.4):

$$Recovery(\%) = \frac{\Delta n_{H\uparrow}}{n_{H,\downarrow}} * 100 \tag{A.4}$$

A.3 Computational Methods

DFT calculations has been performed with kinetic energy cutoffs for plane wave expansion of wavefunctions and charge density values of 55 and 440 Ry, respectively[1]. All structures were fully optimized using force convergence threshold of at least 10^{-4} Ry/a.u. and with a self-consistency convergence criterion of at least 1×10^{-8} . The calculations have been carried

out using the Monkhorst-Pack k-points grid of $2 \times 2 \times 2$ in the reciprocal space. The DFT calculations for isolated cages and zeolite clusters were performed in a cubic simulation cell of volume $30 \times 30 \times 30$ Å^3. The 5^{12} small cage was modeled with a 20-molecule water cluster. In these small (5^{12}) cages, 8 oxygen atoms are located in a perfect cube (O_h). An estimated distance of 3.91 Å separates those 8 oxygen atoms from the cage center. The remaining 12 oxygen are positioned at 3.95 Å from the cage center and transform according to (T_h) subgroup of (O_h)[10]. The results agree with the average obtained from the X-ray structure of sII as well as the optimized crystal model[3, 14]. To represent the zeolite promoters, we have used computationally affordable finite cluster models of zeolite crystals. Cluster models have extensively been employed to understand reactive and absorptive processes in various framework types zeolites[9]. In particular, they have been successfully applied to understand zeolite acidity and water-zeolite interactions [5, 8]. **Figure C.2** shows the optimized configuration of $CH_4@5^{12}$ small cage model.

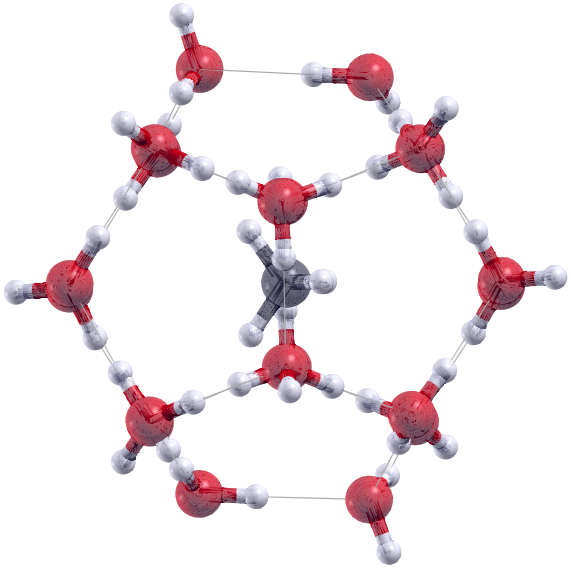

Figure A.2: Optimized configuration of $CH_4@5^{12}$ small cage using vdW-DF2 exchange functional.

A.4 Characterization of Zeolites and Clathrate Hydrates

A.4.1 Zeolite Promoter Characterization

Powder X-ray diffraction (PXRD) , and SEM images confirmed the crystal structures of Na-X and H-Y zeolites as shown in **Figure C.3** and **Figure C.4**. PXRD patterns were obtained with a PANalytical X'Pert Pro ® diffractometer system using Cu-K_α-radiation (λ = 1.5418 Å; 45 kV; 40 mA) in a continuous scan at 25°C. The start position in 2θ was 5.0084° while the end position in 2θ was 49.9734°. We used step size in 2θ of 0.0170° and scan step time of 50.1650

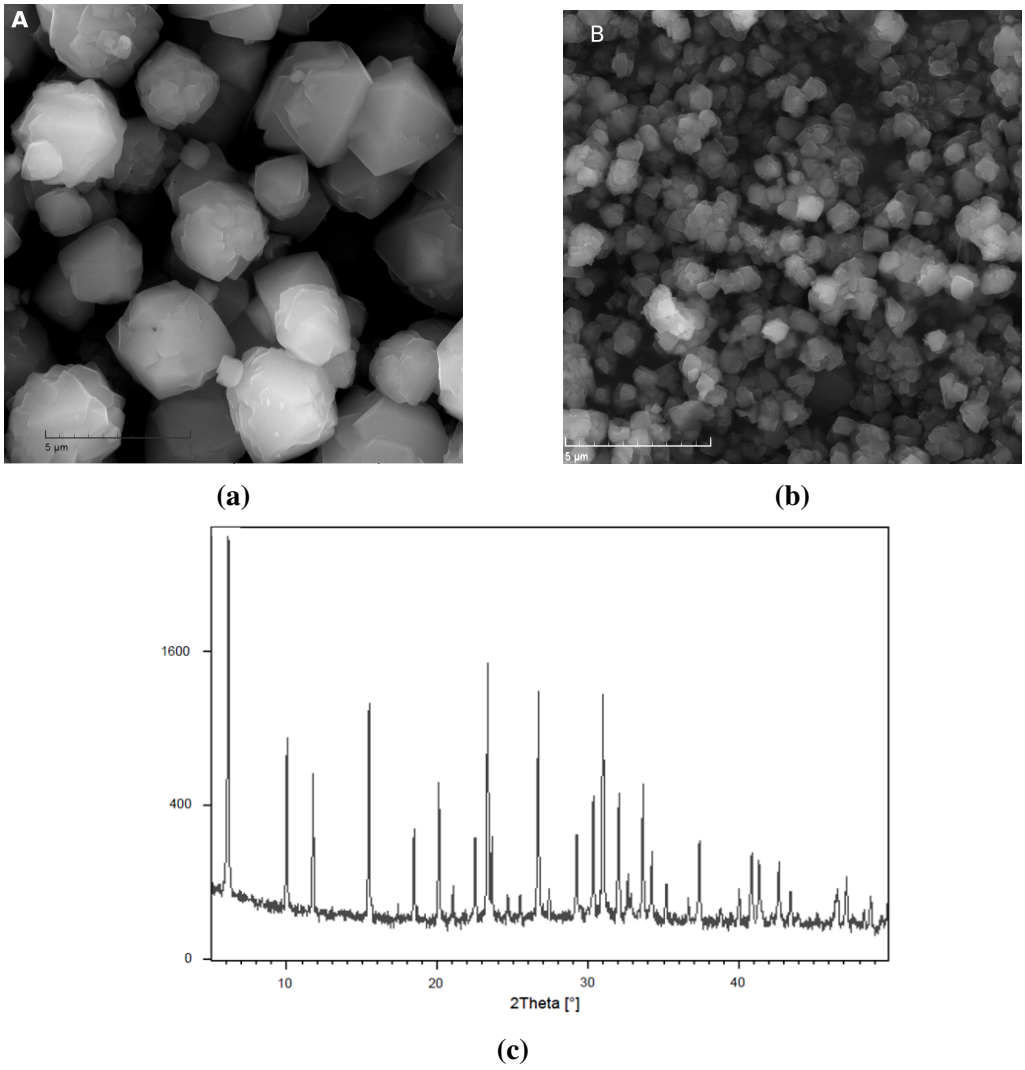

Figure A.3: SEM images of (a) Na-X and (b) H-Y along with XRD pattern of Na-X.

s. The measured specimen had a length of 10 mm. Electron micrographs were taken on a (TESCAN) MIRA-LMH scanning electron microscope (SEM) equipped with electron emission gun and operated at 20 kV. To improve the electrical conductivity of the sample, they were sputtered with platinum.

In general, the surface area and the porous volume measurements can be measured via N_2-adsorption using usual surface area measurements. In particular, surface area measurements such as a BET-measurement (measurement according Brunauer, Emmet, Teller) can be used (ASTM D3663 for the surface area; and ASTM D4365 for the porous volume). Nitrogen adsorption measurements were performed on Micromeritics ASAP 2020 surface area analyzer and all samples were degassed under vacuum at 300°C overnight before measurement. The isotherms were obtained using ASAP 2020 analysis program. The external surface (S_{ext}), the volume of micropores (V_{micro}) were obtained from *t-plot* based on the Harkins-Jura equation. Further, the mesoporous volume was determined as the difference between the total and micro-

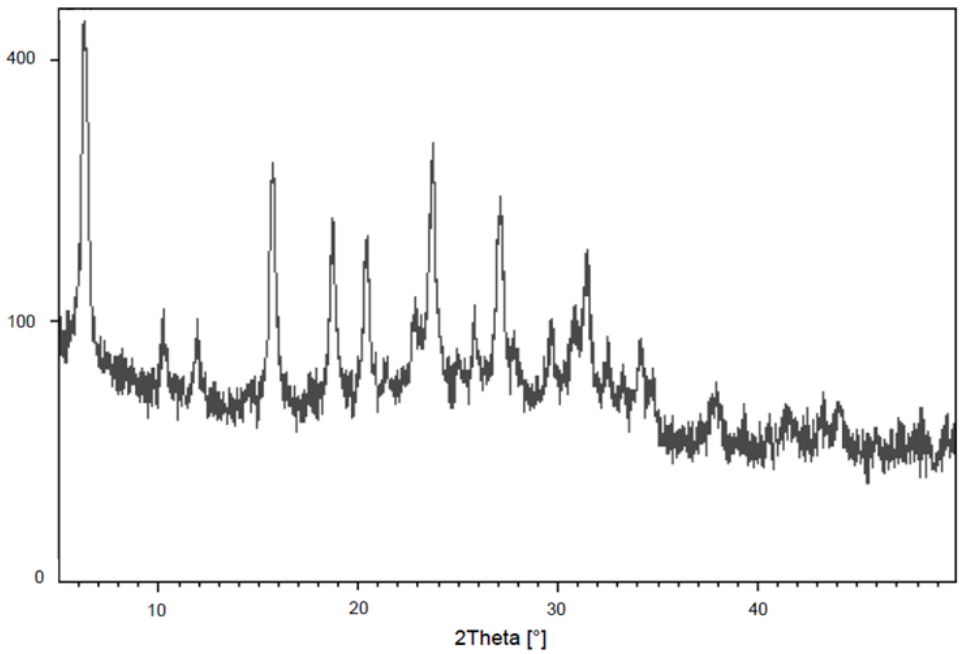

Figure A.4: PXRD pattern of H-Y using Cu-K_α-radiation (λ = 1.5418 Å; 45 kV; 40 mA) in a continuous scan at 25°C.

pore volumes[12] as per Eq.(A.5)

$$V_{meso} = V_{total} - V_{micro} \tag{A.5}$$

Table C.1 describes the BET-surface (S_{BET}), the external surface (S_{ext}), the volume of micropores (V_{micro}), the volume of mesopores (V_{meso}), and the total volume of pores (V_{total}) of the H-Y zeolite and of the Na-X zeolite.

Table A.1: Textural properties, number of Brønsted, Lewis and total acid sites estimated from pyridine (Py) adsorption quantified by infrared (IR) measurements for Na-X and H-Y Zeolites.

Zeolite	S_{BET} (m^2 g−1)	S_{ext} (m^2g^{-1})	V_{micro} (cm^3g-1)	V_{meso} (cm^3g^{-1})	V_{total} (cm^3g^{-1})	ε_{1545} (μmol/g)	ε_{1455} (μmol/g)	Total Brønsted and Lewis acidity (μmol/g)
H-Y	800	72.3	0.34	0.05	0.39	283	464	747
Na-X	833	54	0.30	0.03	0.33		353	353

Inductively coupled plasma-atomic emission spectroscopy (ICP-AES) on an OPTIMA 4300 DV (Perkin-Elmer) was used to determine all chemical compositions. Energy dispersive X-ray spectroscopy (EDX) measurements using the same scanning electron microscope model mentioned above were also performed to confirm the elemental analysis.The acidity of zeolites is measured via temperature programmed desorption (TPD). More specifically, the acidity is measured by pyridine (Py) adsorption quantified via infrared (IR) measurements. IR spectra were recorded on a Nicolet Magna 550 Fourier-Transform (FT)-IR spectrometer with 4 cm^{-1} optical resolution, with one level of zero-filling for the Fourier transform.

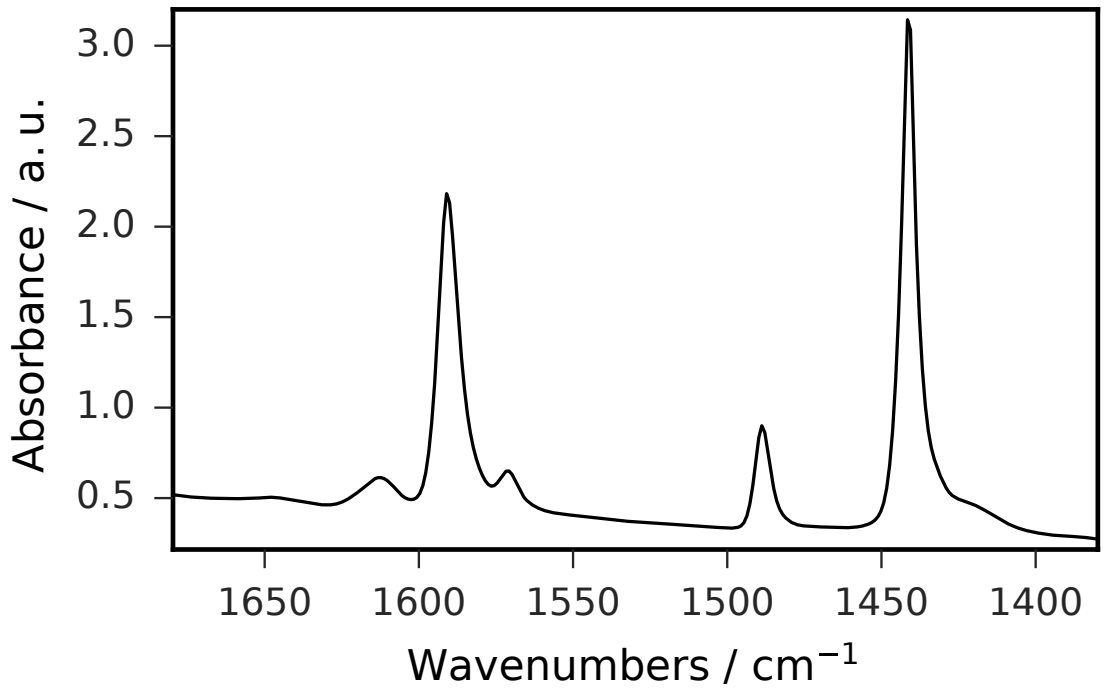

Figure A.5: Infrared spectra of Na-X zeolite between 1400 – 1700 cm^{-1} range after pyridine adsorption and evacuation under vacuum at 250°C. .

Prior to the measurements, the samples were pressed in self-supporting discs (diameter: 1.6 cm, 10 mg cm^{-2}) and activated in the IR cell (attached to a vacuum line) at 723°K for 4 h up to 106 Torr (14132.17 Pa). The IR cell was equipped with KBr windows, which allowed registering the spectra in the spectral region down to 400 cm^{-1}. The pressure of the adsorbed gases was measured by two Barocel gauges. One gauge was attached directly to the sample containing compartment of the cell. Another gauge allowed to measure a dose of gas in the known volume before adsorption thereof into the cell. The sample temperature during the treatment or recording of spectra was monitored by a chromel–alumel thermocouple inserted into the heater or into the coolant compartment of the cell. Adsorption of Py was performed at 423°K. The excess of probe molecules was further evacuated at 423°K. The adsorption–evacuation was repeated several times until no changes in the spectra were observed. The amount of the adsorbed Py was measured by means of the extinction coefficients ε_{1545} at 1545 cm^{-1}; pyridine attached to Brønsted acidic sites) = 1.8 cm/μmol and ε_{1455} (at 1455 cm^{-1}; pyridine attached to Lewis acidic sites) = 1.5 cm/μmol. The pyridine adsorption allowed quantifying the Brønsted acidic sites via ε_{1545} and the Lewis acidic sites via ε_{1455}[11].

The two zeolites are microporous, which does not allow the hydrate to be formed inside

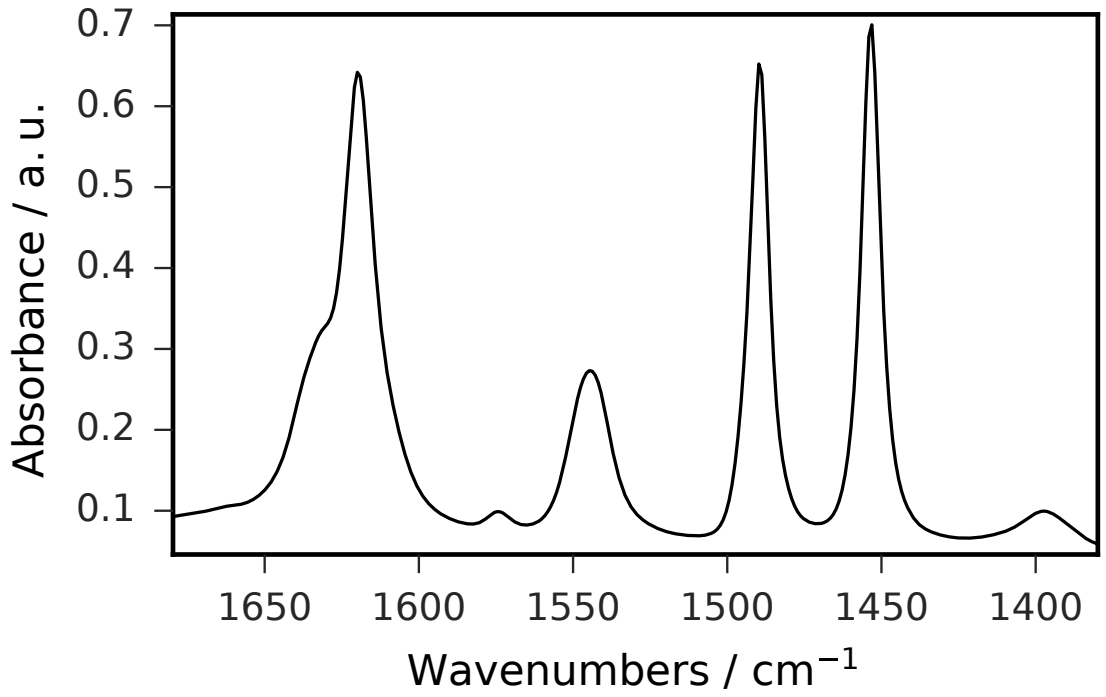

Figure A.6: Infrared spectra of H-Y zeolite between 1400 – 1700 cm^{-1} range after pyridine adsorption and evacuation under vacuum at 250°C.

pores. The measurements also showed that H-Y possesses a slightly higher external surface area than Na-X, which may increase the contact and enhance hydrate nucleation. A higher Si/Al ratio is associated with higher hydrophobicity[2, 4]. (ICP-AES) measurements revealed that while Na-X zeolite maintained high concentration of sodium, most of the sodium extra framework cation has been exchanged, and Si/Al ratio of H-Y is 2.7 compared to 1.2 in the case of Na-X as shown in **Table C.2** Such Si/Al ratios were also confirmed using (EDX) spectroscopy elemental analysis, as shown in **Table C.3**.

The acidity of the H-Y zeolite and of the Na-X zeolite were determined via temperature programmed desorption, i.e., by pyridine adsorption quantified via infrared measurements as described herein. **Table C.1** below reports the results for the two extinction coefficients ε_{1545} (Brønsted acidic sites) and ε_{1455} (Lewis acidic sites) and the total acidities while **Figures C.5** and **C.6** show the corresponding IR-spectra. The IR acidity measurements show that H-Y possesses high Lewis and total acidity than Na-X. More importantly, such results of acidity were reflected in the prepared THF aqueous solutions. To illustrate, the pH of blank 5.56 mol% THF aqueous solution is 7.5 while the same solution prepared with 0.5 wt% of H-Y, or 0.5 wt% Na-X solution were 9.19 and 4.52, receptively. More details can be found the supporting information.

Table A.2: Inductively coupled plasma-atomic emission spectroscopy (ICP-AES) for the Zeolite Promoters

	23Na [HEHe]	27Al [HEHe]	29Si [HEHe]
Zeolite	Concentration [mg/l]	Concentration [mg/l]	Concentration [mg/l]
Na-X	5.54	6.55	8.17
H-Y	0.78	4.95	13.28

Table A.3: Energy dispersive X-ray spectroscopy (EDX) measurements of Zeolite Promoters.

Element	Net	Mass%	Mass% (normalized)	Atom%	Absolute error in % (1 sigma)	Relative error in % (1 sigma)
			H-Y (sample #1)			
Al	328805	5.28	26.83	27.39	0.28	5.25
Si	849005	13.64	69.24	67.9	0.61	4.44
Na	24756	0.77	3.93	4.7	0.08	9.86
	Total:	19.69	100	100		
			H-Y (sample #2)			
Al	146766	6.94	25.55	26.11	0.36	5.15
Si	375371	19.24	70.79	69.5	0.84	4.39
Na	11976	1	3.67	4.4	0.09	9.3
	Total:	27.17	100	100		
			H-Y (sample #3)			
Al	240420	9.32	25.18	25.82	0.47	5.05
Si	618582	26.9	72.66	71.58	1.17	4.35
Na	12025	0.8	2.16	2.6	0.08	9.95
	Total:	37.03	100	100		
			Na-X			
Al	311131	19.6	34.57	33.67	0.96	4.9
Si	368444	23.1	40.73	38.11	1.01	4.37
Na	174806	14	24.69	28.22	0.93	6.62
	Total:	56.7	100	100		

A.4.2 Binary CH_4-THF Hydrate Characterization

Structure II crystal information was obtained by powder X-ray diffraction (PXRD) [7]. The measurement were carried out atmospheric pressure and low temperature with a PANalytical X'Pert Pro ® diffractometer system using Cu-K_α-radiation (λ = 1.5418 Å; 45 kV; 40 mA) in a continuous scan at 25°C. The start position in 2θ was 10.0114° while the end position in 2θ was 39.7500°. We used step size in 2θ of 0.0170° and scan step time of 50.1650 s. The measured specimen had a length of 10 mm. Binary CH_4-THF hydrates were synthesized in high pressure reactor as described in **Experimental Section** using 5.56 mol% THF aqueous solution at 6 MPa and 283.2 K. After the reaction is deemed completed, the unreacted gas is depressurized to atmosphere followed by quick reactor cooling by liquid nitrogen. Under liquid nitrogen to avoid hydrate dissociation, the hydrate sample was grounded by a mortar and pestle to prepare the uniform powder. Then, the sample was compared to standard hydrate pattern. In **Figure C.7**, the obtained PXRD pattern is a typical sII pattern of space group $Fd\bar{3}m$ which is another indication of the presence of sII and absence of sI.

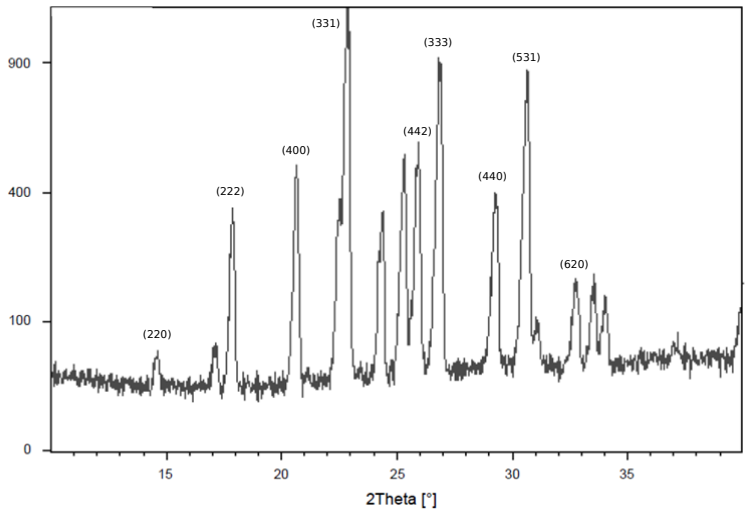

Figure A.7: Powder X-ray diffraction (PXRD) of binary CH_4-THF hydrate synthesized at 6 MPa and 283.2 K

Raman spectra of hydrate samples is obtained using an immersion Raman probe (InPhotonics®) lined to the laser spectrometer (Horiba LabRam Evol®) via optical fibres. A green laser at 532 nm wavelength was used for excitation. The spectral coverage is 50-3500 cm^{-1}.After the reaction is deemed completed, the unreacted gas is depressurized to atmosphere followed by quick reactor cooling by liquid nitrogen for data acquisition.

Raman spectroscopic measurements were performed on the binary hydrate synthesized using 5.56 mol% THF solution and methane gas starting at a pressure of 6 MPa and 283.2 K. As shown in **Figure C.8**, Raman spectra in the low-frequency region of water lattice modes of sII THF hydrate appear around $\sim$ 203 cm^{-1}. Then, a sharp peak of C-C-C-C appears at $\sim$

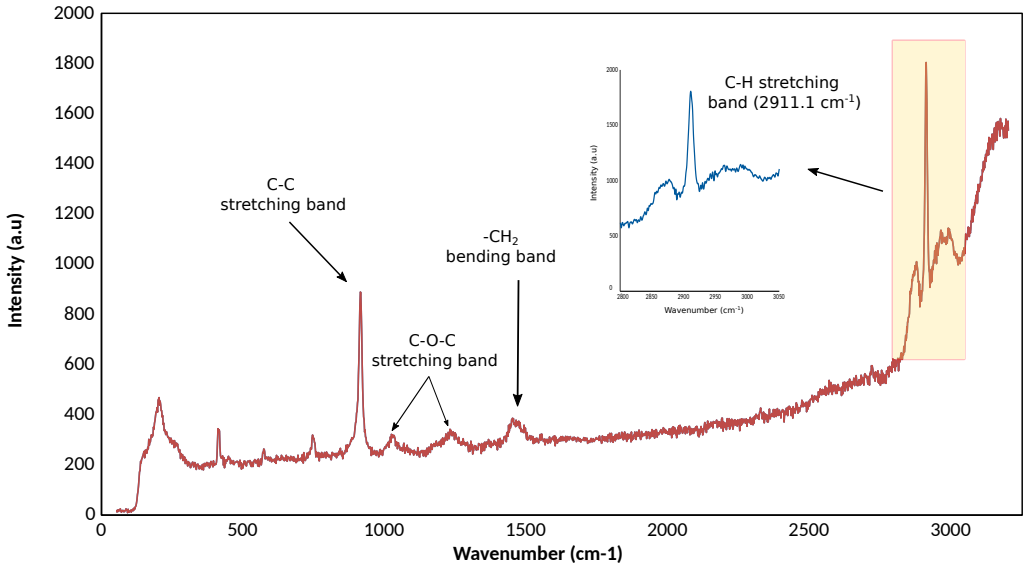

Figure A.8: Raman spectra of binary CH_4-THF hydrate formed at 6 MPa and 283.2 K. C-H stretching band is shown separately in blue.

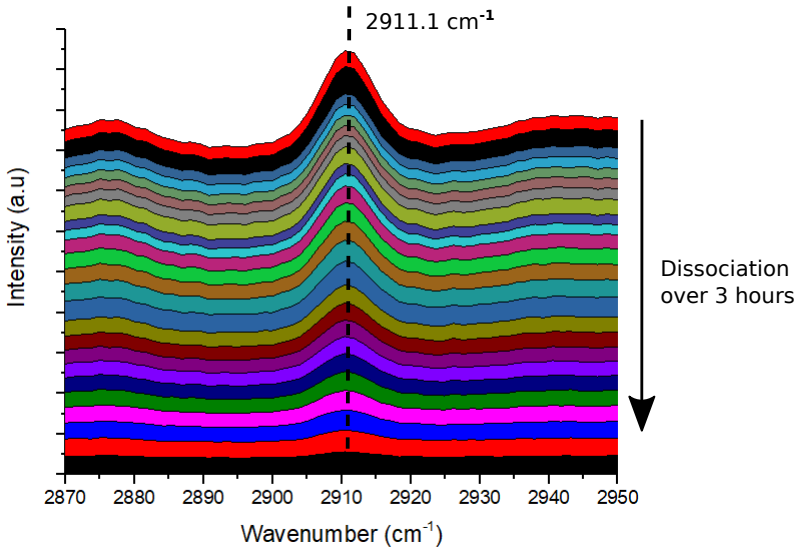

Figure A.9: *Ex-situ* sequential Raman analysis of the dissociation of binary CH_4-THF hydrates shows methane gas disappearance from 5^{12} small cage (peak at 2911.1 cm^{-1}) at 293.2 K and atmospheric pressure. Peaks are shown in different colors for clarity

913.7 cm^{-1} as THF occupies the $5^{12}6^4$ cages of sII hydrates. At 1023.7 cm^{-1} a weak mode of the THF C-O-C stretching could be observed. The peaks at 1451.1 cm^{-1} can be assigned to -CH_2 bending of THF. C-H and O-H stretching modes overlap around 2877.1 cm^{-1}. Methane occupancy in 5^{12} small cages of sII can be clearly seen by the sharp peak at $\sim$ 2911.1 cm^{-1}. The choice of these *P-T* conditions guaranteed that formation conditions are within the stability boundary of sII clathrate. Thus, this eliminates any possibility of sI formation in our sample as

it is thermodynamically stable at 193 K [2].

To further prove the formation of binary CH_4-THF hydrate rather than pure sII THF hydrate, we carried out a sequential Raman analysis of hydrate dissociation. Our focus is to track the methane gas release from hydrate structure following the disappearance of $\sim$ 2911.1 cm^{-1} peak of methane at 5^{12} cage. **Figure C.9** shows Raman spectra measured as a function of time during hydrate dissociation. It reveals a decrease of $\sim$ 2911.1 cm^{-1} peak intensity over 3 hours of methane dissociation at atmospheric pressure and 293.2 K until the signal disappeared. This disappearance indicates that all methane has been released from the solid hydrate.

A.5 Other Figures and Tables

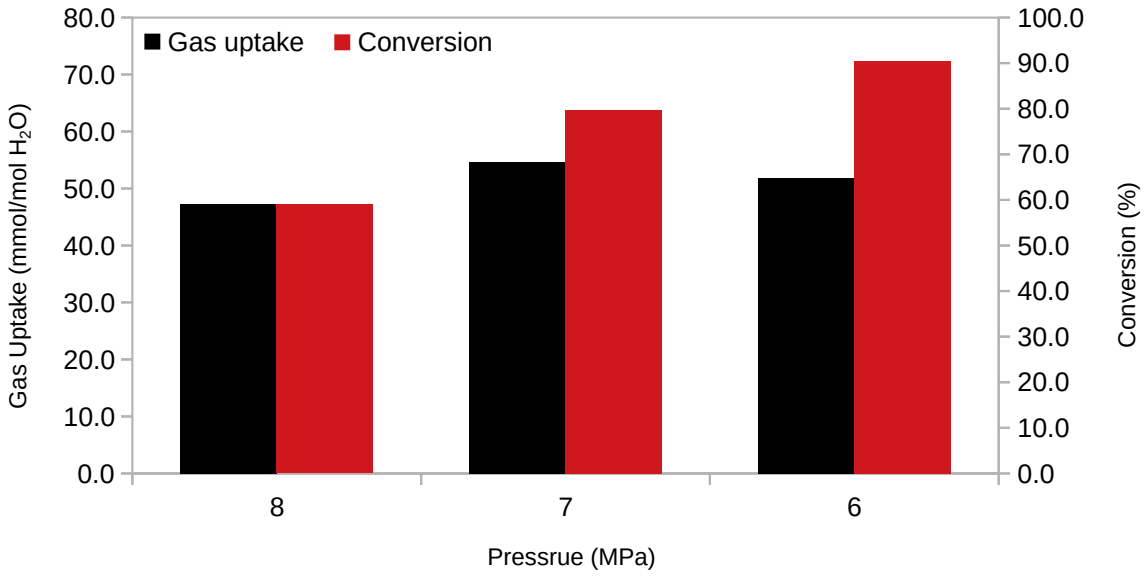

Figure A.10: Effect of pressure on the gas uptake (in black) and conversion (in red) of THF aqueous solution in non-stirred tank reactor.

Table A.4: Hydrate formation at 283.2 K from 5.6 mol% THF aqueous solution at different pressures.

System No.	Zeolite Concen-tertion(% w/v)	P (MPa)	Induction time(min)	Gas up-take(mmol gas/mol H_2O)	Gas Conversion(%)	Hydrate Yield (%)	t_{90} (min)	% Recovery
THF-Blank-80	0	80	7.3	47.21	58.88%	40.13%	254	96.23
THF-Blank-70	0	70	19.3	54.62	79.75%	46.43%	231	95.88
THF-Blank-60	0	60	26.0	51.82	90.37%	40.44%	464	96.71

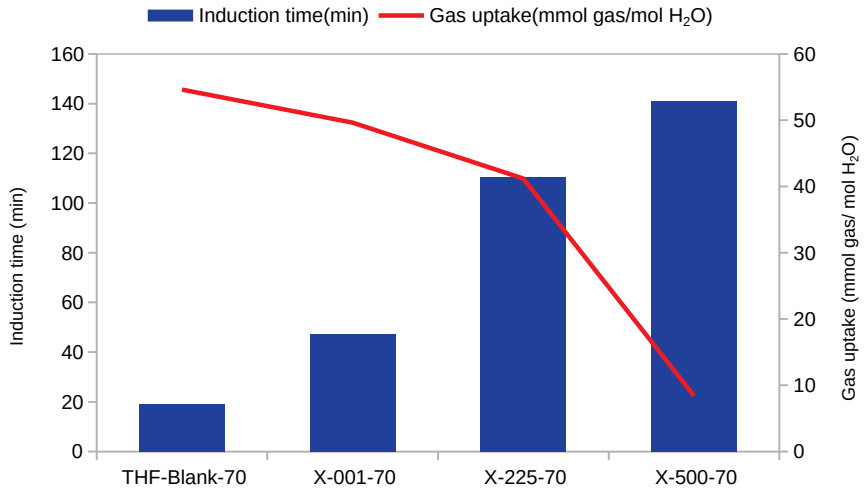

Figure A.11: Effect of zeolite Na-X concentration on the induction time (in green) and gas uptake (in dark red) of THF aqueous solution at 7 MPa and 283.2 K.(For interpretation of the references to colour in this figure legend, the reader is referred to the web version of this article.)

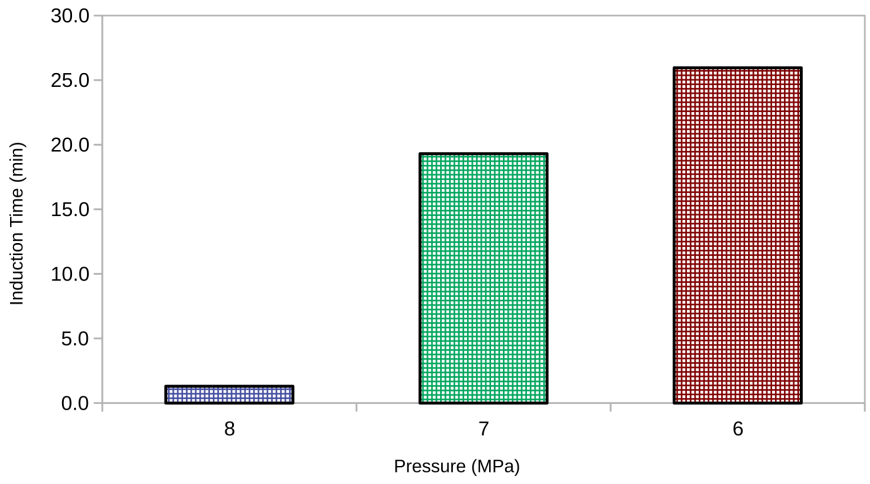

Figure A.12: Effect of Pressure on the induction time of THF aqueous solution in non-stirred tank reactor.

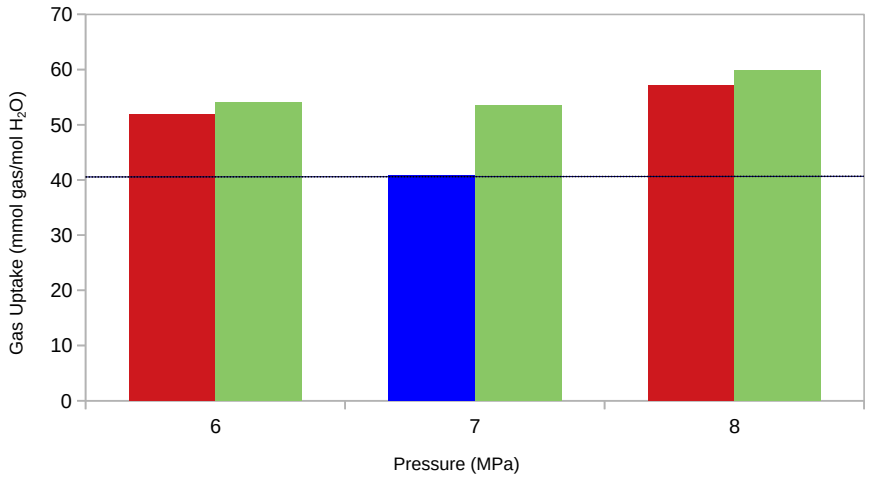

Figure A.13: Comparison methane uptake in presence of H-Y and SDS at different pressures and 283.2 K. The green and blue bars are gas uptake with 0.5 wt% of H-Y and SDS[13], respectively. The light red bars are gas uptake at 0.255 wt% H-Y zeolite.

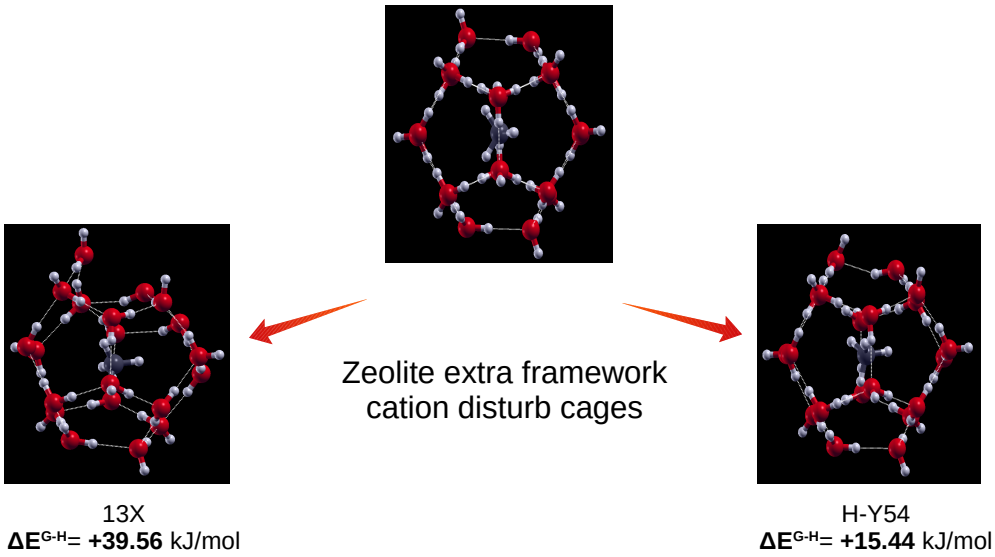

Figure A.14: Optimized structures of $CH_4@5^{12}$ cage (Oxygen and hydrogen atoms are in red and white, respectively) in the absence and presence of Na-X and H-Y. The ΔE^{HG} of the two systems is also included.

References

[1] P. E. Blöchl. Projector augmented-wave method. *Phys. Rev. B*, 50(24):17953–17979, 1994. ISSN 01631829. doi: 10.1103/PhysRevB.50.17953.

[2] N. Y. Chen. Hydrophobic properties of zeolites. *J. Phys. Chem.*, 80(1):60–64, 1976. ISSN 00223654. doi: 10.1021/j100542a013.

[3] Michael T. Kirchner, Roland Boese, W. Edward Billups, and Lewis R. Norman. Gas hydrate single-crystal structure analyses. *J. Am. Chem. Soc.*, 126(30):9407–9412, 2004. ISSN 00027863. doi: 10.1021/ja049247c.

[4] Nikolay Kosinov, Clement Auffret, Gerard J. Borghuis, Venkata G.P. Sripathi, and Emiel J.M. Hensen. Influence of the Si/Al ratio on the separation properties of SSZ-13 zeolite membranes. *J. Memb. Sci.*, 484:140–145, 2015. ISSN 18733123. doi: 10.1016/j.memsci.2015.02.044. URL `http://dx.doi.org/10.1016/j.memsci.2015.02.044`.

[5] Mariann Krossner and Joachim Sauer. Interaction of water with brønsted acidic sites of zeolite catalysts. ab initio study of 1:1 and 2:1 surface complexes. *J. Phys. Chem.*, 100 (15):6199–6211, 1996. ISSN 00223654. doi: 10.1021/jp952775d.

[6] Asheesh Kumar, Rajnish Kumar, and Praveen Linga. Direct use of seawater for rapid methane storage via clathrate (sII) hydrates. *Appl. Energy*, 235(August 2018):21–30, 2019. ISSN 0306-2619. doi: 10.1016/j.apenergy.2018.10.085. URL `https://doi.org/10.1016/j.apenergy.2018.10.085`.

[7] Asheesh Kumar, Hari Prakash Veluswamy, Praveen Linga, and Rajnish Kumar. Molecular level investigations and stability analysis of mixed methane-tetrahydrofuran hydrates: Implications to energy storage. *Fuel*, 236(August 2018):1505–1511, 2019. ISSN 00162361. doi: 10.1016/j.fuel.2018.09.126.

[8] Frédéric Labat, Alain H. Fuchs, and Carlo Adamo. Toward an accurate modeling of the

water-zeolite interaction: Calibrating the DFT approach. *J. Phys. Chem. Lett.*, 1(4):763–768, 2010. ISSN 19487185. doi: 10.1021/jz100011p.

[9] Angela N. Migues, Adina Muskat, Scott M. Auerbach, Woody Sherman, and S. Vaitheeswaran. On the rational design of zeolite clusters. *ACS Catal.*, 5(5):2859–2865, 2015. ISSN 21555435. doi: 10.1021/cs501827p.

[10] Ahmed Omran, Nikolai Nesterenko, and Valentin Valtchev. Ab initio mechanistic insights into the stability, diffusion and storage capacity of sI clathrate hydrate containing hydrogen. *Int. J. Hydrogen Energy*, 47(13):8419–8433, 2022. ISSN 03603199. doi: 10.1016/j.ijhydene.2021.12.186. URL `https://doi.org/10.1016/j.ijhydene.2021.12.186`.

[11] Ana Palčić and Valentin Valtchev. Analysis and control of acid sites in zeolites. *Appl. Catal. A Gen.*, 606(July 2020):117795, 2020. ISSN 0926860X. doi: 10.1016/j.apcata.2020.117795. URL `https://doi.org/10.1016/j.apcata.2020.117795`.

[12] Ana Palčić, Simona Moldovan, Hussein El Siblani, Aurelie Vicente, and Valentin Valtchev. Defect Sites in Zeolites: Origin and Healing. *Adv. Sci.*, 2104414:2104414, 2021. ISSN 2198-3844. doi: 10.1002/advs.202104414.

[13] Burla Sai Kiran, Kandadai Sowjanya, Pinnelli S R Prasad, and Ji Ho Yoon. Experimental investigations on tetrahydrofuran - Methane - water system: Rapid methane gas storage in hydrates. *Oil Gas Sci. Technol. – Rev. IFP Energies Nouv.*, 74:12, 2019. ISSN 19538189. doi: 10.2516/ogst/2018092.

[14] Konstantin A. Udachin, Christopher I. Ratcliffe, and John A. Ripmeester. Single crystal diffraction studies of structure I, II and H hydrates: Structure, cage occupancy andf composition. *J. Supramol. Chem.*, 2(4-5):405–408, 2002. ISSN 14727862. doi: 10.1016/S1472-7862(03)00049-2.

Appendix B

Supporting Information for Chapter 5

B.1 Characterization methods

B.1.1 Zeolite Promoter Characterization

Powder X-ray diffraction (PXRD) patterns were obtained with a PANalytical X'Pert Pro ® diffractometer system using Cu-K_α-radiation (λ = 1.5418 Å; 45 kV; 40 mA) in a continuous scan at 25°C. The start position in 2θ was 5.0114° while the end position in 2θ was 59.99°. We used step size in 2θ of 0.0170° and scan step time of 50.1650 s. The measured specimen had a length of 10 mm. Electron micrographs were taken on a (TESCAN) MIRA-LMH scanning electron microscope (SEM) equipped with electron emission gun and operated at 20 kV. To improve the electrical conductivity of the sample, they were sputtered with platinum.

In general, the surface area and the porous volume measurements can be measured via N_2-adsorption using usual surface area measurements. In particular, surface area measurements such as a BET measurement (measurement according to Brunauer, Emmet, Teller) can be used (ASTM D3663 for the surface area; and ASTM D4365 for the porous volume). Nitrogen adsorption measurements were performed on Micromeritics ASAP 2020 surface area analyzer and all samples were degassed under vacuum at 300°C overnight before measurement. The isotherms were obtained using ASAP 2020 analysis program. The external surface (S_{ext}), and the volume of micropores (V_{micro}) were obtained from ẽxtitt-plot based on the Harkins-Jura equation. Further, the mesoporous volume was determined as the difference between the total and micropore volumes[1] as per Eq.(C.8)

$$V_{meso} = V_{total} - V_{micro} \tag{B.1}$$

All measurements and data plots as utilized herein were made with a Micromeritics Tristar 3000 analyzer. The total surface area was determined by N_2 sorption analysis according to ASTM D 4365 – 95 (reapproved 2008). Volumes of micropores and mesopores were determined according to D4641-94 (reapproved 2006).

Inductively coupled plasma-atomic emission spectroscopy (ICP-AES) on an OPTIMA 4300 DV (Perkin-Elmer) was used to determine all chemical compositions. Energy-dispersive X-ray spectroscopy (EDX) measurements using the same scanning electron microscope model mentioned above were also performed to confirm the elemental analysis.

B.1.2 Seawater-based Mixed CH_4-THF Characterization

Natural seawater was Natural seawater (SW) obtained from Ouistreham coast, Caen, France. After filtration of large particles, an Agilent quadrupole ICP/MS 7900 equipped with a 1.5 mm Quartz torch and a Helium collision cell was used to determine the elemental content of our seawater sample. Then, structure II clathrate crystal information was obtained by powder X-ray diffraction (PXRD) [2]. Variable temperature powder X-ray diffraction (PXRD) data was collected on a PANalytical X'Pert Pro ® diffractometer system using an X-ray tube Co-K_α-radiation (λ = 1.79 Å; 45 kV; 40 mA) and an Anton Paar TTK450 temperature chamber. The XRPD pattern were collected in Bragg-Brentano configuration with an X'Celerator detector from $8^\circ \leq 2\theta \leq 70^\circ$ with a step size of 0.0167° and 180 s/step. Variable temperature PXRD data were also collected between -20 °C and -100 °C under flowing nitrogen. Scattering from the sample holder was avoided by using a Si zero-scattering background slide in the sample holder. The nitrogen was dried by flowing it through a Drierite gas purifier (filled with DRIERITE and 5 A molecular sieve). Structural analysis was performed using the program JANA2020 [3]. Mixed CH_4-THF hydrates were synthesized in the high pressure reactor as described in **Section 2.1** using 5.56 mol% THF freshwater aqueous solution at 9.5 MPa and 298.2 K. After the reaction is deemed complete, the unreacted gas is depressurized to atmosphere followed by quick reactor cooling by liquid nitrogen. Under liquid nitrogen to avoid hydrate dissociation, the hydrate sample was grounded by a mortar and pestle to prepare the uniform powder. Then, the sample was compared to a standard hydrate pattern. Since hydrate conversion is not 100%, the I_h ice in the PXRD data comes from unreacted water. In a similar manner, solid state ^{13}C MAS NMR spectra were obtained using a Bruker DRX400 spectrometer at a Larmor frequency of 100.6 MHz. Spectra were recorded at 250 K by placing the powdered hydrate samples in a 4 mm o.d. Zr-rotor that was loaded into a variable-temperature (VT) probe. All 13C NMR spectra were recorded with magic angle spinning (MAS) between 2 and 4 kHz.

B.1.3 Hydrate formation experiment

First, the reactor was filled with the solution until the desired level was achieved before it is sealed. After purging with N_2 for three-time to ensure oxygen removal, the reactor and related connection were purged with methane too. The system then is cooled down/heated to the target 298.2 K temperature. Once the target temperature was achieved, the system was pressurized

with methane up to 9.5 MPa. Pressure and temperature values were recorded every 10 sec and transmitted with the acquisition system to the PC for recording and monitoring. The time period between this starting point and the formation of the first hydrate crystal is called induction time. The induction time was distinguished by a simultaneous pressure drop and temperature increase due to the exothermic reaction nature of hydrate formation. As the reaction continues, the pressure drops further, and the hydrate formation process is considered complete after 9 hours. After that period, we found that there is no further significant pressure drop for all experiments in this study.

The number of moles of the gas consumed at any time t ($\Delta n_{H\downarrow}$) is equal to the difference between the number of moles of the gas $n_{H,0}$ at time =0 (i.e. the start of the experiment) and the number of moles of the gas present $n_{H,t}$ at any time t in the vessel as shown by Eq.(C.1):

$$\Delta n_{H\downarrow} = n_{H_0} - n_{H_t} = \left(\frac{PV}{zRT}\right)_{G_0} - \left(\frac{PV}{zRT}\right)_{G_t} \tag{B.2}$$

Subscript G_0 and G_t represent the gas phase at the start of the experiment and time t, respectively. Here, P, T, and V are the pressure, temperature, and reactor volume, respectively. R is the universal gas constant, and z is the comprehensibility factor calculated by Pitzer's correction [4].

Normalized methane gas uptake is calculated by the following Eq.(C.2):

$$Normalized \quad uptake \quad = \frac{\Delta n_{H\downarrow}}{n_{H_2O}} \tag{B.3}$$

B.1.4 Hydrate dissociation experiment

To evaluate the methane uptake, the hydrates were dissociated by increasing the temperature at the end of all experiments to 310.2 K for at least 6 hours. The selection of that temperature ensures complete hydrate dissociation as it is beyond the equilibrium phase boundary. After 6 hours, the dissociation is deemed completed when the pressure is not changing for 1 h. During dissociation, the amount of methane released from hydrate at any time t is calculated by Eq.(C.6)

$$\Delta n_{H\uparrow} = n_{H,\downarrow} - n_{H,0} = \left(\frac{PV}{zRT}\right)_{G,t} - \left(\frac{PV}{zRT}\right)_{G,0} \tag{B.4}$$

where $n_{H,\downarrow}$ is the moles of methane gas consumed for the hydrate formation at the end of the experiment. Finally, the methane recovery is calculated as in Eq.(C.7):

$$Recovery(\%) = \frac{\Delta n_{H\uparrow}}{n_{H,\downarrow}} * 100 \tag{B.5}$$

B.1.5 Computational Methods

We performed density functional theory (DFT) calculations [5] using the projected augmented wave (PAW) method and the standard pseudopotentials supplied by Quantum Espresso (QE) software [6]. The kinetic energy cutoff for plane wave expansion of wavefunctions and charge density were 55 and 440 Ry, respectively[7]. All structures were fully optimized using a force convergence threshold of at least 10^{-4} Ry/a.u. and with a self-consistency convergence criterion of at least $1, \times 10^{-8}$. The calculations have been carried out using the Monkhorst-Pack *k*-points grid of $2 \times 2 \times 2$ in the reciprocal space. The DFT calculations for isolated cages and zeolite clusters were performed in a cubic simulation cell of volume $30 \times 30 \times 30$ Å^3. The 5^{12} small cage was modeled with a 20-molecule water cluster. In these small (5^{12}) cages, 8 oxygen atoms are located in a perfect cube (O_h). An estimated distance of 3.91 Å separates those 8 oxygen atoms from the cage center. The remaining 12 oxygen are positioned at 3.95 Å from the cage center and transform according to the (T_h) subgroup of (O_h)[8]. The results agree with the average obtained from the X-ray structure of sII as well as the optimized crystal model[9, 10]. Amino acids' interaction with the above hydrate cages was successfully monitored using DFT calculated as reported by Lee *et al.*[11]. A similar method was used to represent the zeolite promoters and their interaction with hydrate cages. In that method, we have used computationally affordable finite cluster models of zeolite crystals. Cluster models have extensively been employed to understand reactive and absorptive processes in various framework types of zeolites[12]. In particular, they have been successfully applied to understand zeolite acidity and water-zeolite interactions [13, 14].

B.2 Figures and Tables

Table B.1: Textural measurement for Zeolite Promoters obtained from Nitrogen adsorption measurements

Zeolite	S_{BET} (m^2g^{-1})	S_{ext} (m^2g^{-1})	V_{micro} (cm^3g^{-1})	V_{meso} (cm^3g^{-1})	V_{total} (cm^3g^{-1})
USY-40	920.25	341.28	0.23	0.32	0.55
USY-10	956.65	295.09	0.26	0.26	0.53

Table B.2: Summary of experiments carried out with THF 5.56 mol% water (FW) and simulated seawater (SSW). In all listed experiments, temperature and initial pressure were 298.2 K and 9.5 MPa.

System	Experiment No.	Reactor Type	**Gas uptake(mmol gas/mol H_2O)**	Induction Time (min)	t_{90}[a]	**Revovery (%)**[b]
FW+ 5.56 mol% THF+0.03% US-Y-40	F1	NSTR	**60.37** (±2.5)	0.80 (±0.7)	**356.70**	96.09
	F2	NSTR	**53.90** (±3.7)	0.20 (±0.1)	**376.80**	96.41
	F3	NSTR	**55.70** (±1.2)	0.50 (±0.2)	**358.90**	97.95
FW+ 5.56 mol% THF+0.03% L-valine	G1	NSTR	**64.52** (±4.1)	1.00 (±0.5)	**444.00**	97.20
	G2	NSTR	**66.18** (±1.8)	1.20 (±0.3)	**398.80**	97.35
	G3	NSTR	**65.20** (±2.2)	2.30 (±0.8)	**423.00**	98.00
SSW (3 wt% NaCl)+ 5.56 mol% THF+0.03% US-Y-40	H1	NSTR	**29.78** (±4.2)	10.90 (±1.7)	**162.30**	97.20
	H2	NSTR	**30.60** (±1.6)	7.40 (±1.2)	**184.80**	96.70
	H3	NSTR	**31.80** (±3.5)	8.70(±2.2)	**170.50**	97.35
SSW (3 wt% NaCl)+ 5.56 mol% THF+0.03% L-valine	I1	NSTR	**34.79** (±1.8)	1.80 (±0.8)	**396.50**	97.78
	I2	NSTR	**30.60** (±0.9)	2.20 (±0.7)	**385.40**	97.95
	I3	NSTR	**31.50** (±3.8)	1.50 (±0.8)	**375.20**	97.10

[a] average results of t_{90} varied within ±48 min

[b] average results of hydrate %recovery varied within ±1.42 %.

Table B.3: Inductively coupled plasma-atomic emission spectroscopy (ICP-AES) for the Zeolite Promoters

	23Na [HEHe]	27Al [HEHe]	29Si [HEHe]
Zeolite	Concentration [mg/l]	Concentration [mg/l]	Concentration [mg/l]
USY-10	0.15	1.27	16.75
USY-40	0.14	0.48	19.96

Table B.4: Energy-dispersive X-ray spectroscopy (EDX) measurements of Zeolite Promoters.

Element	Net	Mass%	Mass% (normalized)	Atom%	Absolute error in % (1 sigma)	Relative error in % (1 sigma)
			USY-40			
Al	239751	1.02	2.63	2.75	0.070	7.25
Si	11873099	37.27	96.46	96.68	1.61	4.32
Na	3238	0.24	0.63	0.19	0.04	14.67
			USY-10			
Al	269678	1.82	6.53	6.78	0.11	6.01
Si	3584252	25.74	92.49	92.37	1.09	4.24
Na	4041	0.04	0.16	0.20	0.01	11.34

Table B.5: France seawater composition analysis (Total salinity: 2.75 wt%)

Test	Components (mg/L)
23 Na	12415.120
34 S	585.870
39 K	459.110
35 Cl	32670.020
14 N	6628.771
79 Br	8.824
127 I	0.111
24 Mg	1380.400
43 Ca	413.430
27 Al	$\leq$ 0.001
11 B	4.628
88 Sr	1.034
51 v	$\leq$ 0.01
31 P	0.058
60 Ni	$\leq$ 0.001
107 Ag	$\leq$ 0.001
66 Zn	0.001
56 Fe	0.001
63 Cu	0.001
28 Si	0.400
45 Sc	0.110
7 Li	0.120
85 Rb	0.017
89 Y	0.112
95 Mo	0.002
137 Ba	0.003

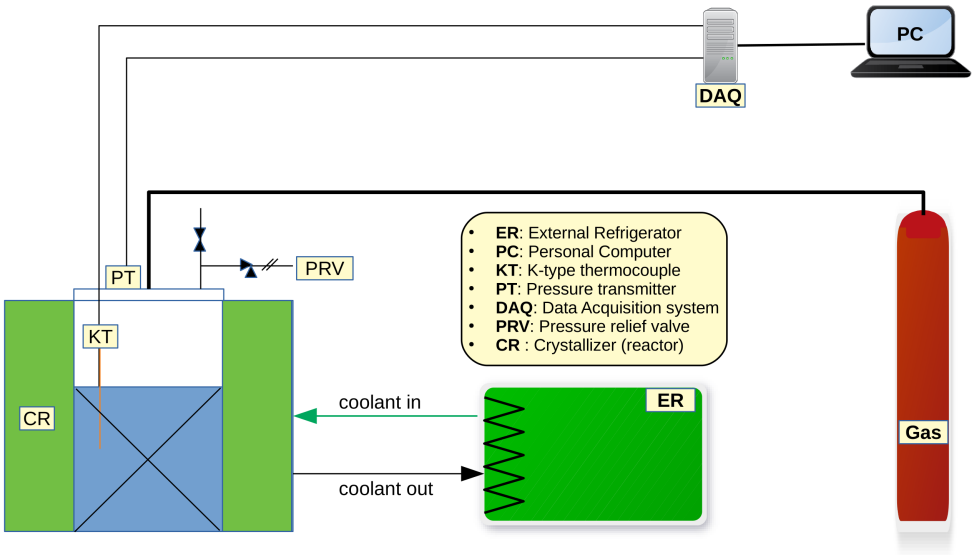

Figure B.1: Schematic diagram of hydrate formation and dissociation setup

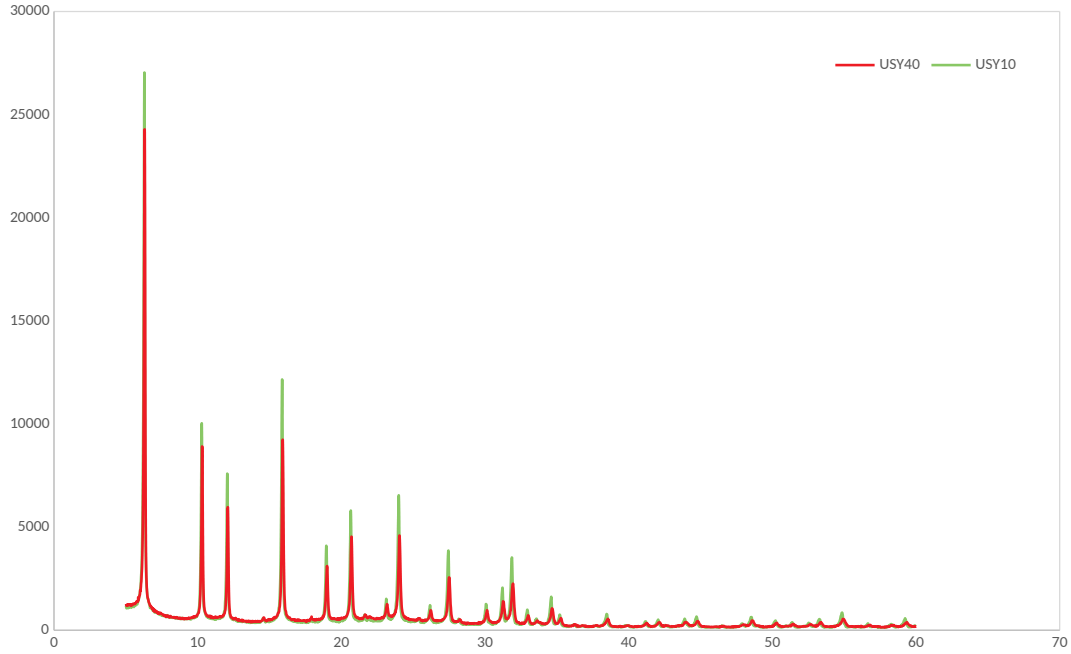

Figure B.2: PXRD pattern of USY-10 and USY-40 using Cu-K_α-radiation (λ = 1.5418 Å; 45 kV; 40 mA) in a continuous scan at 25°C.

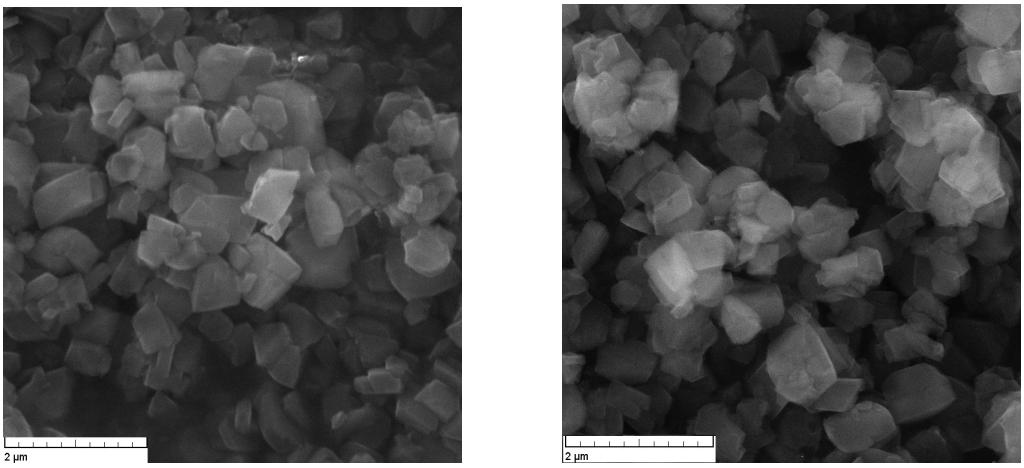

(a) **(b)**

Figure B.3: SEM images of (a) USY-10 and (b) USY-40

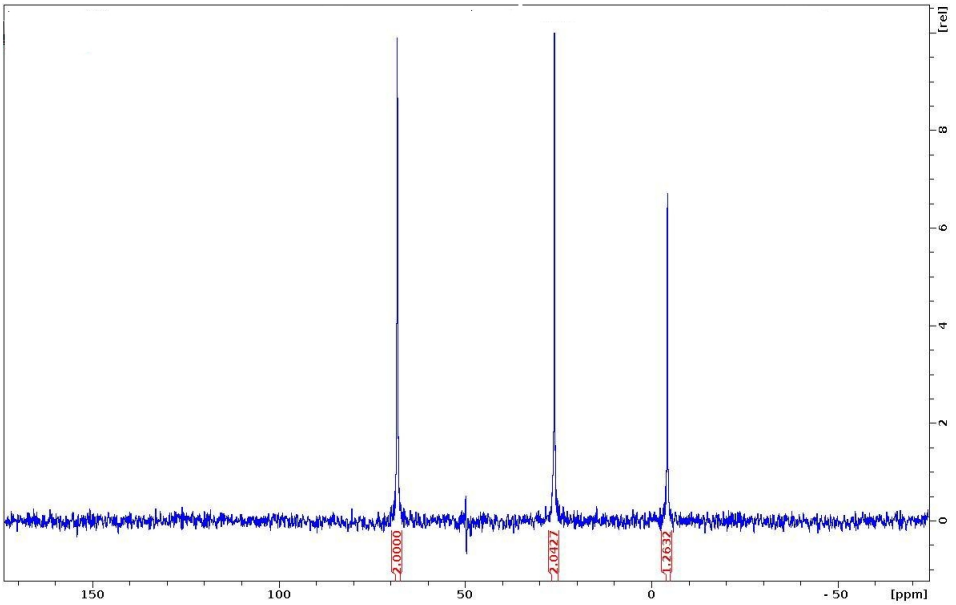

Figure B.4: ^{13}C MAS NMR spectra of seawater-based binary CH_4+THF hydrate (structure II) synthesized at 298.2 K. Methane molecules occupied only in 5^{12} cages and appeared at about -4.3 ppm and THF molecules occupied in $5^{12}6^4$ large cages were represented by two resonances (-C-C- at 26.2 ppm, -C-O-C- at 69.0 ppm).

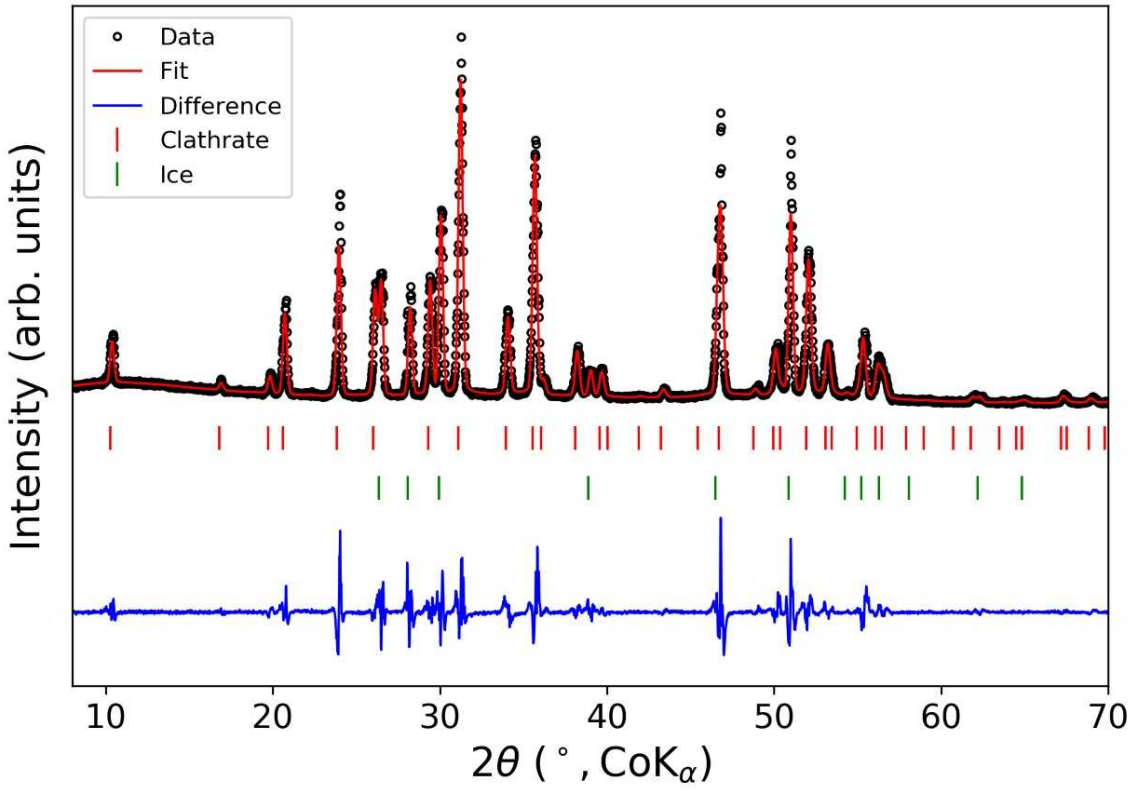

Figure B.5: PXRD pattern of mixed CH_4-THF clathrate using Co-K_α-radiation (λ = 1.79 Å; 45 kV; 40 mA) at -100 °C under flowing nitrogen.

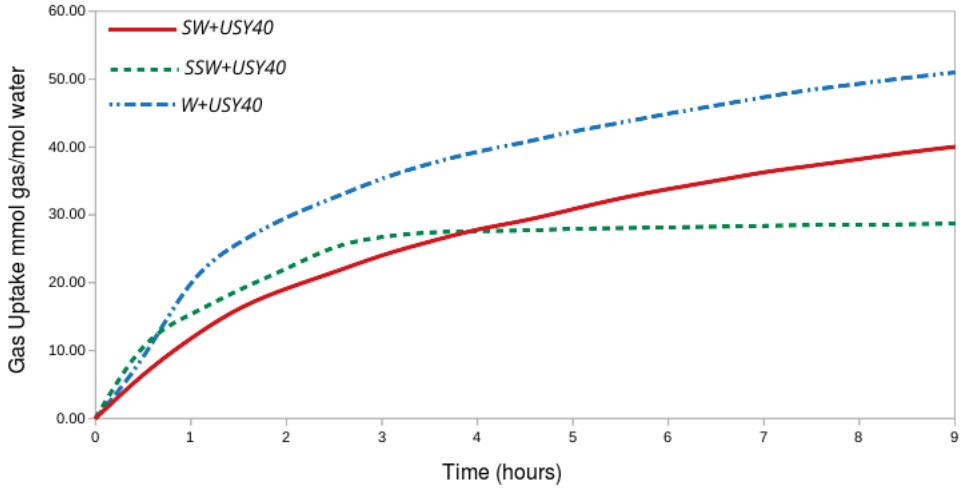

Figure B.6: Comparison of average methane gas uptake owing to hydrate formation runs in presence USY-40 zeolite using seawater, simulated seawater (3 wt% NaCl) and pure water: all solution contain THF in stoichiometric concentration of 5.56 mol% and hydrate synthesis temperature and pressure are 298.2 K and 9.5 MPa, respectively.

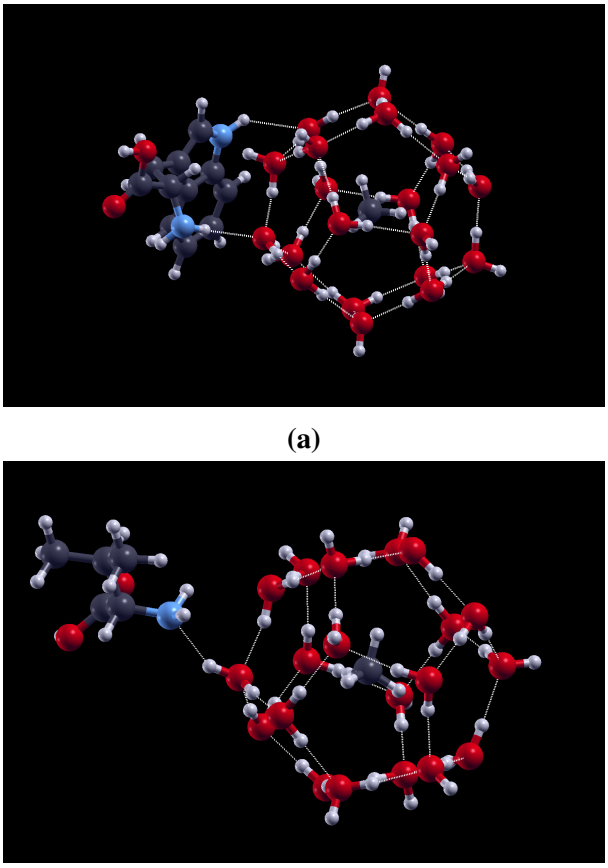

(a)

(b)

Figure B.7: Optimized configurations of small (5^{12}) cage with zeolite clusters of (a) L-tryptophan and (b) L-valine. Nitrogen, hydrogen, and carbon atoms are shown in blue, white, and black colors, respectively.

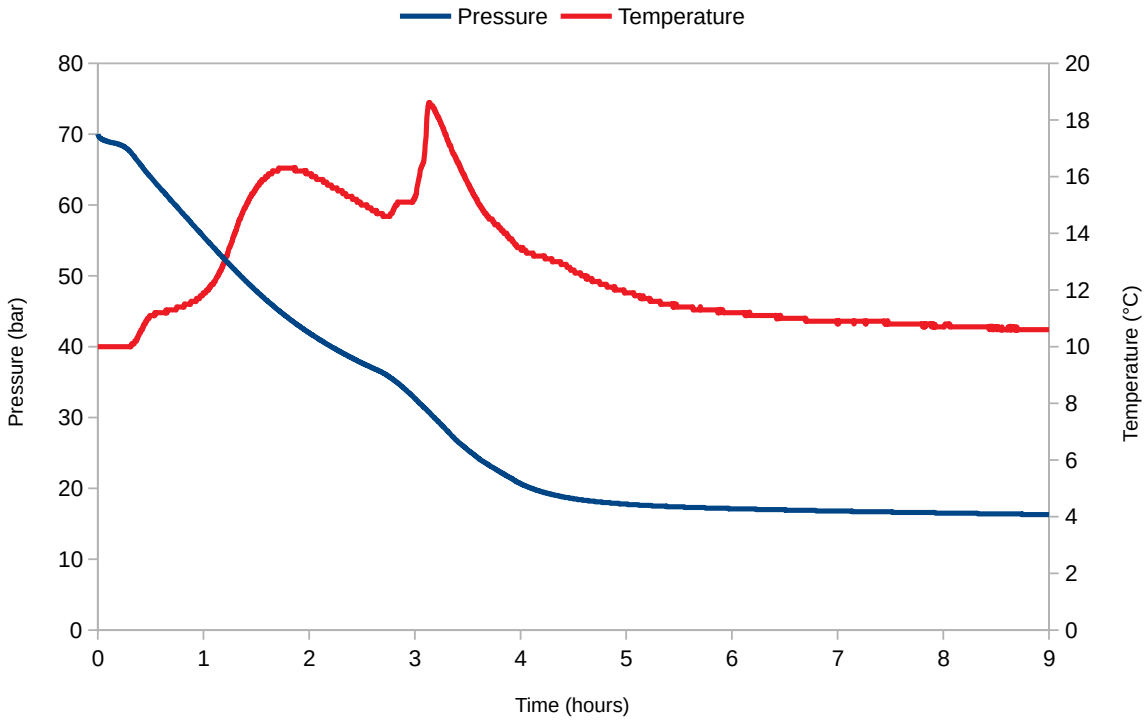

(a)

°

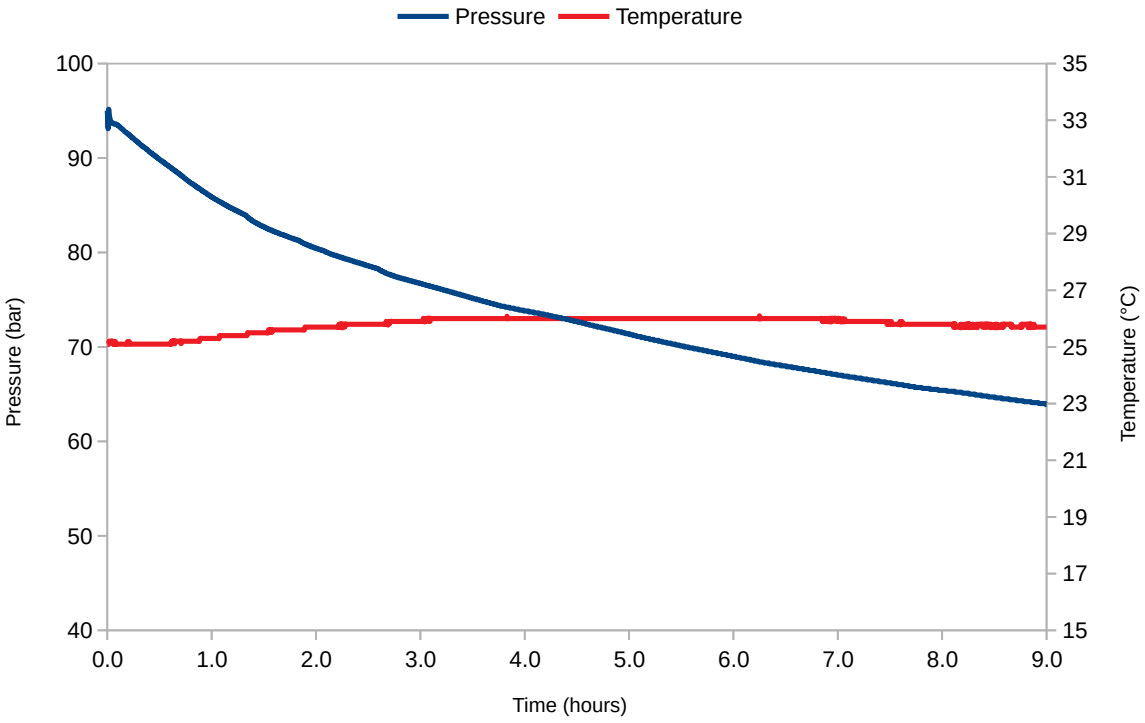

(b)

Figure B.8: *P-T* profile of (a) Typical CH_4-THF hydrate formation from fresh water at 7 MPa and 283.2 K and (b) Seawater-based hydrate formation using USY-valine as KHP at this work.

References

[1] Ana Palčić, Simona Moldovan, Hussein El Siblani, Aurelie Vicente, and Valentin Valtchev. Defect Sites in Zeolites: Origin and Healing. *Adv. Sci.*, 2104414:2104414, 2021.

[2] Asheesh Kumar, Hari Prakash Veluswamy, Praveen Linga, and Rajnish Kumar. Molecular level investigations and stability analysis of mixed methane-tetrahydrofuran hydrates: Implications to energy storage. *Fuel*, 236(August 2018):1505–1511, 2019.

[3] Z. Kristallogr V. Petříček, M. Dušek and L. Palatinus. Crystallographic Computing System JANA2006: General features. *Cryst. Mater*, 229:345–352, 2014.

[4] Kenneth S. Pitzer, David Z. Lippmann, R. F. Curl, Charles M. Huggins, and Donald E. Petersen. The Volumetric and Thermodynamic Properties of Fluids. II. Compressibility Factor, Vapor Pressure and Entropy of Vaporization. *J. Am. Chem. Soc.*, 77(13):3433–3440, 1955.

[5] W. Kohn. Nobel lecture: Electronic structure of matter - Wave functions and density functional. *Rev. Mod. Phys.*, 71(5):1253–1266, 1999.

[6] Paolo Giannozzi, Stefano Baroni, Nicola Bonini, Matteo Calandra, Roberto Car, Carlo Cavazzoni, Davide Ceresoli, Guido L. Chiarotti, Matteo Cococcioni, Ismaila Dabo, Andrea Dal Corso, Stefano De Gironcoli, Stefano Fabris, Guido Fratesi, Ralph Gebauer, Uwe Gerstmann, Christos Gougoussis, Anton Kokalj, Michele Lazzeri, Layla Martin-Samos, Nicola Marzari, Francesco Mauri, Riccardo Mazzarello, Stefano Paolini, Alfredo Pasquarello, Lorenzo Paulatto, Carlo Sbraccia, Sandro Scandolo, Gabriele Sclauzero, Ari P. Seitsonen, Alexander Smogunov, Paolo Umari, and Renata M. Wentzcovitch. QUANTUM ESPRESSO: A modular and open-source software project for quantum simulations of materials. *J. Phys. Condens. Matter*, 21(39), 2009.

[7] P. E. Blöchl. Projector augmented-wave method. *Phys. Rev. B*, 50(24):17953–17979, 1994.

[8] Ahmed Omran, Nikolai Nesterenko, and Valentin Valtchev. Ab initio mechanistic insights into the stability, diffusion and storage capacity of sI clathrate hydrate containing hydrogen. *Int. J. Hydrogen Energy*, 47(13):8419–8433, 2022.

[9] Konstantin A. Udachin, Christopher I. Ratcliffe, and John A. Ripmeester. Single crystal diffraction studies of structure I, II and H hydrates: Structure, cage occupancy andf composition. *J. Supramol. Chem.*, 2(4-5):405–408, 2002.

[10] Michael T. Kirchner, Roland Boese, W. Edward Billups, and Lewis R. Norman. Gas hydrate single-crystal structure analyses. *J. Am. Chem. Soc.*, 126(30):9407–9412, 2004.

[11] Dongyoung Lee, Woojin Go, and Yongwon Seo. Experimental and computational investigation of methane hydrate inhibition in the presence of amino acids and ionic liquids. *Energy*, 182:632–640, 2019.

[12] Angela N. Migues, Adina Muskat, Scott M. Auerbach, Woody Sherman, and S. Vaitheeswaran. On the rational design of zeolite clusters. *ACS Catal.*, 5(5):2859–2865, 2015.

[13] Mariann Krossner and Joachim Sauer. Interaction of water with brønsted acidic sites of zeolite catalysts. ab initio study of 1:1 and 2:1 surface complexes. *J. Phys. Chem.*, 100(15):6199–6211, 1996.

[14] Frédéric Labat, Alain H. Fuchs, and Carlo Adamo. Toward an accurate modeling of the water-zeolite interaction: Calibrating the DFT approach. *J. Phys. Chem. Lett.*, 1(4):763–768, 2010.

Appendix C

Supporting Information for Chapter 6

C.1 Experimental Procedure and Calculations

C.1.1 Hydrate formation experiment

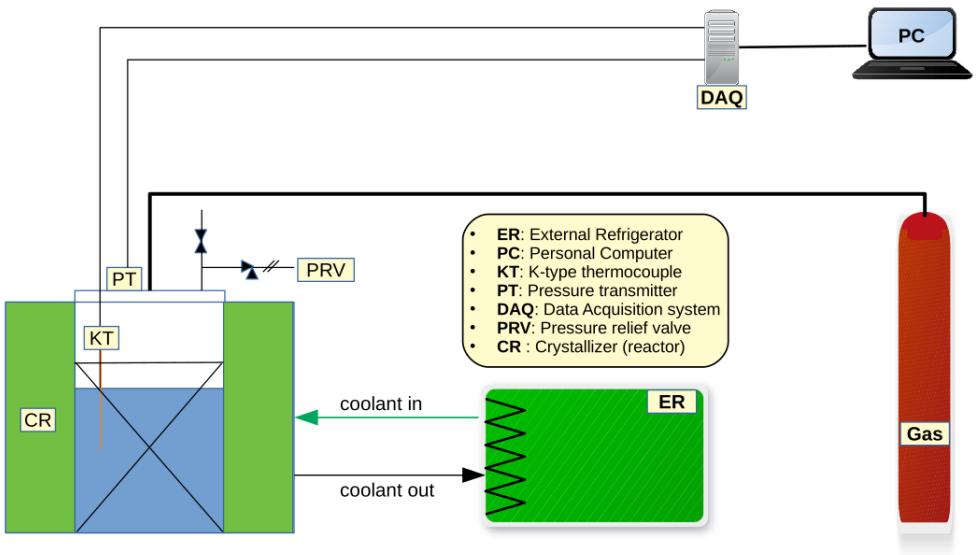

Figure C.1: Schematic diagram of hydrate formation and dissociation setup.

First, the reactor was filled with the solution until the desired level was achieved before it was sealed, and purged with nitrogen. Further, the reactor and related connections were purged with methane to ensure the removal of any contaminants. The system then is cooled down/heated to the target temperature. The system is left to equilibrate at the desired for one hour before it is pressurized with methane up to 6 MPa. During the reaction, pressure and temperature were monitored and recorded every 10 sec via a data acquisition system (DAQ). The induction time is defined as the period between this starting point and the formation of the first hydrate crystal. Here, we monitor the end of the induction period by a simultaneous sudden

pressure drop that is usually accompanied by a temperature increase due to the exothermic nature of hydrate formation. As the reaction continues, the pressure drops further, and the hydrate formation process is considered complete if there is no further significant pressure drop for 1 hour.

The number of moles of the gas consumed ($\Delta n_{H\downarrow}$) at any time t is equal to the difference between the number of moles of the gas ($n_{H,0}$) at time =0 (i.e., the start of the experiment) and the number of moles of the gas present $n_{H,t}$ at any time t in the vessel as shown by Eq.(C.1):

$$\Delta n_{H\downarrow} = n_{H_0} - n_{H_t} = \left(\frac{PV}{zRT}\right)_{G_0} - \left(\frac{PV}{zRT}\right)_{G_t} \tag{C.1}$$

Subscript G_0 and G_t represent the gas phase at the start of the experiment and time t, respectively. Here, P, T, and V are the pressure, temperature, and reactor volume, respectively. R is the universal gas constant, and z is the comprehensibility factor calculated by Pitzer's correction [1].

Normalized methane gas uptake is calculated by the following Eq.(C.2):

$$Normalized \quad uptake \quad = \frac{\Delta n_{H\downarrow}}{n_{H_2O}} \tag{C.2}$$

Finally, the volumetric capacity is calculated following Makagon method [2] where the volume of gas stored in a unit volume of gas hydrate:

$$Q_H = \frac{V_G \delta \times 10^3}{M_h} \tag{C.3}$$

Where the density of hydrate δ is calculated as per Sloan and Koh [3] and the molecular weight of hydrate M_h is defined as:

$$M_h = M + 18.02n \tag{C.4}$$

Then, the volume of gas stored in a unit volume if hydrate at standard conditions is defined by the equation:

$$Q_{SC} = \frac{Q_H P T_0}{Z P_0 T} \tag{C.5}$$

C.1.2 Hydrate dissociation experiment

To evaluate the methane uptake, the hydrates were dissociated by increasing the temperature at the end of all experiments to 310.2 K for at least 6 hours. The selection of that temperature ensures complete hydrate dissociation as it is beyond the equilibrium phase boundary. After 6 hours, the dissociation is deemed completed when the pressure is not changing for 1 h. Dur-

ing dissociation, the amount of methane released from hydrate at any time t is calculated by Eq.(C.6)

$$\Delta n_{H\uparrow} = n_{H,\downarrow} - n_{H,0} = \left(\frac{PV}{zRT}\right)_{G,t} - \left(\frac{PV}{zRT}\right)_{G,0} \tag{C.6}$$

where $n_{H,\downarrow}$ is the moles of methane gas consumed for the hydrate formation at the end of the experiment. Finally, the methane recovery is calculated as in Eq.(C.7):

$$Recovery(\%) = \frac{\Delta n_{H\uparrow}}{n_{H,\downarrow}} * 100 \tag{C.7}$$

C.1.3 Metallic Filament Packing Characterization

Table C.1: Energy-dispersive X-ray spectroscopy (EDX) measurements for metallic packing composition

Element	Net	Mass%	Mass% (normalized)	Atom%	Absolute error in % (1 sigma)	Relative error in % (1 sigma)
Fe	1480026	111.55	69.15	38.82	3.28	2.94
Cr	353350	14.67	9.10	5.48	0.45	3.04
C	299732	33.94	21.04	54.91	3.68	10.83
Si	25698	0.52	0.32	0.36	0.05	9.27
Al	20729	0.49	0.30	0.35	0.05	10.08
Cl	7470	0.14	0.09	0.08	0.03	22.51

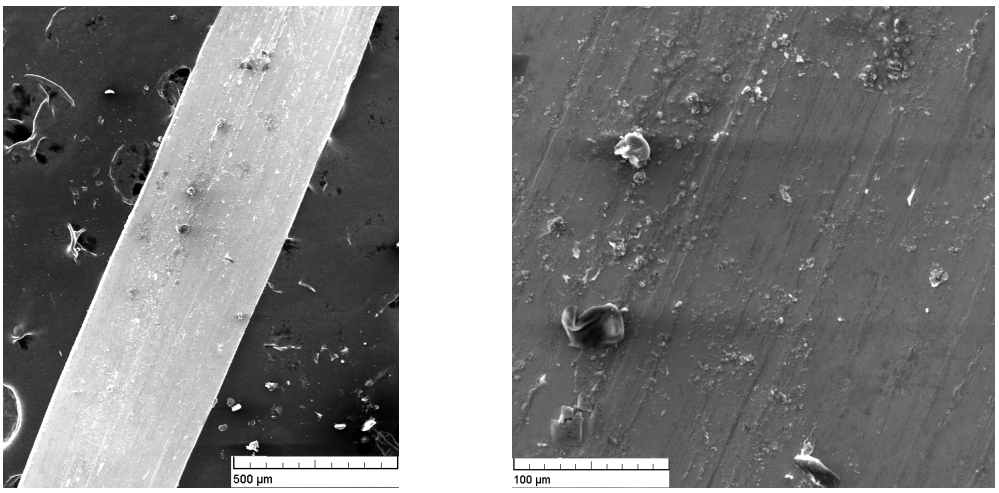

(a) **(b)**

Figure C.2: SEM images of metallic filament packing at (a) 500 μm and (b) 100 μm

(TESCAN) MIRA-LMH scanning electron microscope (SEM) equipped with an electron emission gun and operated at 20 kV was used to obtain the electron micrographs. The same scanning electron microscope model was used for energy-dispersive X-ray spectroscopy (EDX) measurements using to confirm the elemental analysis.

The morphology of light-weight corrosion-resistant metallic filament packing (MFP) in the open container was shown in **Fig.6.5**. One can observe that the packing is not limited to the bottom of the reactor but also extend above the hydrate surface to reach the gas phase. Moreover, the structure of packing works on breaking the hydrate thin film at the liquid-gas interface to allow a better mass transfer. SEM image **Fig.C.2** of MFP showed that SSF with an extended rough surface (the width range is 189-456 μm) increased the thermal conductivity and contributed to nucleation.

Table C.2: Methane hydrate formation with different promoters in a concentration of 300 ppm at 6 MPa and 283.15 K in NSR configuration.

Experiment No.	Kinetic Promoter (KHP)	Temperature (K)	Gas uptake(mmol gas/mol H_2O)	Induction time (min)	t_{90} (min)	Recovery (%)	Storage Capacity (V/V)
1C	L-Try	283.15	109.34	5.67	300.5	97.62	108.68
2C	L-Try	283.15	111.67	3.33	295.17	98.76	110.99
3C	L-Try	283.15	107.01	6.67	305.17	94.36	106.37
4C	SSZ-13	283.15	115.83	10.50	280.33	96.54	115.13
5C	SSZ-13	283.15	118.13	9.67	302.83	97.97	117.4
6C	SSZ-13	283.15	113.52	11.33	275.50	96.50	112.84
7C	Blank	283.15	99.36	167.00	545.67	95.92	99.36
8C	Blank	283.15	104.91	185.33	563.33	96.43	104.28
9C	Blank	283.15	97.12	191.83	531.50	97.53	96.53
10C	L-Meth	283.15	99.73	102.33	305.33	96.23	99.13
11C	L-Meth	283.15	98.78	110.50	302.67	95.68	98.19
12C	L-Meth	283.15	96.41	65.53	312.83	94.89	95.83
13C	L-Leuc	283.15	92.59	77.57	409.50	97.35	92.04
14C	L-Leuc	283.15	94.03	66.67	417.00	96.71	93.46
15C	L-Leuc	283.15	91.16	57.58	420.67	97.92	90.61

Table C.3: Methane hydrate formation with different promoters in a concentration of 300 ppm at 6 MPa and 288.15 K in NSR configuration

Experiment No.	Kinetic Promoter (KHP)	Temperature (K)	Gas uptake(mmol gas/mol H_2O)	Induction time (min)	t_{90} (min)	Recovery (%)	Storage Capacity (V/V)
1B	L-Try	288.15	91.16	6.67	374.33	95.22	90.61
2B	L-Try	288.15	94.27	5.67	355.83	97.30	93.7
3B	L-Try	288.15	97.12	8.50	349.67	96.43	97.12
4B	SSZ-13	288.15	78.57	21.17	343.50	96.55	78.11
5B	SSZ-13	288.15	85.14	20.83	355.33	96.75	84.63
6B	SSZ-13	288.15	77.35	24.33	341.67	97.87	76.88
7B	Blank	288.15	70.46	165.67	550.67	94.95	70.04
8B	Blank	288.15	75.39	150.00	564.33	96.63	74.9
9B	Blank	288.15	76.62	153.17	571.50	95.97	76.16
10B	L-Meth	288.15	93.31	74.00	439.00	96.54	92.75
11B	L-Meth	288.15	81.26	65.33	442.50	98.25	80.77
12B	L-Meth	288.15	77.84	71.33	445.33	98.13	77.38
13B	L-Leuc	288.15	81.50	80.83	428.00	94.78	81.01
14B	L-Leuc	288.15	85.14	75.17	426.67	98.87	84.63
15B	L-Leuc	288.15	87.74	65.33	421.33	95.45	87.75

Table C.4: Methane hydrate formation with different promoters in a concentration of 300 ppm at 6 MPa and 293.15 K in NSR configuration

Experiment No.	Kinetic Promoter (KHP)	Temperature (K)	Gas uptake(mmol gas/mol H_2O)	Induction time (min)	t_{90} (min)	Recovery (%)	Storage Capacity (V/V)
1A	L-Try	293.15	106.78	36.67	231.00	97.12	106.14
2A	L-Try	293.15	105.84	38.17	245.33	95.67	105.21
3A	L-Try	293.15	107.48	32.67	233.17	94.98	107.48
4A	SSZ-13	293.15	77.60	48.00	352.83	96.35	77.13
5A	SSZ-13	293.15	77.11	50.83	355.00	97.00	76.65
6A	SSZ-13	293.15	72.93	76.17	349.67	98.50	72.49
7A	Blank	293.15	46.26	195.33	390.67	97.77	45.98
8A	Blank	293.15	45.23	187.83	385.33	96.12	44.96
9A	Blank	293.15	42.14	128.17	410.67	95.34	41.88
10A	L-Meth	293.15	94.74	84.00	339.00	94.85	94.17
11A	L-Meth	293.15	92.36	80.50	332.17	96.75	91.8
12A	L-Meth	293.15	95.93	86.33	342.17	96.34	95.35
13A	L-Leuc	293.15	97.60	62.00	391.50	96.52	97.01
14A	L-Leuc	293.15	96.14	63.33	399.83	98.67	95.83
15A	L-Leuc	293.15	97.83	67.17	388.67	97.25	97.25

Table C.5: Methane hydrate formation with different promoters in a concentration of 300 ppm at 6 MPa and 293.15 K in FBR configuration

Experiment No.	Kinetic Promoter (KHP)	Temperature (K)	Gas uptake(mmol gas/mol H_2O)	Induction time (min)	t_{90} (min)	Recovery (%)	Storage Capacity (V/V)
1D	L-Try	293.15	104.44	4.33	162.33	98.22	103.81
2D	L-Try	293.15	103.73	3.83	169.50	97.83	103.11
3D	L-Try	293.15	103.03	3.50	149.83	96.12	102.41
4D	SSZ-13	293.15	102.56	2.17	159.00	95.75	101.94
5D	SSZ-13	293.15	104.91	2.00	152.33	98.91	104.91
6D	SSZ-13	293.15	107.25	3.83	150.83	97.32	106.6
7D	Blank	293.15	98.31	76.00	204.50	98.57	97.71
8D	Blank	293.15	93.55	79.83	215.17	94.79	92.98
9D	Blank	293.15	91.16	89.17	222.50	94.77	90.61
10D	L-Meth	293.15	97.12	5.33	165.33	96.19	96.54
11D	L-Meth	293.15	102.79	2.50	156.17	97.84	102.79
12D	L-Meth	293.15	101.85	7.17	153.83	94.63	101.23
13D	L-Leuc	293.15	99.49	4.83	151.17	96.97	98.89
14D	L-Leuc	293.15	104.21	3.50	153.00	95.33	103.5
15D	L-Leuc	293.15	103.03	3.17	160.67	96.47	102.41

Table C.6: Methane hydrate formation with different promoters in a concentration of 300 ppm at 6 MPa and 288.15 K in FBR configuration

Experiment No.	Kinetic Promoter (KHP)	Temperature (K)	Gas uptake(mmol gas/mol H_2O)	Induction time (min)	t_{90} (min)	Recovery (%)	Storage Capacity (V/V)
1E	L-Try	288.15	115.83	3.17	141.00	94.27	115.13
2E	L-Try	288.15	118.13	1.83	152.83	94.83	117.42
3E	L-Try	288.15	112.36	3.00	142.17	97.57	111.68
4E	SSZ-13	288.15	116.98	1.17	140.33	96.89	116.27
5E	SSZ-13	288.15	116.29	2.00	137.00	95.72	115.59
6E	SSZ-13	288.15	110.74	3.83	138.83	94.41	110.07
7E	Blank	288.15	89.96	65.00	192.50	95.79	89.42
8E	Blank	288.15	85.62	77.33	186.33	97.84	85.11
9E	Blank	288.15	80.28	68.17	181.83	98.67	79.8
10E	L-Meth	288.15	103.73	4.17	161.17	96.55	103.11
11E	L-Meth	288.15	104.91	2.50	167.83	98.46	104.27
12E	L-Meth	288.15	100.20	6.83	171.33	97.97	99.59
13E	L-Leuc	288.15	107.71	1.83	139.83	95.23	107.06
14E	L-Leuc	288.15	104.20	2.83	140.17	94.36	103.57
15E	L-Leuc	288.15	111.20	1.83	136.00	97.39	110.53

Table C.7: Methane hydrate formation with different promoters in a concentration of 300 ppm at 6 MPa and 283.15 K in FBR configuration

Experiment No.	Kinetic Promoter (KHP)	Temperature (K)	Gas uptake(mmol gas/mol H_2O)	Induction time (min)	t_{90} (min)	Recovery (%)	Storage Capacity (V/V)
1F	L-Try	283.15	110.74	0.00	78.67	97.50	110.07
2F	L-Try	283.15	113.06	1.00	72.67	95.64	112.37
3F	L-Try	283.15	109.11	0.83	71.00	97.82	108.45
4F	SSZ-13	283.15	114.68	1.33	75.33	96.32	113.98
5F	SSZ-13	283.15	116.98	0.00	77.33	96.86	116.27
6F	SSZ-13	283.15	111.20	0.83	70.83	94.78	110.53
7F	Blank	283.15	77.13	5.83	62.50	96.24	77.13
8F	Blank	283.15	80.77	3.33	57.33	94.28	80.28
9F	Blank	283.15	86.35	7.83	55.17	93.99	85.83
10F	L-Meth	283.15	94.74	5.50	71.83	94.76	94.17
11F	L-Meth	283.15	92.36	4.83	67.17	98.20	91.8
12F	L-Meth	283.15	98.54	2.83	63.33	96.57	97.95
13F	L-Leuc	283.15	97.12	2.33	70.17	95.17	96.53
14F	L-Leuc	283.15	99.02	3.83	67.00	95.25	98.42
15F	L-Leuc	283.15	93.55	4.00	60.33	94.78	92.98

C.2 Characterization methods

C.2.1 Zeolite Promoter Characterization

PANalytical X'Pert Pro ® diffractometer was used to obtain powder X-ray diffraction (PXRD) patterns. The diffractometer system used Cu-K_α-radiation (λ = 1.5418 Å; 45 kV; 40 mA) in a continuous scan at 25°C. The angle 2θ position was between 5.0114° and 35° while the step size in 2θ was 0.0170° in a step time of 50.1650 s. The measured specimen had a length of 10 mm.

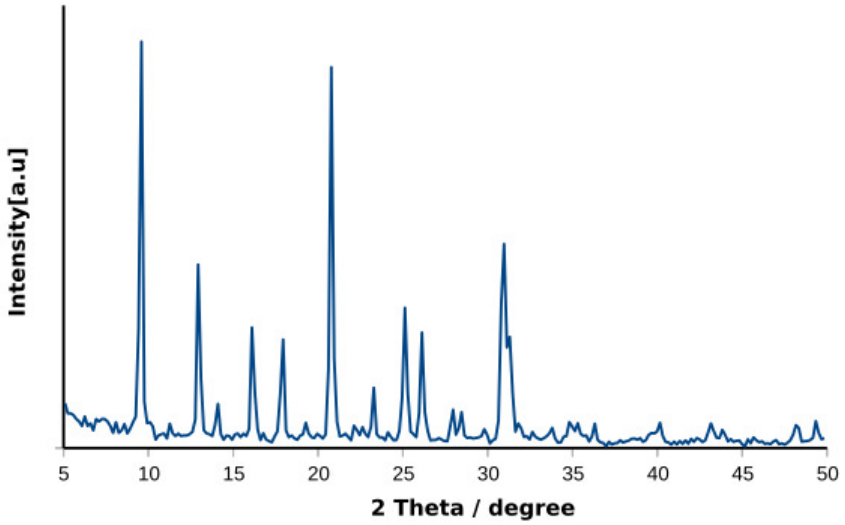

Figure C.3: PXRD pattern of H-SSZ-13 using Cu-K_α-radiation (λ = 1.5418 Å; 45 kV; 40 mA).

(TESCAN) MIRA-LMH scanning electron microscope (SEM) equipped with an electron emis-

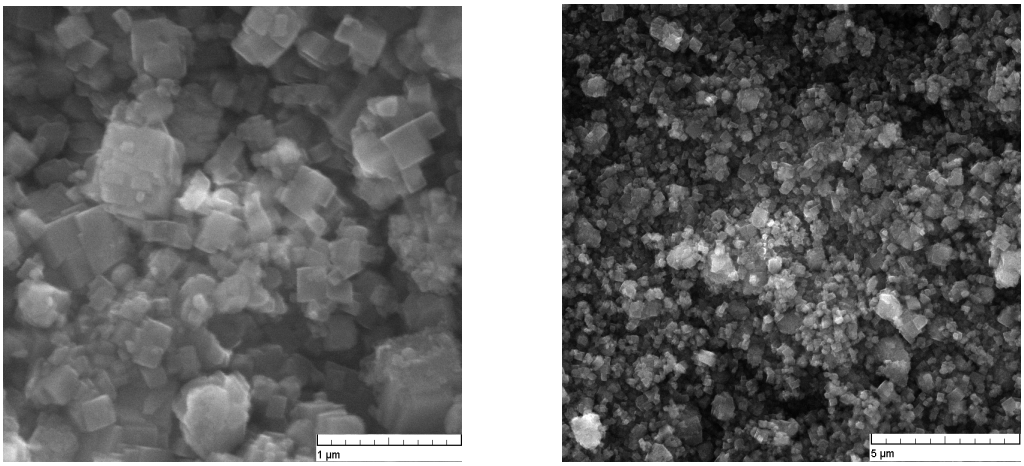

(a) **(b)**

Figure C.4: SEM images of H-SSZ-13

sion gun and operated at 20 kV was used to obtain the electron micrographs.The same scanning electron microscope model was used for energy-dispersive X-ray spectroscopy (EDX) measurements using to confirm the elemental analysis. Prior to the measurements, the samples were sputtered with platinum to improve their electrical conductivity. In addition, chemical composition of H-SSZ-13 was confirmed using inductively coupled plasma-atomic emission spectroscopy (ICP-AES) on an OPTIMA 4300 DV (Perkin-Elmer).

Table C.8: Energy-dispersive X-ray spectroscopy (EDX) measurements of H-SSZ-13.

Element	Mass% (normalized)	Atom%	Relative error in % (1 sigma)
Al	10.84	11.24	0.24
Si	89.10	88.69	1.62
Na	0.05	0.06	0.02

Table C.9: Inductively coupled plasma-atomic emission spectroscopy (ICP-AES) analysis of the zeolite.

	23Na [HEHe]	27Al [HEHe]	29Si [HEHe]
Zeolite	Concentration [mg/l]	Concentration [mg/l]	Concentration [mg/l]
H-SSZ-13	0.21	2.10	18.96

N_2-adsorption was employed to get the surface area and the porous volume measurements were measured via BET surface area measurement (measurement according to Brunauer, Emmet, Teller) with ASTM D3663 for the surface area and ASTM D4365 for the porous volume. The adsorption measurements were performed on Micromeritics ASAP 2020 surface

area analyzer after degassing all samples under vacuum at 300°C overnight before measurement. ASAP 2020 analysis program has been used to obtain the isotherms. The *t-plot* based on the Harkins-Jura equation was used to obtain he external surface (S_{ext}), and the volume of micropores (V_{micro}). The mesoporous volume was estimated as the difference between the total and micropore volumes[4] as per Eq.(C.8)

$$V_{\text{meso}} = V_{\text{total}} - V_{\text{micro}} \tag{C.8}$$

For the data analysis, measurements were plotted with a Micromeritics Tristar 3000 analyzer. The total surface area was determined by N_2 sorption analysis according to ASTM D 4365 – 95 (reapproved 2008). Volumes of micropores and mesopores were determined according to D4641-94 (reapproved 2006).

Table C.10: Textural measurement for Zeolite Promoters obtained from Nitrogen adsorption measurements

Zeolite	S_{BET} (m^2g^{-1})	S_{ext} (m^2g^{-1})	V_{micro} (cm^3g^{-1})	V_{meso} (cm^3g^{-1})	V_{total} (cm^3g^{-1})
H-SSZ-13	760.49	47.28	0.34	0.27	0.07

C.2.2 Binary CH_4-THF Characterization

Structure II clathrate crystal information was obtained by powder X-ray diffraction (PXRD) [5]. The measurement was carried out at atmospheric pressure and low temperature with a PANalytical X'Pert Pro ® diffractometer system using Cu-K_α-radiation (λ = 1.5418 Å; 45 kV; 40 mA) in a continuous scan. The start position in 2θ was 10.0114°, while the end position in 2θ was 39.7500°. We used a step size in 2θ of 0.0170° and a scan step time of 50.1650 s. First, the binary CH_4-THF hydrates were synthesized in high-pressure reactor as described above using 5.56 mol% THF aqueous solution at 6 MPa and 293.2 K. After the reaction is deemed complete, the unreacted gas is depressurized to the atmosphere followed by quick reactor cooling by liquid nitrogen. The hydrate sample was grounded by a mortar and pestle to prepare the uniform powder under liquid nitrogen to avoid sample dissociation. the obtained PXRD pattern is a typical sII pattern of space group $Fd\bar{3}m$ which is another indication of the presence of sII and absence of sI.

Similarly, solid-state ^{13}C MAS NMR spectra were obtained using a Bruker DRX400 spectrometer at a Larmor frequency of 100.6 MHz. Spectra were recorded at 250 K by placing the powdered hydrate samples in a 4 mm o.d. Zr-rotor that was loaded into a variable-temperature (VT) probe. All ^{13}C NMR spectra were recorded with magic angle spinning (MAS) between

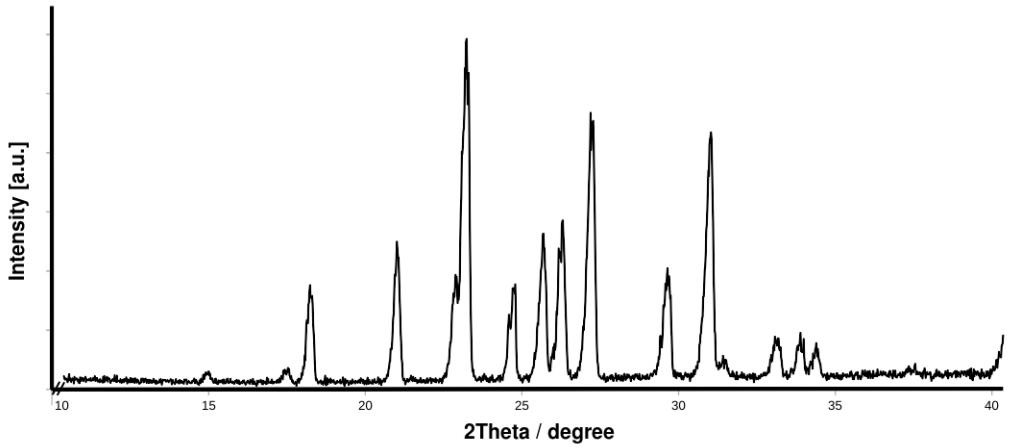

Figure C.5: Powder X-ray diffraction (PXRD) of binary CH_4-THF hydrate synthesized at 6 MPa and 293.2 K.

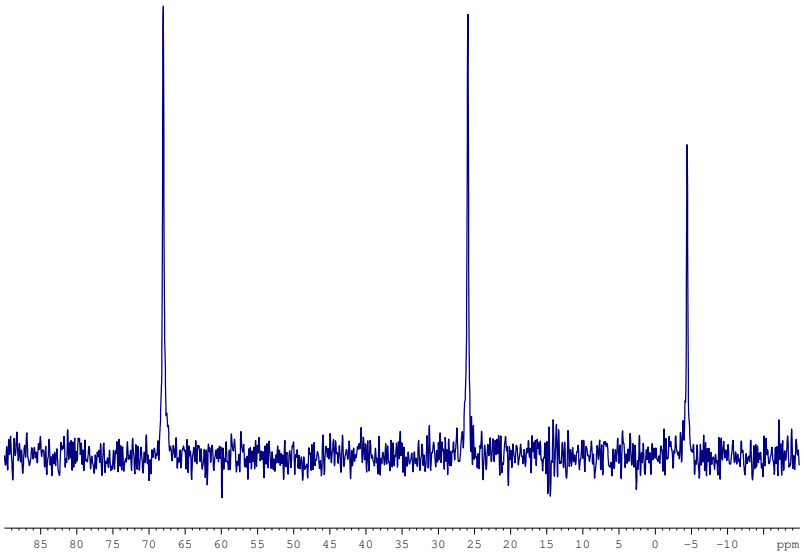

Figure C.6: ^{13}C MAS NMR spectra of binary CH_4+THF hydrate (structure II) synthesized at 293.2 K. Methane molecules occupied only in 5^{12} cages and appeared at about -4.3 ppm, and THF molecules occupied in $5^{12}6^4$ large cages were represented by two resonances (-C-C- at 26.2 ppm, -C-O-C- at 69.0 ppm).

2 and 4 kHz. Spectroscopic data revealed methane occupancy in 5^{12} small cages of sII as a sharp peak at -4.3 ppm, while the other two peaks (26.2 and 69.0 ppm) indicate the large cage occupancy of THF as shown in **Fig.C.6**.

Finally, Raman spectra of binary CH_4-THF clathrate sample are obtained using an immersion Raman probe (InPhotonics®) connected to the laser spectrometer (Horiba LabRam Evol®) via optical fibers. For excitation, a green laser at 532 nm wavelength was used with a spectral coverage of 50-3500 cm^{-1}.

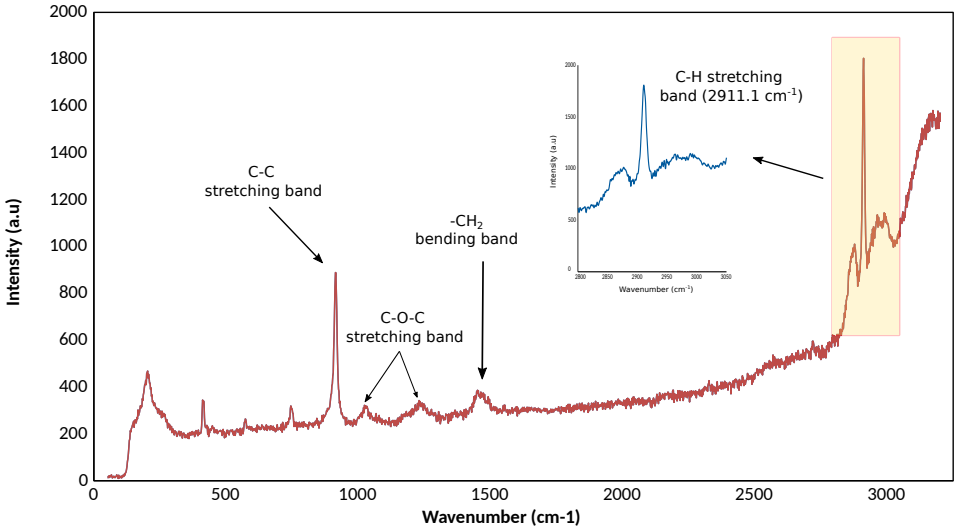

Figure C.7: Raman spectra of binary CH_4-THF hydrate formed at 6 MPa and 283.2 K. C-H stretching band is shown separately in blue.

C.3 Computational Methods

Computational details were described in detail in our previous publication [6] . In brief, density functional theory (DFT) calculations [7] were performed using the projected augmented wave (PAW) method and the standard pseudopotentials implemented by Quantum Espresso (QE) software [8]. The kinetic energy cutoff for plane wave expansion of wavefunctions and charge density were 55 and 440 Ry, respectively[9]. The structures were fully optimized using a force convergence threshold of at least 10^{-4} Ry/a.u. and with a self-consistency convergence criterion of at least $1, \times 10^{-8}$. The calculations have been carried out using the Monkhorst-Pack k-points grid of $2 \times 2 \times 2$ in the reciprocal space. The DFT calculations for isolated cages and amino acids were performed in a cubic simulation cell of volume $30 \times 30 \times 30$ Å^3. The 5^{12} small cage was modeled with a 20-molecule water cluster. In these small (5^{12}) cages, 8 oxygen atoms are located in a perfect cube (O_h). An estimated distance of 3.91 Å separates those 8 oxygen atoms from the cage center. The remaining 12 oxygen are positioned at 3.95 Å from the cage center and transformed according to the (T_h) subgroup of (O_h)[10]. The results agree with the average obtained from the X-ray structure of sII as well as the optimized crystal model[11, 12].

Amino acids' interaction with the above hydrate cages was successfully monitored using DFT calculated as reported by Lee *et al.*[14].**Fig.C.9** shows the optimized configuration of CH_4@5^{12} small cage model.

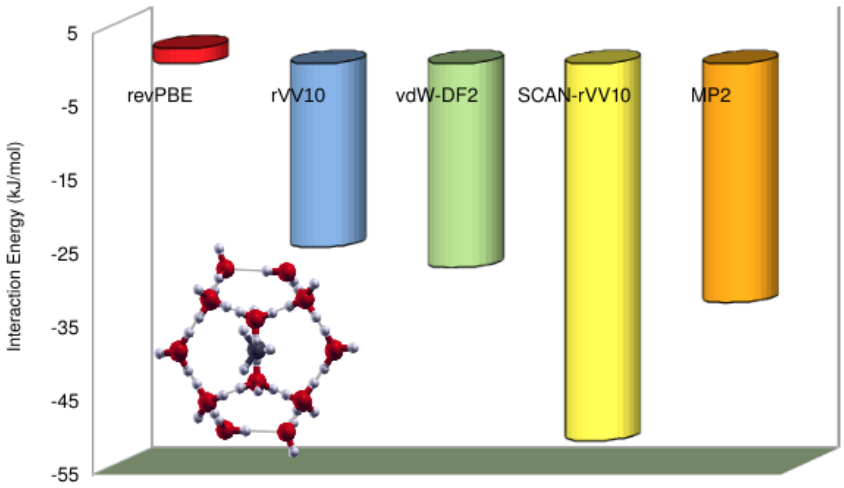

Figure C.8: Comparison of interaction energy of $CH_4@5^{12}$ cage (showed at the corner) estimated by different DFT calculations in this study compared to MP2 calculation [13].

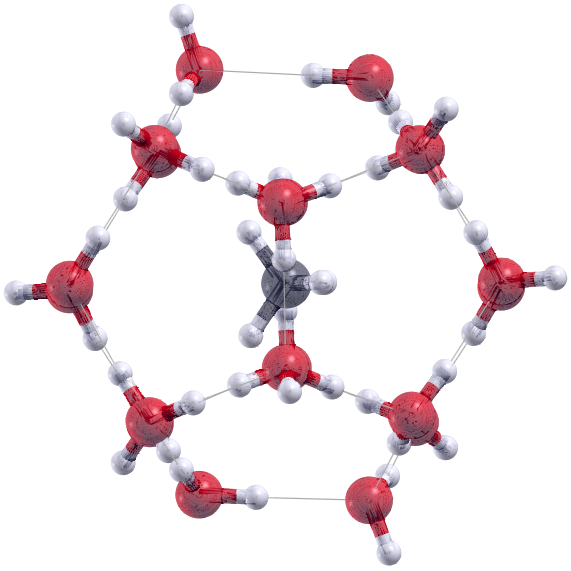

Figure C.9: Optimized configuration of $CH_4@5^{12}$ small cage using vdW-DF2 exchange functional.

References

[1] Kenneth S. Pitzer, David Z. Lippmann, R. F. Curl, Charles M. Huggins, and Donald E. Petersen. The Volumetric and Thermodynamic Properties of Fluids. II. Compressibility Factor, Vapor Pressure and Entropy of Vaporization. *J. Am. Chem. Soc.*, 77(13):3433–3440, 1955.

[2] Makagon Yuri F. *Hydrates of Hydrocarbons*. Pennwell, 1997.

[3] E. Dendy Sloan and Carolyn Ann Koh. *Clathrate hydrates of natural gases, thrid edition*. CRC Press, third edition, 2007.

[4] Ana Palčić, Simona Moldovan, Hussein El Siblani, Aurelie Vicente, and Valentin Valtchev. Defect Sites in Zeolites: Origin and Healing. *Adv. Sci.*, 2104414:2104414, 2021.

[5] Asheesh Kumar, Hari Prakash Veluswamy, Praveen Linga, and Rajnish Kumar. Molecular level investigations and stability analysis of mixed methane-tetrahydrofuran hydrates: Implications to energy storage. *Fuel*, 236(August 2018):1505–1511, 2019.

[6] Ahmed Omran, Nikolay Nesterenko, and Valentin Valtchev. Revealing Zeolites Active Sites Role as Kinetic Hydrate Promoters: Combined Computational and Experimental Study. *ACS Sustain. Chem. Eng.*, 10(24):8002–8010, jun 2022.

[7] W. Kohn. Nobel lecture: Electronic structure of matter - Wave functions and density functional. *Rev. Mod. Phys.*, 71(5):1253–1266, 1999.

[8] Paolo Giannozzi, Stefano Baroni, Nicola Bonini, Matteo Calandra, Roberto Car, Carlo Cavazzoni, Davide Ceresoli, Guido L. Chiarotti, Matteo Cococcioni, Ismaila Dabo, Andrea Dal Corso, Stefano De Gironcoli, Stefano Fabris, Guido Fratesi, Ralph Gebauer, Uwe Gerstmann, Christos Gougoussis, Anton Kokalj, Michele Lazzeri, Layla Martin-Samos, Nicola Marzari, Francesco Mauri, Riccardo Mazzarello, Stefano Paolini, Alfredo Pasquarello, Lorenzo Paulatto, Carlo Sbraccia, Sandro Scandolo, Gabriele Sclauzero, Ari P. Seitsonen, Alexander Smogunov, Paolo Umari, and Renata M. Wentzcovitch.

QUANTUM ESPRESSO: A modular and open-source software project for quantum simulations of materials. *J. Phys. Condens. Matter*, 21(39), 2009.

[9] P. E. Blöchl. Projector augmented-wave method. *Phys. Rev. B*, 50(24):17953–17979, 1994.

[10] Ahmed Omran, Nikolai Nesterenko, and Valentin Valtchev. Ab initio mechanistic insights into the stability, diffusion and storage capacity of sI clathrate hydrate containing hydrogen. *Int. J. Hydrogen Energy*, 47(13):8419–8433, 2022.

[11] Konstantin A. Udachin, Christopher I. Ratcliffe, and John A. Ripmeester. Single crystal diffraction studies of structure I, II and H hydrates: Structure, cage occupancy andf composition. *J. Supramol. Chem.*, 2(4-5):405–408, 2002.

[12] Michael T. Kirchner, Roland Boese, W. Edward Billups, and Lewis R. Norman. Gas hydrate single-crystal structure analyses. *J. Am. Chem. Soc.*, 126(30):9407–9412, 2004.

[13] Mert Atilhan, Nezih Pala, and Santiago Aparicio. A quantum chemistry study of natural gas hydrates. *J. Mol. Model.*, 20(4), 2014.

[14] Dongyoung Lee, Woojin Go, and Yongwon Seo. Experimental and computational investigation of methane hydrate inhibition in the presence of amino acids and ionic liquids. *Energy*, 182:632–640, 2019.

List of Publications and Communications

Publications

Related to this work

1. ***Omran A, Nesterenko N, & Valtchev V.*** Zeolitic ice: A route toward net zero emissions. ***Renewable and Sustainable Energy Reviews***. 2022 Oct 1;168:112768.

2. ***Omran A, Nesterenko N, & Valtchev V.*** Ab initio mechanistic insights into the stability, diffusion and storage capacity of sI clathrate hydrate containing hydrogen. ***International Journal of Hydrogen Energy***. 2022 Feb 12;47(13):8419-33.

3. ***Omran A, Nesterenko N, & Valtchev V.*** Revealing Zeolites Active Sites Role as Kinetic Hydrate Promoters: Combined Computational and Experimental Study. ***ACS Sustainable Chemistry & Engineering***. 2022 Jun 9;12 (24):8002–8010.

4. ***Omran A, Nesterenko N, Paecklar AA, Barrier N, & Valtchev V.*** Toward Economical Seawater-Based Methane Hydrate Formation at Ambient Temperature: A Combined Experimental and Computational Study. ***ACS Sustainable Chemistry & Engineering***. 2022 Aug 18;10 (35):11617–11626.

5. ***Omran A, Nesterenko N, & Valtchev V.*** Sustainable Energy Storage in Hydrates: Combining Predictive First Principle Calculations, Green Kinetic Promoters with Improved Reactor Design. Submitted at September 2022.

Previous

- ***Omran, A., Yoon, S. H., Khan, M., Ghouri, M., Chatla, A., & Elbashir, N.*** Mechanistic Insights for Dry Reforming of Methane on Cu/Ni Bimetallic Catalysts: DFT-Assisted Microkinetic Analysis for Coke Resistance. ***Catalysts***. 2020 Sep 10;10(9):1043.

Patents

- ***Omran A, Nesterenko N, & Valtchev V.*** Promotion of Methane Hydrate Formation. Ref.:IS20-029. Submitted by TotalEnergies and ANR on February 2022.

International Communications

Related to this work

1. ***Omran A, Nesterenko N, & Valtchev V.*** *Ab initio* Mechanistic Insight into the Stability, Diffusion, and Storage Capacity of H_2, CH_4, and CO_2 in sI Clathrate Hydrate. **Oral** communication at European Congress and Exhibition on Advanced Materials and Processes - EUROMAT 2021, Sep 2021, **Hybrid Event-Austria**.

2. ***Omran A, Nesterenko N, & Valtchev V.*** An Eco-Friendly Approach For Improved Methane Hydrate Kinetics In Near-Ambient Temperature and Moderate Pressure. **Oral** communication at **ACS Research Conference**: Chemistry and Chemical Engineering in MENA, May 2022, **Doha, Qatar**.

3. ***Omran A, Nesterenko N, & Valtchev V.*** An Innovative Environmental Benign Approach to Enhance Methane Hydrate Kinetics in Near-Ambient and Moderate Pressure. **Oral** communication at 7^{th} International Conference on Multifunctional, Hybrid and Nanomaterials, October 2022, **Genoa, Italy**.

4. ***Omran A, Nesterenko N, & Valtchev V.*** Toward Economical Seawater-Based Methane Hydrate Formation at Ambient Temperature: A Combined Experimental and Computational Study. **Oral** communication at The international Conference « Matériaux 2022 » October 2022, **Lille, France**.

5. ***Omran A, Nesterenko N, & Valtchev V.*** A Computational Insight of Guest Exchange Mechanism between CH_4 and CO_2 in SI Clathrate: CH_4 Recovery and CO_2 Storage Opportunities. **Oral** communication at TAMUQ-TotalEnergies Workshop" Successful Industry-Academia Collaboration in the Advancement of CO_2 Utilization & Low Carbon Processes", May 2022, **Doha, Qatar**.

6. ***Omran A., Nesterenko N., & Valtchev V.*** Synergistic eco-friendly kinetic promoters for high methane storage in fresh and seawater-based hydrate. **Oral** communication at 8^{th} LCS Workshop 'Zeolites in the Energy Transition' , **Cabourg, France**.

7. ***Omran A, Nesterenko N, & Valtchev V.*** Zeolitic Ice For Energy Transition : Mechanistic Insights From *Ab initio* Calculations. **Poster** at CAMD Summer School 2022 of Electronic Structure Theory and Materials Design, August 2022, **Helsingør, Denmark**.

Previous

- ***Omran A., Ghouri M. & Elbashir N.*** DFT study of Copper-Nickel (111) Catalyst for Methane Dry Reforming .**Oral** at Third International Computational Science and Engineering Conference , Doha, Qatar.

National Communications

1. ***Omran A, Nesterenko N, & Valtchev V.*** Binary H_2-CH_4 Clathrate for better hydrogen Storage. **Oral** communication at Hydrogen Scientific Day (Production, Storage and Valorization) organized by I-EPE (Energie, Propulsion et I-EPE (Energie, Propulsion et Environment), December 2019, Caen, France.

2. ***Omran A, Nesterenko N, & Valtchev V.*** Revealing Acidic Zeolites: Role as New Kinetic Hydrate Promoters: A Combined Computational and Experimental Study. **Oral** communication at 37^{th} meeting of French Group of Zeolite (GFZ), March 2022, Vogüé, France.

3. ***Omran A, Nesterenko N, & Valtchev V.*** Green Kinetic Promoters for Seawater based Methane Hydrate Formation at Ambient Temperature. **Oral** communication at Hydrate Scientific Days "Les Journées « HYDRATES 2022 »" , November 2022, IFPEN, Rueil-Malmaison , France.

4. ***Omran A, Nesterenko N, & Valtchev V.*** Understanding CH_4-CO_2 Guest Exchange Mechanism between in sI Clathrate: CH4 Recovery and CO2 Storage Opportunities. **Oral** communication at Hydrate Scientific Days "Les Journées « HYDRATES 2022 »" , November 2022, IFPEN, Rueil-Malmaison , France.

5. ***Patrick Bousquet-Mélou, Jean-Baptiste Harry, Benoist Gaston, Patrick Amestoy, Jean-Yves L'Excellent, Ahmed Omran, & Valtchev V.*** Technology watch and achievements in programming on long vector processors. **Oral** communication at Journées Calcul Données : Rencontres scientifiques et techniques autour du calcul et des données. "JCAD 2022" , October 2022, Dijon , France.

Technical Communications

1. ***Omran A, Nesterenko N, & Valtchev V.*** Gas Clathrates: Environmentally Benign Materials for The Energy Transition. The Catalyst Review. 2021 Nov.; 34(11):6-13.

2. ***Omran A, Nesterenko N, & Valtchev V.*** Greenhouse Gases as Promoters for Green Hydrogen Storage. Technical communication at Advances in Engineering retrieved at `https://advanceseng.com`

Abstract

In the context of energy and economic crisis, the smooth energy transition will require a proper combination of energy efficiency and integration of renewables to achieve the optimum trade-off between the increasing energy demand and environmental commitments according to Paris Agreement. In that context, the environmental friendly gas hydrates or "zeolitic ice" can play a key role in areas such as methane storage, hydrogen storage and combined carbon capture and sequestration (CCS). Gas hydrates are non-stoichiometric nanoporous crystalline compounds that are mainly composed of 3D water cages encapsulating gases. Using a combination of experimental and computational techniques, this work aims to promoting the slow hydrate formation kinetics, increase the energy content to enable their scale up, as well as enhance fundamental understanding of the gas diffusion in hydrates.

Keywords: zeolitic ice, methane hydrates, hydrogen storage , zeolites , DFT.

Résumé

Dans le contexte de crise énergétique et économique, la transition énergétique en douceur nécessitera une combinaison appropriée d'efficacité énergétique et d'intégration des énergies renouvelables pour atteindre le compromis optimal entre la demande énergétique croissante et les engagements environnementaux selon l'Accord de Paris. Dans ce contexte, les hydrates de gaz ou « glace zéolitique » verts peuvent jouer un rôle clé dans des domaines tels que le stockage du méthane, le stockage de l'hydrogène et la capture et la séquestration combinées du carbone (CSC). Les hydrates de gaz sont des composés cristallins nanoporeux non stoechiométriques qui sont principalement composés de cages d'eau 3D encapsulant des gaz. En utilisant une combinaison de techniques expérimentales et informatiques, ce travail vise à promouvoir la cinétique de formation lente des hydrates, à augmenter le contenu énergétique pour permettre leur mise à l'échelle, ainsi qu'à améliorer la compréhension fondamentale de la diffusion des gaz dans les hydrates.

Mots clés : glace zéolithique, hydrates de méthane, stockage d'hydrogène, zéolithes, DFT.